

N69-33422  
NASA CR-103788

FINAL TECHNICAL REPORT

CHARGED PARTICLE RADIATION DAMAGE IN SEMICONDUCTORS, XIV:

STUDY OF RADIATION EFFECTS IN LITHIUM DOPED  
SILICON SOLAR CELLS

27 MAY 1969

**CASE FILE  
COPY**

10971-6014-R0-00

Contract No. 952251

JET PROPULSION LABORATORY  
CALIFORNIA INSTITUTE OF TECHNOLOGY  
PASADENA, CALIFORNIA

**TRW**  
SYSTEMS GROUP

FINAL REPORT

STUDY OF RADIATION EFFECTS IN LITHIUM DOPED  
SILICON SOLAR CELLS

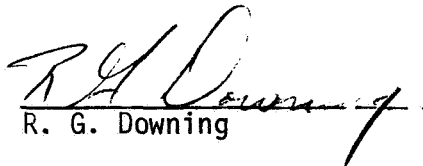
27 May 1969

10971-6014-R0-00

R. G. Downing  
J. R. Carter  
R. E. Scott  
W. K. Van Atta

Prepared by:

Approved:

  
R. G. Downing

  
J. L. Rogers

Contract 952251

Jet Propulsion Laboratory  
California Institute of Technology  
Pasadena, California

TRW Systems  
One Space Park  
Redondo Beach, California 90278

This work was performed for the Jet Propulsion Laboratory, California Institute of Technology, as sponsored by the National Aeronautics and Space Administration under Contract 952251.

## TABLE OF CONTENTS

	<u>PAGE</u>
I. INTRODUCTION	1
II. LITHIUM SOLAR CELL EVALUATION	3
A. Lithium Doped Crucible Silicon Solar Cells	9
B. Lithium Doped Float Zone Silicon Solar Cells	12
C. Conclusions and Recommendations	15
III. KINETICS OF LITHIUM IN SILICON	17
A. Lithium Redistribution Studies	17
B. Carrier Removal Studies	25
C. Recombination Studies	35
IV. EVALUATION TECHNIQUES STUDIES	39
A. Lang X-Ray Topography Study	39
B. Junction Capacitance Measurements	40
C. Diffusion Sources	45
D. Other Solar Cell Structures	46
V. NEW TECHNOLOGY	47
REFERENCES	47

### TABLES

TABLE I	LITHIUM SOLAR CELL MANUFACTURING PARAMETERS	48
TABLE II	CRUCIBLE LI SOLAR CELL RECOVERY CHARACT. @ 100°C	49
TABLE III	F.Z. LITHIUM SOLAR CELL RECOVERY CHARACTERISTICS	50
TABLE IV	RECOVERED LEVEL & HALF RECOVERY TIME	51
TABLE V	PROPERTIES OF LI DIFFUSED SILICON SPECIMENS	52
TABLE VI	RADIATION DEFECT PRODUCTION IN N-TYPE SILICON	53

### FIGURES

FIG. 1	ELECTRON DEGRADATION OF CONTEMPORARY N/P SILICON SOLAR CELLS	54
FIG. 2	LITHIUM DOPED SOLAR CELL I-V CHARACTERISTIC EXHIBITING DEGRADATION AND COLLAPSE OF POWER POINT	55
FIG. 3	LITHIUM DOPED SOLAR CELL I-V CHARACTERISTIC EXHIBITING $I_{SC}$ REDEGRADATION WITH CONTINUED $V_{OC}$ RECOVERY	56
FIG. 4	ANNEALING TIME VS. STORAGE TEMPERATURE FOR CRUCIBLE LITHIUM DOPED SOLAR CELLS	57

<u>FIGURES</u> (Cont.)	<u>PAGE</u>
FIG. 5 INITIAL $I_{SC}$ VERSUS LITHIUM CONCENTRATION AT JUNCTION FOR CRUCIBLE AND FLOAT ZONE LI DOPED SOLAR CELLS	58
FIG. 6 RECOVERED $I_{SC}$ VERSUS LITHIUM CONCENTRATION AT JUNCTION FOR CRUCIBLE AND FLOAT ZONE LI DOPED SOLAR CELLS	59
FIG. 7 RECOVERY OF GROUP C1 LITHIUM SOLAR CELLS AT 100°C	60
FIG. 8 RECOVERY OF GROUP C1 LITHIUM SOLAR CELLS AT 80°C	61
FIG. 9 RECOVERY OF GROUP C1 LITHIUM SOLAR CELLS AT 60°C	62
FIG. 10 RECOVERY OF GROUP C2 LITHIUM SOLAR CELLS AT 100°C	63
FIG. 11 RECOVERY OF GROUP C2 LITHIUM SOLAR CELLS AT 80°C	64
FIG. 12 RECOVERY OF GROUP C2 LITHIUM SOLAR CELLS AT 60°C	65
FIG. 13 RECOVERY OF GROUP C6A LITHIUM SOLAR CELLS AT 100°C	66
FIG. 14 RECOVERY OF GROUP C6A LITHIUM SOLAR CELLS AT 80°C	67
FIG. 15 RECOVERY OF GROUP C6A LITHIUM SOLAR CELLS AT 60°C	68
FIG. 16 RECOVERY OF GROUP C6B LITHIUM SOLAR CELLS AT 100°C	69
FIG. 17 RECOVERY OF GROUP C6B LITHIUM SOLAR CELLS AT 80°C	70
FIG. 18 RECOVERY OF GROUP C6B LITHIUM SOLAR CELLS AT 60°C	71
FIG. 19 RECOVERY OF GROUP C6C LITHIUM SOLAR CELLS AT 100°C	72
FIG. 20 RECOVERY OF GROUP C6C LITHIUM SOLAR CELLS AT 80°C	73
FIG. 21 RECOVERY OF GROUP C6C LITHIUM SOLAR CELLS AT 60°C	74
FIG. 22 RECOVERY OF GROUP C5A LITHIUM SOLAR CELLS AT 100°C	75
FIG. 23 RECOVERY OF GROUP C5A LITHIUM SOLAR CELLS AT 80°C	76
FIG. 24 RECOVERY OF GROUP C5A LITHIUM SOLAR CELLS AT 60°C	77
FIG. 25 RECOVERY OF GROUP C5A LITHIUM SOLAR CELLS AT 25°C	78
FIG. 26 RECOVERY OF GROUP C5C LITHIUM SOLAR CELLS AT 100°C	79
FIG. 27 RECOVERY OF GROUP C5C LITHIUM SOLAR CELLS AT 80°C	80
FIG. 28 RECOVERY OF GROUP C5C LITHIUM SOLAR CELLS AT 60°C	81
FIG. 29 RECOVERY OF GROUP H1 LITHIUM SOLAR CELLS AT 100°C	82
FIG. 30 RECOVERY OF GROUP H1 LITHIUM SOLAR CELLS AT 80°C	83
FIG. 31 RECOVERY OF GROUP H1 LITHIUM SOLAR CELLS AT 60°C	84
FIG. 32 RECOVERY OF GROUP H2 LITHIUM SOLAR CELLS AT 100°C	85
FIG. 33 RECOVERY OF GROUP H2 LITHIUM SOLAR CELLS AT 80°C	86
FIG. 34 RECOVERY OF GROUP H2 LITHIUM SOLAR CELLS AT 60°C	87
FIG. 35 RECOVERY OF GROUP H6 LITHIUM SOLAR CELLS AT 100°C	88
FIG. 36 RECOVERY OF GROUP H6 LITHIUM SOLAR CELLS AT 80°C	89
FIG. 37 RECOVERY OF GROUP H6 LITHIUM SOLAR CELLS AT 60°C	90



<u>FIGURES (Cont.)</u>	<u>PAGE</u>
FIG. 38 RECOVERY OF GROUP T2 LITHIUM SOLAR CELLS AT 100°C	91
FIG. 39 RECOVERY OF GROUP T2 LITHIUM SOLAR CELLS AT 80°C	92
FIG. 40 RECOVERY OF GROUP T2 LITHIUM SOLAR CELLS AT 60°C	93
FIG. 41 RECOVERY OF GROUP T7 LITHIUM SOLAR CELLS AT 100°C	94
FIG. 42 RECOVERY OF GROUP T7 LITHIUM SOLAR CELLS AT 80°C	95
FIG. 43 RECOVERY OF GROUP T7 LITHIUM SOLAR CELLS AT 60°C	96
FIG. 44 RECOVERY OF GROUP T7 LITHIUM SOLAR CELLS AT 25°C	97
FIG. 45 RECOVERY OF GROUP T8 LITHIUM SOLAR CELLS AT 100°C	98
FIG. 46 RECOVERY OF GROUP T8 LITHIUM SOLAR CELLS AT 80°C	99
FIG. 47 RECOVERY OF GROUP T8 LITHIUM SOLAR CELLS AT 60°C	100
FIG. 48 RECOVERY OF GROUP C5B LITHIUM SOLAR CELLS AFTER $3 \times 10^{14}$ e/cm <sup>2</sup>	101
FIG. 49 RECOVERY OF GROUP C5B LITHIUM SOLAR CELLS AFTER $3 \times 10^{15}$ e/cm <sup>2</sup>	102
FIG. 50 RECOVERY OF GROUP C5D LITHIUM SOLAR CELLS AFTER $3 \times 10^{14}$ e/cm <sup>2</sup>	103
FIG. 51 RECOVERY OF GROUP C5D LITHIUM SOLAR CELLS AFTER $3 \times 10^{15}$ e/cm <sup>2</sup>	104
FIG. 52 RECOVERY OF GROUP H4 LITHIUM SOLAR CELLS AFTER $3 \times 10^{14}$ e/cm <sup>2</sup>	105
FIG. 53 RECOVERY OF GROUP H4 LITHIUM SOLAR CELLS AFTER $3 \times 10^{15}$ e/cm <sup>2</sup>	106
FIG. 54 RECOVERY OF GROUP H5 LITHIUM SOLAR CELLS AFTER $3 \times 10^{14}$ e/cm <sup>2</sup>	107
FIG. 55 RECOVERY OF GROUP H5 LITHIUM SOLAR CELLS AFTER $3 \times 10^{15}$ e/cm <sup>2</sup>	108
FIG. 56 RECOVERY OF GROUP H7 LITHIUM SOLAR CELLS AFTER $3 \times 10^{14}$ e/cm <sup>2</sup>	109
FIG. 57 RECOVERY OF GROUP H7 LITHIUM SOLAR CELLS AFTER $3 \times 10^{15}$ e/cm <sup>2</sup>	110
FIG. 58 RECOVERY OF GROUP T3 LITHIUM SOLAR CELLS AFTER $3 \times 10^{14}$ e/cm <sup>2</sup>	111
FIG. 59 RECOVERY OF GROUP T3 LITHIUM SOLAR CELLS AFTER $3 \times 10^{15}$ e/cm <sup>2</sup>	112
FIG. 60 RECOVERY OF GROUP T4 LITHIUM SOLAR CELLS AFTER $3 \times 10^{14}$ e/cm <sup>2</sup>	113
FIG. 61 RECOVERY OF GROUP T4 LITHIUM SOLAR CELLS AFTER $3 \times 10^{15}$ e/cm <sup>2</sup>	114
FIG. 62 RECOVERY OF GROUP T5 LITHIUM SOLAR CELLS AFTER $3 \times 10^{14}$ e/cm <sup>2</sup>	115
FIG. 63 RECOVERY OF GROUP T5 LITHIUM SOLAR CELLS AFTER $3 \times 10^{15}$ e/cm <sup>2</sup>	116
FIG. 64 RECOVERY OF GROUP T6 LITHIUM SOLAR CELLS AFTER $3 \times 10^{14}$ e/cm <sup>2</sup>	117
FIG. 65 RECOVERY OF GROUP T6 LITHIUM SOLAR CELLS AFTER $3 \times 10^{15}$ e/cm <sup>2</sup>	118
FIG. 66 CHANGES IN DONOR CONCENTRATION DURING REDISTRIBUTION	119
FIG. 67 CHANGES IN SHORT CIRCUIT CURRENT DURING REDISTRIBUTION	120
FIG. 68 CHANGES IN SHORT CIRCUIT CURRENT DURING RECOVERY	121
FIG. 69 VARIATION OF RECOVERY HALF TIME WITH LI CONCENTRATION	122
FIG. 70 REMOVAL RATE AT JUNCTION FOR VARIOUS LI CONCENTRATIONS	123
FIG. 71 CHANGES IN LI CONCENTRATION DURING RECOVERY	124

<u>FIGURES</u> (cont.)	<u>PAGE</u>
FIG. 72 CHANGES IN LI CONCENTRATION AND SHORT CIRCUIT CURRENT DURING RECOVERY	125
FIG. 73 HALL MOBILITIES OF LITHIUM DOPED SILICON	126
FIG. 74 CARRIER REMOVAL, LITHIUM DOPED F.Z. SILICON	127
FIG. 75 CARRIER REMOVAL, LITHIUM DOPED F.Z. SILICON	128
FIG. 76 REMOVAL CONSTANT VS. DONOR CONCENTRATION	129
FIG. 77 HALL COEFFICIENT CHANGES DURING IRRADIATION, LI DOPED F.Z. SILICON	130
FIG. 78 ANNEALING OF IRRADIATED LITHIUM DOPED SILICON	131
FIG. 79 MOBILITY CHANGES DURING IRRADIATION AND ANNEALING, F.Z.	132
FIG. 80 MOBILITY CHANGES DURING IRRADIATION AND ANNEALING, Q.C.	133
FIG. 81 CARRIER REMOVAL, PHOSPHORUS DOPED F.Z. SILICON	134
FIG. 82 MOBILITY CHANGES DURING IRRADIATION AND ANNEALING, PHOSPHORUS FLOAT ZONE	135
FIG. 83 LIFETIME VERSUS RECIPROCAL TEMP, P/N NON-LITHIUM CELLS	136
FIG. 84 LIFETIME VERSUS RECIPROCAL TEMP, LITHIUM F.Z. CELLS	137
FIG. 85 LIFETIME VERSUS RECIPROCAL TEMP, LITHIUM F.Z. CELLS	138
FIG. 86 LIFETIME VERSUS RECIPROCAL TEMP, LITHIUM Q.C. CELLS	139
FIG. 87 LIFETIME VERSUS RECIPROCAL TEMP, LITHIUM Q.C. CELLS	140
FIG. 88 TOPOGRAPH OF LI DOPED F.Z. SILICON (0.1 ohm-cm), AS RECEIVED	141
FIG. 89 TOPOGRAPH OF LI DOPED F.Z. SILICON (21 ohm-cm), AFTER 18 HRS. AT 400°C, SLOW COOLED	142
FIG. 90 CAPACITANCE VS. VOLTAGE FOR GROUP H5 LI SOLAR CELLS SHOWING -1/2 POWER SLOPE	143
FIG. 91 CAPACITANCE VS. VOLTAGE FOR GROUP C1 LI SOLAR CELLS SHOWING -1/3 POWER SLOPE	144
FIG. 92 CAPACITANCE VS. VOLTAGE FOR GROUP T3 LI SOLAR CELLS SHOWING -1/4 POWER SLOPE	145
FIG. 93 DONOR CONCENTRATION DETERMINED BY CAPACITANCE	146

ABSTRACT

Studies of the annealing of irradiated lithium doped silicon solar cells indicate considerable improvement over previous devices. Float zone lithium doped solar cells after  $3 \times 10^{14}$  e/cm<sup>2</sup> at 1.0 MeV have exhibited recovered maximum power points as high as 95% under solar illumination and about 90% under tungsten illumination. Similarly after  $3 \times 10^{15}$  e/cm<sup>2</sup> recovered maximum power points of 80% under solar illumination and 70% under tungsten illumination have been observed. In each case room temperature half anneal times are of the order of an hour. Crucible lithium doped solar cells exhibit the same recovery characteristics at about 80°C while being considerably slower at room temperature. However, wide deviations in response characteristics are observed between groups and manufacturers which can not be reconciled by any of the known material or processing variables utilized in the production of the solar cells. Redistribution and carrier removal studies indicate a lithium removal rate during irradiation of  $0.05 \text{ cm}^{-1}$  which appears to result in a lithium-vacancy defect site active as a recombination center. Subsequent annealing results in further loss of lithium, implying a lithium-vacancy-lithium defect site which is inactive in the recombination process resulting in recovery of electrical characteristics. Minority carrier lifetime versus temperature measurements on both crucible and float zone lithium doped solar cells further confirm the absence of the A-center as a dominant recombination site in lithium doped n-type silicon.

## I. INTRODUCTION

This final report covers activities during a one-year period of performance on JPL Contract No. 952251. The work presented here includes evaluation of current state-of-the-art lithium doped silicon solar cells under electron irradiation and some basic determinations of various semiconductor parameters of interest under the influence of lithium interactions with radiation induced defects. The evaluation program consisted of time dependent measurements of float zone lithium doped silicon solar cells irradiated at  $3 \times 10^{14}$  e/cm<sup>2</sup> and  $3 \times 10^{15}$  e/cm<sup>2</sup> with 1 MeV electrons followed by storage at room temperature. The evaluation of crucible lithium doped silicon solar cells was performed at storage temperatures of 60°, 80° and 100°C after irradiation to  $3 \times 10^{15}$  e/cm<sup>2</sup> with 1 MeV electrons. Lithium concentration and gradient near the junction were determined through capacitance voltage measurements.

In addition to the evaluation program a number of techniques were used to evaluate the physical properties of lithium doped silicon in an effort to better understand the kinetics of the lithium interactions that result in rapid radiation damage annealing. Lithium redistribution studies were performed to determine the optimum diffusion schedule for the production of an adequate lithium concentration in the active volume of a silicon solar cell. Carrier removal studies have been performed to determine the role of the various impurities in the formation and removal of radiation induced defect sites. Minority carrier lifetime versus temperature recombination studies have been performed in an attempt to identify the dominant recombination center in lithium doped n-type silicon. In addition capacitance versus temperature measurements have been performed to demonstrate useability of this technique for the acquisition of additional information on the energy levels of radiation induced defect sites. Lang X-ray

topography was attempted in an effort to determine if large lithium precipitation sites could be observed in silicon. Finally, other types of defect sources such as lithium hydride and other types of cell structures such as n/p lithium doped cells have been investigated for their potential value. The following sections of this report describe in detail the results of the principle efforts mentioned here and their resulting impact on the potential future worth of the lithium doped silicon solar cell as a useable radiation resistant device.

## II. LITHIUM SOLAR CELL EVALUATION

In this phase of the program a considerable number of lithium doped silicon solar cells manufactured by Centralab, Heliotek and Texas Instruments have been evaluated as a function of time and temperature after electron irradiation. A large number of processing and material parameters were varied in an effort to optimize the lithium solar cell annealing characteristics and to determine the effect of the various parameters on these characteristics. The principal variables were time and temperature of initial lithium diffusion, time and temperature of the redistribution diffusion, manner of applying the lithium source, type of silicon base material, primary dopant, resistivity, and sequence of processing. For all of the various groups of cells evaluated, the associated material and processing variables are given in Table I.

There were two test schedules utilized for the solar cell evaluations. For the float zone lithium doped solar cells two levels of irradiations were performed at  $3 \times 10^{14}$  e/cm<sup>2</sup> and  $3 \times 10^{15}$  e/cm<sup>2</sup> at 1 MeV. I-V characteristics were then obtained as a function of time with storage at room temperature. For the crucible lithium doped solar cells, the irradiation was performed at only one level of  $3 \times 10^{15}$  e/cm<sup>2</sup> and time dependent I-V characteristics were obtained for three different storage temperatures of 60°, 80°, and 100°C. This approach was necessary since room temperature annealing for the crucible solar cells is too slow to acquire sufficient meaningful data in a reasonable period of time. Extrapolations of the temperature dependent annealing times to room temperature were then acquired.

The detailed response of each individual group of cells will be discussed in detail later. The general characteristics of the response of the entire group of cells can be summarized as shown in Tables II and III. Table II illustrates for crucible lithium doped solar cells the various response parameters of interest.

Each cell group is identified by its code number, diffusion schedule, lithium concentration at the junction, and irradiation level. The initial levels and recovered levels are shown for short circuit current only inasmuch as principal interest is in the effect of lithium on radiation response under tungsten illumination. Although there were some minor differences in I-V characteristics among the groups, which will be discussed later, the short circuit current represents the principal measurement of interest for this evaluation. The recovered levels given in the table are the peak of the recovery curve and do not take into account any redegradation that occurred in some instances. The one-half recovery time is that point at which one-half of the recovery that was ultimately achieved occurred. The C versus V slope is an indication of the gradient of the dopant concentration at the junction and as such is indicative of the presence of lithium near the junction region. In the event of a step function junction or very low lithium concentration at the junction, a  $-1/2$  slope is evidenced. A  $-1/3$  slope implies a linear gradient of carriers near the junction, which is indicative of a moderate amount of lithium diffusion to the junction region. A  $-1/4$  slope implies a quadratic donor concentration gradient near the junction indicative of heavy lithium concentration due to the typical diffusion characteristic which exhibits an error function relationship. In general it can be observed that the higher lithium concentrations result in lower initial characteristics, higher recovered levels, and rapid annealing rates. In those cases where low lithium concentrations are observed as evidenced by both lithium concentration and the capacitance voltage slope, higher initial levels with little or very slow annealing rates are observed. There are, however, many deviations from these general response characteristics which will be discussed in detail in later sections. One of the important factors illustrated by the data in Table II is the fact that at slightly elevated temperatures the crucible

lithium solar cells have annealing rates equal to room temperature annealing of float zone cells.

In Table III the results of the evaluation of the float zone lithium doped silicon solar cells are shown. The various parameters illustrated are the same as those discussed in the previous table. The response characteristics at room temperature are very similar to those of the crucible cells at elevated temperatures and exhibit the same general trends. As in the case of the crucible cells, however, there are a number of large deviations, in particular the remarkable performance, both initially and after irradiation, of the T6 group of cells. One fact that remains evident throughout the course of the program is that large deviations in lithium doped solar cell characteristics occur which can not be accounted for by any of the variables identified at this time. It is suspected that some material parameter such as oxygen concentration or manufacturing techniques associated with either the boron or the lithium diffusion may account for some of the wide differences observed. In any event, the results clearly show that for certain groups of cells the radiation resistance of the lithium doped silicon solar cell is remarkably good and represents a considerable improvement over the contemporary 10 ohm-cm n/p silicon solar cell.

The recovery ability of the entire group of cells is summarized in Table IV which illustrates the rank of the various groups of cells, their maximum recovered level, and their associated one-half recovery time. Those cells which exhibit little or no annealing are not included. Presentation of the data in this form implies that as a group the Texas Instruments solar cells performed remarkably well. Although this fact is evident for the recovered level of the short circuit current, the tendency of the Texas Instruments cells as a whole to exhibited deterioration of the maximum power point negates some of their superior response. Furthermore, since all these measurements were performed under tungsten illumination, differences between the groups of cells in their radiation response is



considerably amplified. Under solar illumination a considerably smaller fraction of the output is associated with the bulk response and hence differences between the cells would be considerably reduced.

For purposes of adequate comparison of lithium doped cells to conventional n/p 10 ohm-cm contemporary cells, a group of standard cells provided by Heliotek and Centralab has also been irradiated with 1 MeV electrons as shown in Figure 1. As is evident in the figure, which contains within the band data on 12 separate cells from both manufacturers, the reproducibility of the conventional cell within a group and between manufacturers is very good. It is observed that after  $3 \times 10^{15}$  e/cm<sup>2</sup> the standard cells exhibit a degraded short circuit current of 33-35 ma. In comparison with some lithium doped p/n cells which exhibit annealed short circuit currents of greater than 35 ma., it is clear that the annealed lithium cell is significantly better than the conventional cell under electron bombardment to these moderately high fluences. Under proton and neutron irradiation, it has also been shown that the lithium cell when annealed is clearly superior to the conventional cell. A similar comparison can be made for fluences of  $3 \times 10^{14}$  e/cm<sup>2</sup> where the conventional cell has an output of 46-49 ma. compared to the lithium doped groups with an annealed output of about 52 ma. short circuit current. In all of the recovery curves to be presented in later sections the corresponding n/p 10  $\Omega$ -cm degradation levels shown in Figure 1 are indicated for rapid comparison of the maximum recovered level of the lithium doped solar cell with the contemporary n/p solar cell response.

There were in general several instances of anomalous behavior of two different types. The first type of anomalous behavior was apparent failure of the junction characteristic due to lithium diffusion or depletion resulting in reduction in the I-V characteristic at the maximum power point. The second type of anomalous behavior is short circuit current redegradation accompanied by continued annealing of the open circuit voltage. Figures 2 and 3 illustrate the power point degradation and short circuit current redegradation observed in some cases. The groups of cells evidencing maximum power degradation were C5C, C5B, C6A, H6, T7 and T4. Although in most cases this effect was minor, there were several incidences of complete collapse which will be discussed later. The group of cells exhibiting redegradation tendencies included C1, T2, T3, T4, T5 and T6. As in the previous case, these tendencies were minor and usually amounted to 10% or less.

In Figure 4 a summary of annealing time versus storage temperature is presented for the crucible cells. As is evident in the figure, the slopes are consistent with lithium diffusion in the presence of oxygen with an activation energy of slightly less than 1 ev. The only departure from this characteristic is the T7 group of cells which do not respond in a normal fashion or exhibit a meaningful slope. Room temperature annealing times are obtained for each group of cells through extrapolation of this data. Due to the very rapid annealing rate and peculiar activation energy of the T7 group, the room temperature annealing rate was determined experimentally and, as shown in Figure 4, does not agree with the higher temperature slope.

Figures 5 and 6 illustrate the initial output and the recovered output as a function of lithium concentration. The solid lines in Figure 5 are the data obtained in the previous year's efforts whereas the data points show the characteristics of the various groups of cells evaluated in this year's program. The general trend of decreasing output with increasing lithium concentration, although widely scattered, is fairly evident. Of particular interest, however, is the fact that the Texas Instruments cells as a whole exhibit a significantly higher output than the other groups of cells for given lithium concentrations. In Figure 6 the maximum recovered short circuit current is plotted as a function of lithium concentration at the junction. In general, the float zone lithium doped cells exhibit higher recovered short circuit currents than crucible lithium doped cells for a given lithium concentration. However, once again the T7 group of crucible lithium doped cells was anomalous in that it exhibited characteristics more typical of float zone lithium doped cells in maximum recovered short circuit current.

It has been previously hypothesized that edge effects produced by different lithium concentrations at the edge of the cells relative to the center of the cells may be responsible for the lack of complete recovery of short circuit current. To test this hypothesis, Texas Instruments manufactured several groups of cells in an identical fashion with the exception that one group was diffused as a whole slice and then cut after lithium diffusion to produce a uniform edge while the other group was lithium diffused as cut cells in the normal fashion. In the crucible cells, this group is represented by T7 fabricated in a normal manner, and T8 fabricated as whole slices. A similar process was performed for the float zone cells as T3 was fabricated in a normal manner whereas T5 was fabricated as whole slices. The data indicates insignificant differences due to edge effects and in fact in each case the cells fabricated as whole slices appear

slightly inferior to cells fabricated in the normal fashion. It is concluded, therefore, that edge effects are not of primary importance in the Texas Instruments manufacturing process and are probably not important in the manufacturing process used by other manufacturers.

A. Lithium Doped Crucible Silicon Solar Cells

The recovery characteristics of the C1 group of cells as a function of time and temperature are shown in Figures 7 through 9. These cells exhibited relatively good initial characteristics and were among the more superior groups of cells in maximum recovered levels even though their lithium concentration was relatively low. These cells, however, did exhibit rather slow recovery rates and have redegraded slightly less than 5% at this time. The C2 group of cells shown in Figures 10 through 12 responded in a very anomalous fashion in that very little annealing was observed and no lithium was detectable in the junction region as evidenced by capacitance measurements and capacitance versus voltage slope. Considering the diffusion schedule that was used, the apparent lack of lithium in the bulk region of the cell and near the junction is not readily explainable. Anticipating that the antimony dopant may have been responsible for this anomalous behavior, since arsenic or phosphorus doped silicon is normally used, a second group of cells (C6) was fabricated to determine the effect of dopant on lithium diffusion. The groups C6A and C6B consisted of two resistivities of antimony doped silicon and group C6C consisted of phosphorus doped silicon. The C6A group of antimony doped silicon consisted of rather low resistivity material in the 3 to 16 ohm-cm range similar to the C2 group which was in the 5 to 10 ohm-cm range. The C6A group, shown in Figures 13 through 15, responded in a fashion similar to the C2 group in that little annealing was observed and lithium detection was not possible through capacitance measurements.

The C6B group, however, utilizing a slightly higher starting resistivity in the 17 to 85 ohm-cm range exhibited good initial characteristics and good recovery characteristics, as shown in Figures 16 through 18. The C6C group utilizing phosphorus doped silicon in the same resistivity range as the C6B group exhibited identical characteristics both initially and during recovery, as shown in Figures 19 through 21. It is concluded, therefore, that antimony as a dopant is not responsible for the anomalous behavior of the C2 group but rather the use of a starting material resistivity which is too low and apparently inhibits lithium diffusion. This effect can not be confirmed, however, since these two groups represent the only groups evaluated using starting material resistivities less than 20 ohm-cm. The C5A and C5C groups of cells utilized identical starting material with different diffusion and redistribution schedules. The C5A group, shown in Figures 22 through 25, was diffused at a higher temperature for a shorter period of time with no redistribution and exhibited a high lithium concentration with corresponding poor initial outputs; however, their recovery rates were very fast. The C5C group, shown in Figures 26-28, by utilizing the slightly lower diffusion temperature for a longer period of time with a redistribution diffusion, exhibited good initial characteristics and high recovery levels very similar to the C1 group previously discussed. This group of cells, however, showed a tendency toward failure in the maximum power point of the I-V characteristic of 5 to 10% after several hundred hours of storage.

The recovery characteristics of the H1 cell group as a function of time and temperature are shown in Figures 29 through 31. The H1 group exhibited relatively poor initial characteristics and only average maximum recovered levels; however, their recovery rate was very fast, i.e. of the order of 1 hour at 100°C. These response characteristics are typical of cells with high lithium concentrations as

indicated by capacitance measurements and the  $-1/4$  capacitance versus voltage slope. The H2 group was processed in an identical manner except 20 ohm-cm material was used instead of 100-200 ohm-cm material. This group, shown in Figures 32 through 34, exhibited considerably better initial outputs but slightly poorer maximum recovery characteristics relative to the H1 group. The H6 group, shown in Figures 35 through 37, was diffused at a slightly higher temperature which should have raised the lithium concentration considerably. Although the capacitance measurements did not indicate a significantly higher lithium concentration near the junction, the initial outputs were very low indicative of high bulk lithium concentration. In addition, the maximum recovered levels were poorer than the previous group. The performance of this group of cells as a whole was relatively inferior to cells previously obtained from this manufacturer utilizing the same diffusion schedules and also seemed inconsistent with the C groups of cells which, while utilizing similar materials and diffusion schedule, exhibited significantly different characteristics.

The performance of the Texas Instruments group of cells as a whole is inconsistent with the two previous groups in that high initial outputs and high maximum recovered levels are observed with very rapid annealing rates. These cells are fabricated in a different fashion than the previous groups in that the lithium source is evaporated on the back surface instead of painted on and the boron diffusion is performed using a different diffusion source. It is not known at this time whether the better than average response of these cells is due to either one or both of these factors. The T2 group of cells, shown in Figures 38 through 40, though diffused at a lower temperature, exhibited a very rapid recovery rate relative to considerably slower recovery rates exhibited by the C groups of cells with an identical diffusion schedule. In addition the initial characteristics were very good and the maximum recovered level was the highest

for this group of cells. The rapid annealing rate in conjunction with the implied lower lithium concentrations suggests a considerably lower oxygen concentration in this group of cells relative to the C groups of cells. Some short circuit current redegradation of approximately 3% is observed while the open circuit voltage continues to anneal. The T7 and T8 groups of cells, shown in Figures 41 through 47, were both diffused at a significantly lower temperature for a much longer period of time and in addition the T8 group of cells was fabricated as a whole slice to determine if edge effects, as previously discussed, were an important factor. Since the T8 group of cells in general was inferior in both initial output and maximum recovered level, the edge effect does not appear to be a dominate factor in the recovery characteristic. The T7 group exhibited excellent recovery characteristics similar to the T2 group. However, considerable degradation of the maximum power point of 5 to 15% occurred. In addition, as shown in Figure 4, the temperature dependence of the annealing characteristic of the T7 group was not consistent with any of the other groups of cells. The fact that the T7 group of cells was so different from the T8 group of cells when particular attention was devoted to duplicating the manufacturing parameters for the edge effect test was not reconcilable, but may be due to the use of starting material differences which were unspecified, such as oxygen concentration. In any event the T2 group of cells was the most superior of the groups investigated from the point of view of initial characteristics, recovery characteristics, and long term stability of the I-V characteristic.

#### B. Lithium Doped Float Zone Silicon Solar Cells

The recovery characteristics of the C5 groups of cells, as a function of time, are shown in Figures 48 through 51. The C5B and C5D groups were diffused with

significantly different diffusion schedules to determine the effect of the diffusion schedule on their radiation response characteristics. The C5B group contained extremely high lithium concentration with a correspondingly poor initial output characteristic. The observed low recovery levels are due to this poor initial output characteristic. The C5D group exhibited a considerably lower lithium concentration with an average initial output and a very good maximum recovered level. However, the  $3 \times 10^{15}$  e/cm<sup>2</sup> irradiations appeared to deplete the lithium concentrations since all of the cells exhibited a complete collapse of the I-V characteristic within a few hours after irradiation. Immediately prior to the collapse of the I-V characteristic, the maximum recovered level of one cell for the  $3 \times 10^{15}$  e/cm<sup>2</sup> irradiation had reached the highest value observed to date for any lithium doped cells. Basic inconsistencies exist for these two groups of cells since all of the identified manufacturing and material parameters normally result in excellent cell characteristics as opposed to the apparent collapse of this particular group of cells. As has been pointed out before, there remains some unidentified material or processing variable which strongly influences the characteristics of lithium doped silicon solar cells.

The recovery characteristics of the H4 group of cells are shown in Figures 52 and 53. The H4 group of cells, though utilizing a relatively standard diffusion schedule, exhibited very poor initial output characteristics and associated poor recovery levels. This group of cells represents another instance in which, using standard diffusion schedules and material parameters, lithium doped cells are produced which are not consistent with previously evaluated cells or cells of very similar processing parameters. The H5 group of cells, shown in Figures 54 and 55, which was diffused at a significantly lower temperature of 350°C, exhibited negligible recovery characteristics which is consistent



with the absence of a detectable lithium concentration at the junction. Clearly, this diffusion schedule is insufficient to produce the required lithium concentrations and normal recovery characteristics. The H7 group of cells, shown in Figures 56 and 57, utilized the same diffusion schedule as the H4 group but exhibited very good initial outputs and excellent maximum recovered levels as opposed to the poor characteristics of the H4 group. The H7 group was made from Lopex material instead of conventional float zone material which might imply that, other things being equal, Lopex material produces a significantly better lithium doped solar cell. However, previous evaluations and evaluations of the Texas Instruments cells to be discussed later both indicate the use of Lopex or float zone material has no effect on lithium doped solar cell characteristics. Hence, comparison of the H4 and H7 groups of cells once again indicates the presence of an unidentified variable in the production of lithium doped solar cells which strongly influences their recovery characteristics.

The recovery characteristics of the T3 group of cells as a function of time are shown in Figures 58 and 59. The T3 group of cells was diffused at a slightly lower temperature utilizing no redistribution diffusion. These cells had good initial characteristics and exhibited good recovery levels very similar to the H7 group previously discussed. However, the T3 group of cells exhibited a slightly inferior I-V characteristic relative to the H7 cells and have indicated short circuit current redegradation of approximately 10% to date. The T4 group of cells, shown in Figures 60 and 61, was processed in the same fashion as the T3 group except float zone material was used instead of Lopex. The T4 group of cells responded in an almost identical fashion to the T3 group of cells indicating no strong dependence on type of material used. The T5 group, shown in Figures 62 and 63, was processed in the same fashion as the T3 group except that the T5 group was processed as whole slices through the lithium diffusion to determine

the existence of edge effects. As in the previous case with the crucible cells processed in this fashion, there is no significant difference in response between the T5 and T3 groups of cells, implying once again the lack of the existence of a strong edge effect. In general the T3, T4 and T5 groups all tend to exhibit significant short circuit current redegradation and are only as good as a contemporary 10  $\Omega$ -cm n/p solar cell at best. The T6 group of cells was diffused at a significantly lower temperature, 325°C, for a much longer period of time, 8 hours, in a fashion similar to the T7 and T8 crucible groups. Although the T7 and T8 crucible groups did not exhibit any startling effects due to this somewhat different diffusion schedule, the T6 group exhibited the best initial characteristics and the highest recovered levels of any cells observed to date by a significant amount, as evidenced in Table III and Figures 64 and 65. The recovery times, however, were considerably slower than normally observed for float zone cells and the short circuit current exhibited redegradation of 5 to 10% to date while the open circuit voltage continues to anneal.

### C. Conclusions and Recommendations

The results of this year's evaluation program clearly indicate that as a whole the lithium doped silicon solar cells currently being fabricated, both crucible and float zone, are greatly improved over cells previously tested. Better initial efficiencies and higher recovered levels are being obtained with some sacrifice in recovery rates, but with evidence of better long term stability. Preliminary measurements made with a sun simulator indicate that for the better groups of cells with initial efficiencies of 9 to 10%, recovery of maximum power of about 95% can be obtained after  $3 \times 10^{14}$  e/cm<sup>2</sup> and 80% after

$3 \times 10^{15} \text{ e/cm}^2$ . It is envisioned that as the lithium cell is optimized more simulator measurements will be utilized in the evaluation program.

It is also evident, however, from the results of this year's efforts that there remains an unidentified material or processing parameter which exerts a strong influence on the production of good lithium doped silicon solar cells. It has been proposed that a possible important material parameter, which to date remains unspecified, may be oxygen concentration. On the other hand, differences between manufacturers in both the lithium and the boron diffusion techniques may have a considerable effect. Further it is evidenced that lower temperature diffusions for longer periods of time may yield superior lithium doped solar cells. There does not appear to be a strong influence of type of material, i.e. Lopex versus float zone, or material dopant and resistivity as long as resistivity ranges remain within 20 to 200 ohm-cm.

It is recommended that future efforts consider the different boron and lithium diffusion techniques currently being utilized as well as the lower temperature longer time diffusions initiated late in the program by Texas Instruments. Finally, the data presented here seems to indicate a fairly narrow range of diffusion time-temperature profiles which can produce desirable lithium concentrations allowing a heavier concentration in future efforts on other variables within this fairly narrow range of lithium diffusion schedules.

### III. KINETICS OF LITHIUM IN SILICON

#### A. Lithium Redistribution Studies

Centralab Semiconductor prepared two groups of lithium diffused silicon solar cells for redistribution studies. One group was diffused for 5 minutes at 425°C and the other 30 minutes at 350°C. These lithium diffusions were planned to place a high concentration of lithium in the back of the cells without allowing detectable quantities of lithium to reach the junction. After this diffusion, the silicon blank was fabricated into a completed solar cell. In this way the effects of the redistribution of lithium can be observed by changes of cell parameters and junction capacitance. The silicon used was float zone crystal of 65 ohm-cm resistivity. The lithium redistribution was performed at 250°C. Figure 66 is a plot of donor concentration at the junction versus the redistribution time. Cells C3-1, 2 were lithium diffused 30 minutes @ 350°C. Cells C3-33, 34 were lithium diffused 5 minutes @ 425°C. The phosphorus concentration of the original silicon is also indicated on the figure. It is apparent that these cells have no detectable lithium at the junction before redistribution. After a short time at 250°C the junction donor concentration begins to rise at a rapid rate. This rapid increase continues until a maximum is reached. In the case of cells diffused 30 minutes at 350°C (C3-1, 2), a maximum of about  $3 \times 10^{14}$  donor atoms/cm<sup>3</sup> at the junction is reached after 13 hours of redistribution. If the phosphorus concentration is subtracted from the previous figure a maximum lithium concentration of  $2.25 \times 10^{14}$  atoms/cm<sup>3</sup> at the junction is determined. The maximum for cells diffused 5 minutes @ 425°C,  $0.5 \times 10^{14}$  Li atoms/cm<sup>3</sup>, is reached after 18 hours at 250°C. After 100 hours at 250°C the lithium concentration at the junction is again reduced to an undetectable value. It is interesting to note that cells diffused for 30 minutes at 350°C

achieve a higher maximum lithium concentration and in a shorter time than those diffused 5 minutes at 425°C. The lithium concentrations found in these cells are in general much lower than those of previously studied lithium diffused cells.

Figure 67 is a plot of the short circuit current densities of cells C3-1, 2, 33, 34 as a function of redistribution time. Cells C3-33, 34 have initially higher  $J_{sc}$  values than the other cells shown. This condition persists throughout the redistribution. As previously noted, cells C3-33, 34 also contain several times more lithium than cells C3-1, 2. Since the cells with the greater lithium concentration have superior  $J_{sc}$ , these results indicate that the diffusion of significant quantities of lithium into a solar cell do not necessarily result in an inferior cell. It does, however, degrade the  $J_{sc}$  a certain amount. This decrease occurs during the first 10 hours of redistribution at 250°C. The decrease does not appear to be greatly dependent upon the quantity of lithium reaching the junction. The decrease in  $J_{sc}$  appears to correspond timewise to the maximum increase of lithium at the junction. The most curious aspect of this change is the manner in which  $J_{sc}$  remains constant after the lithium concentration at the junction begins to decrease. When the redistribution has proceeded to the extent that concentrations of lithium are no longer detectable at the junction of a cell, the  $J_{sc}$  of the cell remains at the same value it degraded to when the maximum concentration of lithium was present. Since the  $J_{sc}$  is largely a function of the minority carrier lifetime in the base regions, one must assume that additional recombination centers are formed in the base region during the presence of the lithium. These defects remain after the lithium donors are no longer present. Their concentration is too small to be detected in any way other than lifetime or  $J_{sc}$  changes.

Although the changes in lithium concentration and short circuit current reflected in Figures 66 and 67 were the result of thermally activated processes operating at 250°C, the very slow progress of these processes can be expected at room temperature. For this reason some cells will show very significant changes in lithium concentration and short circuit current during room temperature storage of several months. The nature of the decrease in lithium at the junction after the maximum is reached is not clear. This effect could be caused by outdiffusion, precipitation or diffusion of lithium into the boron doped layer. Further work is necessary to determine the exact cause.

The redistribution time of several cells was varied to produce a group of cells which differed only by the concentration of lithium found at the junction. These cells were irradiated to study the effect of lithium concentration on the recovery kinetics. Figure 68 shows the changes in short circuit current which result after irradiation. The data indicates that the times necessary to reach half recovery, after an irradiation of  $3 \times 10^{14} \text{ e/cm}^2$ , vary considerably depending on the concentration of lithium detected at the junction. Some variation can also be seen in the maximum recovered value of short circuit current. In general the cells with higher initial  $I_{sc}$  values recover to highest output values. In Figure 69 the half recovery time of  $I_{sc}$  after irradiation is plotted versus the concentration of lithium at the junction. This plot indicates a negative slope of 1.23. This type of data can be useful in determining nature of a chemical reaction. In the general case of a second order reaction between two species of greatly unequal concentration, the half time for disappearance of the low concentration species will vary inversely with the concentration of the higher concentration species. In the lightly irradiated lithium cell, the concentration of lithium will greatly exceed the concentration of radiation produced recombination

centers. If the centers are annihilated by lithium in a bimolecular manner, the half recovery time would be inversely proportional to the lithium concentration. The experimental results are very close to such a relationship. Since the lithium concentrations are known to increase rapidly with distance from the junction, the average lithium concentration in the active region of the cell will be considerably higher than that determined by capacitance. Despite this difference, the lithium concentration at the junction must be directly related to the average concentration in the base region because of diffusion considerations. Because of these considerations the slope of slightly greater than unity is not too disturbing. Previous work reported by RCA, in which the half recovery time was determined by diffusion length changes, showed a nearly identical slope to that reported in this work.<sup>1</sup>

Although the lithium concentration increased with distance from the junction, it is possible to use the donor concentrations at the junction determined by capacitance to monitor important changes occurring during and after irradiation. If the junction capacitance is monitored as a function electron fluence, the carrier removal rate can be determined. These measurements were made for a series of cells, and the removal rate appeared to be linear in the range of electron fluence investigated. The values of the removal rate for several lithium cells are plotted versus the concentration of lithium at the junction in Figure 70. The experimental results indicated that this removal rate is independent of the concentration of lithium at the junction. This result is marked contrast to those previously reported by RCA.<sup>2</sup> The RCA results are shown by dashed lines on the graph. It is also noted that these experimentally determined removal rates reported here are nearly 1/100 of the calculated displacement rate of silicon by 1 MeV electrons, and similarly lower than the

initial removal rates found in lithium doped float zone silicon by Hall measurements. The reasons for these differences are not clear; however, some of the differences may be due to the widely differing ranges of lithium concentration. The determination of this junction removal rate has considerable practical influence on the design of lithium solar cells. It has been experimentally observed that when the product of the electron fluence and removal rate ( $0.05\text{cm}^{-1}$ ) exceeds the concentration of lithium at the junction, the cell will not recover from the degraded condition in the usual room temperature pattern.

In addition to the changes in lithium concentration during irradiation, a very significant effect can be observed during the recovery period. The changes in lithium concentration at the junction during and after electron irradiation are shown for two cells in Figure 71. The short circuit current recovery of these two cells was previously described in Figure 68. The lithium concentration is stable immediately after irradiation, but a decrease begins several hours after the irradiation, and continues for several hundred hours after the irradiation. The decrease of lithium concentration appears to correlate in time with the recovery of short circuit current after irradiation. It appears that one can safely conclude that the observed consumption of lithium is directly related to the recovery process. A curious point is raised by the continued decrease in lithium concentration after 300 hours when the short circuit current has recovered to its maximum. If this lithium consumption is directly affecting the recombination center population, the lithium concentration should stabilize when the short circuit current becomes stable. Further study of these cells is necessary before any other conclusions can be reached. To confirm these changes a similar study was done on two Heliotek cells. This data is presented in Figure 72. These cells have considerably higher lithium concentrations and an electron fluence of  $3 \times 10^{15} \text{ e/cm}^2$  was used. The results are similar to those



for cells C3-14, 15 with two exceptions. In this case the lithium decrease finally stabilizes but the recovery appears to proceed ahead of the lithium decrease. The short circuit current recovery is half complete in 4 hours, whereas the lithium decrease is only half complete after about 40 hours. Despite this displacement in time, it is highly likely that the two changes are directly related. Since donor concentrations are determined by capacitance measurements, they only sense in the extremity of the active region. The bulk of the active region in which the  $I_{sc}$  is determined has a much higher lithium concentration than that found at the junction. Our previous work has shown that this higher lithium concentration results in a lower half time to recovery. The loss of donors during irradiation was previously shown to be directly proportional to the electron fluence. A similar study of the loss of donors after irradiation would help in defining a model for the behavior of lithium in the recovery process. The data presented in Figures 71 and 72 indicate that the lithium consumed during the recovery process is about 1.5 times greater than which was consumed during the irradiation. This larger lithium decrease during recovery may be related to the fact that the edge of the junction is deeper in the cell after the irradiation.

Caution must be used in interpreting these results, because the consumption of lithium during irradiation may not necessarily result entirely in the production of recombination centers. Likewise, the consumption of lithium after the irradiation or during recovery need not be due entirely to the neutralizing of radiation produced recombination centers. An indirect argument can be made to consider all of the lithium loss during irradiation to be involved in formation of recombination centers. Other work described in this report has shown that an irradiation of a typical float zone lithium solar cell with  $3 \times 10^{14}$  e/cm<sup>2</sup> of 1 MeV electrons results in minority carrier lifetime of about 0.2  $\mu$ sec. If

every lithium atom lost during irradiation results in a recombination center, there would be  $3 \times 10^{14} \text{ e/cm}^2 \times 0.05 \text{ cm}^{-1}$  or  $1.5 \times 10^{13} \text{ cm}^{-3}$  centers produced.

The lifetime studies indicate the following relationship would hold:

$$\tau_{po} = \frac{1}{N_r \sigma_p V}$$

where:  $\tau_{po}$  = minority carrier lifetime

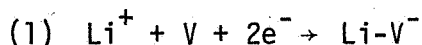
$N_r$  = concentration of recombination centers

$V$  = thermal velocity

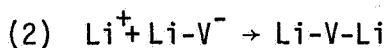
$\sigma$  = capture cross-section

If our previous assumptions are correct, the above relation indicates the recombination center would have a capture cross-section of roughly  $10^{-14} \text{ cm}^2$ . This is a large but reasonable value for the cross-section and any significantly lower introduction rate of centers would require similarly larger capture cross-section. Any assumptions requiring significantly larger cross-sections can be discarded as unrealistic.

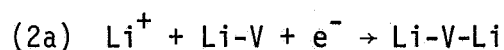
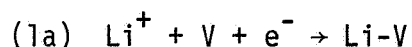
An explanation for a loss of lithium during irradiation and recovery has been presented by workers at RCA.<sup>2</sup> They proposed that recombination centers are generated by the following reaction:



In addition to the one lithium atom which this reaction consumes, two electrons must be removed from the conduction band to satisfy the charge equality necessary on both sides of the equation. The  $\text{Li-V}^-$  defect would be an acceptor, lying below the level of Fermi level in the forbidden band. The proposed reaction by the annihilation of the recombination centers by lithium atoms is as follows:



Although this proposed reaction will destroy the recombination centers, no change will occur in the population of electrons in the conduction band. Therefore, such a reaction would not cause the large reduction in capacitance which was observed during the recovery. If the model were altered so as to place the energy level of Li-V defect above the Fermi level, the previously discussed reactions would be as follows:



Such a model provides for equal loss of carrier electrons during irradiation and recovery. Although this such a model does not provide a mechanism for 1.5 times greater carrier loss during recovery compared to that during irradiation, it is close enough for very serious consideration. The added restriction that the energy level of the Li-V acceptor be above the Fermi level, only need apply in the lightly doped region adjacent to the depleted region. If this restriction also applied in the bulk of the active region, the neutrality of the defect would not promote effective recombination. For this role it is necessary for the Fermi level to move above the acceptor defect energy level, allowing it to become filled and negatively charged. Since the lithium concentration is known to increase rapidly with distance from the junction in these cells, the Fermi level will move much closer to the band edge in the bulk of the active region.

In summary the results of the redistribution studies are the following conclusions:

1. During the redistribution process the lithium concentration at the junction rises rapidly to a maximum, and then slowly decreases.
2. The short circuit current decreases during the period of lithium increase at the junction.

3. The half recovery time for irradiated lithium cells is roughly inversely proportional to the concentration of lithium at the junction. Such a relationship suggests a second order bimolecular process in which one species (lithium) greatly exceeds the population of the other (recombination center).

4. The removal rate during irradiation measured at the junction by capacitance is about  $0.05\text{cm}^{-1}$  for a wide variation of lithium concentrations. This removal appears to be largely related to recombination center production.

5. During the recovery of short circuit current from degradation, capacitance measurements indicate similar loss of lithium.

6. In general the results support the model proposed by RCA workers in which a lithium-vacancy is formed during irradiation to become the dominate recombination center. If other lithium atoms are present they will later react with these centers and form a species which is not active in recombination.

#### B. Carrier Removal Studies

Our previously reported work in this area has involved silicon which was doped with lithium during crystal growth. Our recent efforts are concentrated upon similar studies in silicon doped by diffusion of lithium into the sample. Float zone silicon with an n-type resistivity of 75 ohm-cm is used for most studies. The lithium was diffused in at  $600^{\circ}\text{C}$  to provide uniform saturation. The sample is then allowed to approach equilibrium at a lower temperature. In this manner samples have been prepared with lithium donor concentrations between  $10^{15}$  and  $10^{18}$  atoms/cm<sup>3</sup>. Table V summarizes the various electrical properties of the samples prepared to date. The electrical properties of this material are typical of phosphorus or arsenic doped silicon in regard to Hall mobility and Hall coefficient variation with temperature. In Figure 73, the Hall mobilities of these samples are compared to the published experimental and

computed values of Morin and Maita for arsenic doped silicon.<sup>3</sup> In nearly all cases the values found for our lithium doped specimens are very close to previously mentioned data. This would indicate that the scattering centers are largely the singly charged lithium donor atoms.

Most of the studies of irradiation carrier removal and defect production in silicon have either confirmed or assumed a linear change in radiation defect population with increasing electron fluence. One exception to this occurs when the Fermi level lies close to ionization level of the radiation defect. In this case the removal rate changes rapidly as the Fermi crosses the defect level. This occurrence has been proposed as a method of determining defect energy levels.<sup>4</sup> The early work by Wertheim demonstrated that carrier removal is linear at low electron fluences, but as defect concentration approaches the original impurity concentration, the rate becomes nonlinear.<sup>5</sup> Since the production of a defect complex often involves the consumption of a donor, a rapid decrease in the introduction rate should occur as its constituent impurity is near exhaustion. The irradiation of lithium doped silicon was studied by observing changes in the removal rate as a function of electron fluence. In this manner some information can be obtained regarding structure of radiation defects.

The electron irradiation results of this material are shown in Figure 74. Sample D-1, described in Table V, was irradiated with 1 MeV electrons at room temperature in increments. When the irradiation was interrupted, the resistivity and Hall coefficient were determined. The electron carrier concentration, as determined by the Hall coefficient, is plotted as a function of electron fluence. Since the logarithm of the carrier concentration versus fluence yields a straight line, it appears that this material has again demonstrated the same exponential dependence of carrier concentration upon electron fluence which was previously found in float zone silicon doped with lithium in the melt. The results of these

irradiations are described by the following equation:

$$n = n_0 \exp (-\phi/\alpha)$$

where:  $n_0$  = initial electron concentration

$\phi$  = electron fluence

$\alpha$  = a constant

$n$  = electron concentration after irradiation

Such a relationship indicates that the instantaneous removal rate ( $dn/d\phi$ ) is not a constant, as has been found in other cases, but is directly related to the instantaneous carrier concentration as follows:

$$\frac{dn}{d\phi} = - \frac{n}{\alpha}$$

In the case of D-2 the constant  $\alpha = 5 \times 10^{16} \text{ e/cm}^2$ . This exponential relation was found in all our recent investigations. Although one might expect the same value of  $\alpha$  in samples with different lithium concentrations, in fact this condition was not found. The appearance of an exponential removal is in no way in conflict with previously published work indicating linear removal. Because of the mathematical similarities between linear and exponential functions, the two behaviors can not be distinguished during small initial changes in carrier concentration. There was considerable variation in values found for the constant  $\alpha$ . The irradiation of a similar sample, with a lower lithium concentration, is shown in Figure 75. In this case the removal is exponential with an  $\alpha$  value of  $1.05 \times 10^{16} \text{ e/cm}^2$ . In Figure 76 the experimental values of  $\alpha$  are plotted versus the lithium donor concentration (carriers) of the sample irradiated. The points on this log-log plot indicate  $\alpha$  is a linear function of the initial lithium donor concentration of the specimen. The relationship appears to be:

$$\alpha = n_0/2.2$$

If this relationship is substituted into the instantaneous carrier concentration expression, the following expression results:

$$\frac{dn}{d\phi} = 2.2 \frac{n}{n_0}$$

This would result in:

$$\frac{dn}{d\phi} = 2.2$$

at the start of irradiation when  $n = n_0$ . The physical reasons for this relationship are not apparent at this time. If, as one might expect,  $\alpha$  was independent of lithium concentration, and the value of  $\alpha$  found for a  $10^{16}$  Li/cm<sup>2</sup> were to apply for samples of  $10^{17}$  Li/cm<sup>3</sup> and greater the value of  $dn/d\phi$  would initially exceed that of the displacement rate for 1 MeV electrons. Such a situation would be very difficult to account for theoretically. The value of the initial removal rate found here (2.2/cm) is roughly equal to the calculated displacement rate of 1 MeV electrons in silicon. The Hall coefficient of lithium doped silicon was examined as a function of temperature to investigate the nature of the defects generated by the irradiation. This type of data is shown in Figure 77 for sample A-1, before and after irradiation. The predominant change after irradiation is a reduction in the reciprocal Hall coefficient at all temperatures. These results indicate that the loss in carrier electrons is caused largely by the formation of deep acceptor or neutral defect-lithium complexes. If the defects are acceptor type, the energy level must be greater than 0.3 eV from bottom of the conduction band.

The annealing behavior of radiation damage in the subject specimens is in marked contrast to that previously reported in silicon. Sample A-1 was irradiated with  $4 \times 10^{16}$  e/cm<sup>2</sup> and isochronally annealed for 15 minutes at 75°C and other higher temperatures at 25°C intervals. The annealing data for sample A-1 is shown in Figure 78. In the vicinity of 100°C about 10% of the removal damage is

recovered. At 200°C what appears to be a second annealing stage begins. After annealing for 15 minutes at 275°C the carrier concentration has increased to approximately the same value found in the specimen prior to irradiation. Isochronal annealing at temperatures above 275°C produced rather startling results. Each successive annealing step increased the carrier concentration. After the anneal at 350°C the carrier concentration was five times greater than that found prior to irradiation. The apparent explanation of this behavior lies in the comparison of the isochronal annealing data to the lithium solubility of Pell, which is also plotted in Figure 78.<sup>8</sup> Since the specimen was originally saturated with lithium at 600°C and then held at 200°C, the lower temperature produced a precipitated second phase of lithium silicide rather than outdiffusion of lithium as expected. The annealing above 200°C allowed the silicon to redissolve the precipitate, with subsequent increase of lithium donor concentration. The annealing data show a tendency to approach the solubility data as temperature increases. The annealing data for sample D-2 is also shown on Figure 78. The results are very similar to those just discussed, in that an annealing stage occurs near 100°C, redissolution occurs when the solubility of lithium at the annealing temperature exceeds the concentration of ionized lithium previously detected in the specimen, and concentration present after the highest temperature anneal exceeded that initially present before the irradiation. If the observed effect is indeed lithium redissolving, it may mask the annealing of the remaining fraction of removal damage after annealing at 175°C. Further work is necessary to clarify these effects.

A second view of the irradiation and annealing of sample A-1 can be seen in Figure 79. In this figure the Hall mobility of the specimen is plotted versus the lithium donor concentration after various irradiations and anneals. In addition to the data points, the arsenic data of Morin and Maita is shown as a solid line.<sup>3</sup> It can be seen that the irradiation of this sample results in an increase in the



Hall mobility in addition to the loss of lithium donors. Even after an irradiation of  $4 \times 10^{16}$  e/cm<sup>2</sup> the Hall mobility is equal to that of an unirradiated sample of the same donor concentration. Since Hall mobility is increased, the irradiation results in no additional charged scattering centers, but rather a reduction of charged scattering centers. This conclusion rules out the production of charged acceptor type defects by the irradiation. Thus the irradiation appears to electrically resemble the precipitation process. The anneal has the exact opposite effect as irradiation, as each higher temperature increases the donor concentration and decreases the Hall mobility. The redissolving of lithium donors to concentrations greater than the before irradiated values is also illustrated in Figure 79. The irradiation and annealing of this material appears to be identical to the precipitation and redissolving lithium. Some of the major defect reactions which are known or hypothesized in n-type silicon are presented in Table VI. An examination of the table indicates that reactions 1 or 4 will cause the necessary changes in the population of carrier electrons and scattering centers to produce the observed changes in Hall coefficient and Hall mobility. Reaction 4 is actually the sum of reactions 2 and 3. Since reactions 2 and 3 have already been proposed as the degradation and recovery process in lithium cells, the assumption of reaction 4 or 2 + 3 presents an explanation of the Hall measurements which is consistent with the observations on cells. In the cells, reaction 3 proceeds much slower than reaction 2. Since it has been shown that the time constant of reaction 3 is decreased by presence of greater lithium concentration, it is possible that in these Hall specimens the lithium concentration is sufficient to allow completion during the irradiation.

Because quartz crucible silicon is also under consideration for use in lithium solar cells, a sample of this material was also lithium diffused and fabricated into a Hall specimen.<sup>7</sup> The initial data for this sample is included

in Table V. The electron irradiation results of this sample (Q-1) was very similar to that of the float zone silicon. The removal constant  $\alpha$ , for the lithium doped Q.C. silicon, was roughly twice the value found for float zone silicon of similar lithium concentration. This data is presented in Figure 76. The isochronal annealing after irradiation of sample Q-1, shown in Figure 78, produced a significant decrease in the carrier or lithium donor concentration in the 75-100°C range. This behavior is in marked contrast to that observed in annealing of irradiated, float zone, lithium doped silicon. The decrease or "reverse anneal" observed in sample Q-1 reduces the carrier concentration present after irradiation by about 50%. This change represents a roughly 25% increase in number of carriers removed during the irradiation.

The behavior of sample Q-1 can be explained by the model previously used to explain behavior in lithium cells and bulk float zone silicon. There is considerable evidence to indicate that a principle effect of oxygen in lithium doped silicon is to reduce the effective diffusion constant for lithium in silicon.<sup>6,7</sup> It is therefore reasonable to expect that reaction 4 in Table VI would be considerably slower in the presence of large quantities of oxygen. After the irradiation of sample Q-1, reaction 4 is partially complete and still proceeding at a very slow room temperature rate. When sample Q-1 is raised to the 75-100°C range, reaction 3 goes to completion very quickly. This increased reaction rate is permitted by increased effective lithium diffusion constant at the higher temperature. The consumption of lithium during the completion of reaction 3 causes the "reverse anneal" observed in sample Q-1. The experimental results of room temperature Hall mobility measurements during the irradiation and annealing of sample Q-1 tend to confirm the above explanation of the changes. This data is presented in Figure 80. If the irradiation of sample Q-1 resulted in both reactions 2 and 3 (i.e. 4) going to completion, the Hall mobility, after

a fluence of  $10^{17}$  e/cm<sup>2</sup>, would be close to that of unirradiated silicon of the same carrier concentration (1280 cm<sup>2</sup>/volt-sec.). After such an irradiation, the observed mobility is 1180 cm<sup>2</sup>/volt-sec. The mobility before irradiation was 935 cm<sup>2</sup>/volt-sec. These figures indicate that the total assumed reaction (4) is about 75% complete, if one assumes the presence of only singly charged scattering centers. Another way of expressing these results would be to say that for every loss of 4 carrier electrons from the conduction band during the irradiation, only 3 charge scattering centers are destroyed. During the "reverse anneal" an additional 20% loss of carrier electrons is observed. The additional scattering centers lost during the reverse anneal is 60% of that lost during irradiation. The net result of both the irradiation of crucible silicon and a reverse anneal culminating at 125°C is a loss of carrier electrons and an equal loss scattering centers. This is the same result observed for irradiation float zone silicon doped with lithium. Hence it is believed the oxygen only serves to slow the progress of reaction 4.

Since the irradiation of lithium doped silicon is mainly a relatively simple interaction of donors with the displacement products, it is interesting to compare the behavior with that of phosphorus doped silicon. Although considerable work has been done on phosphorus doped silicon, most of the data reported relates to more lightly doped material than that considered in the lithium studies previously described. To make comparative studies, two samples of phosphorus doped float zone silicon were obtained. The starting resistivities were roughly 0.1 and 0.2 ohm-cm. These resistivities were selected to maximize the population of phosphorus over oxygen, without reaching resistivities which require unreasonably large electron fluences to cause the desired carrier removal. The previous investigations<sup>8</sup> have shown that E-centers (a phosphorous-vacancy pair, acceptor) and A-center (an oxygen-vacancy pair, acceptor) are the most likely defects to form

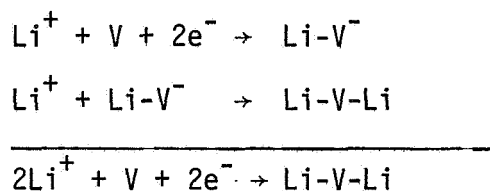
in irradiated silicon of this type.

The changes in carrier concentration during electron irradiation were monitored by Hall measurements. The results are shown in Figure 81. It can be seen that the carrier removal in these samples also tends to follow the exponential behavior observed for lithium doped silicon. The  $\alpha$  values for these samples also plotted on Figure 76. The general trend indicates that in this material  $\alpha = n_0$ , the initial concentration of phosphorus before irradiation, whereas in the lithium doped material  $\alpha = 0.45 n_0$ . The Hall mobility data from the above study is shown in Figure 82. The mobility values before irradiation are very close to the values published for unirradiated silicon. In the case of both phosphorus doped samples, the increasing electron fluence reduces the carrier concentration, but does not change the mobility. This result is in marked contrast to that found in lithium doped float zone silicon, as shown in Figure 79. The behavior observed in Figure 82 can most easily be explained by assuming that reaction 5 in Table VI describes the radiation process. Since this reaction causes the loss of two carrier electrons and no changes in scattering center population per reacting vacancy, this reaction will produce no change in the Hall mobility. If A-centers are formed during irradiation (reaction 6), the mobility will decline. Since no change in mobility is observed, it can be concluded that all the changes observed can be explained by the formation only E-centers and no A-centers.

The relationships between  $\alpha$  and  $n_0$  in Figure 76 indicate that carrier removal rates in lithium doped float zone silicon are roughly twice those found in the phosphorus doped material. Since both reaction 4 and 5 cause the loss of two carrier electrons per reacting vacancy, the removal data indicates that twice as many vacancies are captured before annihilation by lithium atoms compared to a similar concentration of phosphorus atoms in silicon.

The following conclusions can be drawn from the experimental results:

1. The carrier removal rate for electron irradiation of lithium doped float zone silicon is an exponential function of electron fluence.
2. During the initial stages of irradiation the removal rate is  $2.2\text{cm}^{-1}$  for the above described material.
3. The damage process in the heavily lithium doped Hall specimens, consists of the loss of carrier electrons with an equal loss of charge scattering centers.
4. The best available atomistic model to describe the damage is the following series reaction:



Since the equilibrium phase for a lithium-silicon solution is  $\text{Li}_2\text{Si}$ , the radiation process stiochiometrically resembles the precipitation of a second phase. The presence of oxygen appears to slow the above reaction.

5. The isochronal annealing is characterized by a low temperature partial anneal in the  $75\text{-}100^\circ\text{C}$  range and resolution of lithium at higher temperatures.
6. No evidence was found for the formation of "A" centers in the lithium doped silicon.
7. In similar material doped with phosphorus rather than lithium, the damage can be described entirely by the formation of E-centers.

### C. Recombination Studies

Although several models of radiation damage have been advanced to explain the behavior of recombination centers in lithium doped silicon solar cells, the conclusions have been reached by rather indirect means. The most direct measurement possible is the determination of minority carrier lifetime as a function of temperature. Such an experiment can often be analyzed in terms of theoretical recombination statistics to determine the position of the energy level of the recombination center which aids in identifying the defect. The method of lifetime measurement used here involves the determination of the minority carrier diffusion length.<sup>9</sup> The diffusion length can be converted to lifetime by use of the following relation:

$$L^2 = D\tau$$

This method was used to obtain the data shown in Figure 83 for conventional p on n solar cells made with crucible grown silicon. The experimental data in Figure 83 have been fitted to an expression describing recombination through an acceptor level located 0.17 eV below the conduction band. This energy level is associated with the silicon A-center (oxygen-vacancy pair). The temperature dependence of the density of states was considered in making this fit; however, the temperature variation of  $\sigma_p$  (capture cross-section and thermal velocity) were ignored.

There is some difficulty in directly applying this technique to lithium solar cells. The lithium cell is characterized by a steep gradient of lithium concentration in the portion of the cell where the diffusion length is measured. Since the concentration of lithium ( $n_0$ ) enters the theoretical expression, it must be known in most cases. A second difficulty involves tendency of the lithium solar cells to recover after irradiation. The recovery process is actually an increase in the lifetime that often is half complete within an hour after irradiation.

To make a determination of diffusion length versus temperature requires at least a 4 hour period in which the concentration of recombination centers remains constant. This was achieved by two different means. By using float zone cells, with a lower lithium concentration, it was possible to slow the recovery after irradiation enough to permit several hours for diffusion length measurements. A second method of slowing the recovery is achieved by use of crucible silicon for cells. In this material the recovery rate is greatly reduced by the presence of oxygen.

A cell from the redistribution studies, C3-10 was selected for the diffusion length measurements. This cell had a concentration of lithium at the junction of  $3 \times 10^{14} \text{ cm}^{-3}$ . This is low enough to insure no significant recovery during the first few hours after irradiation. In Figure 84 the before irradiation measurements for cell C3-10 are shown. The after irradiation measurements are plotted in Figure 85. The general expression for the lifetime for low injection involving one recombination center is:

$$\tau = \frac{1}{N_r \sigma v} \left( 1 + \frac{N_c}{n_0} e^{-\frac{\Delta E}{kT}} \right)$$

where  $N_r$  = concentration of recombination centers

$\sigma$  = capture cross-section

$v$  = thermal velocity

$N_c$  = density of states

$n_0$  = majority carrier concentration

$\Delta E$  = ionization energy of recombination centers

$kT$  = thermal energy

Most attempts to fit the above expression to experimental data assume the quantity  $1/N_r \sigma v$  to be independent of temperature and adjust  $\Delta E$  for the best fit. The quantity  $N_c$  varies as the 3/2 power of temperature and significantly lowers

the apparent activation derived from the slope of a simple lifetime -reciprocal temperature plot.

If the process is applied to the data in Figure 85, the value of  $\Delta E$  obtained for the best possible fit is 0.06 eV. The solid line in Figure 85 was obtained by such a fit. The present concept of a recombination center indicates that a defect with such a shallow energy level could not function effectively in recombination. The alternate explanation of the experimental data is obtained if one assumes that  $n_0$  is much larger than  $N_C \exp(-\Delta E/kT)$ . In this case the quantity  $1/N_C \sigma v$  will dominate the lifetime. Although the slight increase of thermal velocity will tend to decrease the lifetime as temperature increases, theoretical considerations indicate roughly an order of magnitude decrease in capture cross-section with temperature increase for the range under consideration.<sup>10</sup> Such a decrease comes close to providing the necessary increase in lifetime to explain the observed variation with temperature. If the preceding statements are an accurate representation of the recombination factors, the theory can say very little about the nature of the recombination centers except the quantity  $\Delta E$  must be very large compared to  $kT$ . This restriction would place the ionization level deep in the forbidden band. The dashed line in Figure 85 represents the results of temperature variation of lifetime found for non-lithium cells as shown in Figure 83. This is included to illustrate that, regardless of the theoretical considerations, the results in lithium cells are very different from those in non-lithium cells.

Cell C3-10 was allowed to recover to its original lifetime to permit an additional lifetime-temperature analysis. This data is also presented in Figure 84. It can be seen that, after recovery, the results are identical to those obtained before irradiation. This is sufficient reason to conclude that recovery consists of complete annihilation of the recombination centers produced by the electron



irradiation. Such a conclusion is in good agreement with the model previously considered.

A similar series of experiments was done on a crucible silicon lithium solar cell. This data is presented in Figures 86 and 87. The problems of making a theoretical fit to the data for this irradiated cell are identical to those encountered for the float zone cell. The data for cell H6-4508 in the irradiated condition (Figure 87) is very similar to that for the float zone cell in Figure 85. Within the limitations of this experiment, the results of irradiation in float zone and crucible cells can not be distinguished. Although this is not conclusive evidence, it supports the hypothesis of the same damage reaction in both float zone and crucible lithium solar cells. The major differences between behavior in the two types of cells is the slower recovery in crucible material. This is due to the slower diffusion of lithium rather than any differences in recovery damage mechanism. In addition to the before irradiation results for Cell H6-4508, results are shown for the sample in the partially annealed condition. The temperature variation of lifetime in the partially annealed sample is identical to that of the sample in the unirradiated and irradiated condition.

The following conclusions can be drawn;

1. The lifetime versus temperature results observed for irradiated lithium cells are radically different from those observed for non-lithium cells.
2. The irradiation of float zone and crucible lithium cells give similar results when analyzed by lifetime versus temperature studies.
3. The annealing of an irradiated float zone silicon lithium cell returns the cell to the unirradiated condition.
4. The irradiation generated recombination center in lithium cells appears to be a very deep acceptor level.

#### IV. EVALUATION TECHNIQUES STUDIES

##### A. Lang X-Ray Topography Study

When lithium doped silicon is raised to temperatures above 300°C and cooled to room temperature, the resistivity increases. Such a change could be caused by precipitation or outdiffusion of lithium. The times and temperatures involved suggest outdiffusion. To further investigate this behavior lithium doped float zone silicon wafers were annealed at various temperatures and slow-cooled to room temperature. The resistivities of these wafers were measured with a four-point probe after sufficient material was removed to insure uniform lithium distribution. The resistivity results are shown below:

As received	0.035 $\Omega$ -cm	$5.1 \times 10^{17}$ Li/cm <sup>3</sup>
1 hr @ 200°C	0.035 $\Omega$ -cm	$5.1 \times 10^{17}$ Li/cm <sup>3</sup>
1 hr @ 300°C	0.035 $\Omega$ -cm	$5.1 \times 10^{17}$ Li/cm <sup>3</sup>
18 hr @ 400°C	21.2 $\Omega$ -cm	$2.4 \times 10^{14}$ Li/cm <sup>3</sup>

These wafers were examined by the Lang X-ray topography technique after all treatments. This X-ray technique uses Bragg reflection from a given set of crystal planes to give an unmagnified image of the crystal. Stressed areas of the crystal reflect the X-rays more strongly and appear darker on a photographic plate, or lighter on a positive print such as those shown. Figures 88 and 89 are 9x enlargements of (220) topographs of the as-received and 18-hrs-at-400°C specimens, respectively. The topographs are taken in transmission through the specimens, using Mo characteristic radiation, and show a projection of the structural defects throughout the volume of the specimens, not just the surface. Instrumental resolution is less than 10 microns in the direct specimen image, which is less than 0.1 mm on the enlargements.

The highly dislocated structure normally associated with float-zone silicon is clearly shown in Figures 88 and 89. Individual dislocations are easily seen in many parts of the topographs. The spot at the edge nick is distortion associated with a zone spill during zone-refining of the crystal. The small white spot in Figure 88 is spurious, and is probably due to a scratch during handling of the photographic plate. The light area in Figure 89 near the edge and 90 degrees from the zone spill is due to the specimen mounting post, which did not appear in Figure 88 because that specimen was mounted at the unseen edge. The prominent white spot in Figure 89 appeared with the first heat treatment and is due to improper handling by tweezers.

No separate precipitate particles which might be interpreted as lithium metal precipitates are seen. If present, such particles should be visible because of the extremely high strain sensitivity of this technique. However, it is entirely possible that lithium may precipitate at existing dislocations, causing very little change in specimen appearance.

#### B. Junction Capacitance Measurements

Measurements of junction capacitance as a function of bias voltage, and the derivative of this quantity, are used to deduce the net impurity concentration and the form of its profile. An abrupt junction is assumed because of the very shallow diffusions employed in these solar cells. Then, with  $C$  the junction capacitance,  $V$  the junction voltage (including the contact potential of about 0.5 volt)  $q$  the electronic charge,  $\epsilon$  the dielectric permittivity,  $A$  the area, and  $N(x)$  the impurity concentration on the low-doped side of the junction, which is at  $x = 0$ , we have the well-known relationships

$$\begin{aligned} N &= C^3/q\epsilon A^2(-dC/dV) \\ D &= \epsilon A/C \end{aligned} \tag{1}$$

where  $D$  is the depletion depth.

When  $\log C$  is plotted against  $\log V$  from measured values, the plot is usually a straight line over some appreciable range of  $V$ , i.e.

$$C = BV^{-s}$$

where  $B$  is a constant and  $-s$  is the slope on the plot. This leads to the relationship

$$N(D) = B'D^{(1/s)-2}$$

where  $B'$  is another constant.

Commonly observed values for  $s$  are  $1/2$ ,  $1/3$  and  $1/4$  as shown in Figures 90 through 92. Then, since  $D$  is merely the value of  $x$  at the positive boundary of the space-charge region at each point of capacitance measurement, we have:

for  $s = 1/2$ ,  $N = \text{constant}$

for  $s = 1/3$ ,  $N \sim x$

for  $s = 1/4$ ,  $N \sim x^2$

over whatever limited range of voltage the slope may be considered constant.

The concentration  $N$  may be calculated from Eq (1) using differential capacitance measurements, or if the shape of the profile has been sufficiently well established from the slope measurement, from derived formulas such as, for  $s = 1/3$ ,

$$N(D) = 3VC^2/2\epsilon qA^2$$

where the evaluation may conveniently be done at  $V = 0.5$  volts (zero applied bias), since the contact potential is essentially unchanged throughout these studies.

An additional use of capacitance studies is their use in the determination of energy levels produced by irradiation. The kinetics of carrier capture and emission at a defect (trap or recombination center) is described by Hall-Shockley-Read theory in terms of four rate constants:  $c_n$ ,  $c_p$ ,  $e_n$ ,  $e_p$ . The constants

pertain to, respectively, capture of electrons from the conduction band, capture of holes from the valence band, emission of electrons to the conduction band, and emission of holes to the valence band. The principle of detailed balance leads to relationships among these constants and the defect energy level,  $E_d$ .

In general, the time constant for equilibration of charge state for a given type of defect is given by

$$\tau = 1/[c_n(n+n_1) + c_p(p+p_1)]. \quad (2)$$

Here  $n$  and  $p$  are the ambient electron and hole densities, which control the capture processes, and the fictitious densities  $n_1$  and  $p_1$  are equal to the thermal equilibrium densities which would result if the fermi level were at  $E_d$ . The emission processes are characterized by  $n_1$  and  $p_1$ .

Measurement of the ac capacitance of a junction gives an opportunity to obtain information on defect parameters if temperature, frequency and junction bias are varied. In principle, capture constants, energy level, and defect density can be determined, provided mainly that the effects of only one type of defect can be isolated, and if conditions can be adjusted to favor predominance of only one of the terms in the above equation.

The measurements may be interpreted through Eq (2) as follows. The capacitance measurement consists in applying a small ac voltage in series with the junction bias, thus causing small excursions of the boundary of the space-charge region. In this way, defects near this boundary are alternately exposed more or less to the environments of the space-charge region and the bulk. The time constant of Eq (2) will be limited in the course of one cycle by the emission processes which dominate in the space-charge region, where  $n$  and  $p$  are negligible. Then

$$\tau = 1/(c_n n_1 + c_p p_1).$$

According to whether frequency or temperature is varied, a relaxation or freeze-out, respectively, occurs when the driving frequency exceeds the ability of deep levels to keep pace with the signal through thermal emission.

A set of such measurements is shown in Figure 93. The specimen is a standard 10 ohm-cm n/p solar cell which has been irradiated with  $3 \times 10^{15}$  1-MeV e/cm<sup>2</sup>. The quantity plotted as a function of 1/kT is the net acceptor density N, derived from differential capacitance measurements by means of the well-known relationship

$$N = C^3 / q \epsilon A^2 (-dC/dV), \quad (3)$$

where C is the ac capacitance, q is the electronic charge,  $\epsilon$  is the dielectric permittivity, A is the area (2 cm<sup>2</sup> here), and dC/dV is the voltage derivative of the capacitance.

The measurements show a drop in the apparent net acceptor concentration at lower temperatures. Furthermore, the drop-off is frequency dependent. This immediately suggests that the effect is associated with carrier-defect kinetics at the edge of the space-charge region, rather than with changes in the fermi level in the bulk, since the bulk effects would not depend on the measurement frequency.

Now, referring to the figure, we see that the freeze-out results in a net loss of acceptors. The corresponding emission process is that of holes, so that we are left with the term in  $c_p$ . The term in  $c_n$  would have been kept instead, if there had been a net gain of acceptors upon freeze-out. Finally, then,

$$\tau = 1/c_p p_1 = 1/c_p N_v \exp[-\beta(E_d - E_v)], \quad (4)$$

where  $N_v$  is the effective density of states in the valence band,  $\beta = 1/kT$ , and  $E_d - E_v$  is the height of the defect energy level above the valence band.

If we define a cutoff frequency  $f_c$  as the frequency at which  $N$  is halfway between the high and low limiting values, we recognize that  $f_c$  is of the order of  $1/\tau$ . (It is difficult to define  $f_c$  more exactly here, because of uncertainty in the degeneracy factor of the transition, but it is probably appropriate to within a factor of 2, and in any event will not matter much in the evaluation immediately following.)

If we now read  $f_c$  at two temperatures, we obtain

$$\frac{f_{c1}}{f_{c2}} = \frac{N_{v1}}{N_{v2}} \exp (E_d - E_v)(\beta_2 - \beta_1)$$

or

$$\Delta E = (E_d - E_v) = \frac{1}{\beta_2 - \beta_1} \left[ \ln \frac{f_{c1}}{f_{c2}} - \ln \frac{N_{v1}}{N_{v2}} \right]. \quad (5)$$

Since  $N_v$  does not vary rapidly with temperature we expect roughly equal spacing of the freeze-out curves for equal ratios of frequencies, which is apparently true in the figure. From these curves,  $\Delta E = .27$  ev. This corresponds to a very well known radiation defect just below .3 ev above the valence band in irradiated silicon, suspected to be the divacancy.

The capture constant  $c_p$  and the capture cross-section  $\sigma_p = c_p/v_{th}$ , where  $v_{th}$  is the electron thermal velocity, may be evaluated from each freeze-out curve. The value calculated depends on the definition of  $f_c$ , and so is of limited accuracy pending further study of the degeneracy, or determination of  $\tau$  directly. Values calculated for  $\sigma_p$  are  $1.7 \times 10^{-14}$  cm<sup>2</sup> at 193°K,  $2.5 \times 10^{-14}$  cm<sup>2</sup> at 170°K, and  $2.7 \times 10^{-14}$  cm<sup>2</sup> at 153°K. These values may be compared with  $3 \times 10^{-14}$  cm<sup>2</sup> measured by Vavilov et.al.<sup>11</sup> at 100°K, and with  $8 \times 10^{-13}$  cm<sup>2</sup> measured by Wertheim.<sup>12</sup> The latter value, however, was referred to room temperature under the assumption that  $c_p$  is independent of temperature and therefore is not directly comparable. Again, our values are only preliminary and tentative. The above measurements

serve to illustrate that this technique is in reasonable agreement with other reported techniques, when comparison is made on a rather well-known defect level. The capacitance technique will be applied in the future to lithium-doped irradiated silicon.

### C. Diffusion Sources

A series of diffusion experiments have been performed to evaluate the usefulness of  $\text{LiAlH}_4$  as a diffusion source. The material was used in the form of a 5 molar solution in diethyl ether. The silicon wafers were painted with a thick coating of solution. The first problem involved in use of this material is the evaporation of the solvent to obtain a uniform coating of the hydride. There is a strong tendency for the coating to bubble in some areas. A second problem is the tendency of the hydride to easily oxidize. The oxidation problem was eliminated by evacuating the diffusion furnace before heating. The one clear advantage of this material is lack of physical attack of the silicon surface which is common with a lithium-mineral oil paste. The surface of the hydride diffused wafers remained flat with no pitting and the residue is easily removed. During the initial work it was not possible to produce any surface concentrations in excess of  $10^{17}$  Li atom/cm<sup>3</sup>.

In subsequent work, all the heating for decomposition of the hydride and diffusion of lithium was done under a dry nitrogen atmosphere. This change eliminated all oxidation problems and permitted much higher lithium surface concentrations to be achieved. As mentioned in other sections of this report, this material was used to saturate silicon with lithium for use in carrier removal studies. In these diffusions the surface concentrations achieved were roughly equal to the equilibrium lithium solubilities for the diffusion temperatures used. A sample of the  $\text{LiAlH}_4$  solution was furnished to Centralab for evaluation



in cell manufacture. The initial cells showed much reduced surface pitting attack and a slightly lower surface concentration when compared to those produced with lithium paste.

#### D. Other Solar Cell Structures

Since n/p solar cells are inherently more radiation resistant than p/n cells, it would be highly desirable to incorporate the advantages of lithium annealing into the n/p cell. Two different approaches to this problem have been attempted. The first method involved the diffusion of lithium into p-type silicon to form a p-n junction. Since the concentration of lithium in the bulk of the cell must remain below that of the acceptor concentration, 0.1 ohm-cm p-type silicon was used. In such a material the lithium concentration could rise to  $10^{17} \text{ cm}^{-3}$  without any danger of changing to n-type. In this way it was possible to make devices of very low photovoltaic efficiency. When these devices were irradiated they degraded and did not show any room temperature recovery. Since the available time did not allow more than a cursory study, their results are not conclusive.

A second approach was attempted by removing the back contact of 1 ohm-cm n/p solar cells, and diffusing lithium into the cells from the back. After lithium diffusion the back contacts were reapplied. Unfortunately the resulting device had very high series resistance as a result of the lithium diffusion. Because of this problem no radiation evaluation was attempted. Further work in this field should be preceded by a systematic study of lifetime in irradiated p-type silicon counterdoped with lithium. Such work would establish the value of lithium in the p-type device. If such work indicated that lithium was desirable, the more complicated problem of putting lithium into a p-type cell structure could be approached at a later time.

## V. NEW TECHNOLOGY

No items of new technology are reportable for this program.

## REFERENCES

1. J. J. Wysocki, et. al. Annual Report, Contract No. NAS5-10239, 20 June 1967.
2. G. Brucker, et. al., First Progress Report, Contract No. NAS5-10239, 20 November 1967.
3. F. J. Morin and J. P. Maita, Phys. Rev., 96, 28 (1954).
4. H. Y. Fan, and K. Lark-Horovitz, "Report on the Conference on Defects in Crystalline Solids", Phys. Soc., London, (1954).
5. G. K. Wertheim, Phys. Rev. 105, 1730 (1957).
6. E. M. Pell, Solid State Physics in Electronics and Telecommunicators, Vol. I, p. 261, Academic Press, New York (1960).
7. J. R. Carter, Jr., and R. G. Downing, Semiannual Progress Report, Contract No. NAS5-10322, 28 August 1966.
8. G. D. Watkins, et. al., J. Appl. Phys. 30, 1198 (1959).
9. H. W. Rosenzweig, Bell Systems Tech. T. 41, 1573 (1962).
10. M. Lax, Phys. Rev., 119, 1502 (1960).
11. V. S. Vavilov, et. al., J. Phys. Chem. Solids 22, 31 (1961).
12. G. K. Wertheim, Phys. Dev. 110, 1272 (1958).

Cell Group	<u>Lithium Introduction</u>		<u>Base Material</u>			
	Diffusion Schedule °C/Min/Min	Li. Conc. @ Junction $\text{cm}^{-3}$	Lithium Source	Mat'l Type	Dopant	Resistivity $\Omega\text{-cm}$
C1	450/5/40	$2 \times 10^{14}$	Paint-on	Cruc	As	25-35
C2	425/90/120	---	Paint-on	Cruc	Sb	5-10
C5A	450/40/0	$1 \times 10^{15}$	Paint-on	Cruc	As	30
C5B	450/40/0	$4 \times 10^{15}$	Paint-on	F.Z.	P	90
C5C	425/90/120	$1 \times 10^{14}$	Paint-on	Cruc	As	30
C5D	425/90/120	$3 \times 10^{14}$	Paint-on	F.Z.	P	90
C6A	425/90/120	$\sim 10^{14}$	Paint-on	Cruc	Sb	3-16
C6B	425/90/120	$\sim 10^{14}$	Paint-on	Cruc	Sb	17-85
C6C	425/90/120	$\sim 10^{14}$	Paint-on	Cruc	P	16-57
H1	425/90/60	$4 \times 10^{14}$	Paint-on	Cruc	As	100-200
H2	425/90/60	$4 \times 10^{14}$	Paint-on	Cruc	P	20
H4	425/90/60	$1 \times 10^{15}$	Paint-on	F.Z.	P	80-120
H5	350/30/60	---	Paint-on	F.Z.	P	$\sim 20$
H6	450/90/60	$3 \times 10^{14}$	Paint-on	Cruc	P	$\sim 20$
H7	425/90/60	$1 \times 10^{15}$	Paint-on	Lopex	P	$\sim 20$
T2	400/90/120	$\sim 10^{14}$	Evaporated	Cruc	P	$> 20$
T3	400/90/0	$4 \times 10^{15}$	Evaporated	Lopex	P	$> 50$
T4	400/90/0	$4 \times 10^{15}$	Evaporated	F.Z.	P	$> 50$
T5	400/90/0*	$4 \times 10^{15}$	Evaporated	Lopex	P	$\sim 50$
T6	325/480/0	$7 \times 10^{14}$	Evaporated	Lopex	P	$\geq 50$
T7	325/480/0	$5 \times 10^{14}$	Evaporated	Cruc	P	$\geq 20$
T8	325/480/0*	$3 \times 10^{14}$	Evaporated	Cruc	P	$> 20$

\*Li diffused into whole slices to eliminate non-uniform edges

TABLE I. LITHIUM SOLAR CELL MANUFACTURING PARAMETERS

Cell Group	Diffusion Schedule °C/Min/Min	$N_{Li}$ cm <sup>-3</sup>	Electron Fluence e/cm <sup>2</sup> , 1 MeV	Initial Level I <sub>SC</sub> , mA	Damaged Level I <sub>SC</sub> , mA	Recovered Level I <sub>SC</sub> , mA	Time (hrs.) to 1/2 Recovery Pt.	Average C vs V Slope	Extrapolated Time (days) to 1/2 Recovery Pt. at Room Temp.
C1	450/5/40	2x10 <sup>14</sup>	3x10 <sup>15</sup>	61-64	23-25	38-41	7	-.3	2800
C2	425/90/120	---	3x10 <sup>15</sup>	52-60	18-22	none	----	-.4	----
C5A	450/40/0	1x10 <sup>15</sup>	3x10 <sup>15</sup>	44-48	17	32-33	.16	-.24	12
C5C	425/90/120	2x10 <sup>14</sup>	3x10 <sup>15</sup>	58-62	24-27	40-42	8	-.33	3500
C6A	425/90/120	~10 <sup>14</sup>	3x10 <sup>15</sup>	59-61	22-23	28-33	30	-.39	----
C6B	425/90/120	~10 <sup>14</sup>	3x10 <sup>15</sup>	59	25	36-40	15	-.33	1600
C6C	425/90/120	~10 <sup>14</sup>	3x10 <sup>15</sup>	56-61	25-26	40	15	-.37	----
H1	425/90/60	4x10 <sup>14</sup>	3x10 <sup>15</sup>	46-48	21-23	38-39	1.2	-.24	56
H2	425/90/60	5x10 <sup>14</sup>	3x10 <sup>15</sup>	50-55	20-21	36	.6	-.28	62
H6	450/90/60	4x10 <sup>14</sup>	3x10 <sup>15</sup>	38-41	21	35	1.5	-.30	290
T2	400/90/120	~10 <sup>14</sup>	3x10 <sup>15</sup>	59-62	19-22	42-45	.4	-.3	12
T7	325/480/0	6x10 <sup>14</sup>	3x10 <sup>15</sup>	61-62	17	42	.25	-.26	2*
T8	325/480/0	3x10 <sup>14</sup>	3x10 <sup>15</sup>	55-56	19-21	36-39	2	-.28	150

\*Actually observed

TABLE II. CRUCIBLE LITHIUM SOLAR CELL RECOVERY CHARACTERISTICS @ 100°C

Cell Group	Diffusion Schedule °C/Min/Min	$N_{Li}$ cm <sup>-3</sup>	Electron Fluence e/cm <sup>2</sup> , 1 MeV	Initial Level I <sub>SC</sub> , mA	Damaged Level I <sub>SC</sub> , mA	Recovered Level I <sub>SC</sub> , mA	Time (hrs.) to 1/2 Recovery Pt. @ 25°C	Average C vs V Slope
C5B(F.Z.)	450/40/0	4x10 <sup>15</sup>	3x10 <sup>14</sup>	29-33	23-25	29-32	1.5	-.37
C5D(F.Z.)	425/90/120	3x10 <sup>14</sup>	3x10 <sup>14</sup>	43-45	27-29	43-45	3	-.39
H4(F.Z.)	425/90/60	1x10 <sup>15</sup>	3x10 <sup>14</sup>	33-37	25-28	34-36	.5	-.29
H5(F.Z.)	350/90/60	<10 <sup>14</sup>	3x10 <sup>14</sup>	59-65	29-31	32-38	----	-.45
H7(L)	425/90/60	1x10 <sup>15</sup>	3x10 <sup>14</sup>	44-50	27-28	42-45	.5	-.3
T3(L)	400/90/0	4x10 <sup>15</sup>	3x10 <sup>14</sup>	51-54	24	44-46	.5	-.24
T4(F.Z.)	400/90/0	4x10 <sup>15</sup>	3x10 <sup>14</sup>	45-48	24-25	43-44	.25	-.24
T5(L)	400/90/0	4x10 <sup>15</sup>	3x10 <sup>14</sup>	43-48	22	41-42	.4	-.25
T6(L)	325/480/0	6x10 <sup>14</sup>	3x10 <sup>14</sup>	60-62	27-29	51-52	3	-.27
C5B(F.Z.)	450/40/0	5x10 <sup>15</sup>	3x10 <sup>15</sup>	31-35	19-21	30-33	3	-.37
*C5D(F.Z.)	425/90/120	5x10 <sup>14</sup>	3x10 <sup>15</sup>	44	20	44	10	-.39
H4(F.Z.)	425/90/60	1x10 <sup>15</sup>	3x10 <sup>15</sup>	32-35	21	33	3	-.29
H5(F.Z.)	350/90/60	<10 <sup>14</sup>	3x10 <sup>15</sup>	55-61	19-22	none	----	-.45
H7(L)	425/90/60	1x10 <sup>15</sup>	3x10 <sup>15</sup>	43-48	19-21	36-37	3	-.3
T3(L)	400/90/0	4x10 <sup>15</sup>	3x10 <sup>15</sup>	49-53	15	32-34	2	-.24
T4(F.Z.)	400/90/0	4x10 <sup>15</sup>	3x10 <sup>15</sup>	45-47	16-17	32-34	2.5	-.24
T5(L)	400/90/0	4x10 <sup>15</sup>	3x10 <sup>15</sup>	44-49	15-16	31-32	1	-.25
T6(L)	325/480/0	8x10 <sup>14</sup>	3x10 <sup>15</sup>	60-62	18	39-40	18	-.27

\*One cell only, see text

TABLE III. FLOAT ZONE LITHIUM SOLAR CELL RECOVERY CHARACTERISTICS

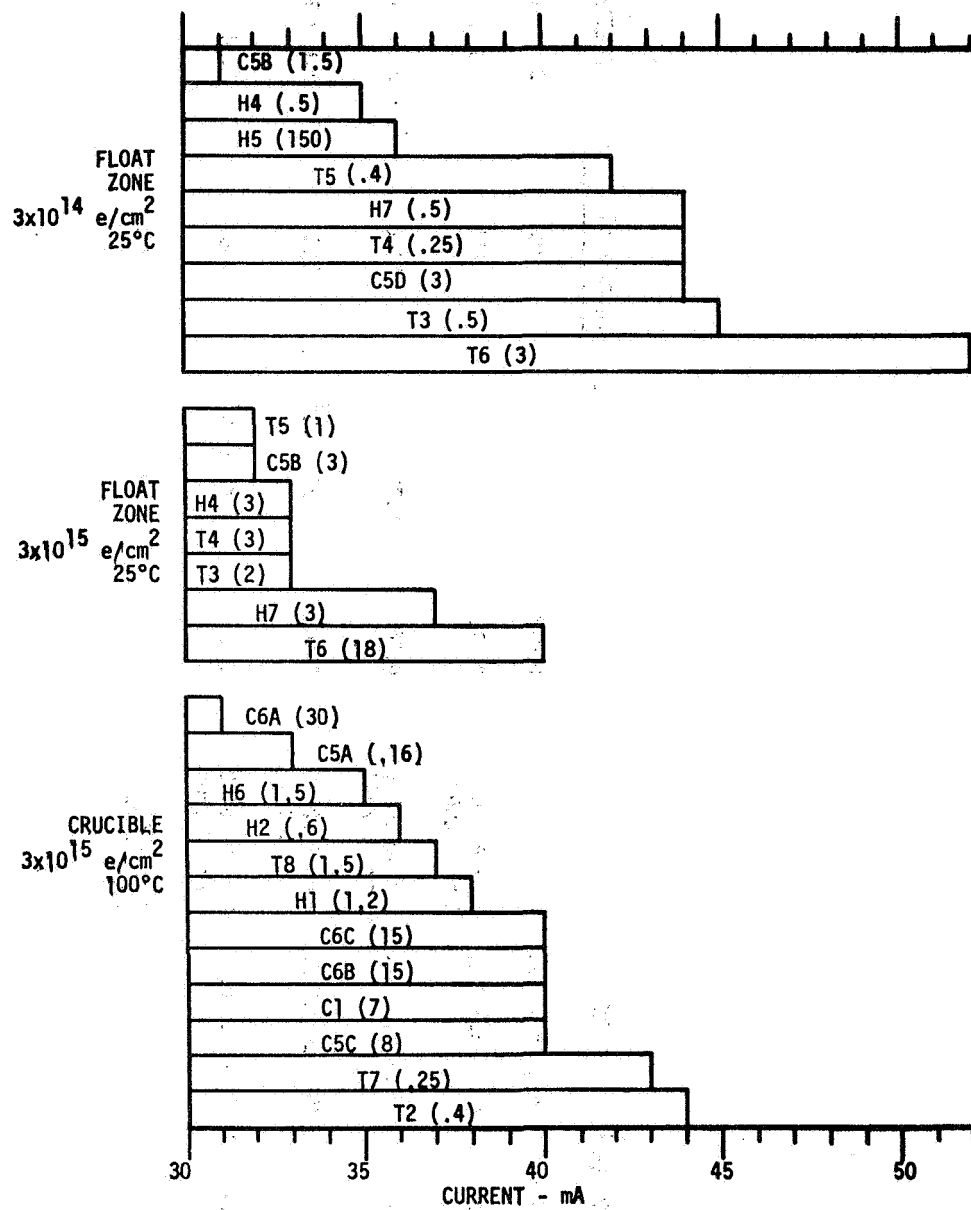


TABLE IV. RECOVERED LEVEL & HALF RECOVERY TIME (IN PARENTHESIS)

<u>Sample #</u>	<u>Silicon</u>	<u>Li Diffusion</u>	<u><math>\rho(\Omega\text{-cm})</math></u>	<u><math>R(\text{cm}^3/\text{coulomb})</math></u>	<u><math>\mu_H(\text{cm}^2/\text{volt-sec})</math></u>	<u><math>\text{Li(atoms/cm}^3\text{)}</math></u>
B-1	75 $\Omega\text{-cm}$ , n, F. Z.	1 hr @ 600°C	0.012	$2.18 \times 10^0$	180	$3.4 \times 10^{18}$
D-2	75 $\Omega\text{-cm}$ , n, F. Z.	1 hr @ 600°C, 8 hr @ 200°C	0.078	$6.35 \times 10^1$	815	$1.2 \times 10^{17}$
A-1	75 $\Omega\text{-cm}$ , n, F. Z.	1 hr @ 600°C 60 hrs @ 200°C	0.26	$2.72 \times 10^2$	1150	$2.7 \times 10^{16}$
C-1	75 $\Omega\text{-cm}$ , n, F. Z.	1 hr @ 600°C 48 hrs @ 150°C	0.50	$6.32 \times 10^2$	1280	$1.6 \times 10^{16}$
E-2	1000 $\Omega\text{-cm}$ , n, F. Z.	1 hr @ 600°C 60 hrs @ 150°C	2.3	$3.46 \times 10^3$	1500	$2.14 \times 10^{15}$
Q-1	50 $\Omega\text{-cm}$ , n, A. C.	1 hr @ 600°C 60 hrs @ 200°C	0.12	$1.10 \times 10^2$	935	$6.7 \times 10^{16}$

TABLE V. PROPERTIES OF LI DIFFUSED SILICON SPECIMENS

	<u>Defect Reaction</u>	<u>Change in Conduction Electrons</u>	<u>Change in Scattering Centers</u>	<u>Nature of Defect</u>
1.	$V + Li^+ + e^- \rightarrow Li-V^0$	Lose One	Lose One	Shallow acceptors, deep donor, or neutral defect
2.	$V + Li^+ + 2e^- \rightarrow Li-V^-$	Lose Two	No Change	Deep Acceptor
3.	$Li-V^- + Li^+ \rightarrow Li-V-Li$	No Change	Lose Two	Neutral (Inactive)
4.(2+3)	$V + 2Li^+ + 2e^- \rightarrow Li-V-Li$	Lose Two	Lose Two	Neutral (Inactive)
5.	$V + P^+ + 2e^- \rightarrow P-V^-$ ("E" Center)	Lose Two	No Change	Deep Acceptor
6.	$V + O + e^- \rightarrow O-V^-$ ("A" Center)	Lose One	Gain One	Deep Acceptor
7.	$O-V^- + Li^+ \rightarrow Li-V-O$	No Change	Lose Two	Neutral

TABLE VI. RADIATION DEFECT PRODUCTION IN N-TYPE SILICON



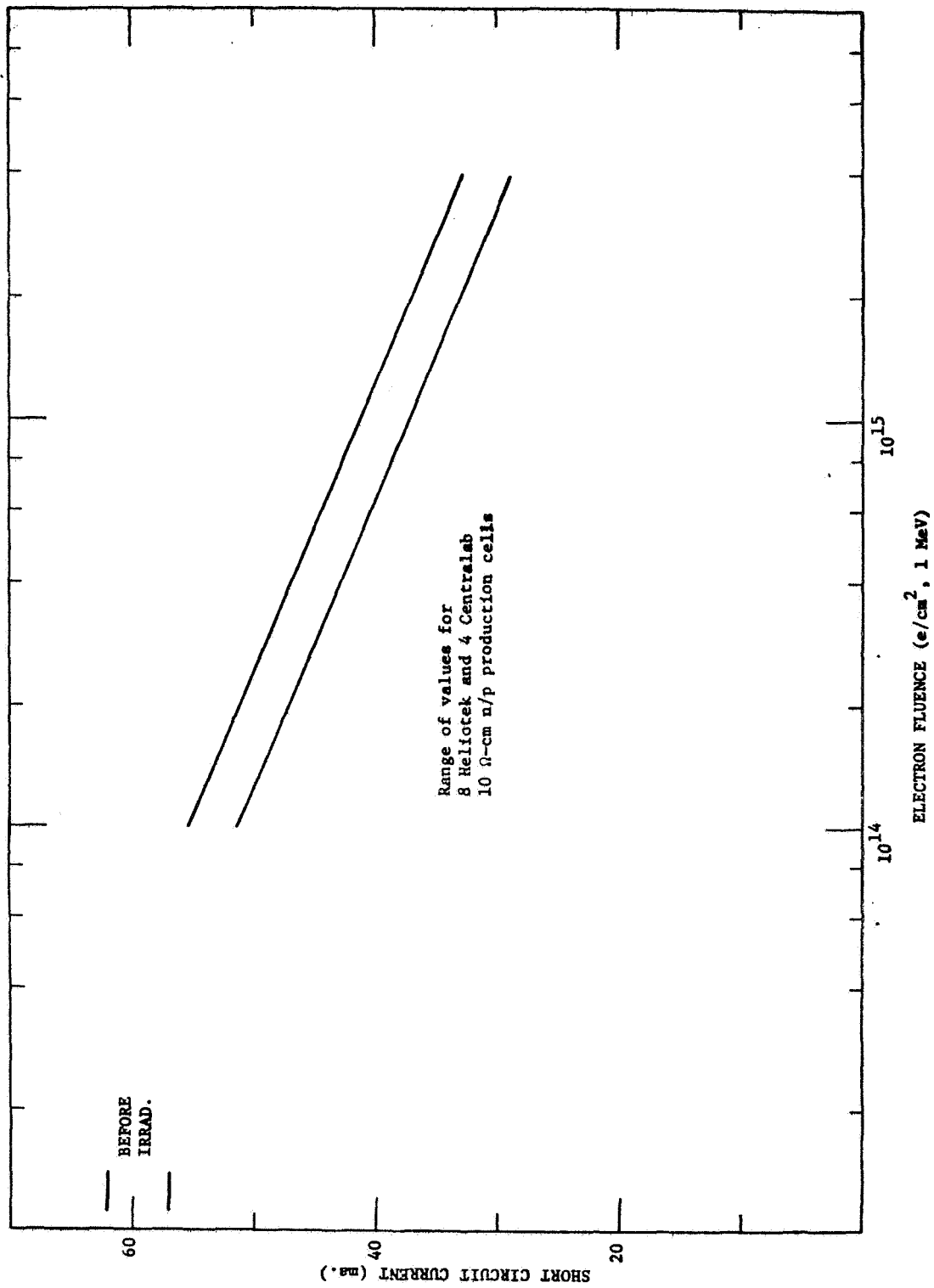


FIG. 1 ELECTRON DEGRADATION OF CONTEMPORARY N/P  
SILICON SOLAR CELLS

# SOLAR CELL CURRENT - VOLTAGE CHARACTERISTICS

Cell Mfg. CENTRALAB Designation C5C-66 Cover Material \_\_\_\_\_ Thickness \_\_\_\_\_  
 Cell Size 1 X 2 PinN ☒ NonP ☐ Cover Coating \_\_\_\_\_  
 Light Source TUNGSTEN Special Conditions  $3 \cdot 10^{15} \text{ e/cm}^2, 1 \text{ Mev}$   
 Intensity \_\_\_\_\_  $\text{mw/cm}^2$  Std. Cell No. 2 30 a-cm, As, Crucible, 425°-70-120  
 Tested By \_\_\_\_\_ Date 4-17-69 Storage temp. 80° C.

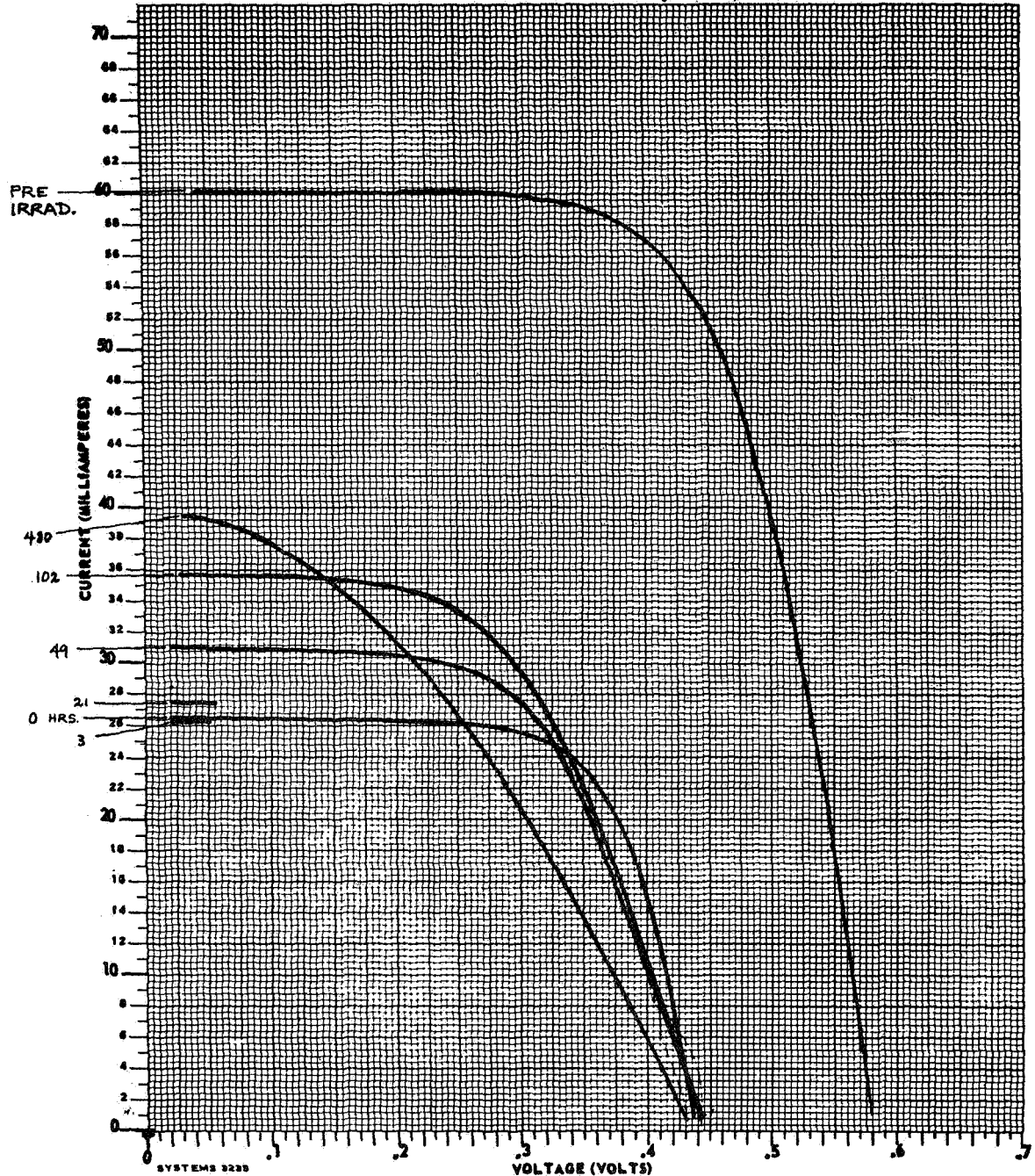


FIG. 2. LITHIUM DOPED SOLAR CELL I-V CHARACTERISTIC EXHIBITING DEGRADATION AND COLLAPSE OF POWER POINT

# SOLAR CELL CURRENT - VOLTAGE CHARACTERISTICS

Cell Mfg. TEXAS INST. Designation T5-6 Cover Material \_\_\_\_\_ Thickness \_\_\_\_\_  
 Cell Size 1 X 2 PpnN ☒ NonP ☐ Cover Coating \_\_\_\_\_  
 Light Source TUNGSTEN Special Conditions  $3 \cdot 10^{15} \text{ e/cm}^2$  1 Mev.  
 Intensity \_\_\_\_\_ mw/cm<sup>2</sup> Std. Cell No. 2 ~ 50  $\Omega$ -cm, Phos., LOPEX, 408-90-0  
 Tested By \_\_\_\_\_ Date 4-1-69 Storage temp. 25°C

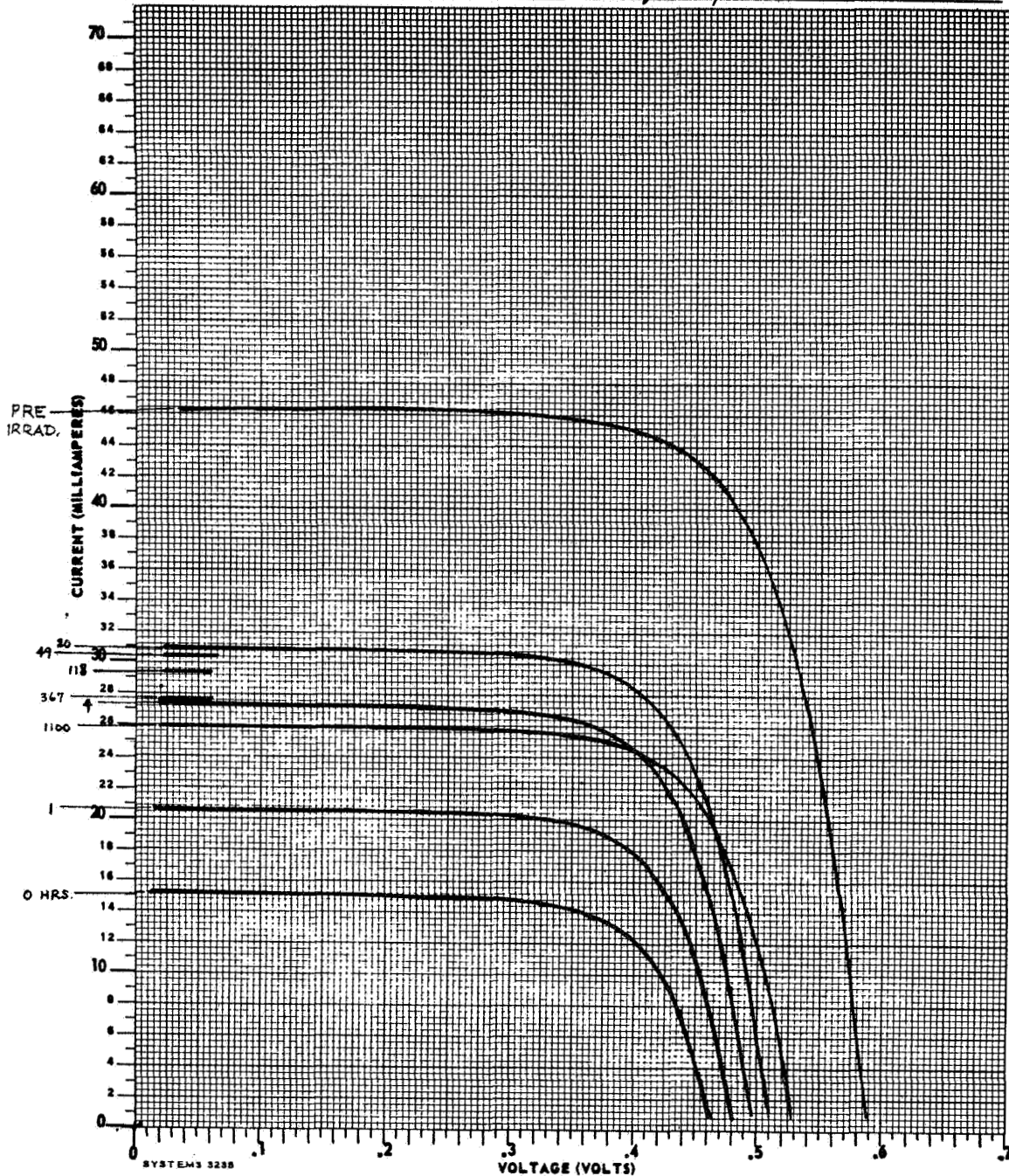


FIG. 3. LITHIUM DOPED SOLAR CELL I-V CHARACTERISTIC EXHIBITING  
 $I_{SC}$  REDEGRADATION WITH CONTINUED  $V_{OC}$  RECOVERY

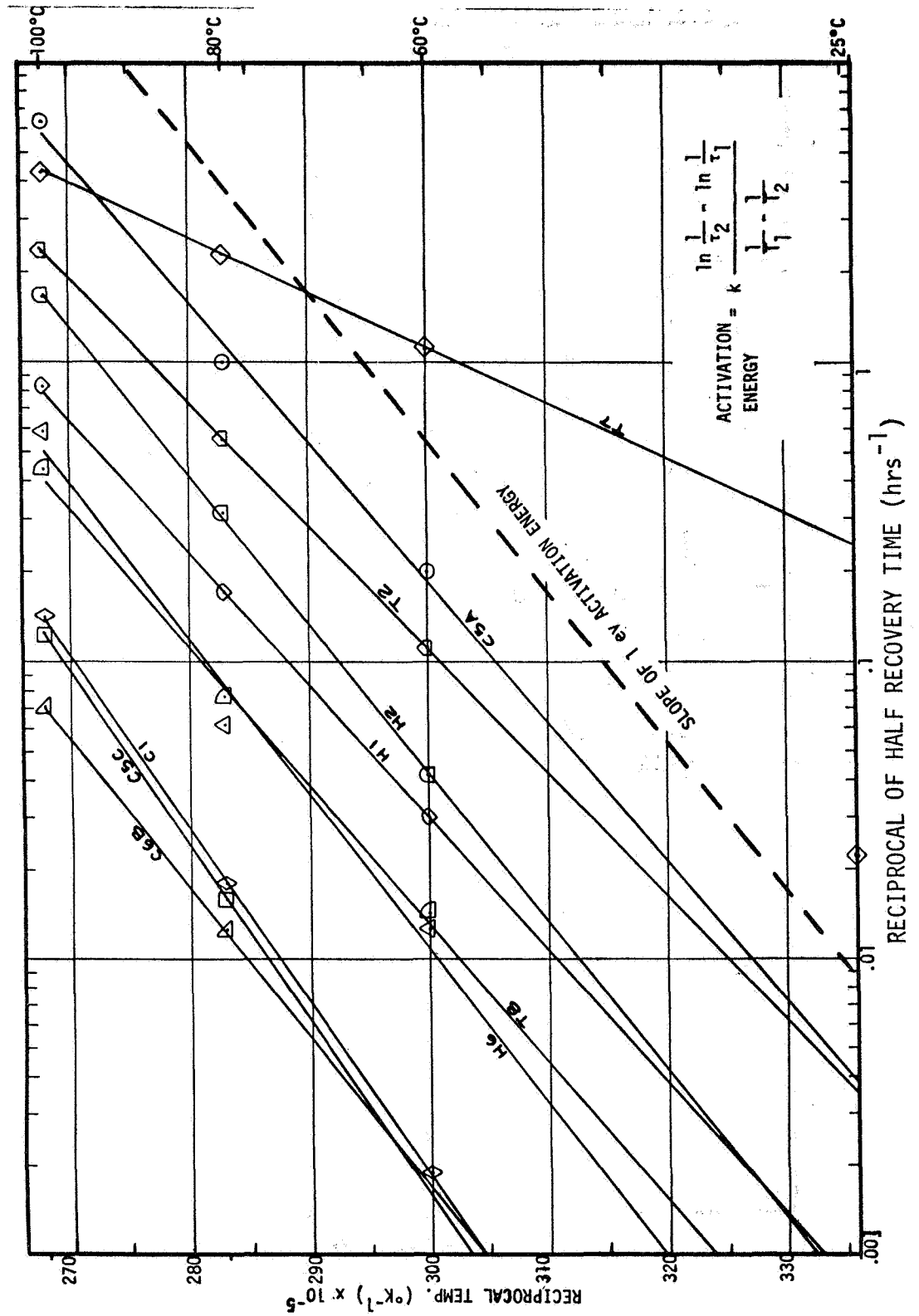


FIG. 4. ANNEALING TIME VERSUS STORAGE TEMPERATURE FOR CRUCIBLE LITHIUM DOPED SOLAR CELLS

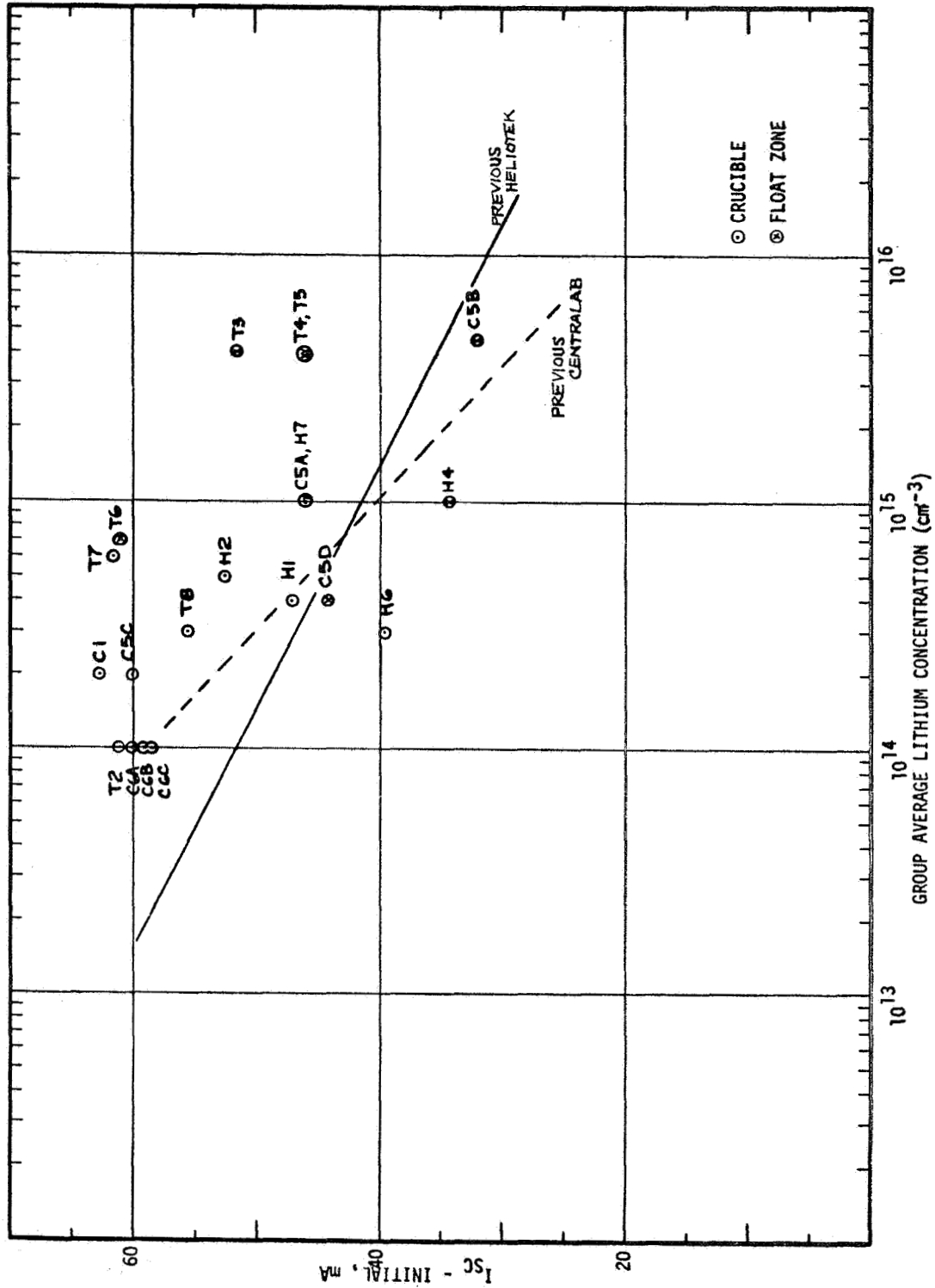


FIG. 5. INITIAL  $I_{SC}$  VERSUS LITHIUM CONCENTRATION AT JUNCTION FOR CRUCIBLE AND FLOAT ZONE LITHIUM DOPED SOLAR CELLS

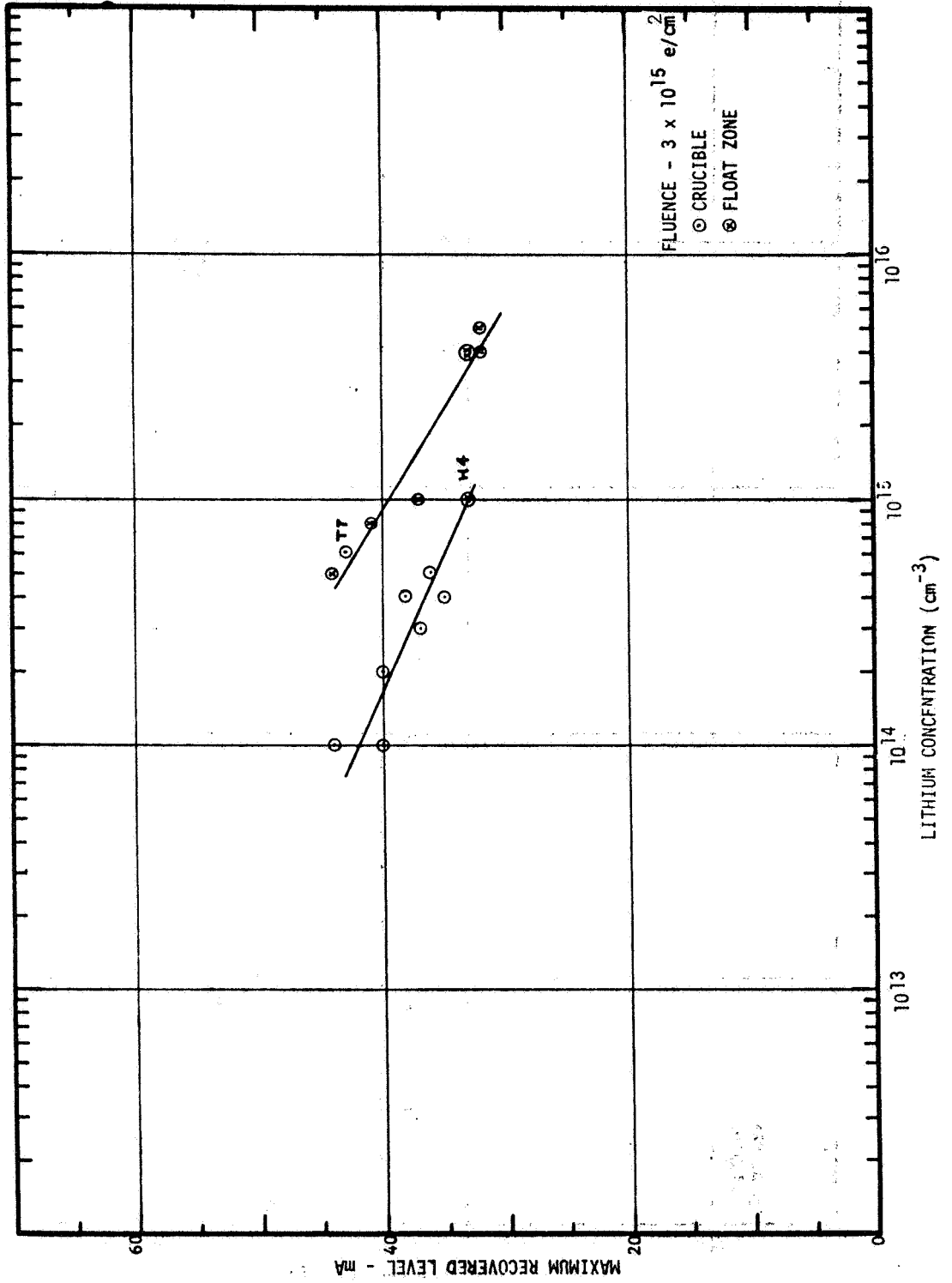


FIG. 6. RECOVERED  $I_{SC}$  VERSUS LITHIUM CONCENTRATION AT JUNCTION FOR CRUCIBLE AND FLOAT ZONE LITHIUM DOPED SOLAR CELLS

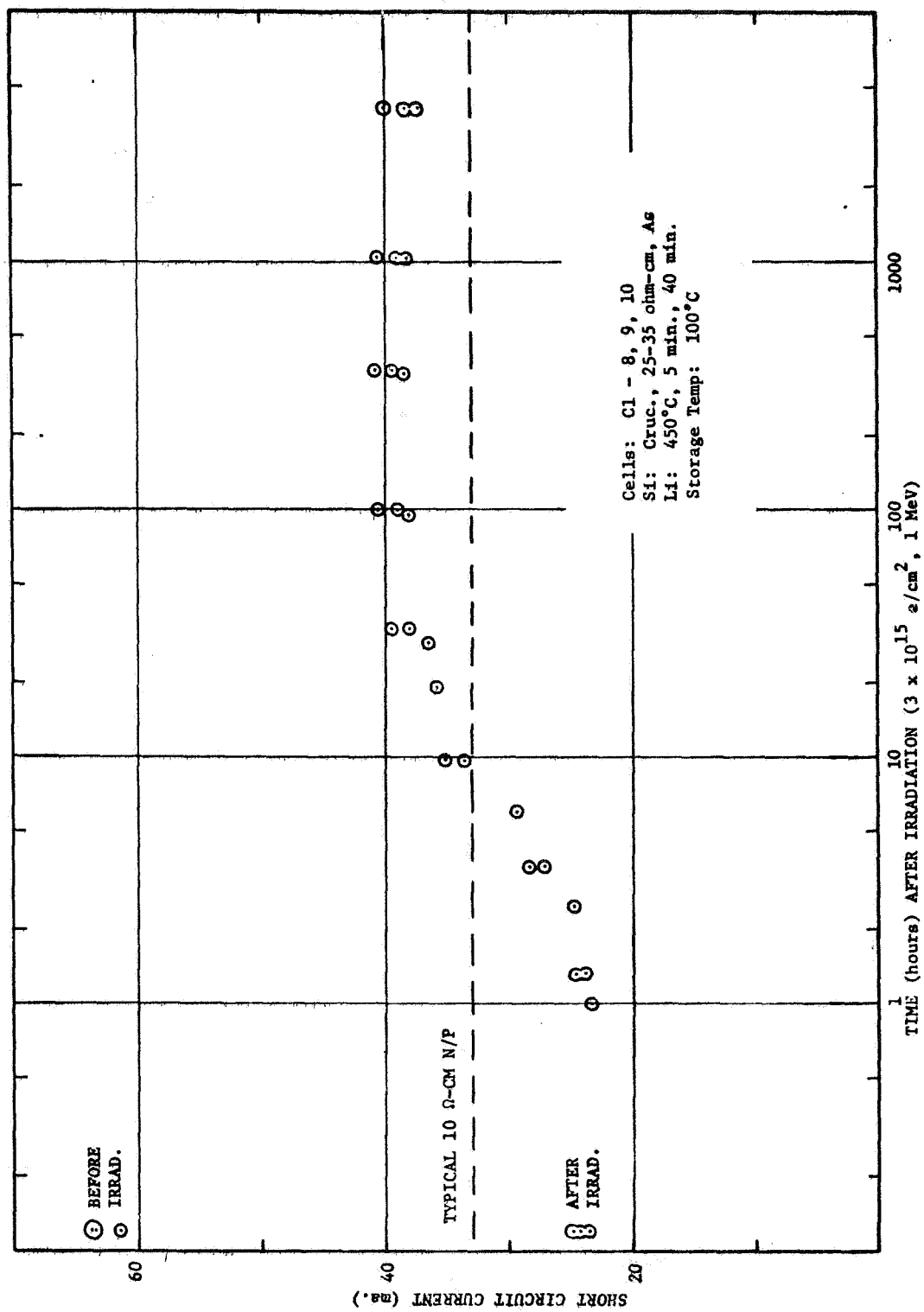


FIG. 7 RECOVERY OF GROUP C1 LITHIUM SOLAR CELLS AT 100°C

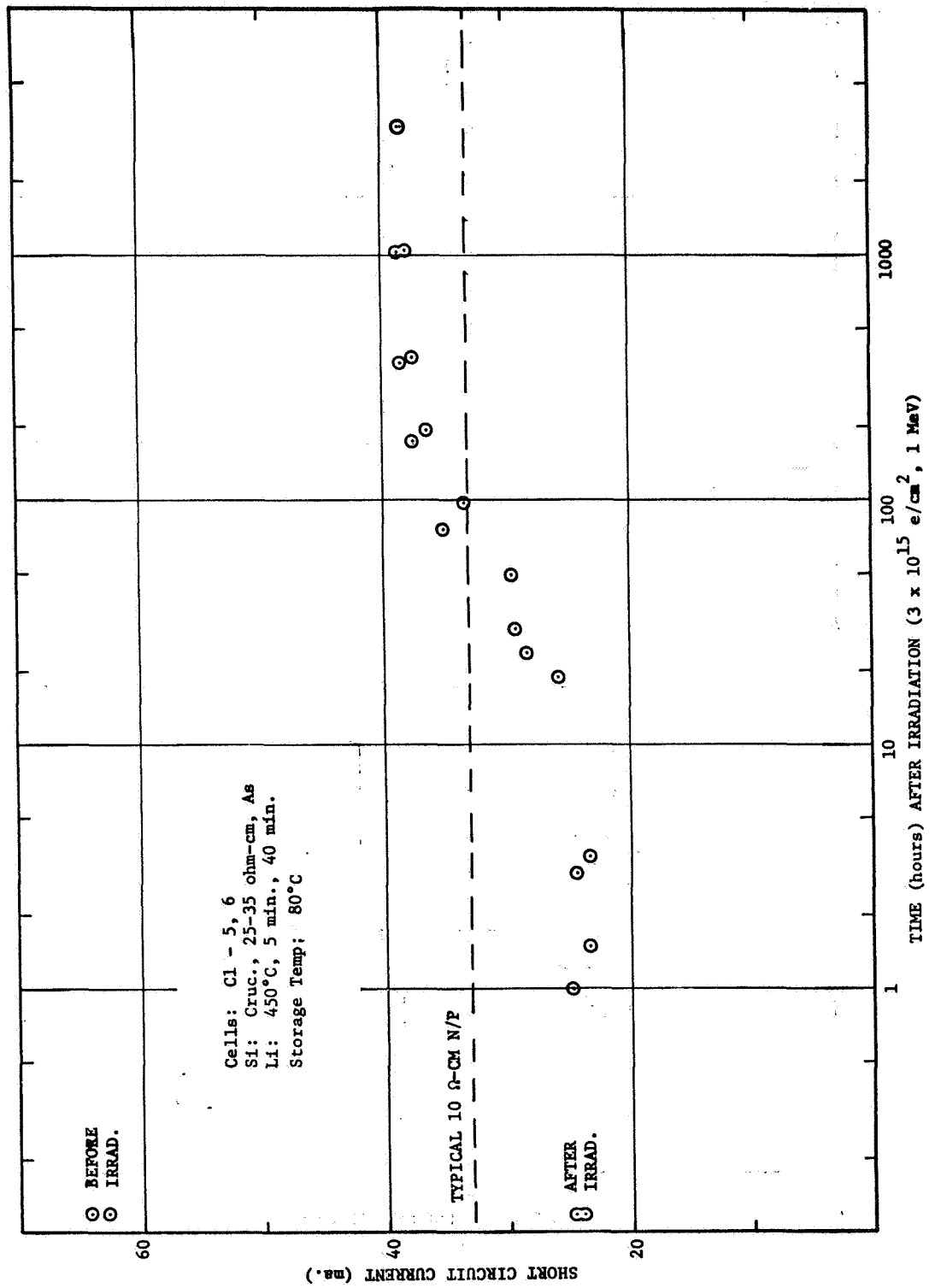


Fig. 8. RECOVERY OF GROUP C1 LITHIUM SOLAR CELLS AT 80°C



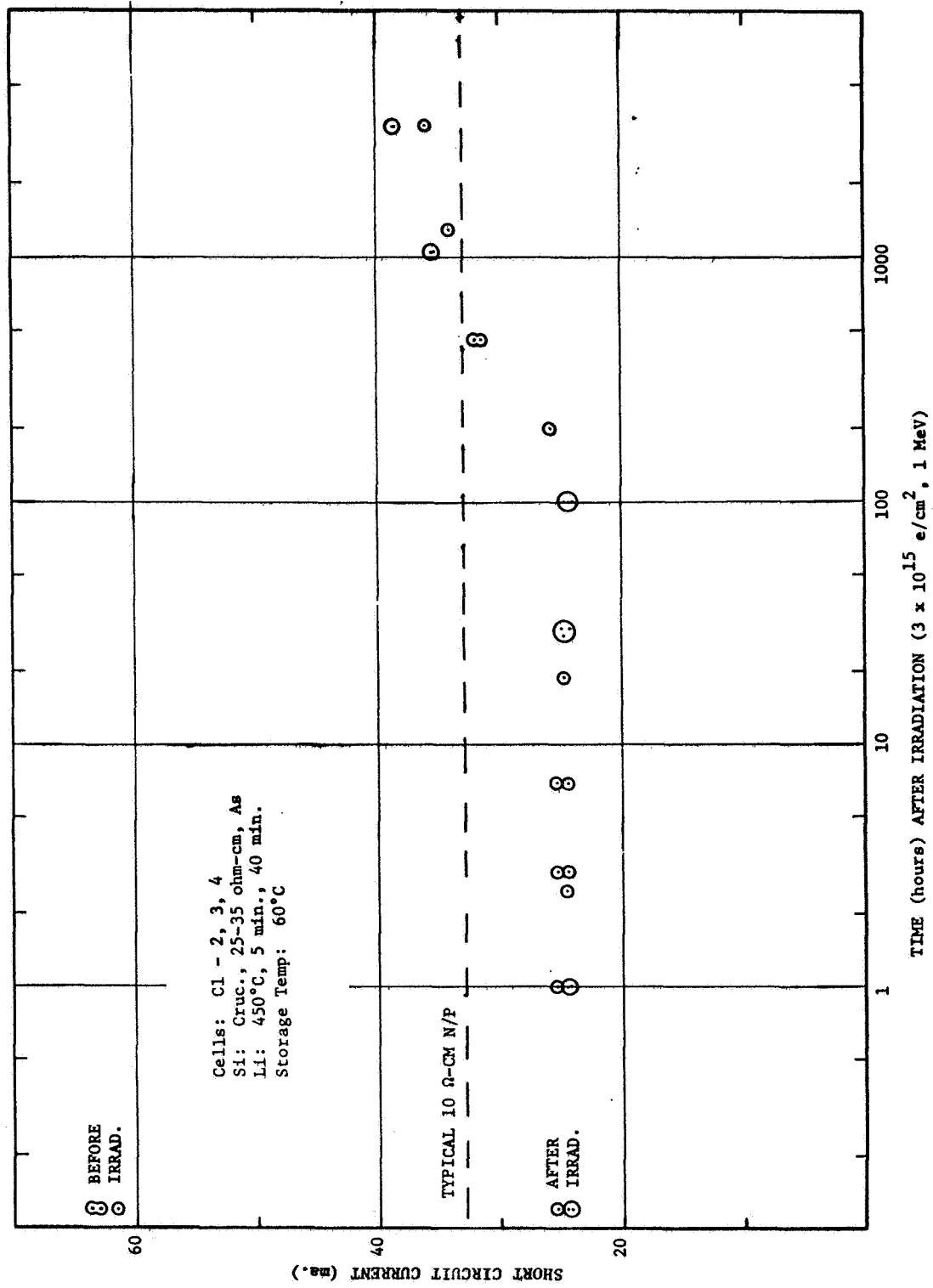


FIG. 9. RECOVERY OF GROUP C1 LITHIUM SOLAR CELLS AT 60°C

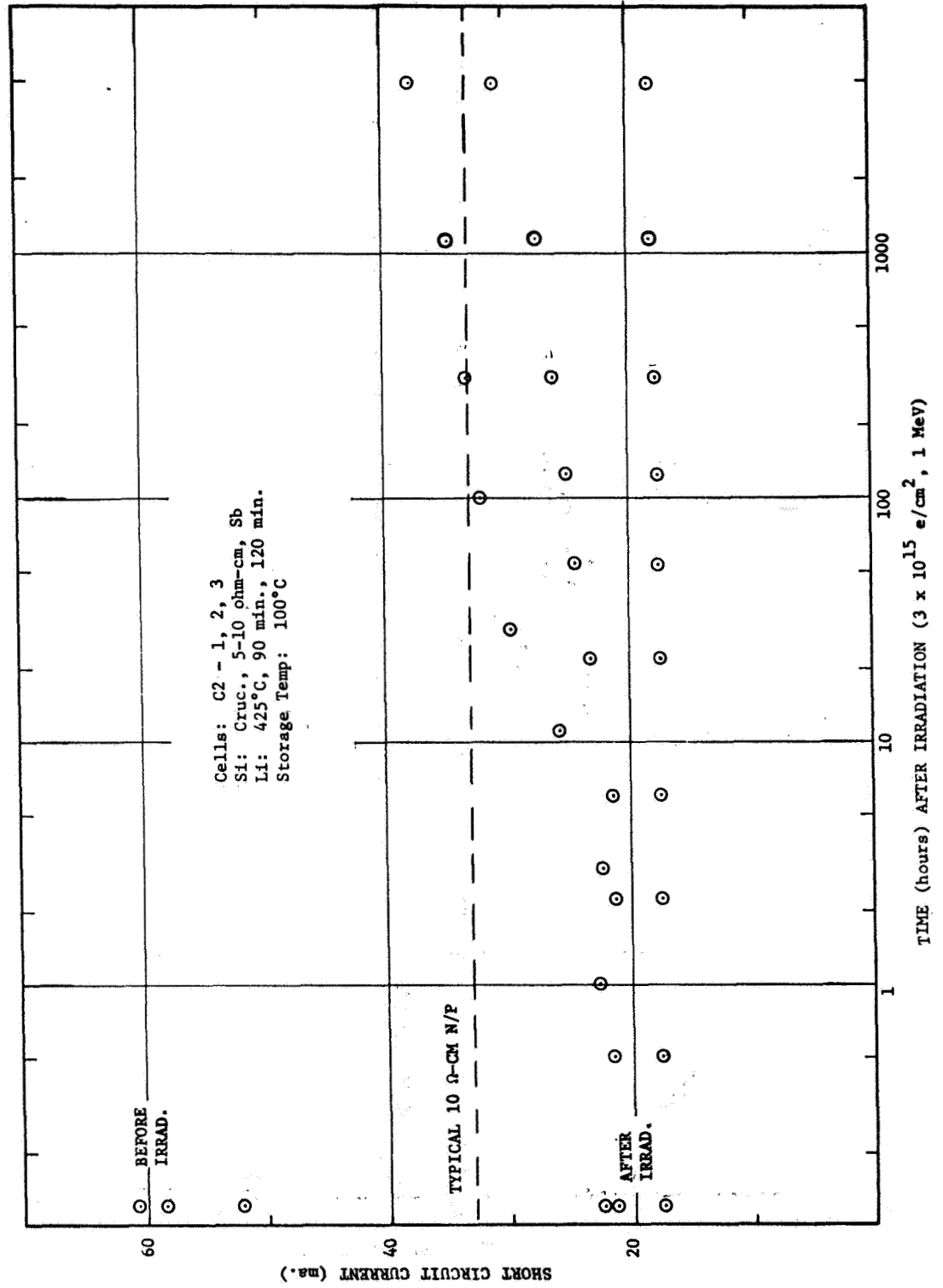


FIG. 10. RECOVERY OF GROUP C2 LITHIUM SOLAR CELLS AT 100°C

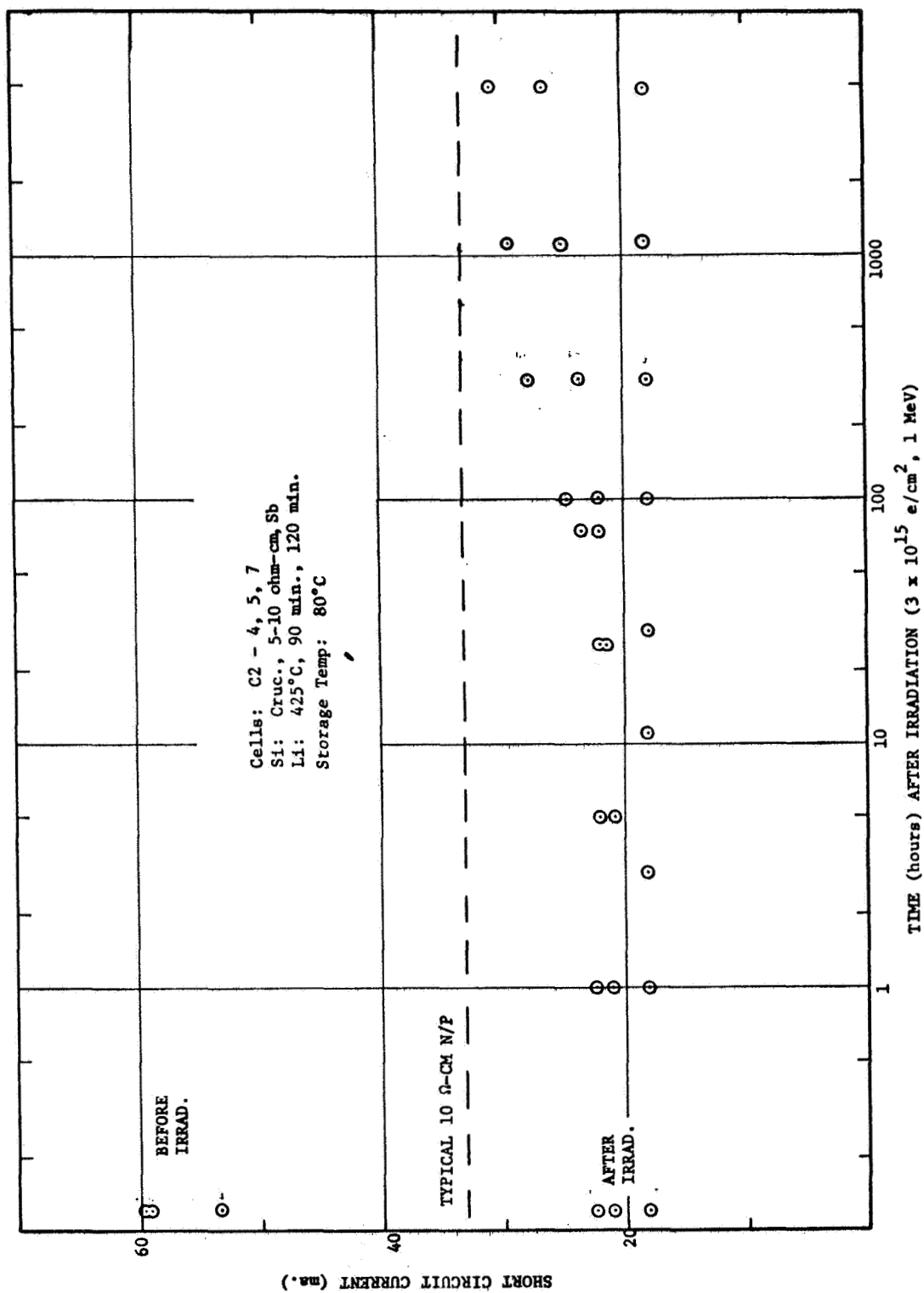


FIG. 11. RECOVERY OF GROUP C2 LITHIUM SOLAR CELLS AT 80°C

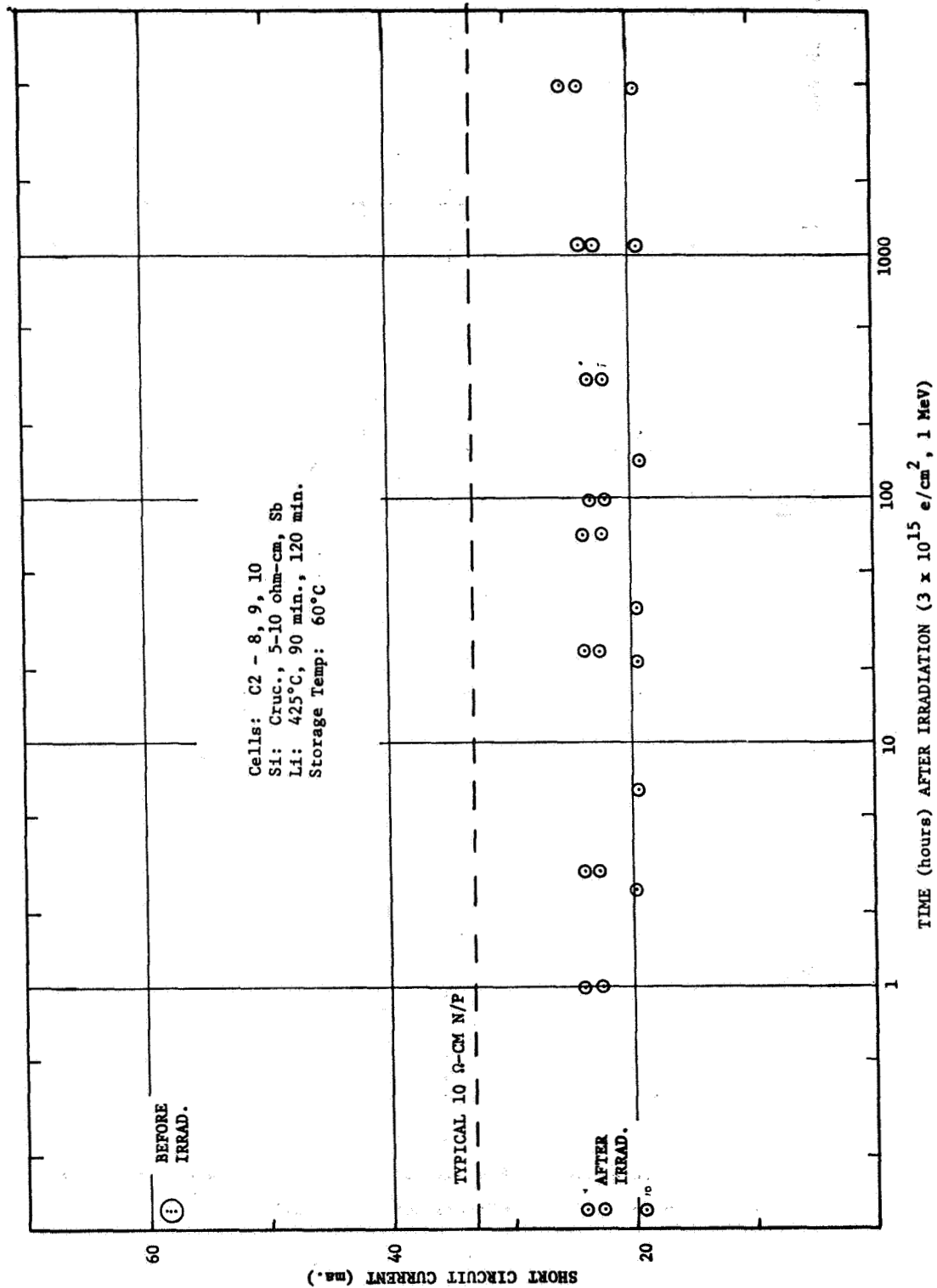


FIG. 12 RECOVERY OF GROUP C2 LITHIUM SOLAR CELLS AT 60°C

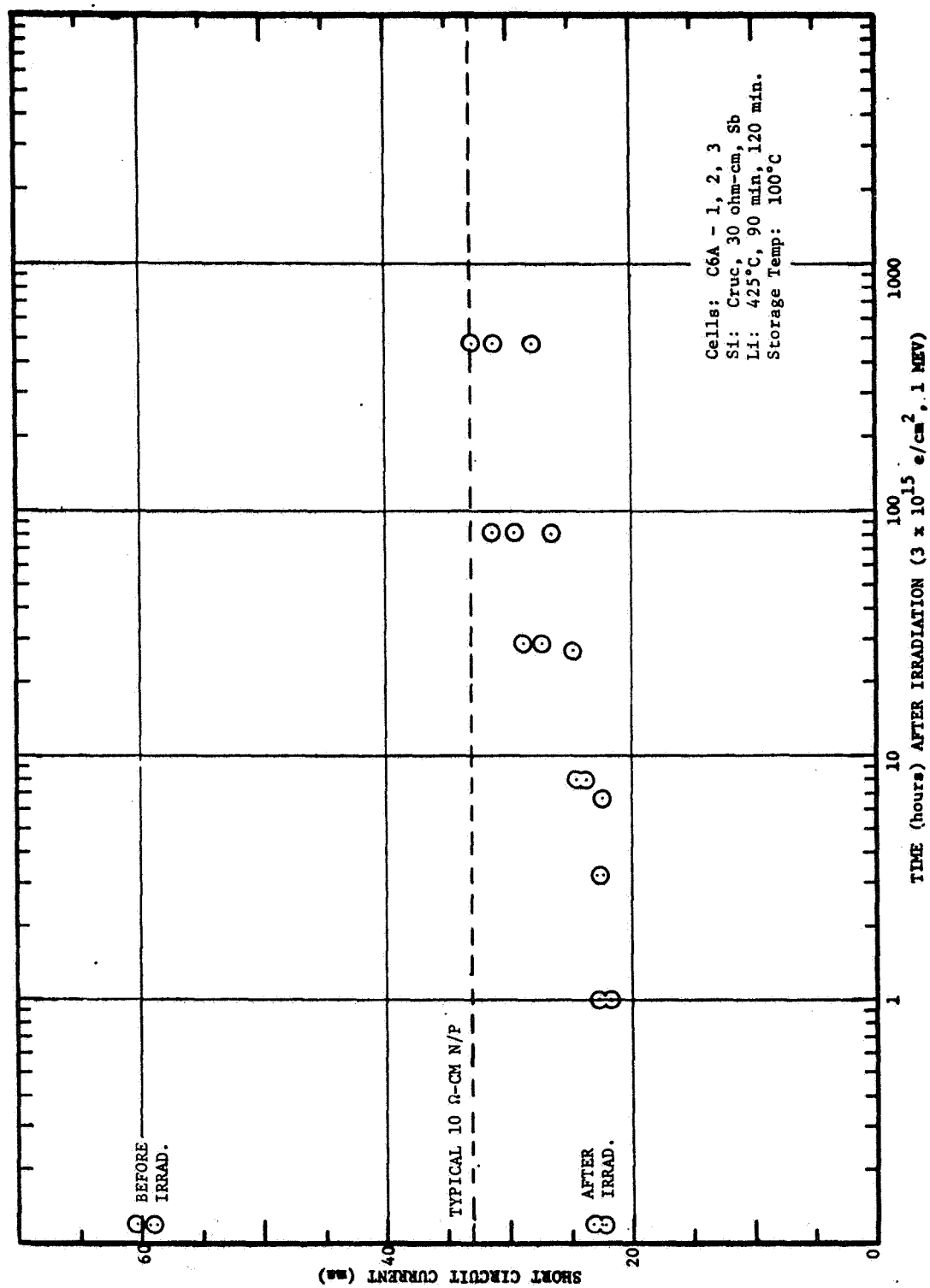


FIG. 13 RECOVERY OF GROUP C6A LITHIUM SOLAR CELLS AT 100°C

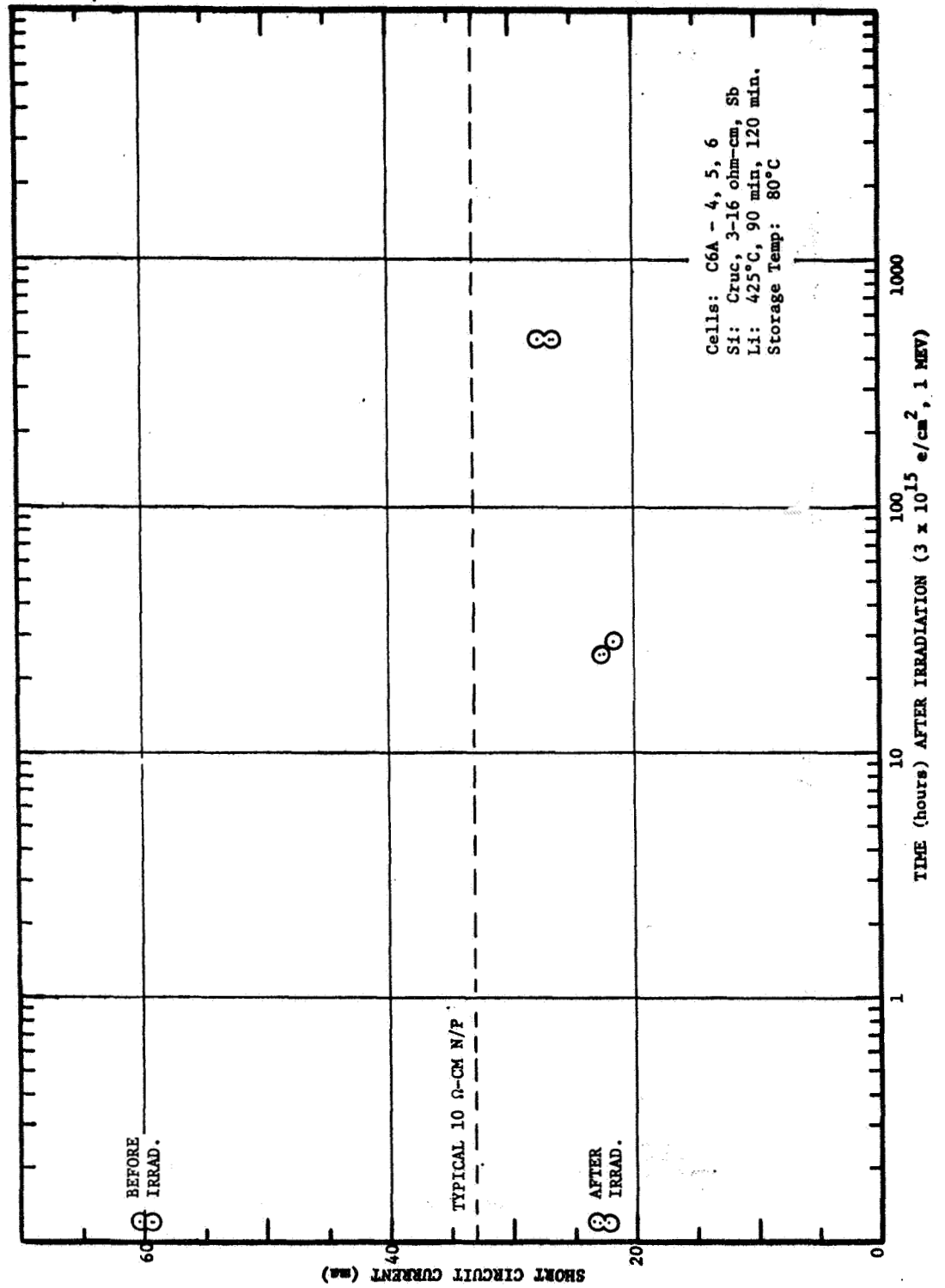


FIG. 14 RECOVERY OF GROUP C6A LITHIUM SOLAR CELLS AT 80°C

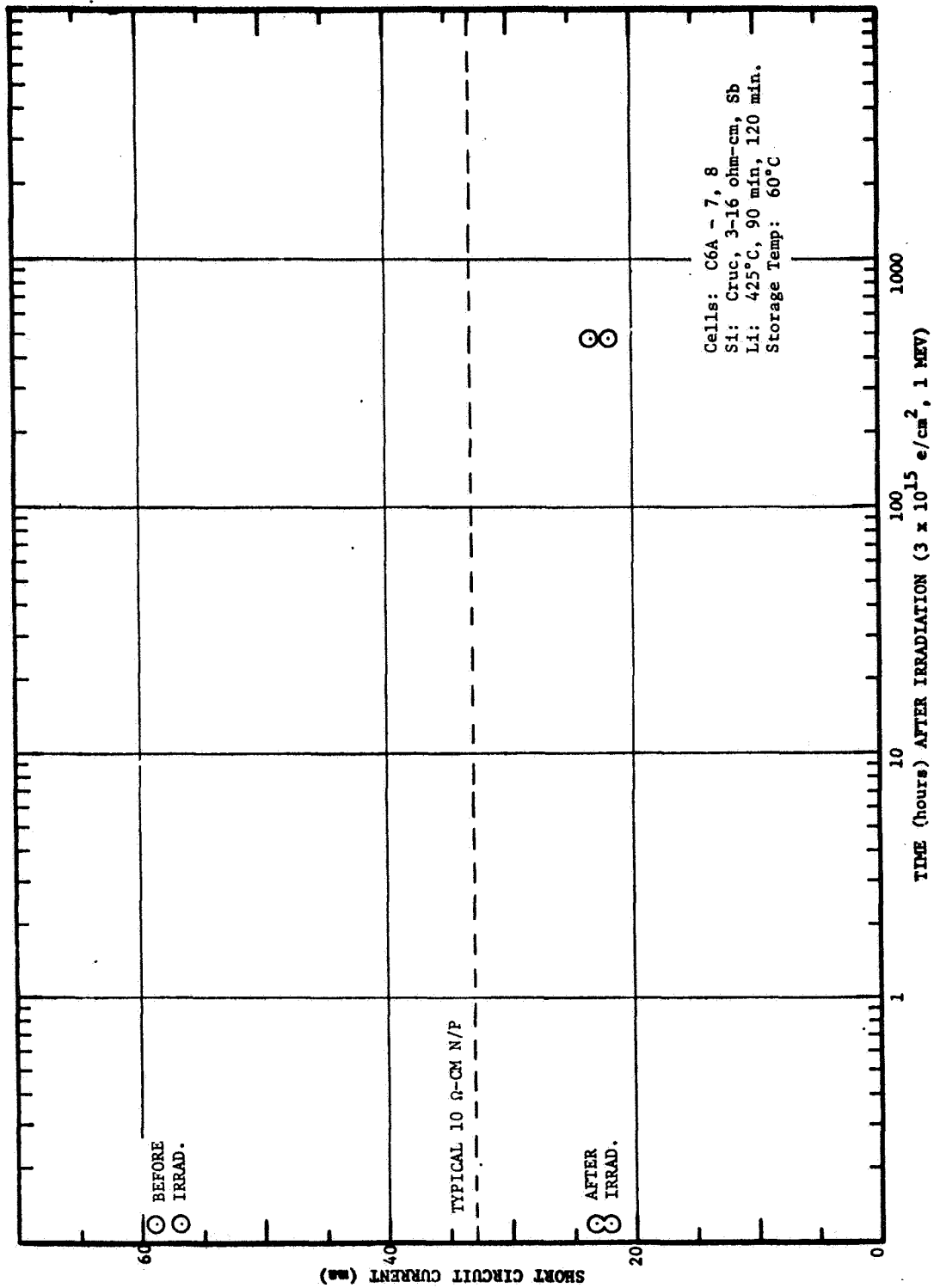


FIG. 15 RECOVERY OF GROUP C6A LITHIUM SOLAR CELLS AT 60°C

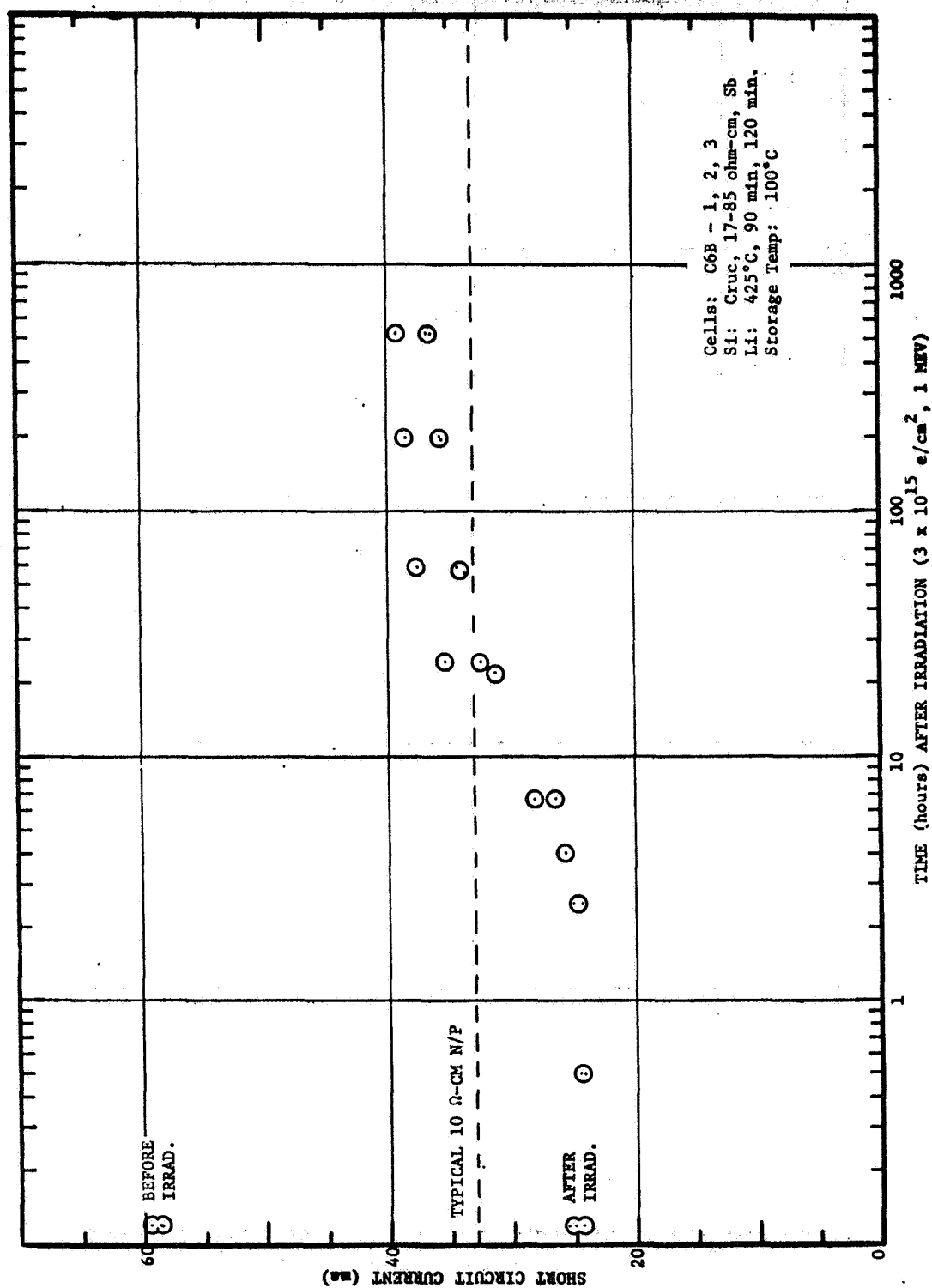


FIG. 16 RECOVERY OF GROUP C6B LITHIUM SOLAR CELLS AT 100°C



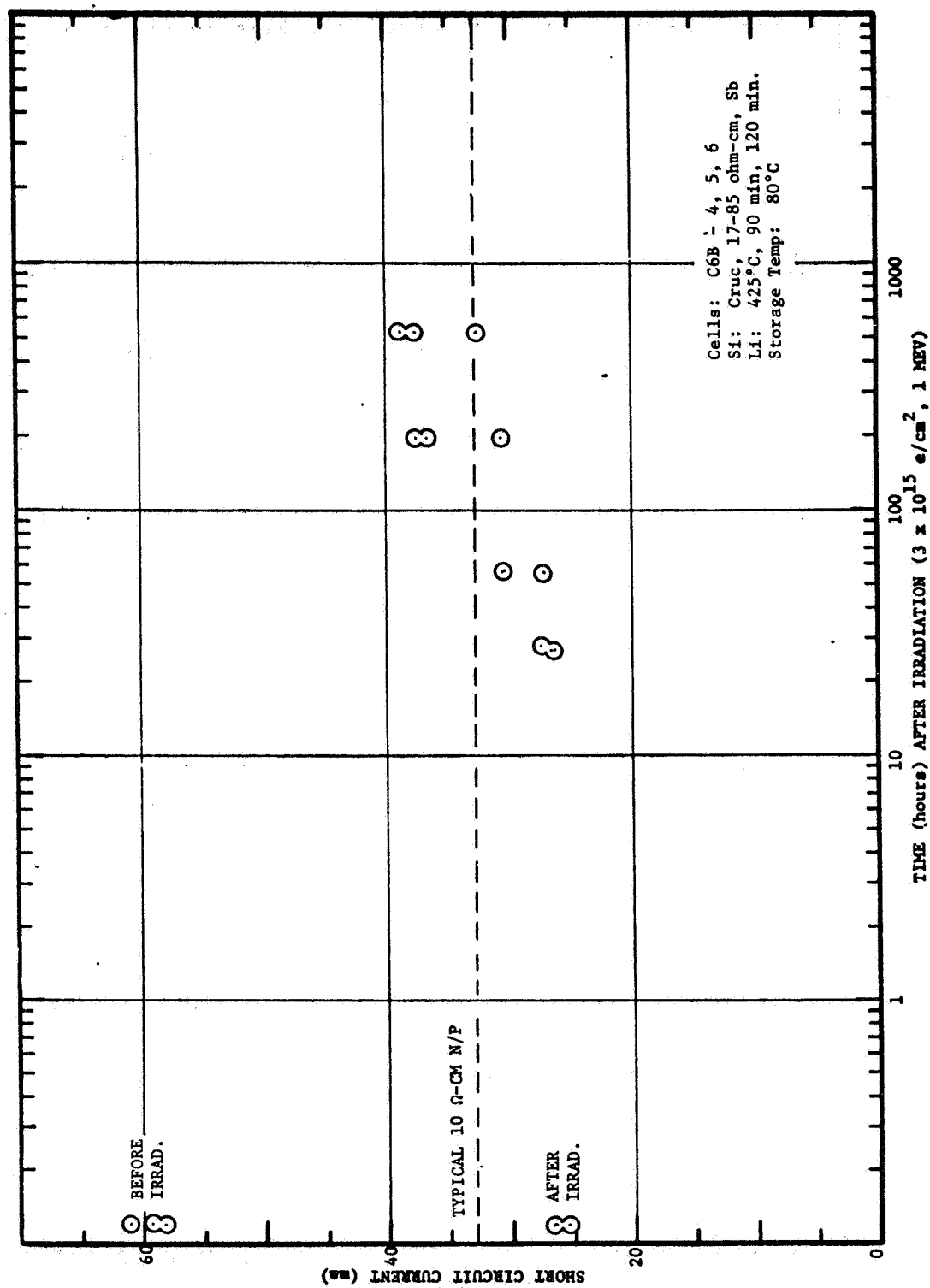


FIG. 17 RECOVERY OF GROUP C6B LITHIUM SOLAR CELLS AT 80°C

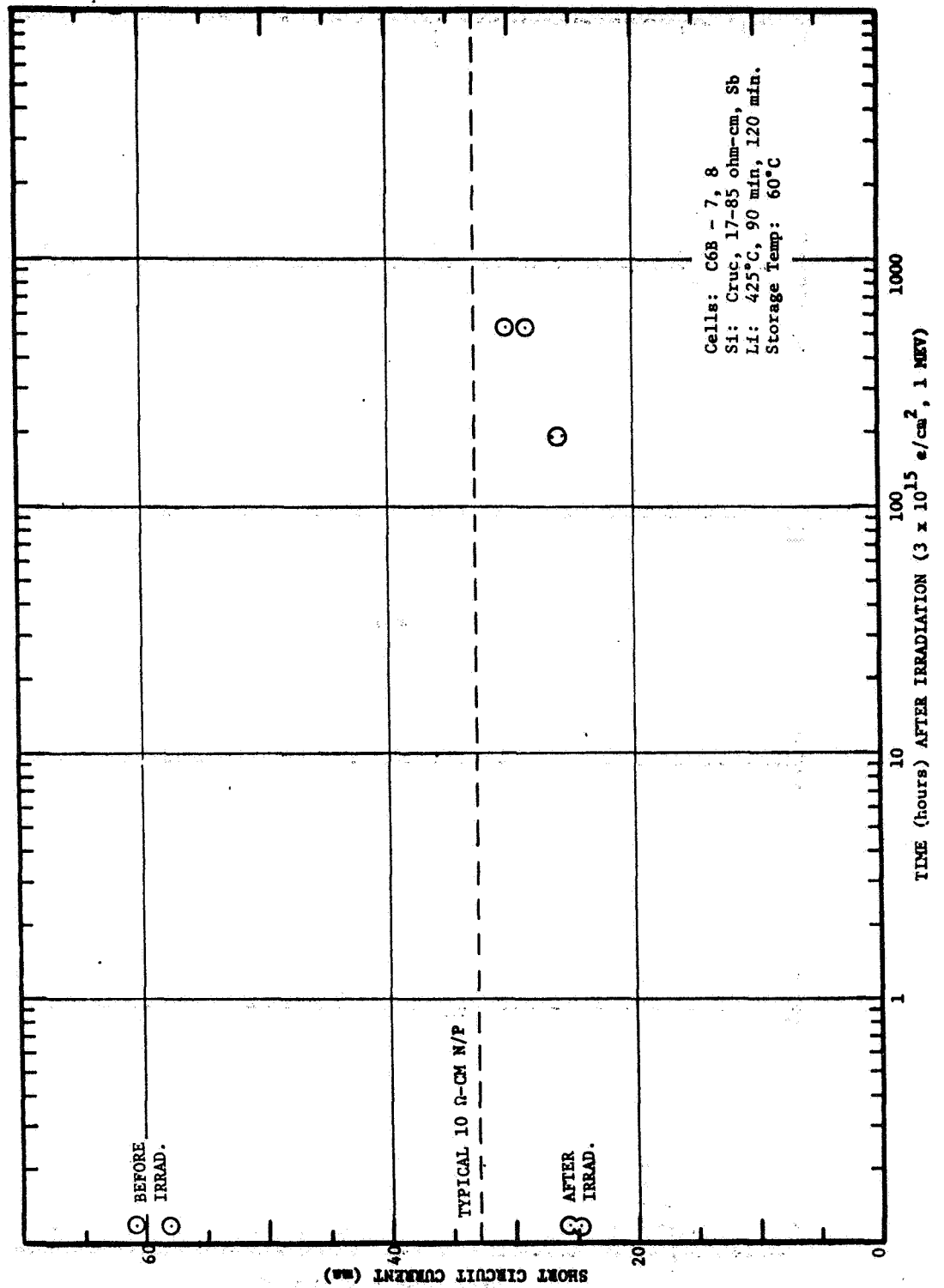


FIG. 18 RECOVERY OF GROUP C6B LITHIUM SOLAR CELLS AT 60°C

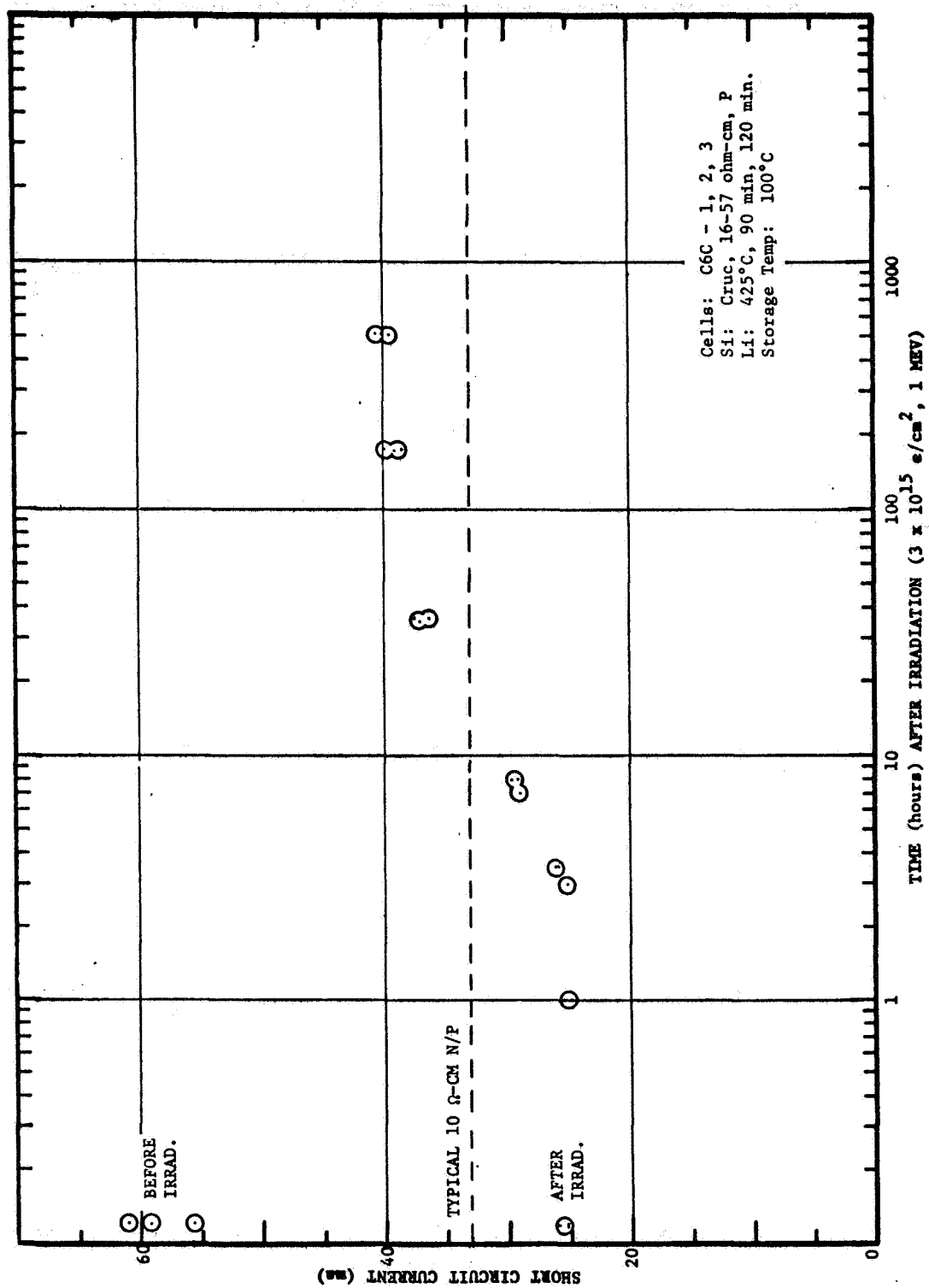


FIG. 19 RECOVERY OF GROUP C6C LITHIUM SOLAR CELLS AT 100°C

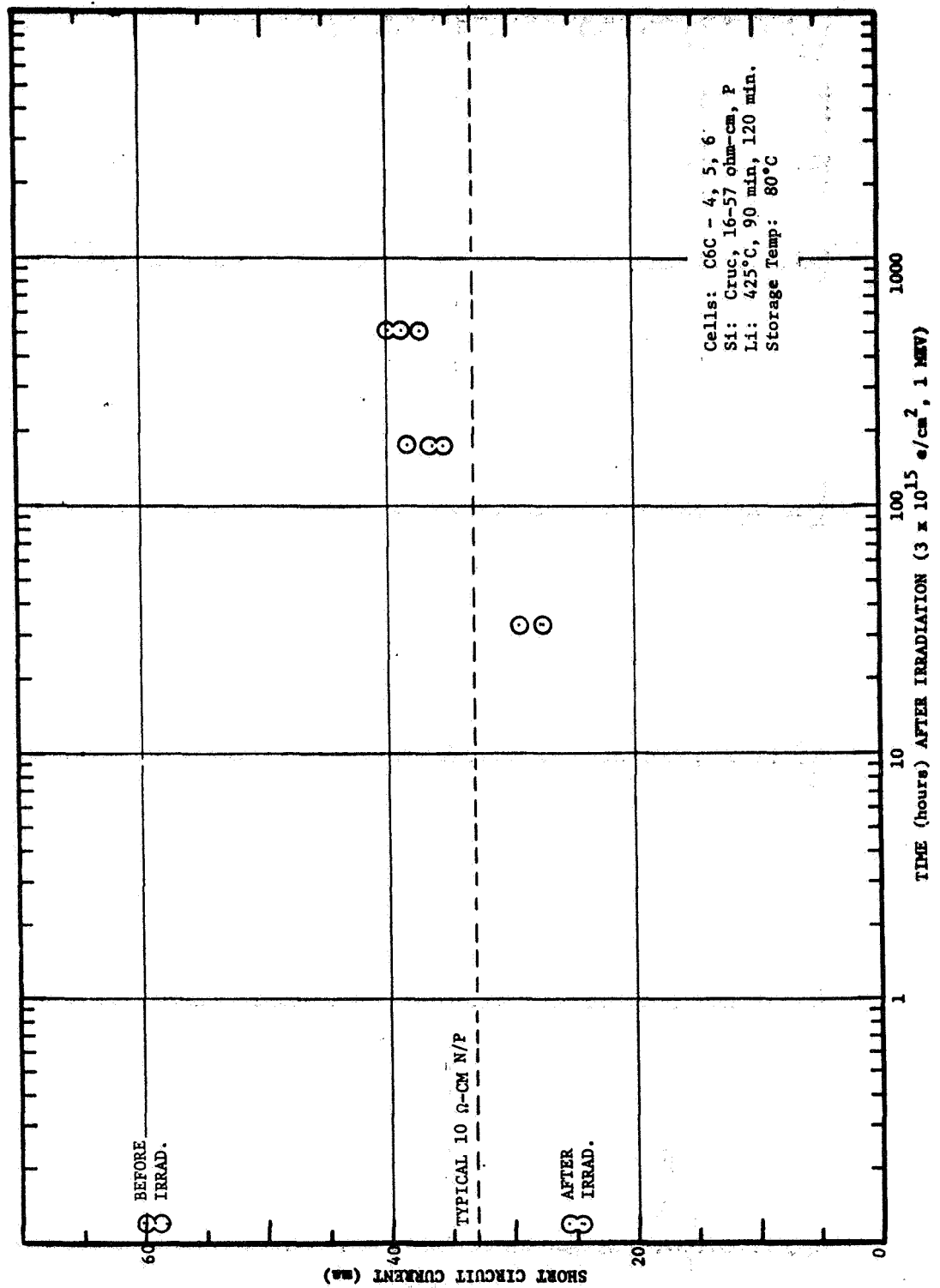


FIG. 20 RECOVERY OF GROUP C6C LITHIUM SOLAR CELLS AT 80°C

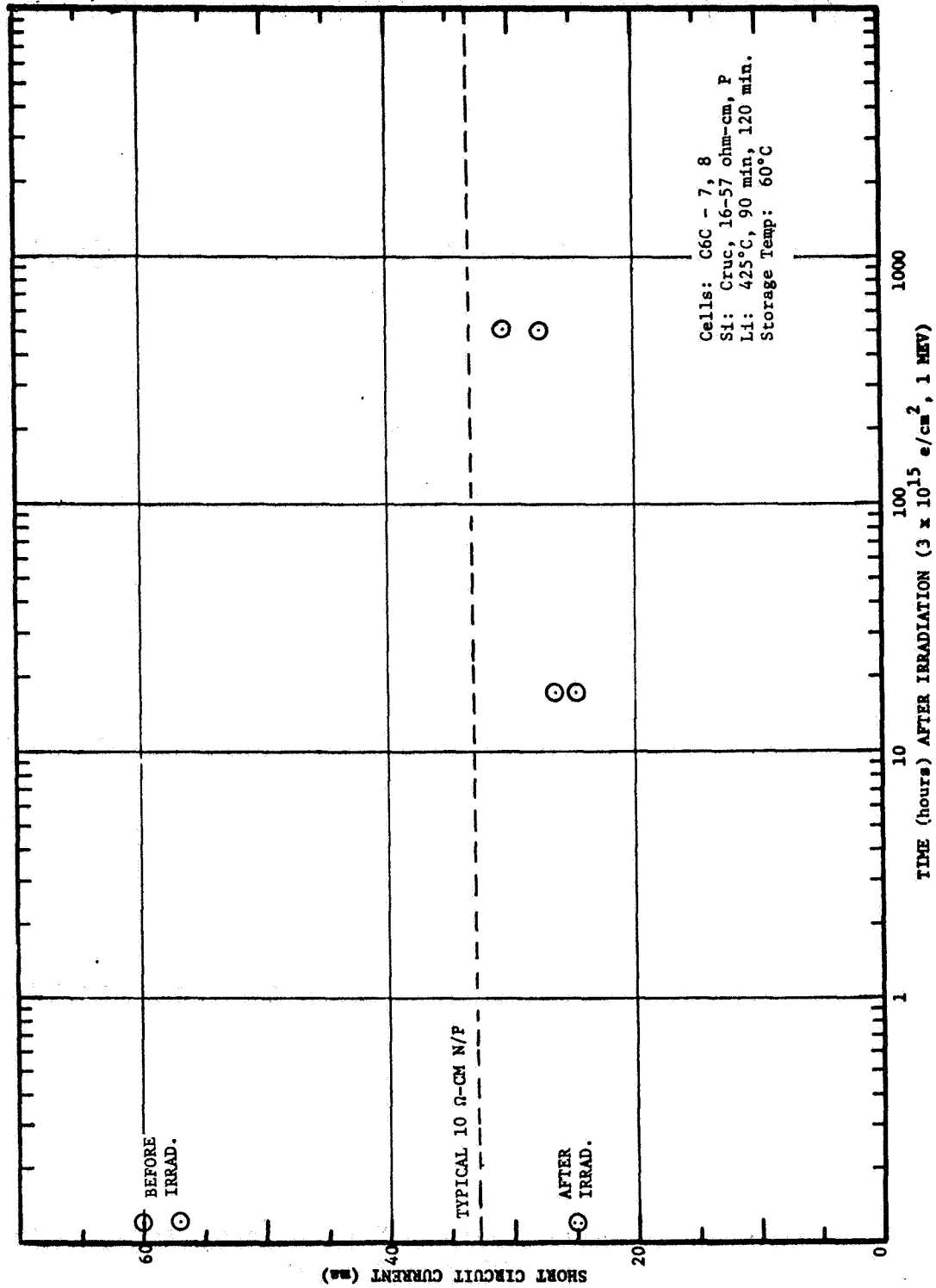


FIG. 21 RECOVERY OF GROUP C6C LITHIUM SOLAR CELLS AT 60°C

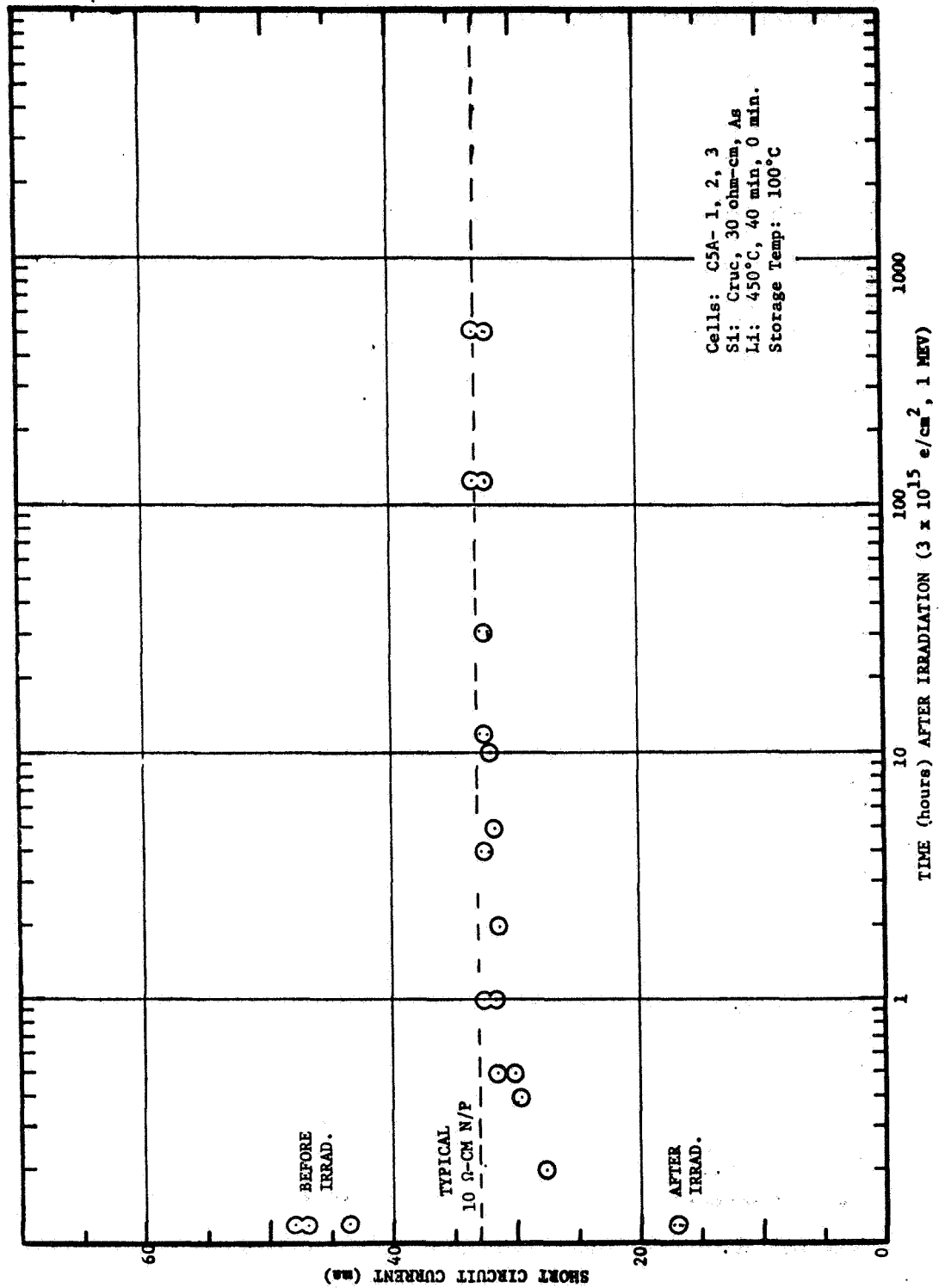


FIG. 22 RECOVERY OF GROUP C5A LITHIUM SOLAR CELLS AT 100°C

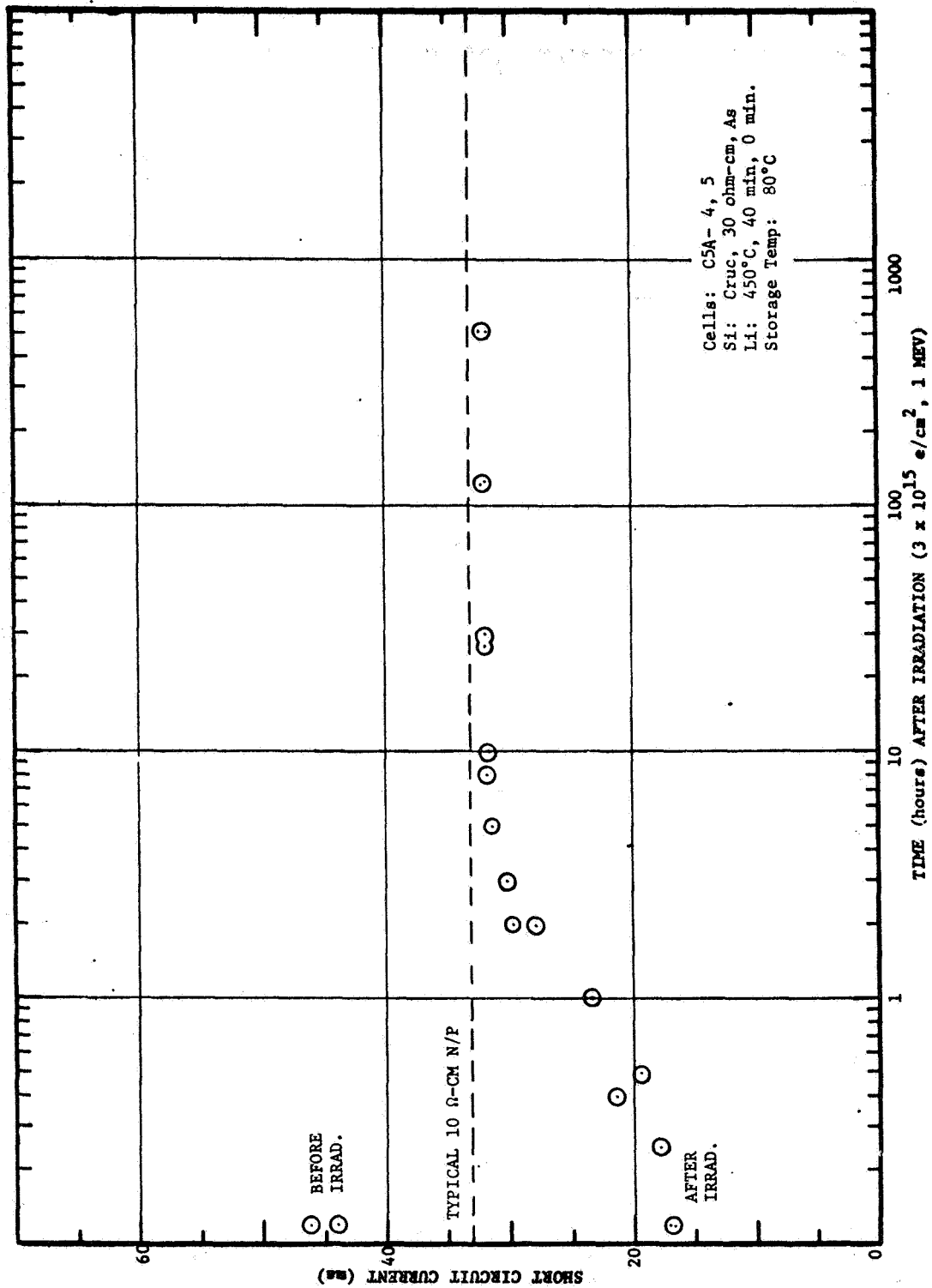


FIG. 23 RECOVERY OF GROUP C5A LITHIUM SOLAR CELLS AT 80°C

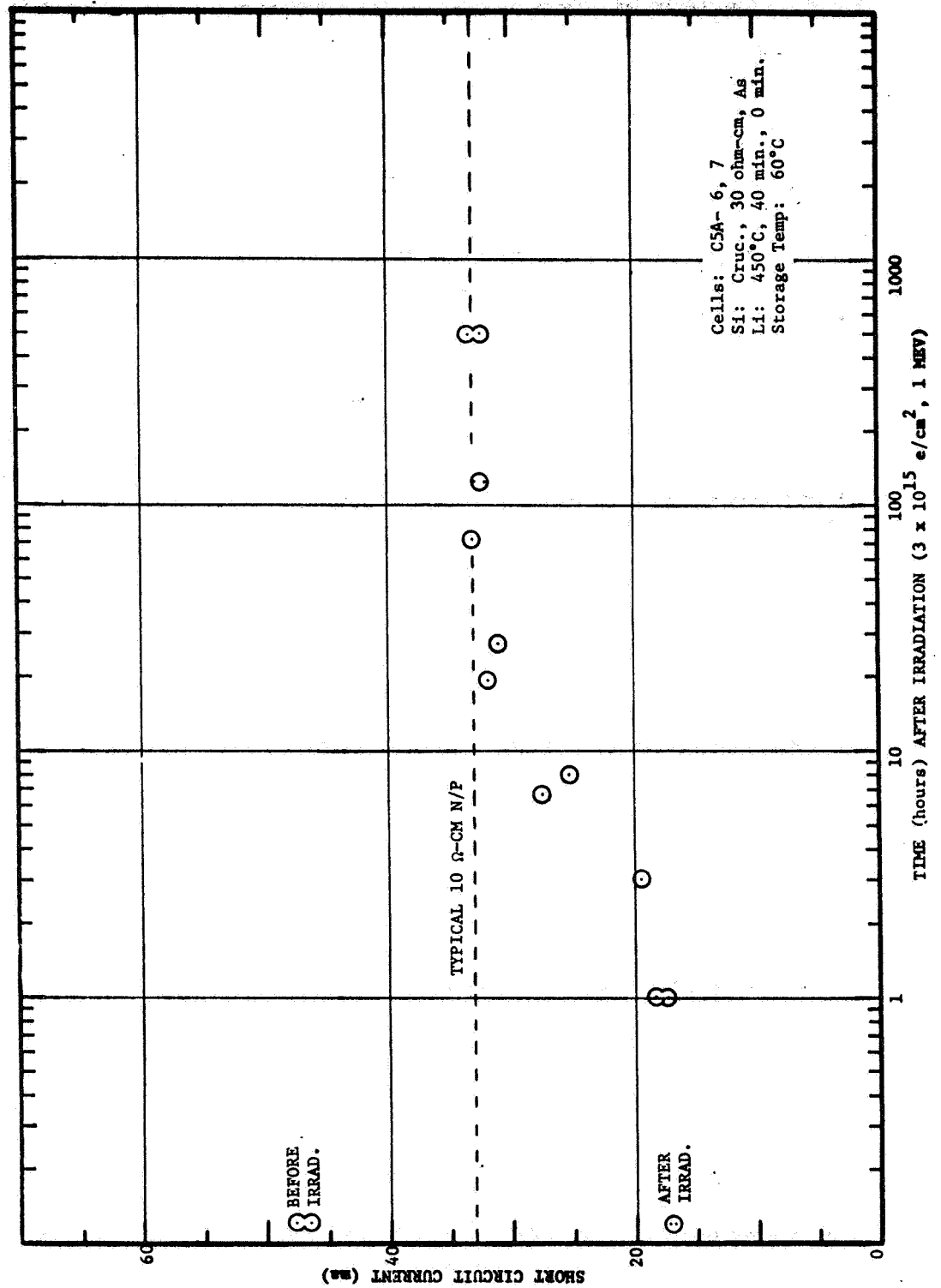


FIG. 24 RECOVERY OF GROUP C5A LITHIUM SOLAR CELLS AT 60°C



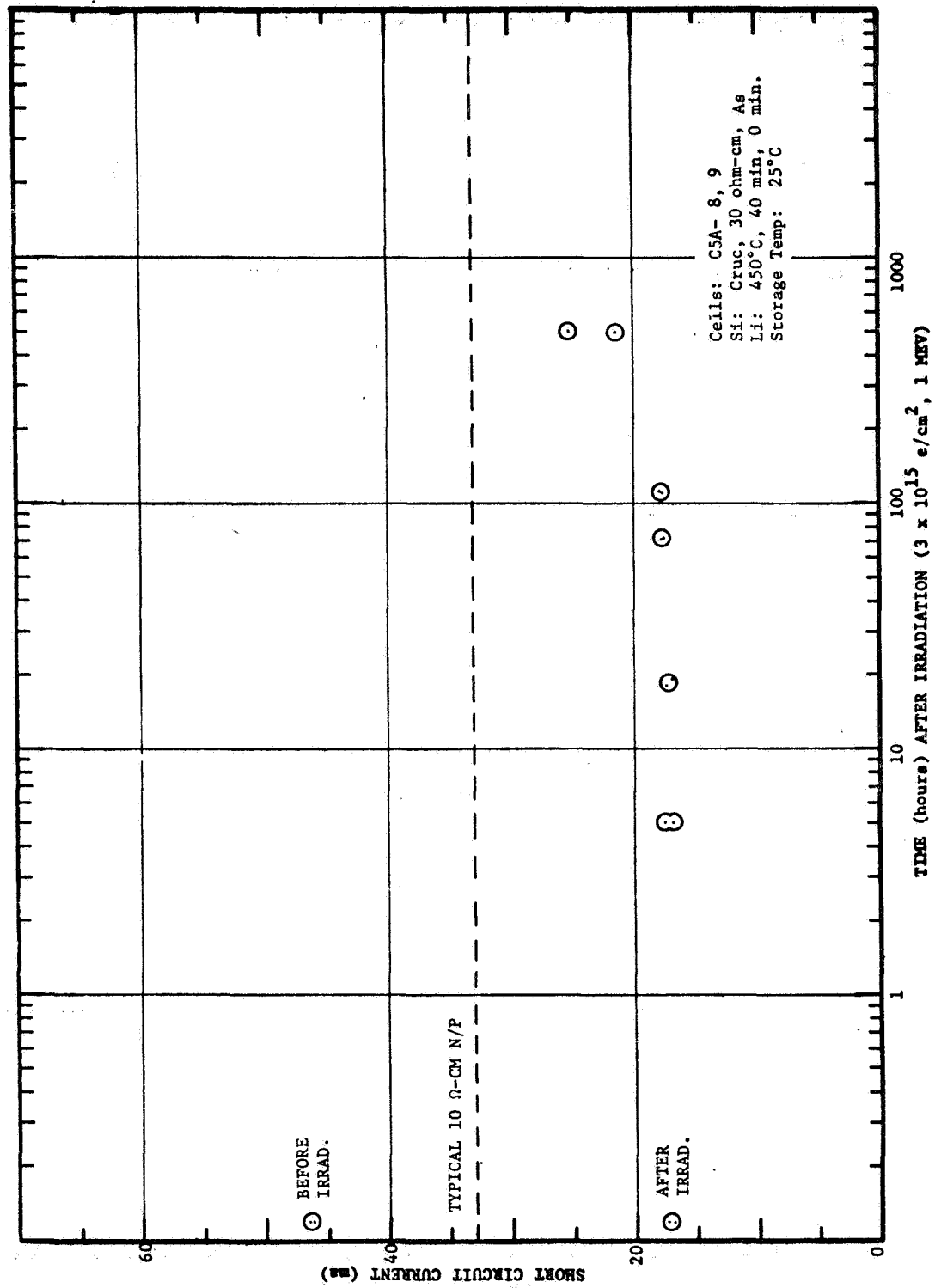


FIG. 25 RECOVERY OF GROUP C5A LITHIUM SOLAR CELLS AT 25°C

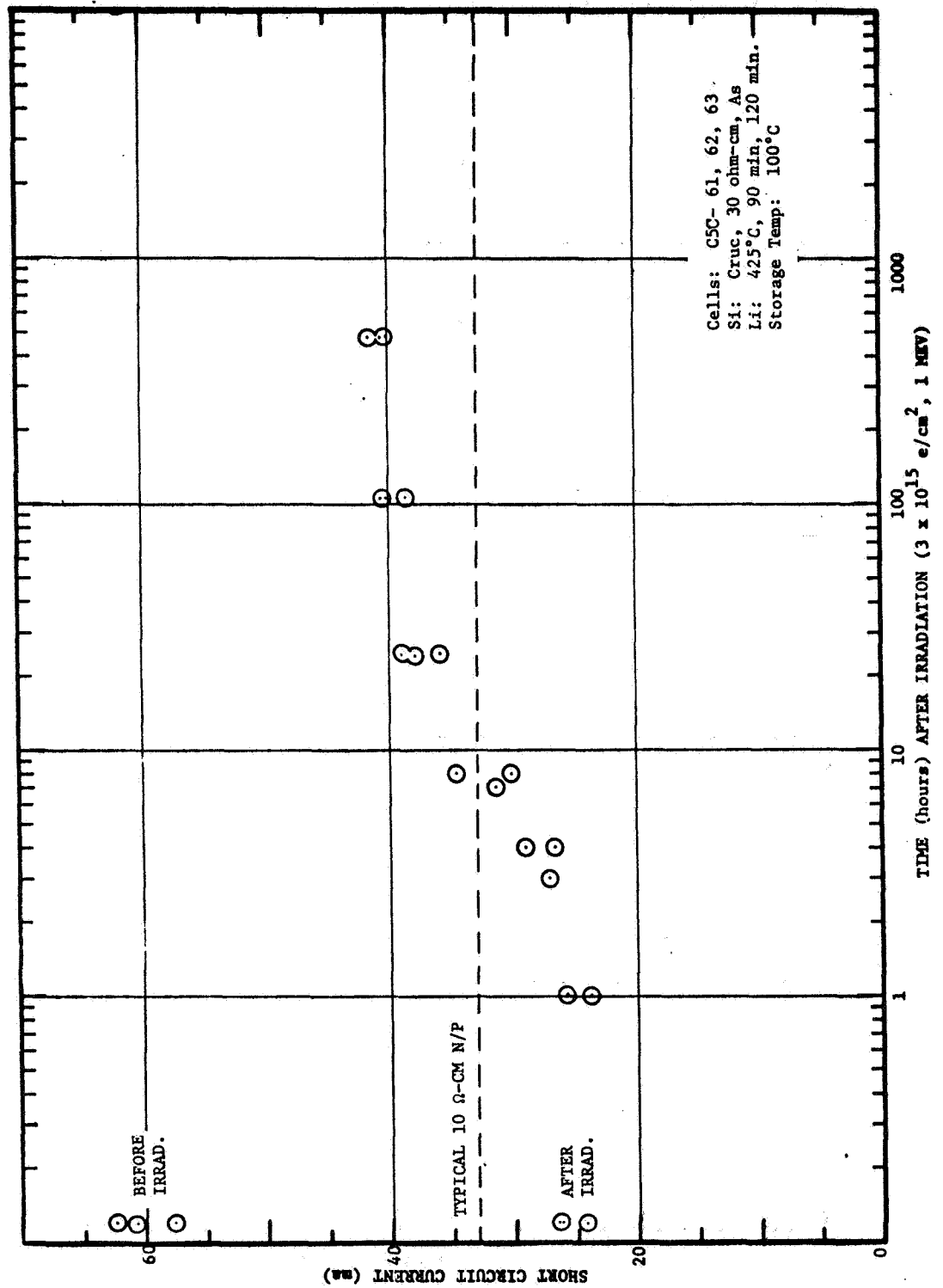


FIG. 26 RECOVERY OF GROUP C5C LITHIUM SOLAR CELLS AT 100°C

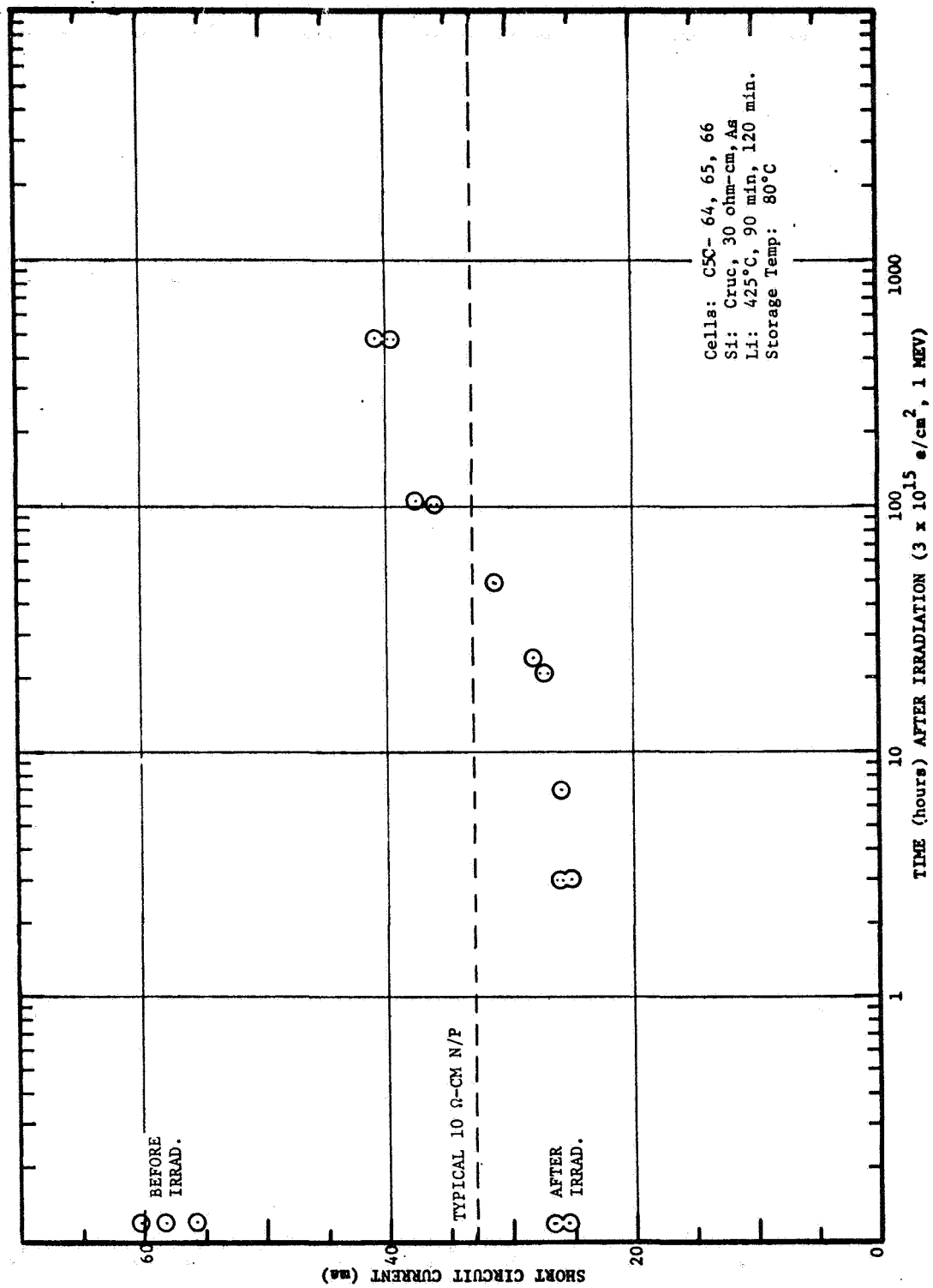


FIG. 27 RECOVERY OF GROUP C5C LITHIUM SOLAR CELLS AT 80°C

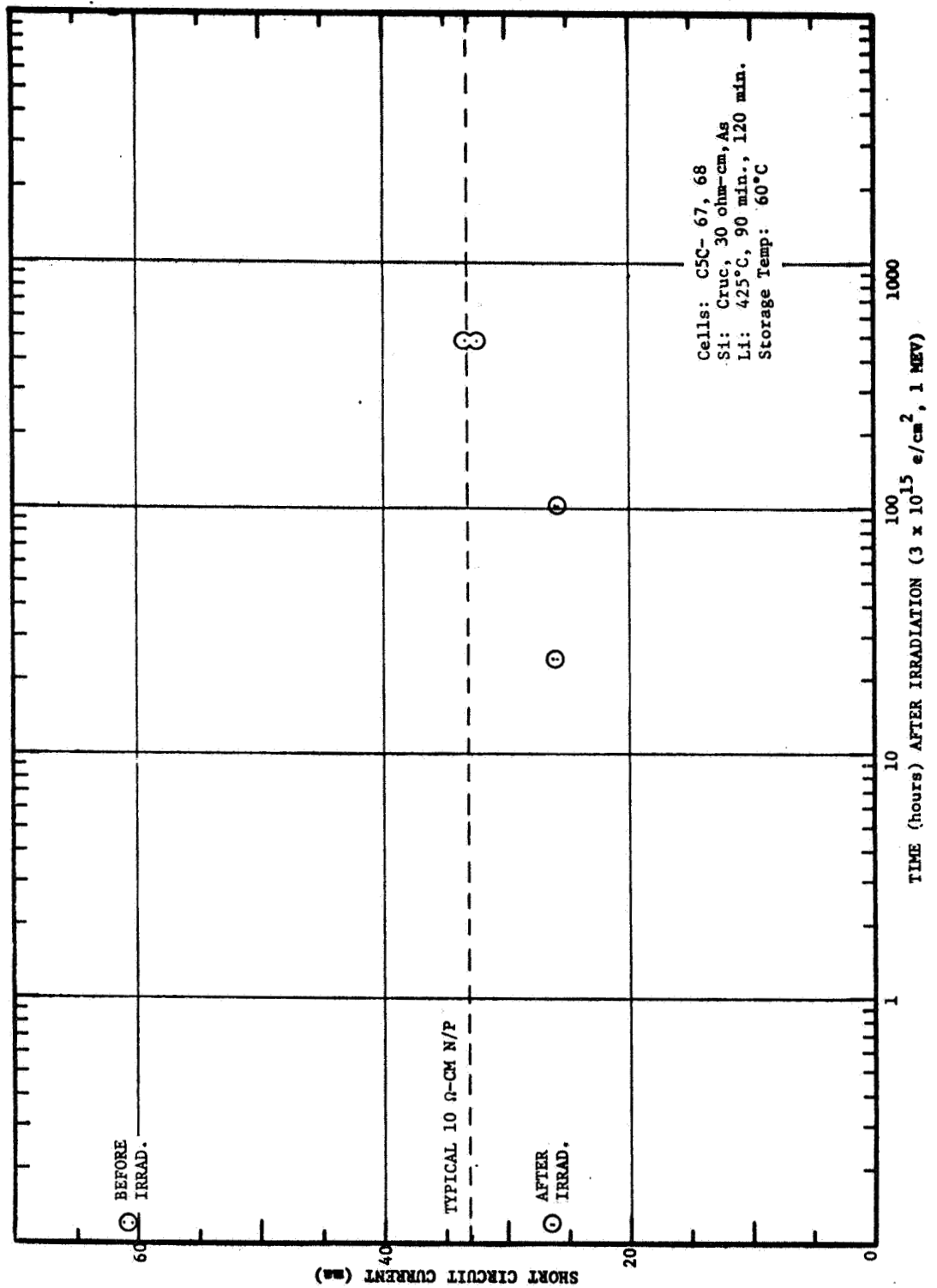


FIG. 28 RECOVERY OF GROUP C5C LITHIUM SOLAR CELLS AT 60°C

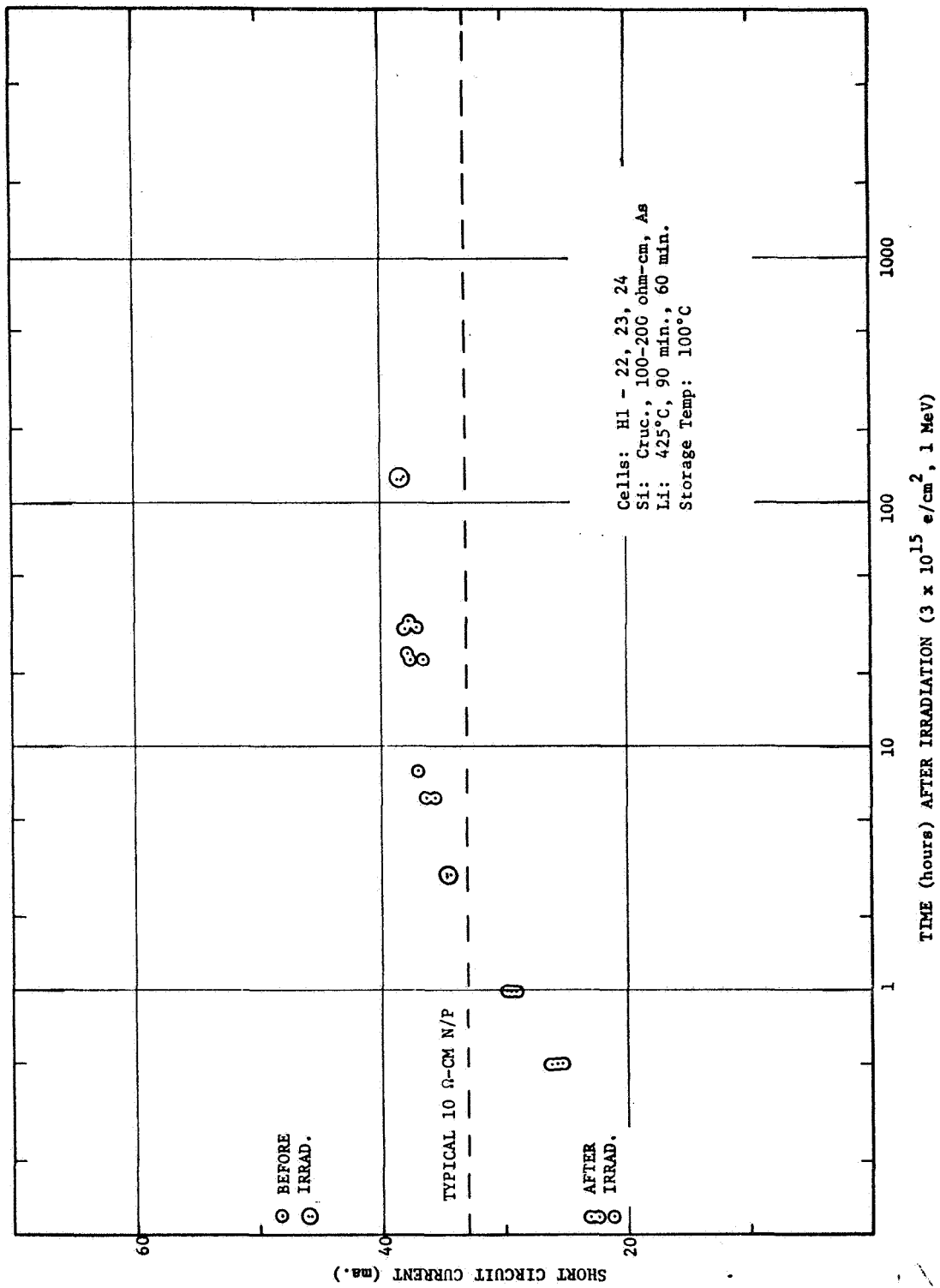


FIG. 29 RECOVERY OF GROUP H1 LITHIUM SOLAR CELLS AT 100°C

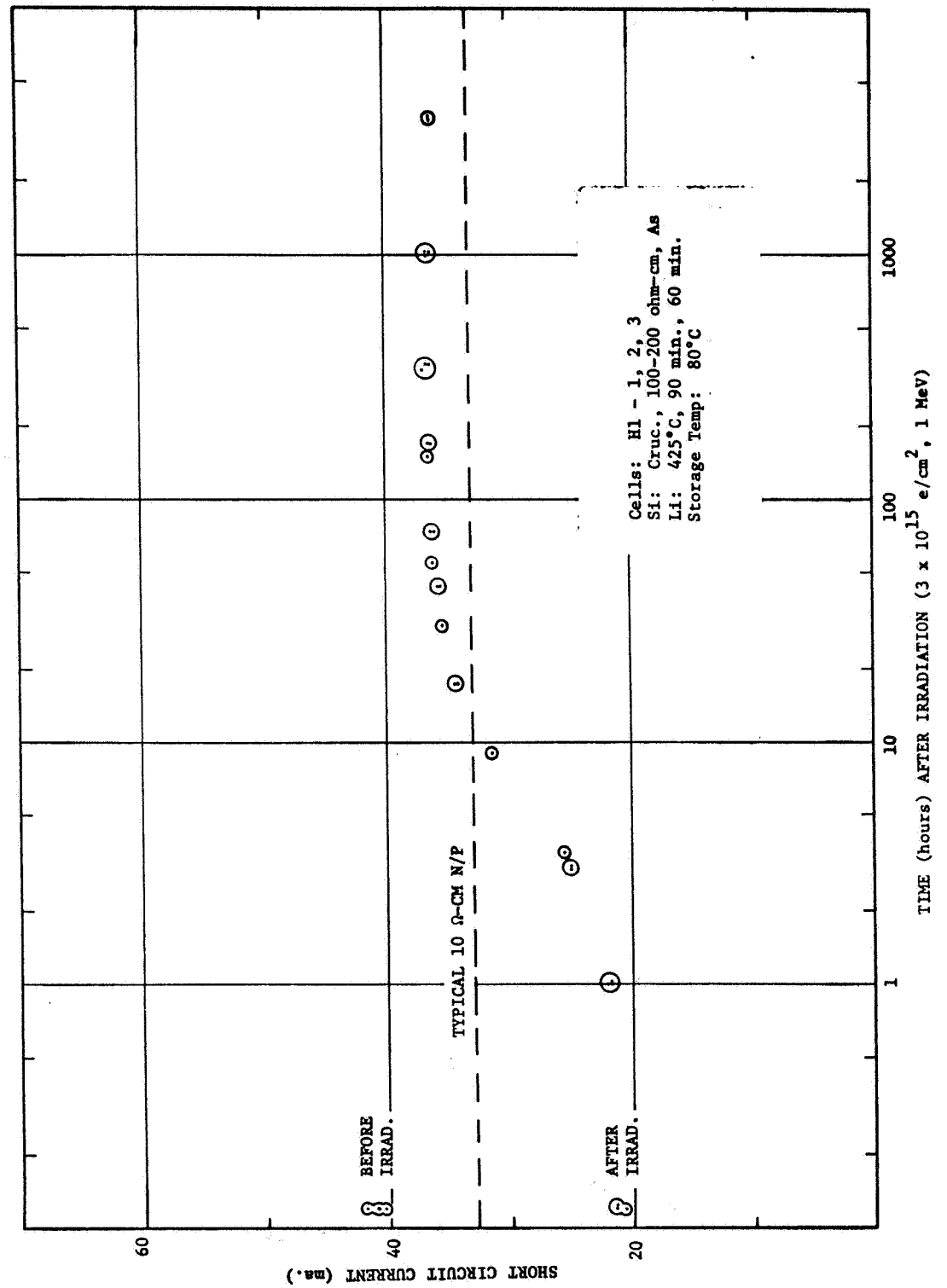


FIG. 30 RECOVERY OF GROUP H1 LITHIUM SOLAR CELLS AT 80°C

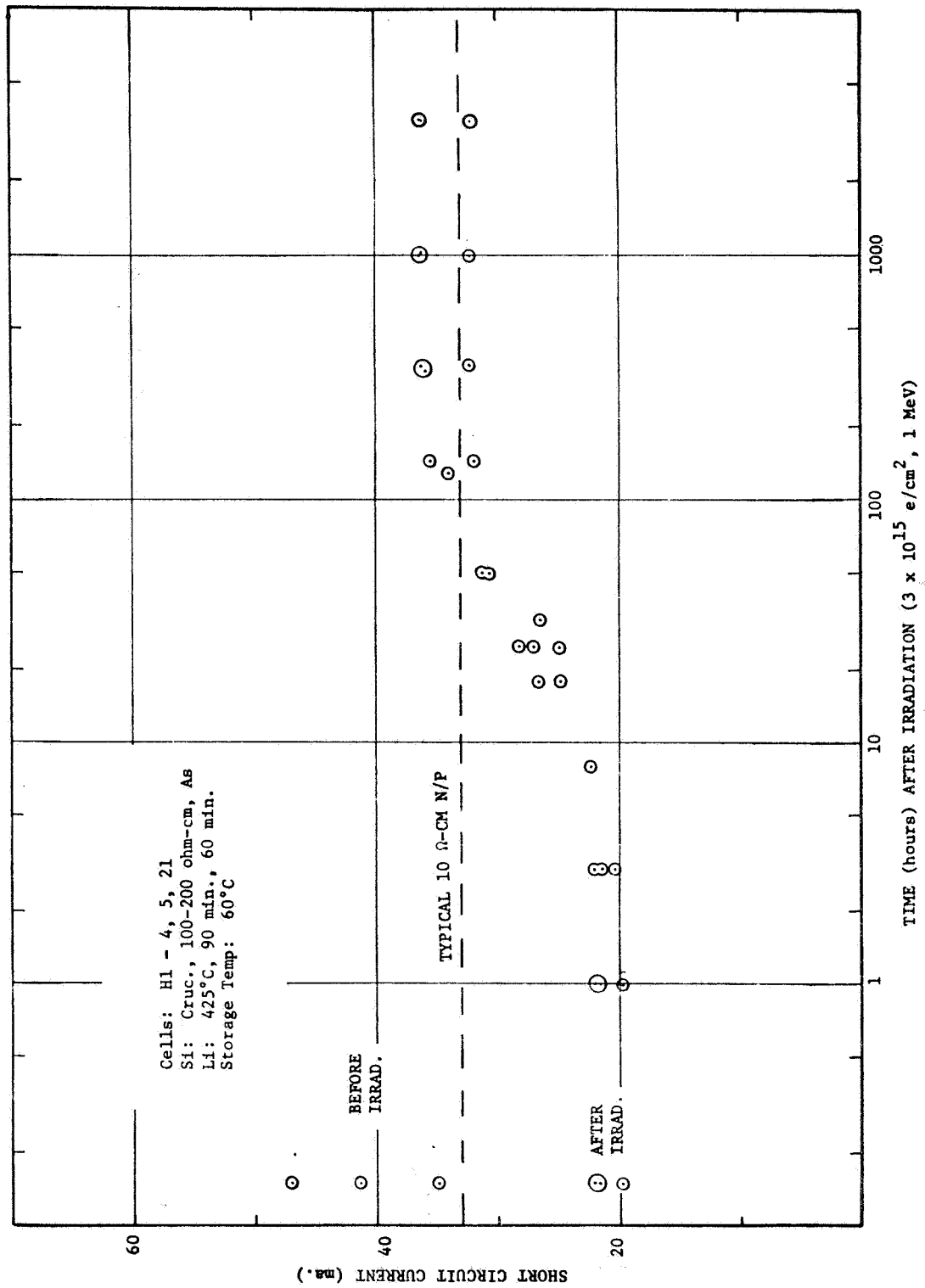


FIG. 31 RECOVERY OF GROUP H1 LITHIUM SOLAR CELLS AT 60°C

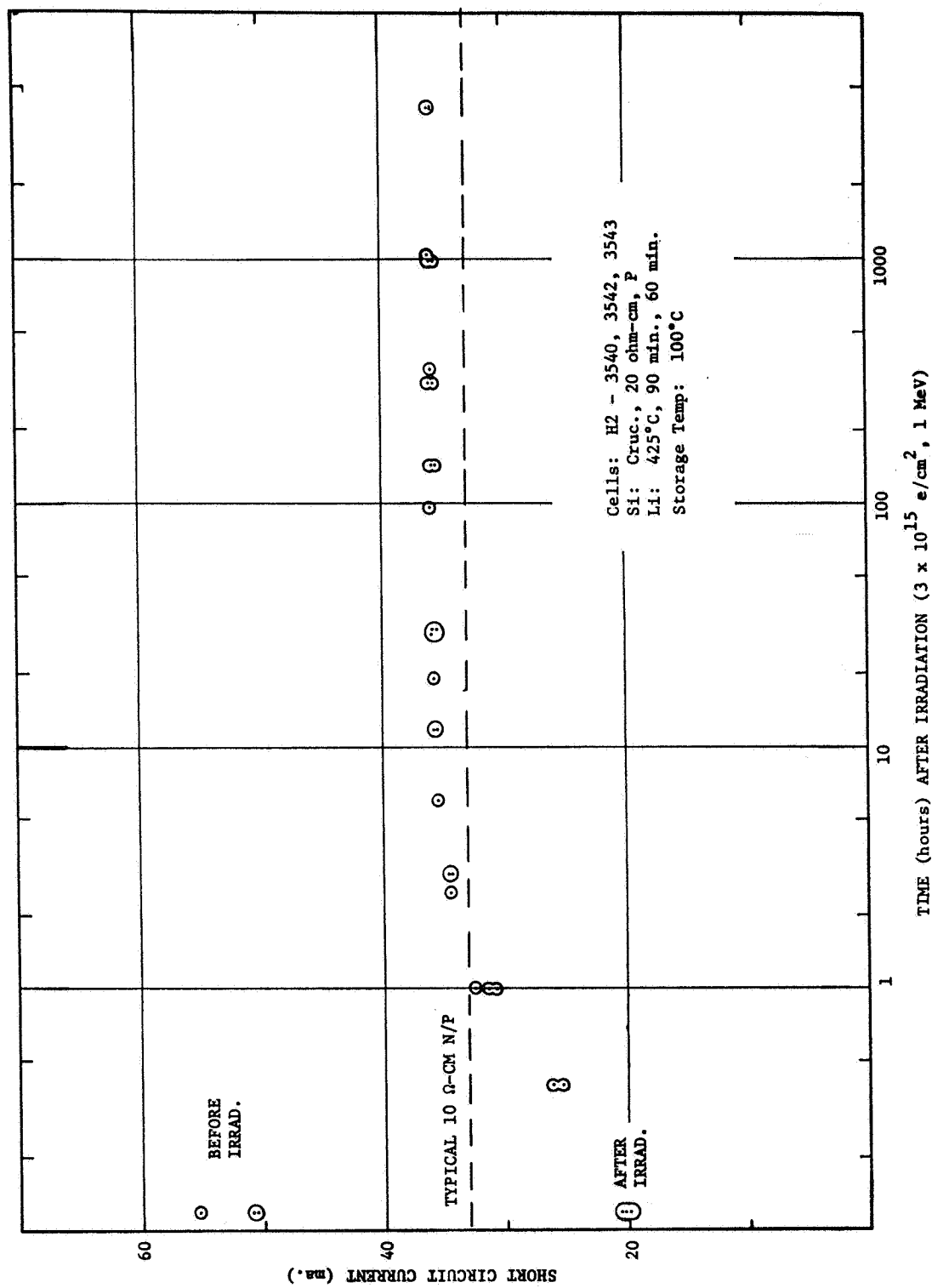


FIG. 32 RECOVERY OF GROUP H2 LITHIUM SOLAR CELLS AT 100°C



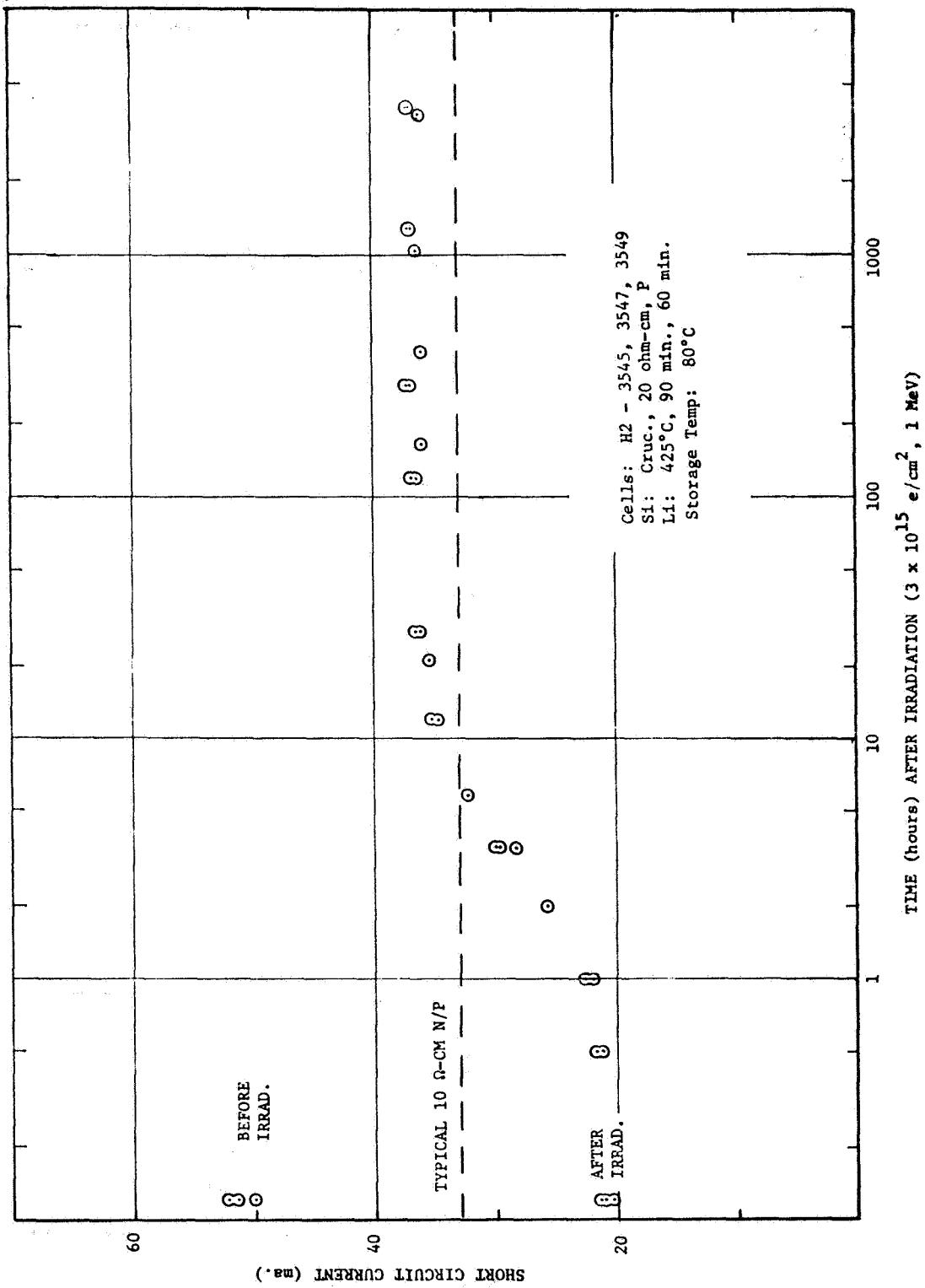


FIG. 33 RECOVERY OF GROUP H2 LITHIUM SOLAR CELLS AT 80°C

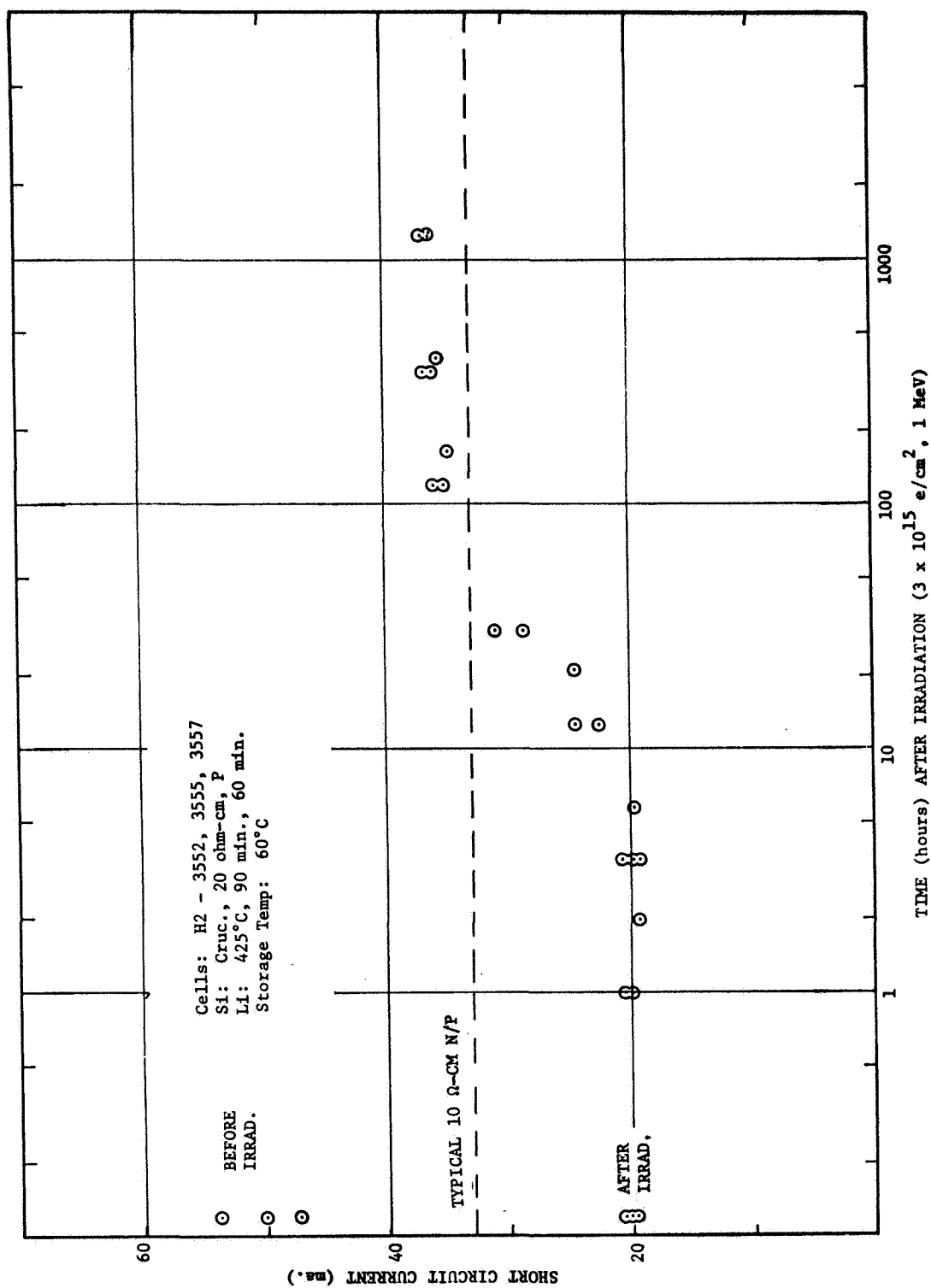


FIG. 34 RECOVERY OF GROUP H2 LITHIUM SOLAR CELLS AT 60°C

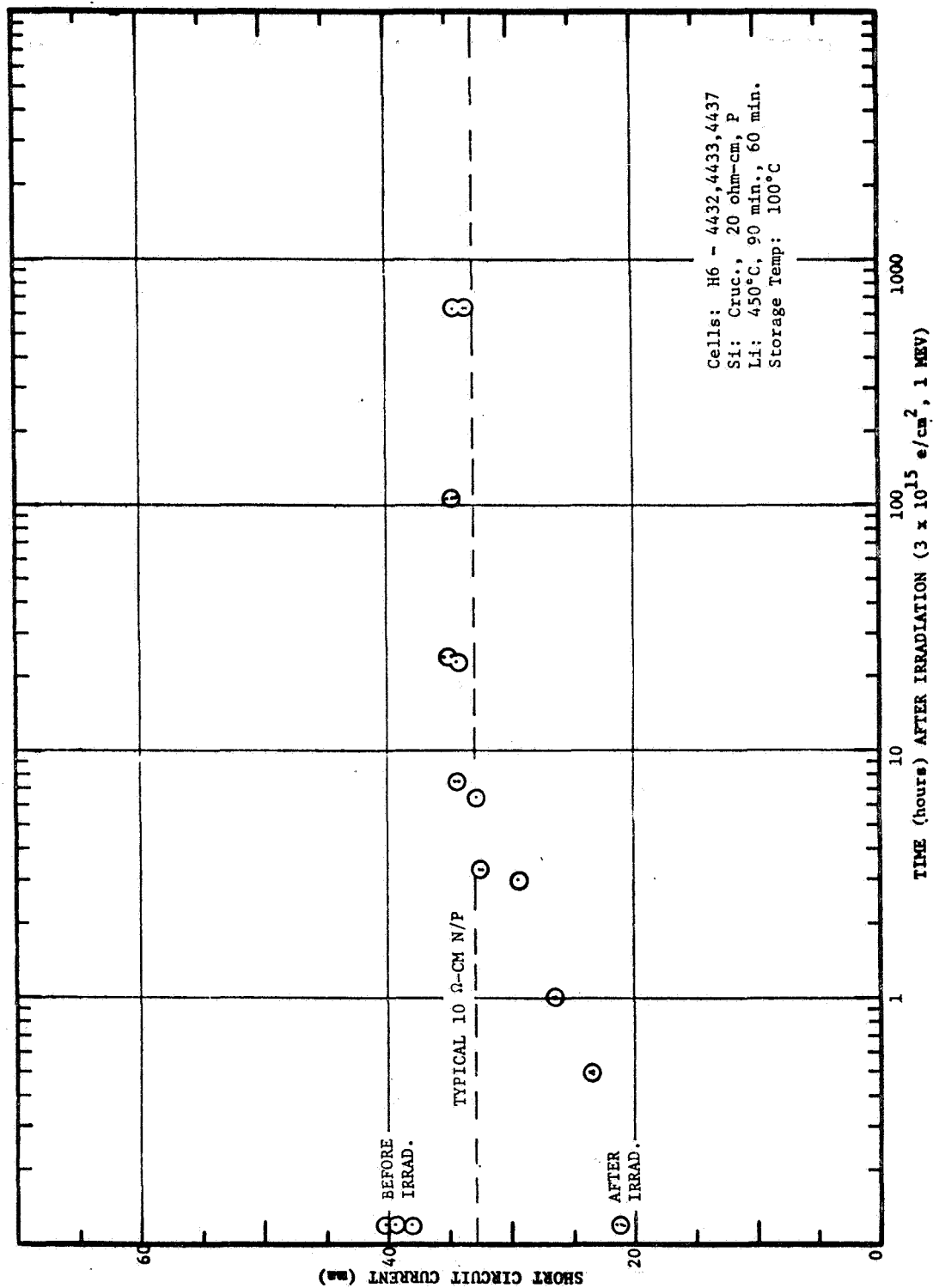


FIG. 35 RECOVERY OF GROUP H6 LITHIUM SOLAR CELLS AT 100°C

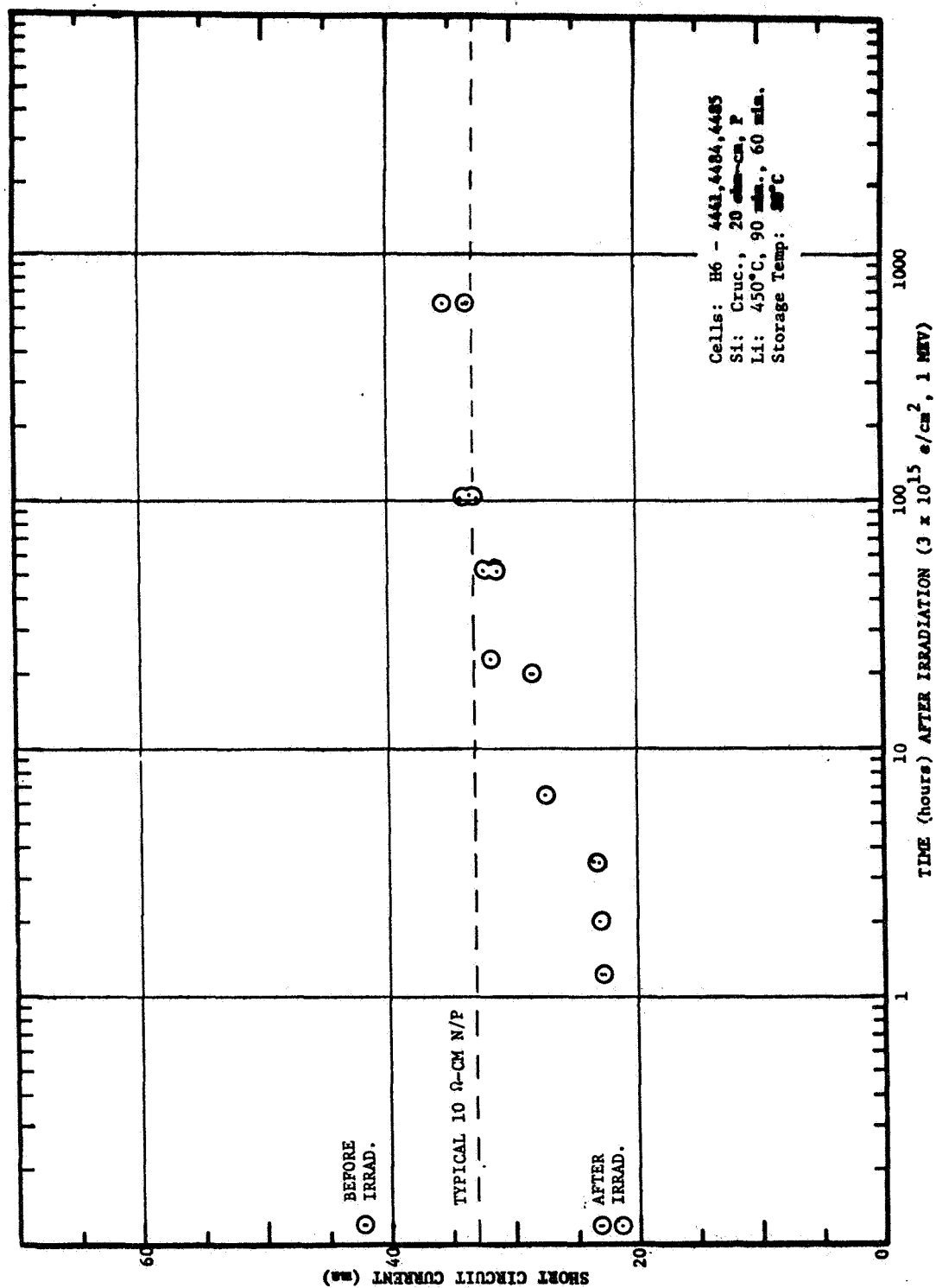


FIG. 36 RECOVERY OF GROUP H6 LITHIUM SOLAR CELLS AT 80°C

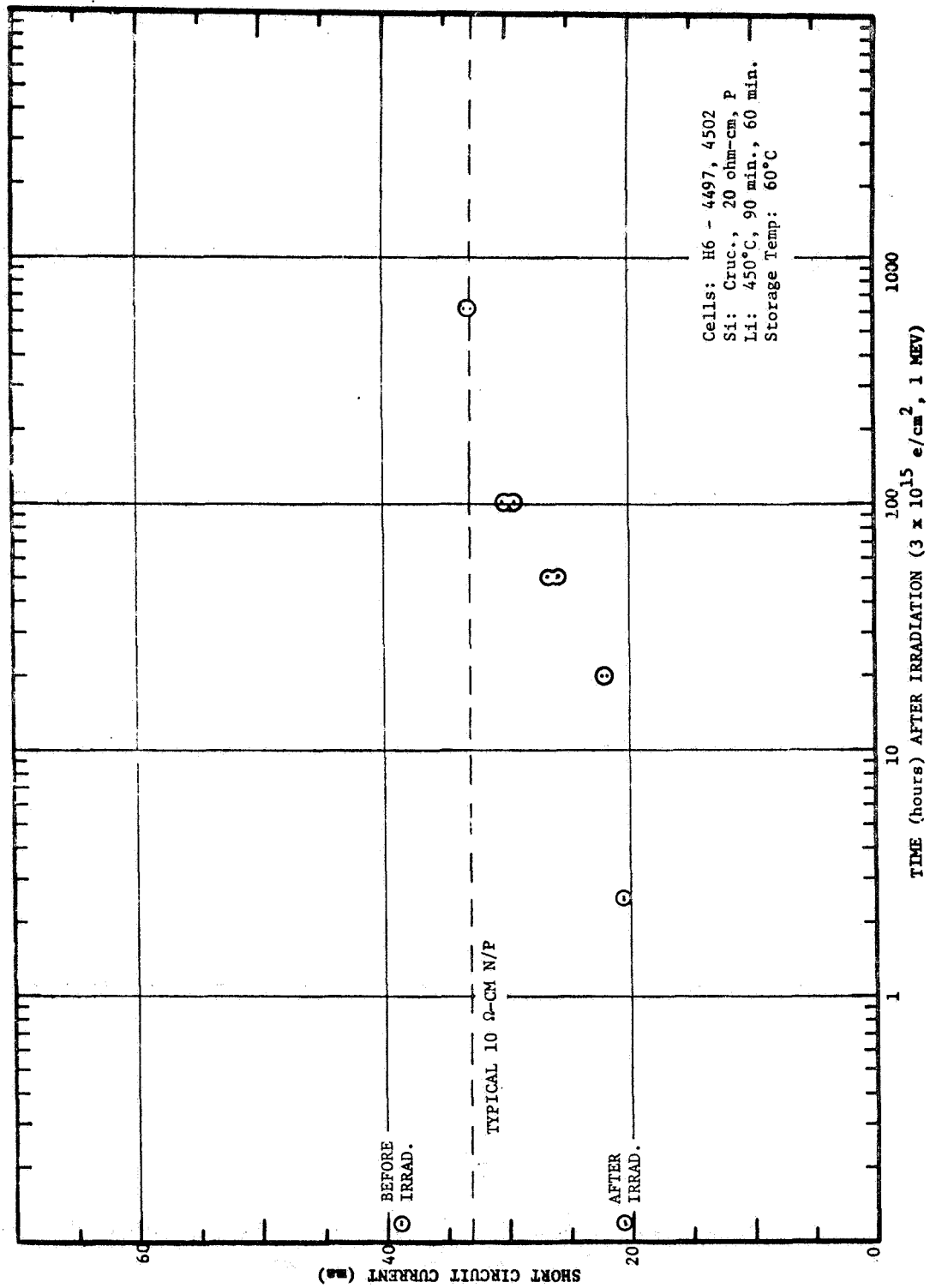


FIG. 37 RECOVERY OF GROUP H6 LITHIUM SOLAR CELLS AT 60°C

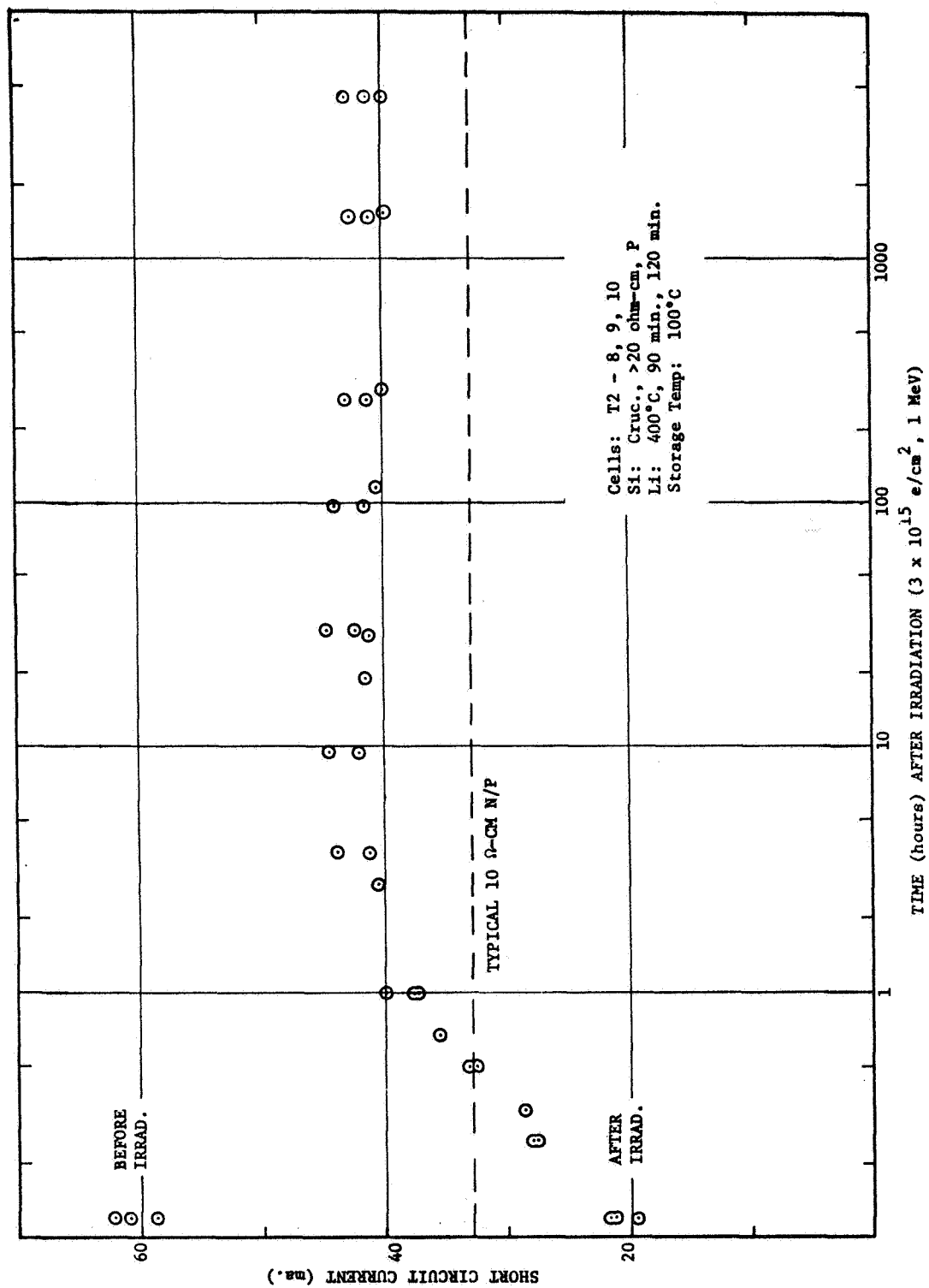


FIG. 38 RECOVERY OF GROUP T2 LITHIUM SOLAR CELLS AT 100°C

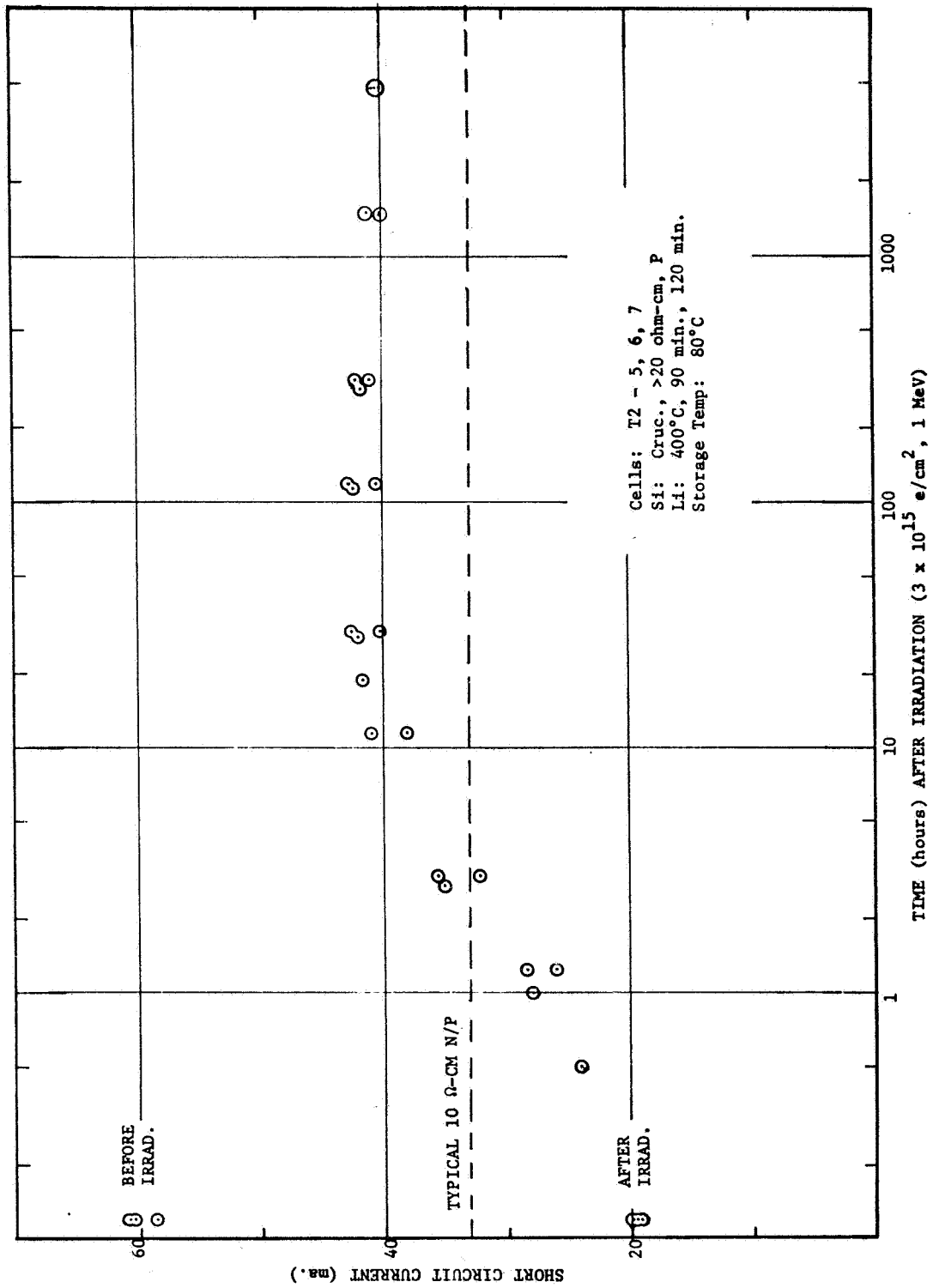
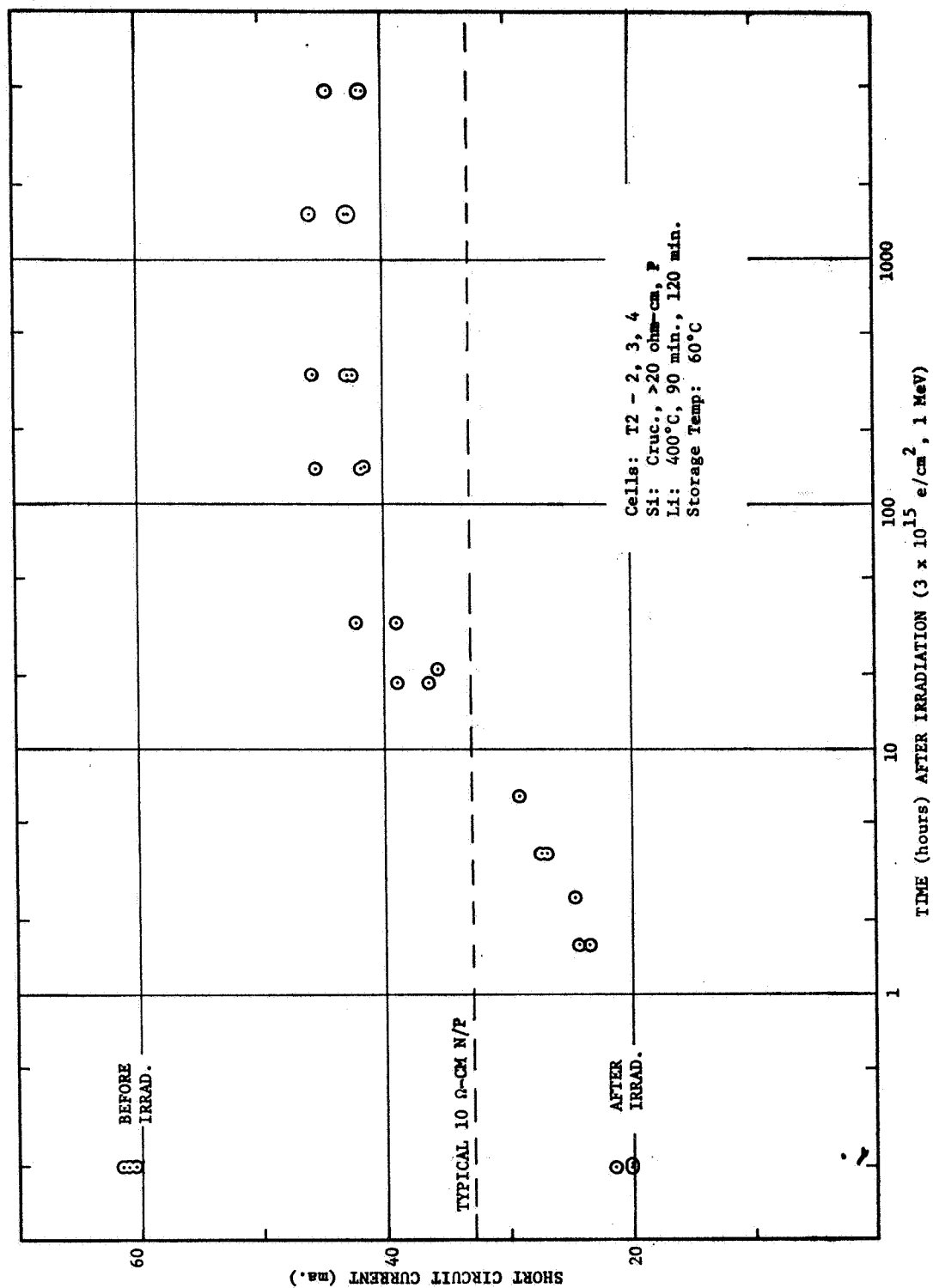


FIG. 39 RECOVERY OF GROUP T2 LITHIUM SOLAR CELLS AT 80°C





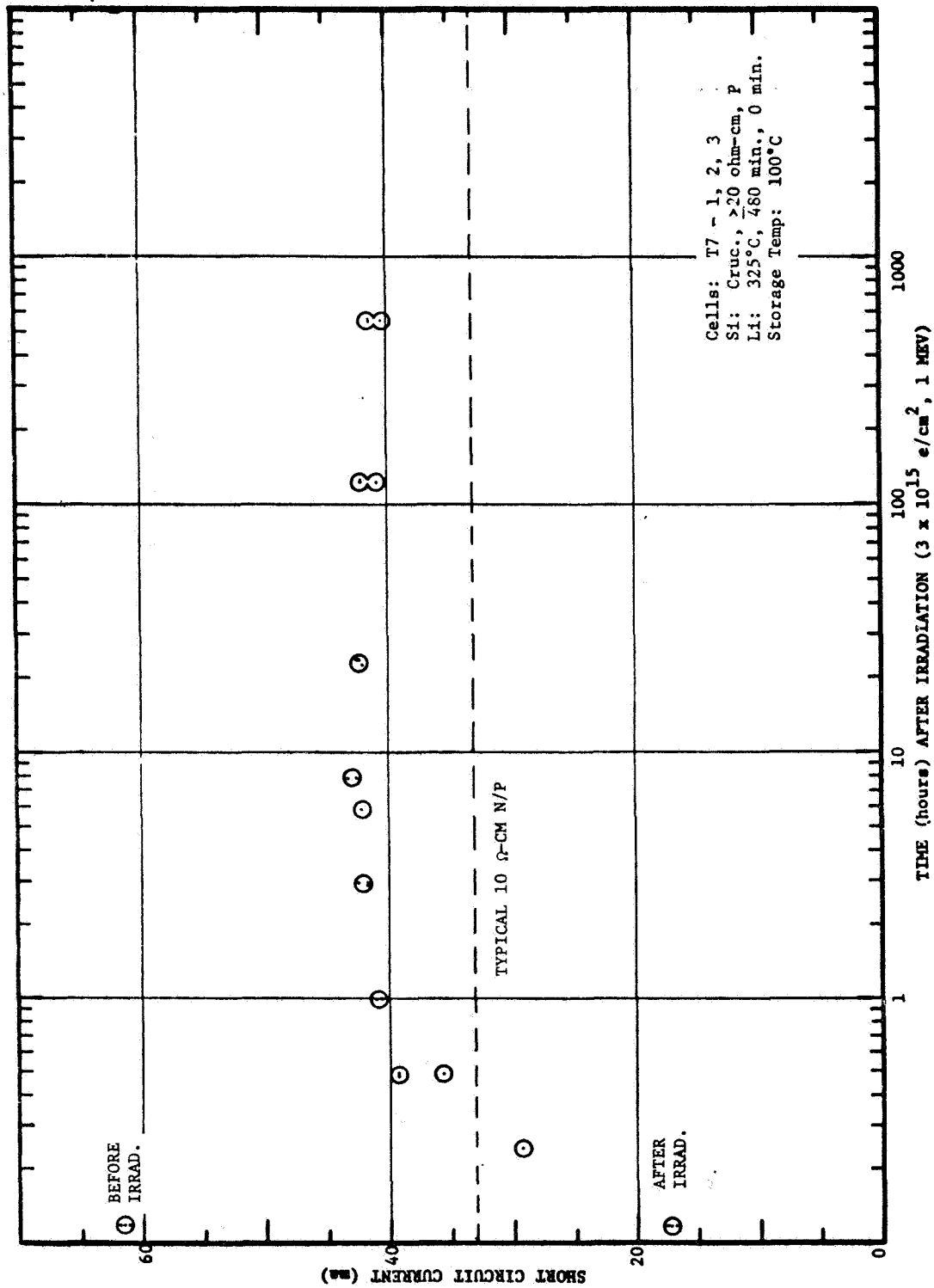


FIG. 41 RECOVERY OF GROUP T7 LITHIUM SOLAR CELLS AT 100°C

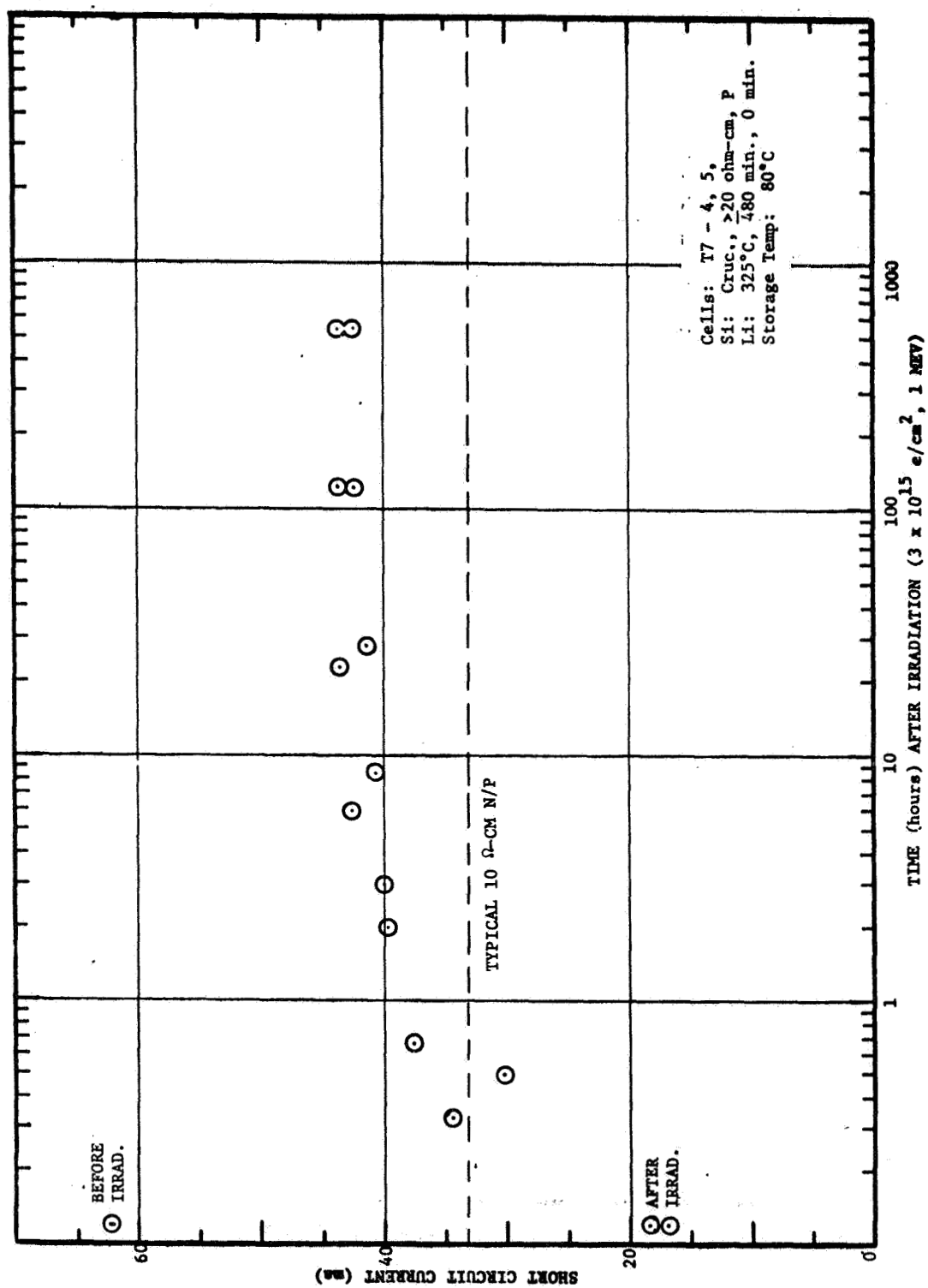


FIG. 42 RECOVERY OF GROUP T7 LITHIUM SOLAR CELLS AT 80°C

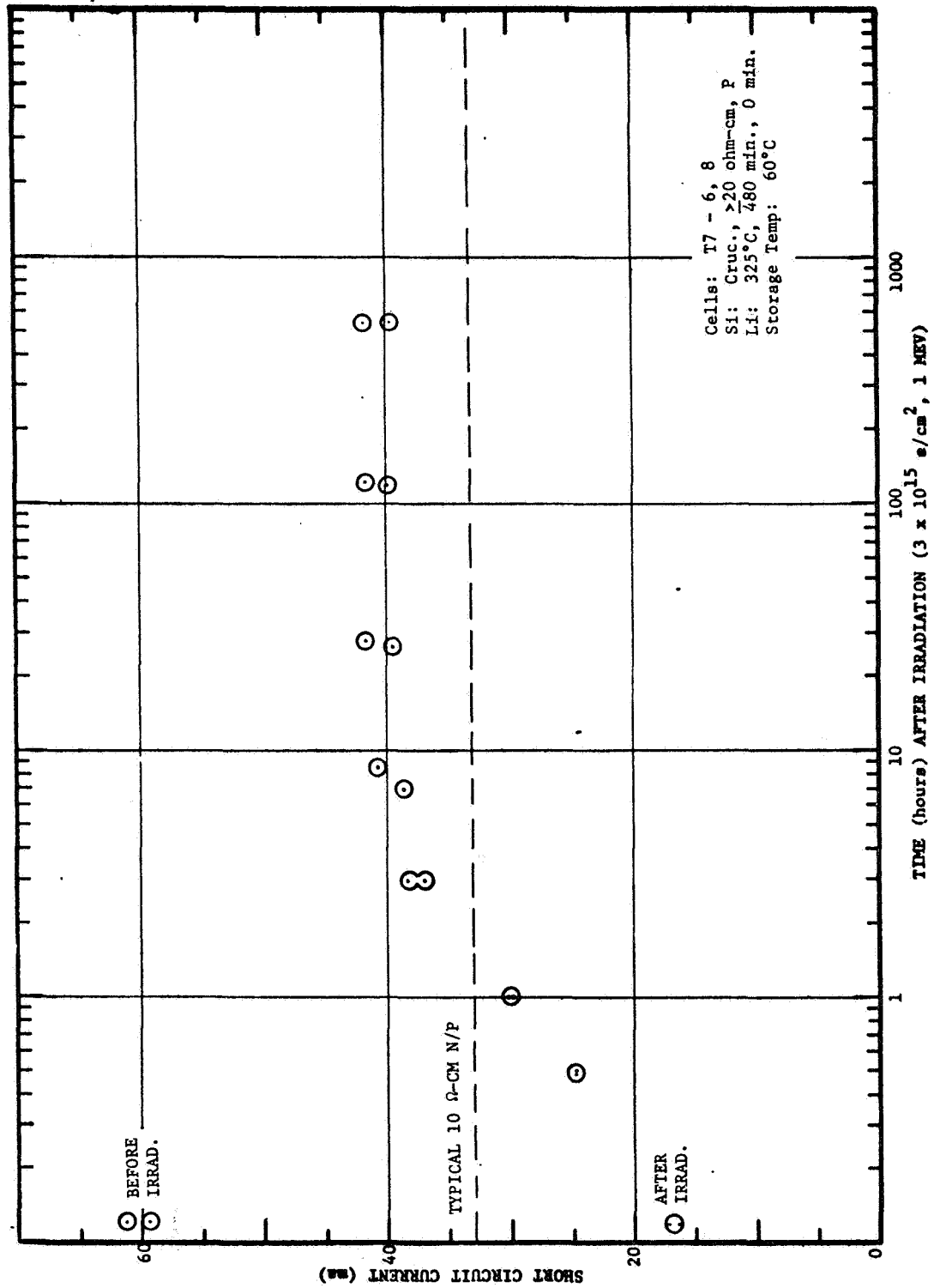


FIG. 43 RECOVERY OF GROUP T7 LITHIUM SOLAR CELLS AT 60°C

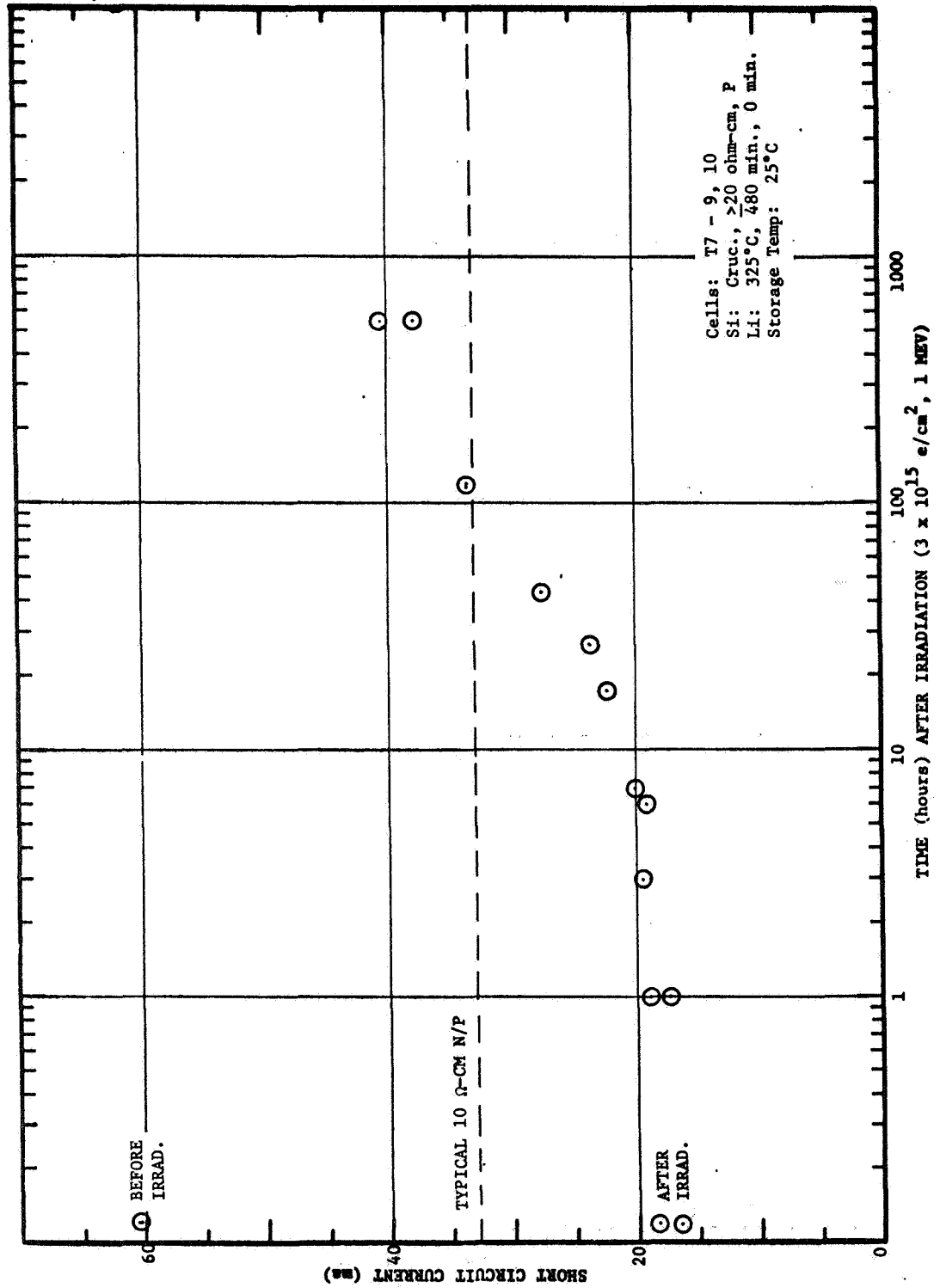


FIG. 44 RECOVERY OF GROUP T7 LITHIUM SOLAR CELLS AT 25°C

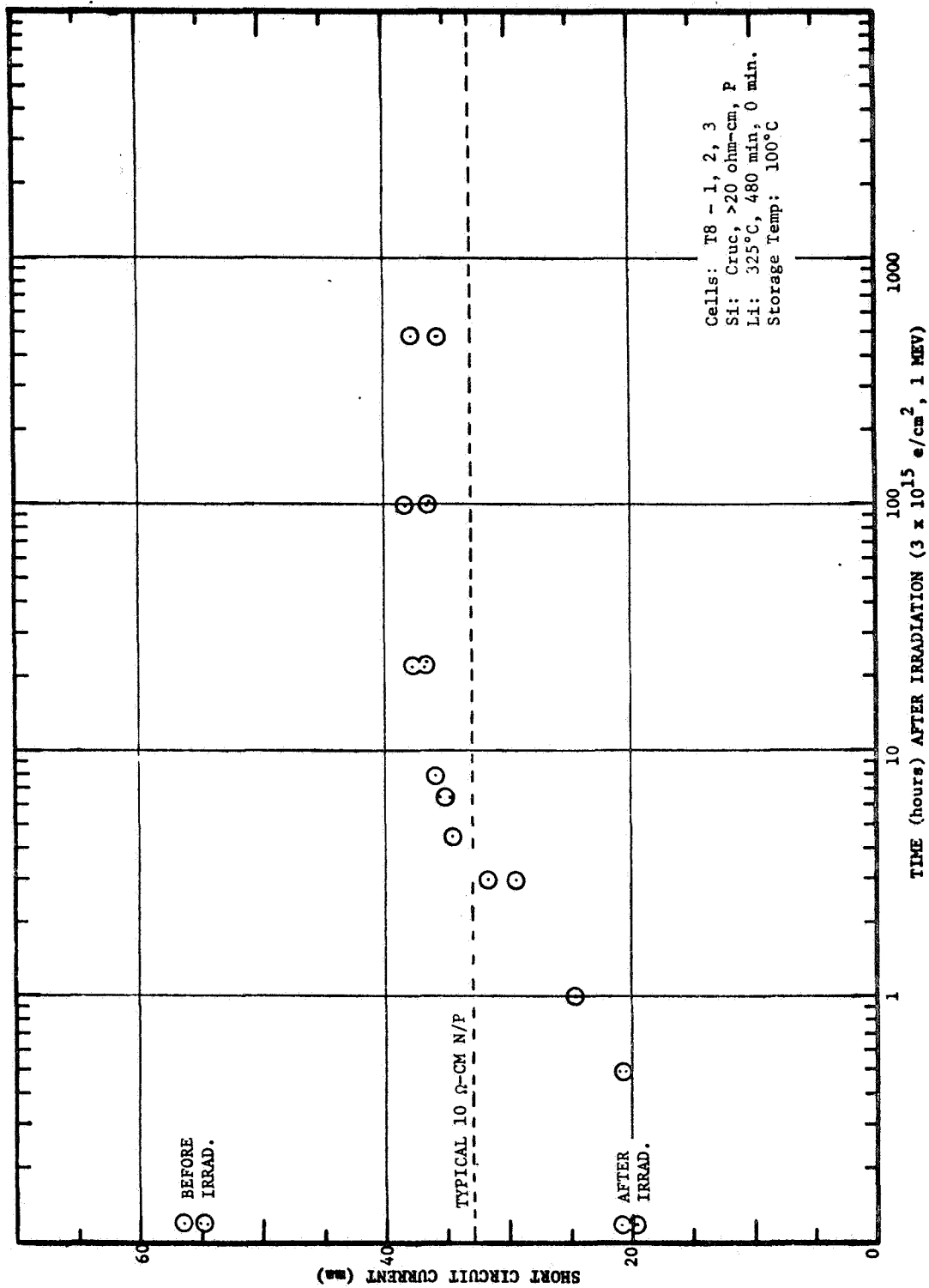


FIG. 45 RECOVERY OF GROUP T8 LITHIUM SOLAR CELLS AT 100°C

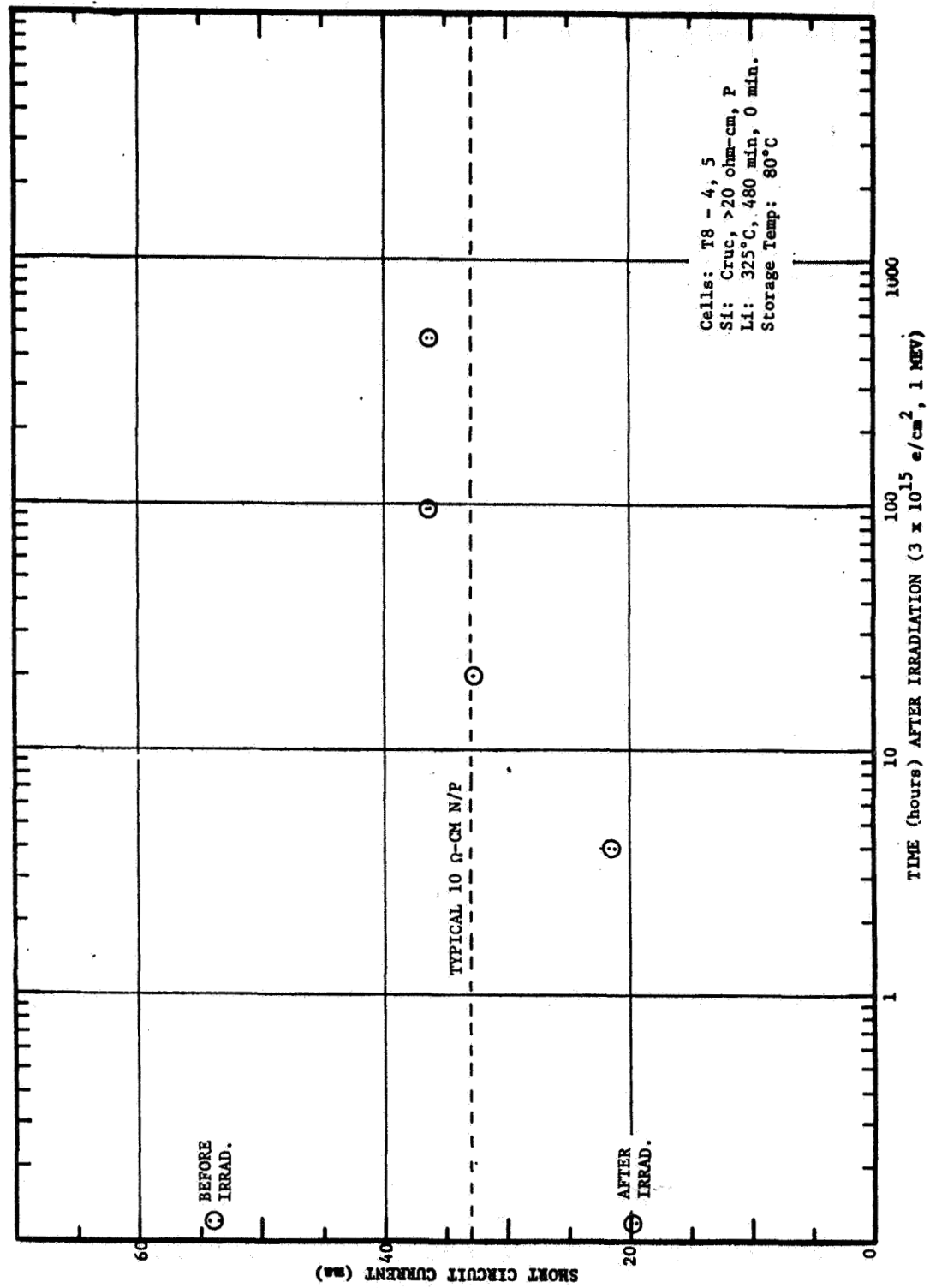


FIG. 46 RECOVERY OF GROUP T8 LITHIUM SOLAR CELLS AT 80°C

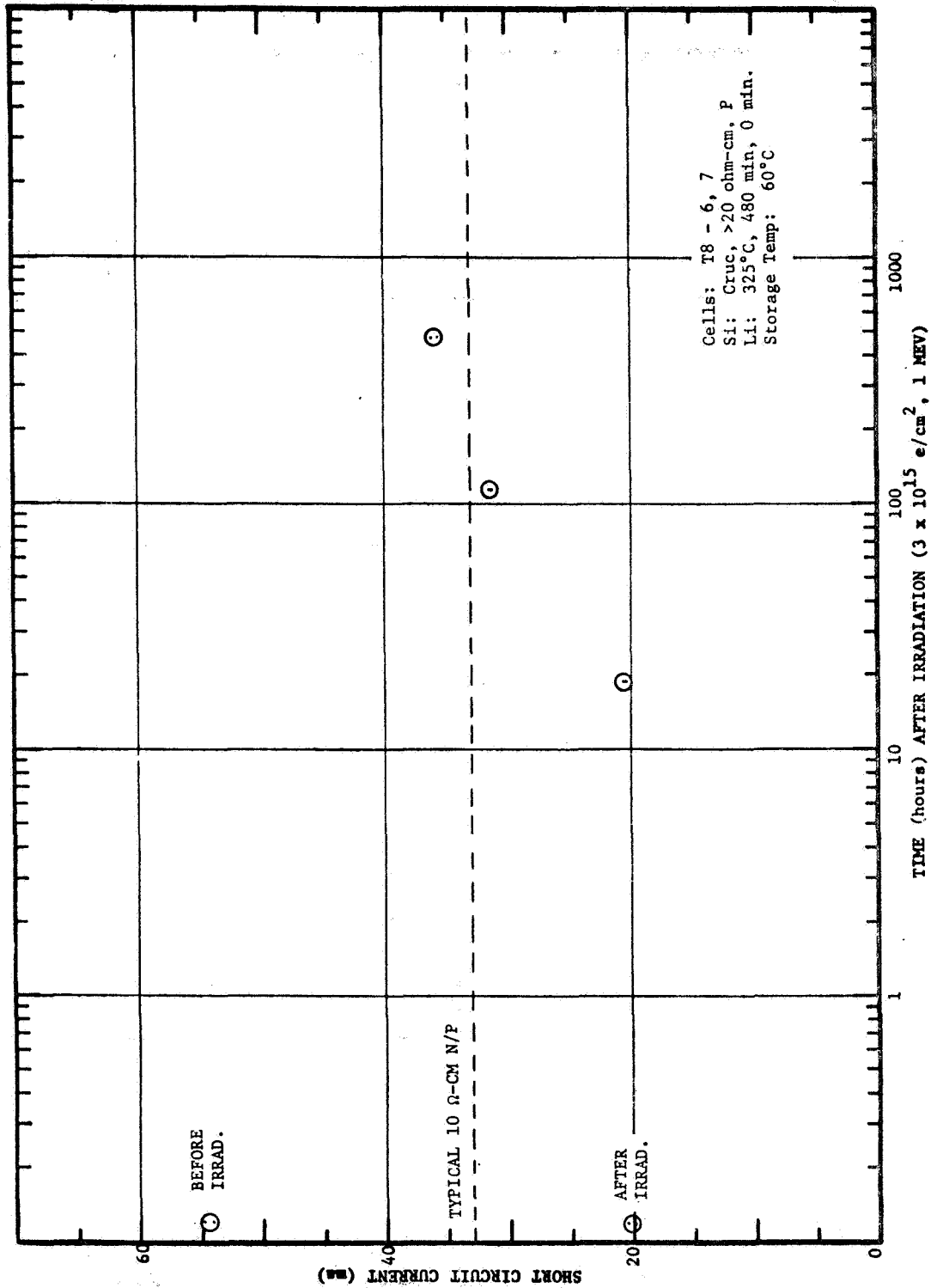


FIG. 47 RECOVERY OF GROUP T8 LITHIUM SOLAR CELLS AT 60°C

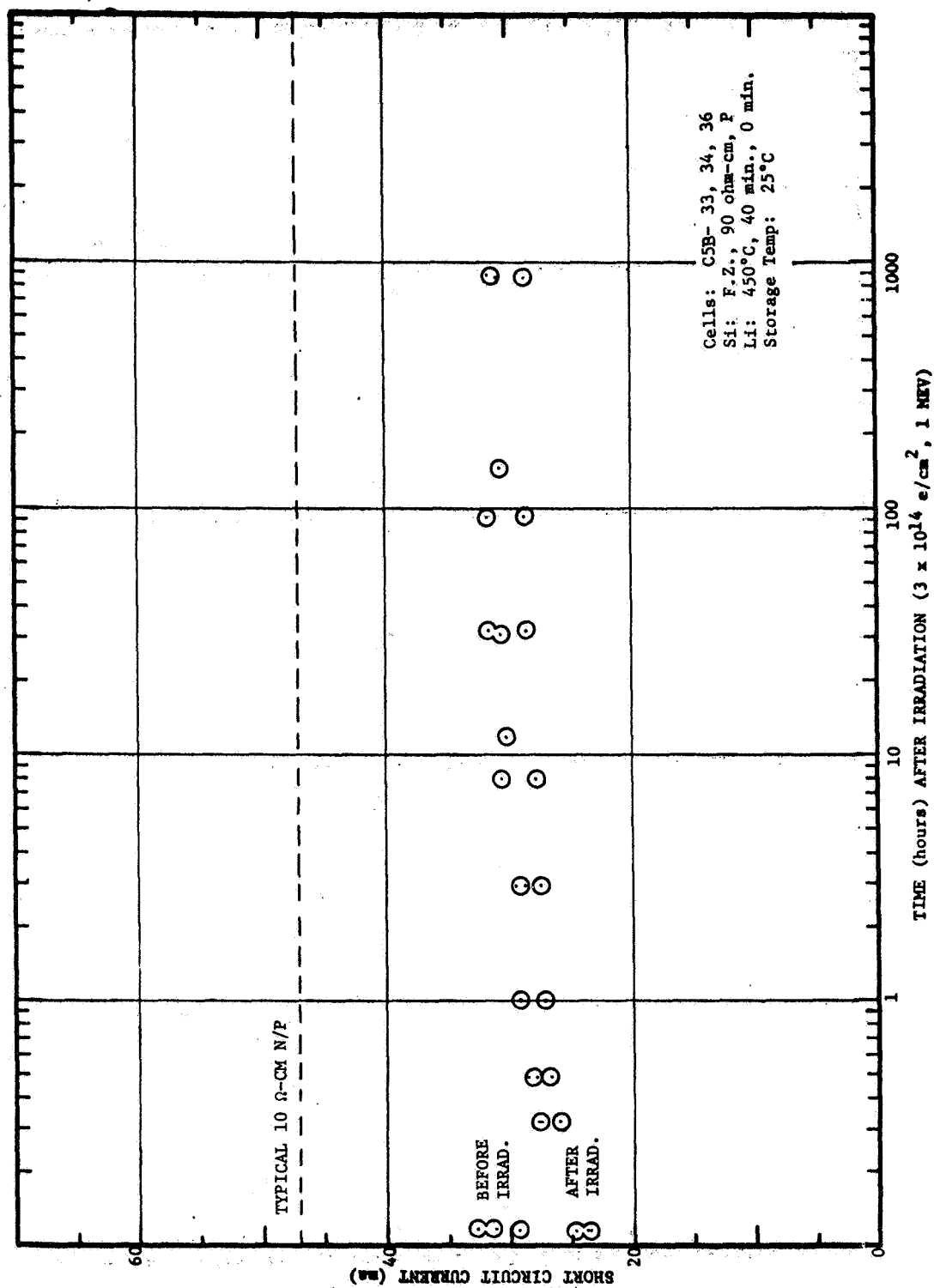


FIG. 48 RECOVERY OF GROUP C5B LITHIUM SOLAR CELLS AFTER  
 $3 \times 10^{14} \text{ e/cm}^2$



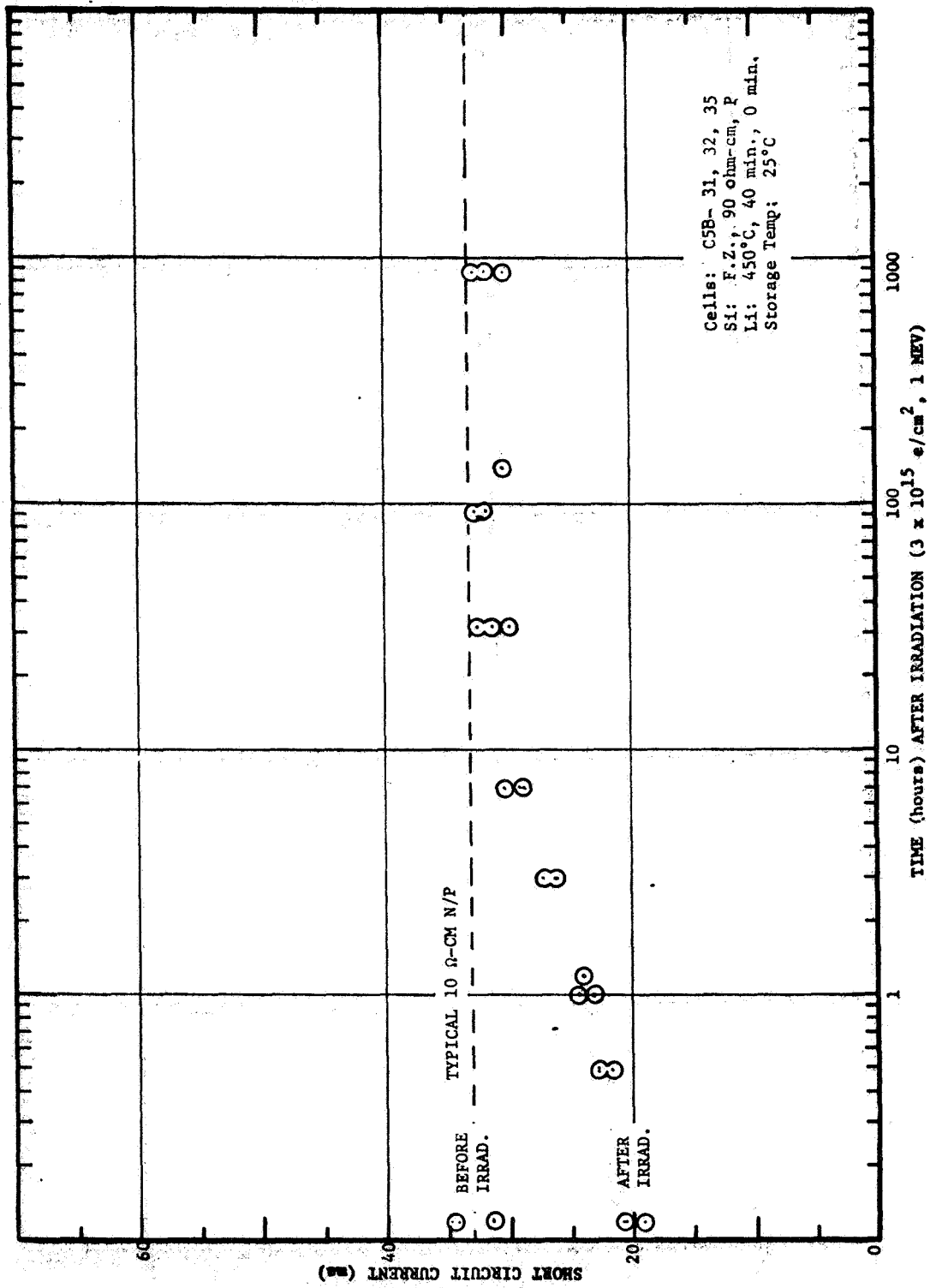


FIG. 49 RECOVERY OF GROUP C5B LITHIUM SOLAR CELLS AFTER  
 $3 \times 10^{15} \text{ e/cm}^2$

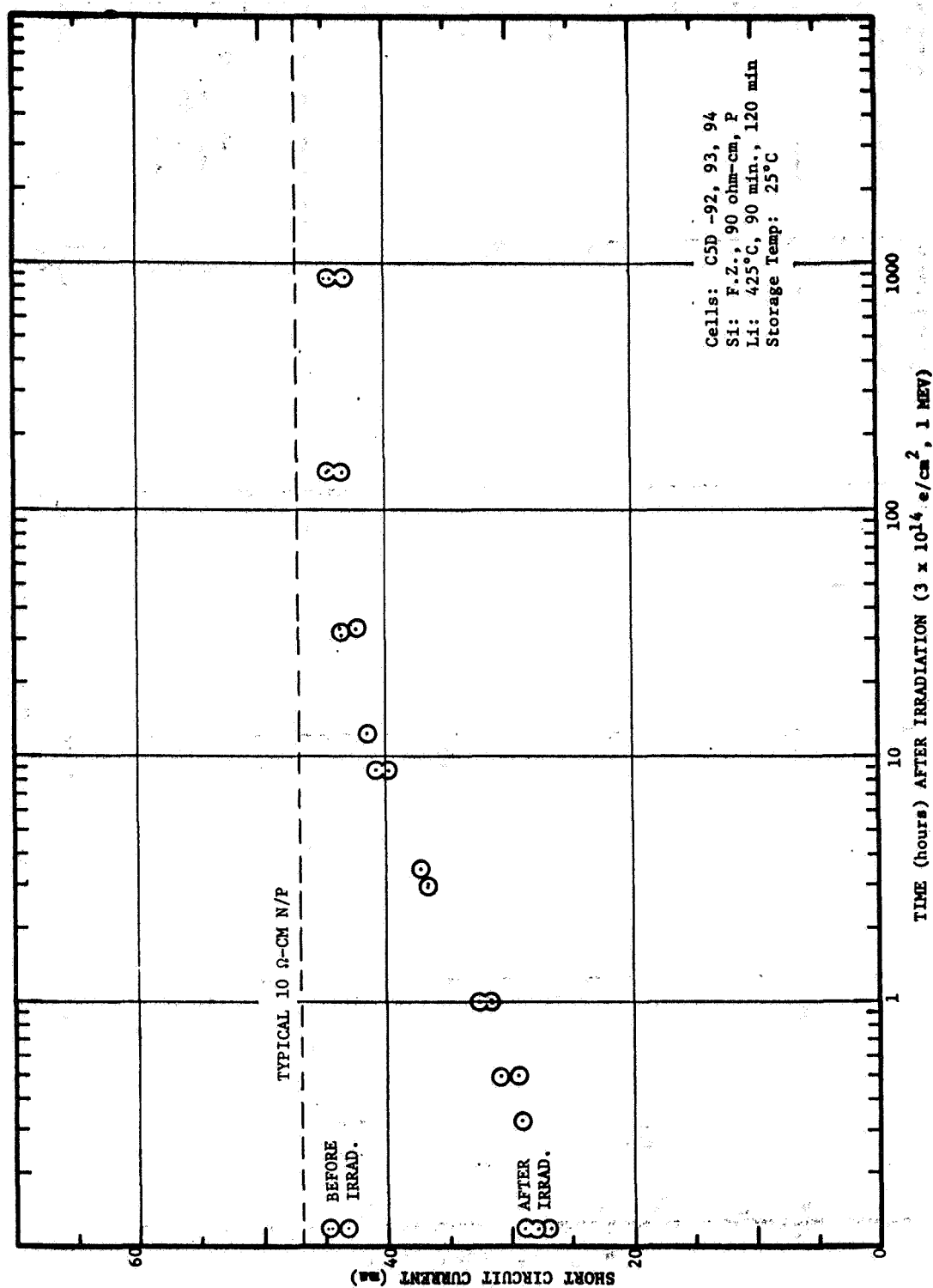


FIG. 50 RECOVERY OF GROUP C5D LITHIUM SOLAR CELLS AFTER  
 $3 \times 10^{14} \text{ e/cm}^2$

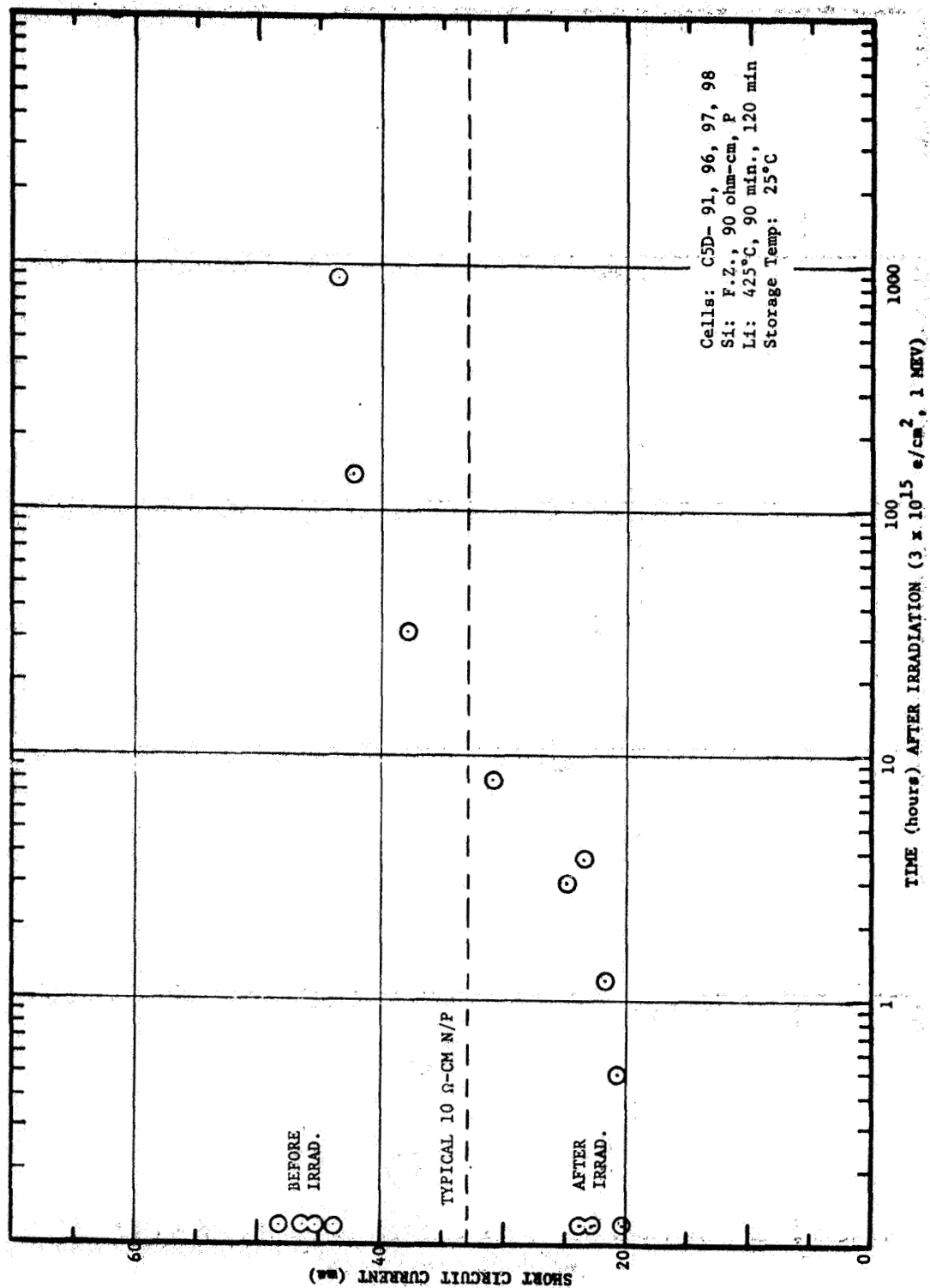


FIG. 51 RECOVERY OF GROUP C5D LITHIUM SOLAR CELLS AFTER  
 $3 \times 10^{15} \text{ e/cm}^2$

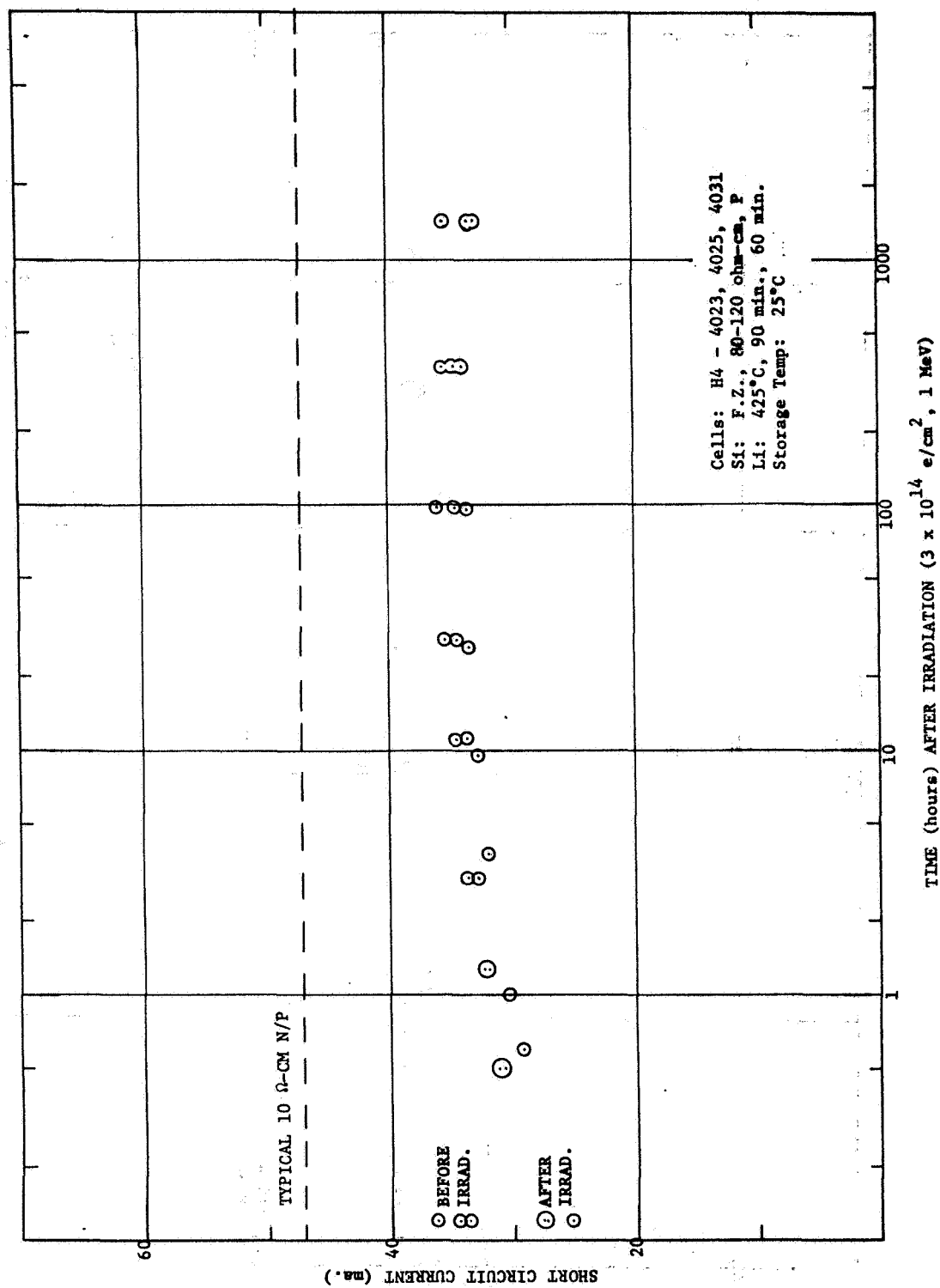


FIG. 52 RECOVERY OF GROUP H4 LITHIUM SOLAR CELLS AFTER  $3 \times 10^{14} \text{ e/cm}^2$

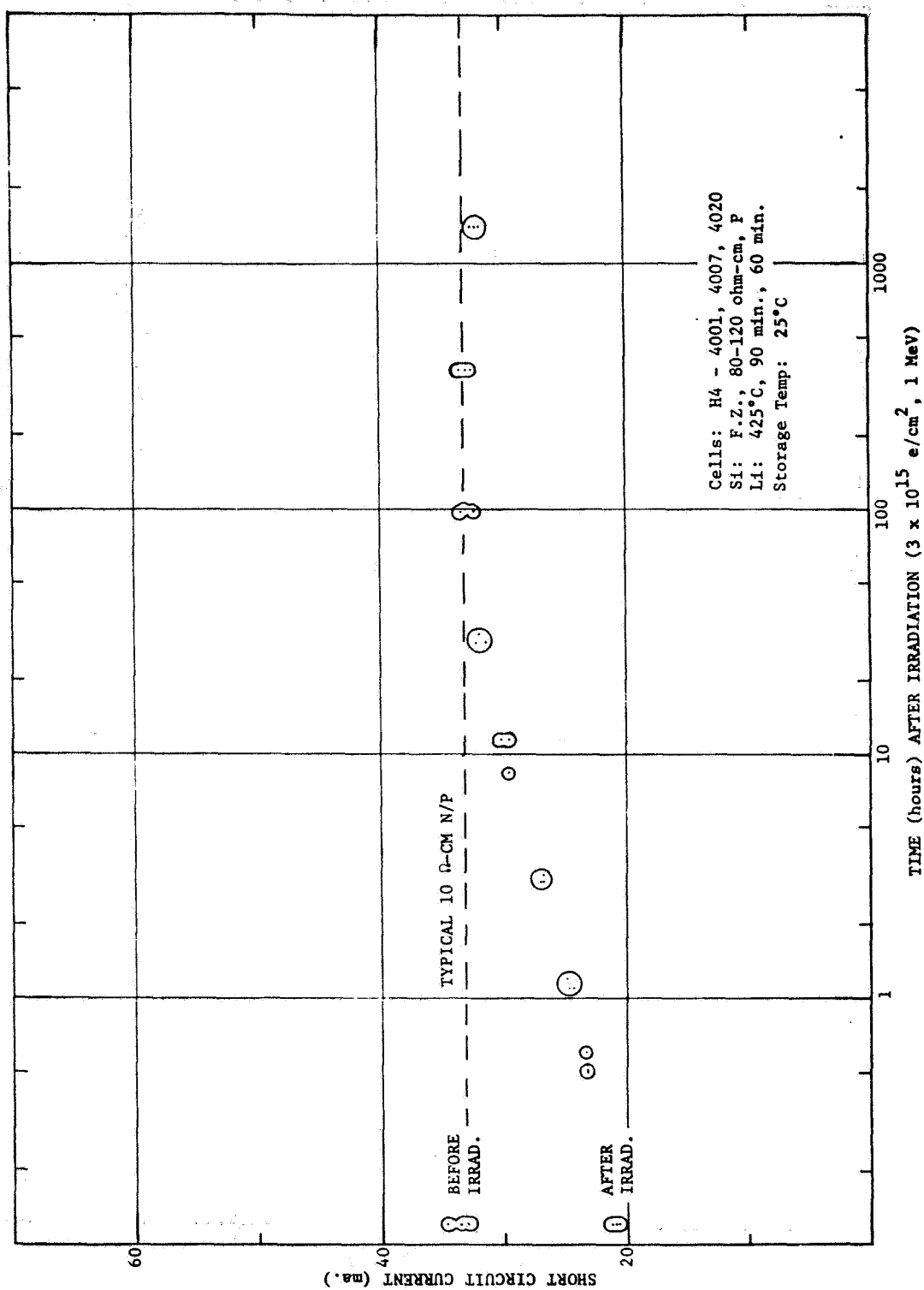


FIG. 53 RECOVERY OF GROUP H4 LITHIUM SOLAR CELLS AFTER  $3 \times 10^{15} \text{ e/cm}^2$

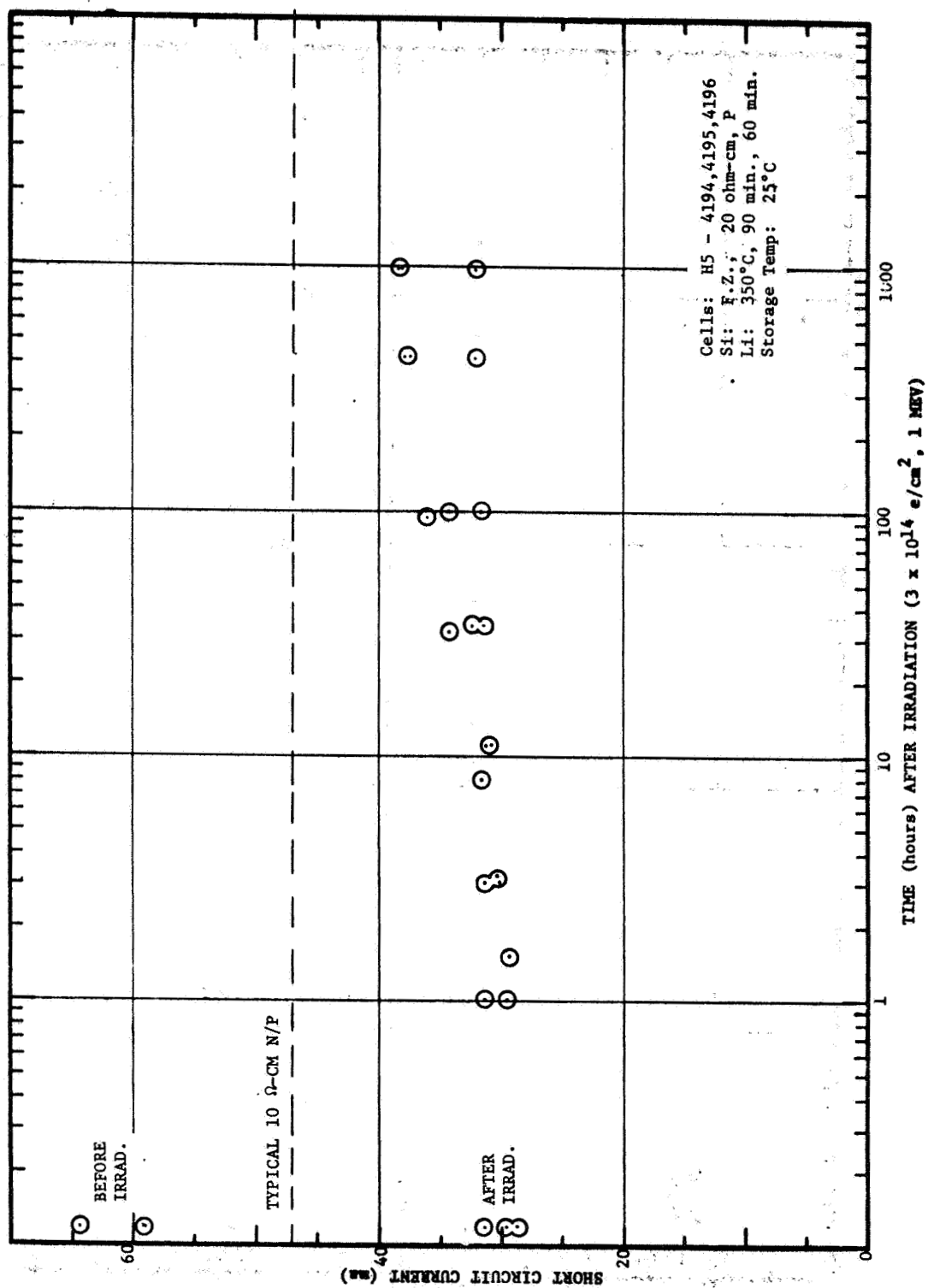


FIG. 54 RECOVERY OF GROUP H5 LITHIUM SOLAR CELLS AFTER  
 $3 \times 10^{14} \text{ e/cm}^2$

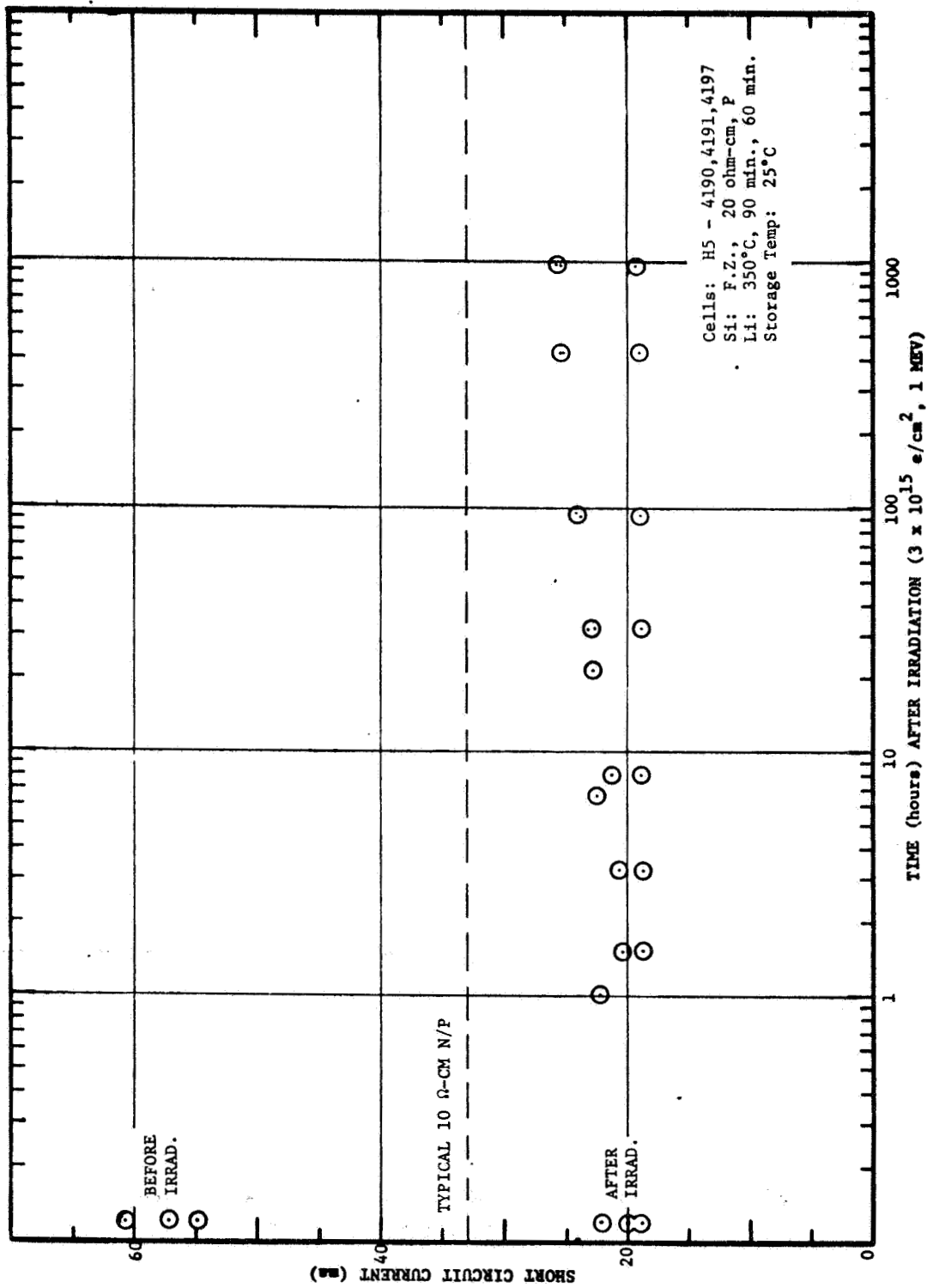


FIG. 55 RECOVERY OF GROUP H5 LITHIUM SOLAR CELLS AFTER  
 $3 \times 10^{15} \text{ e/cm}^2$

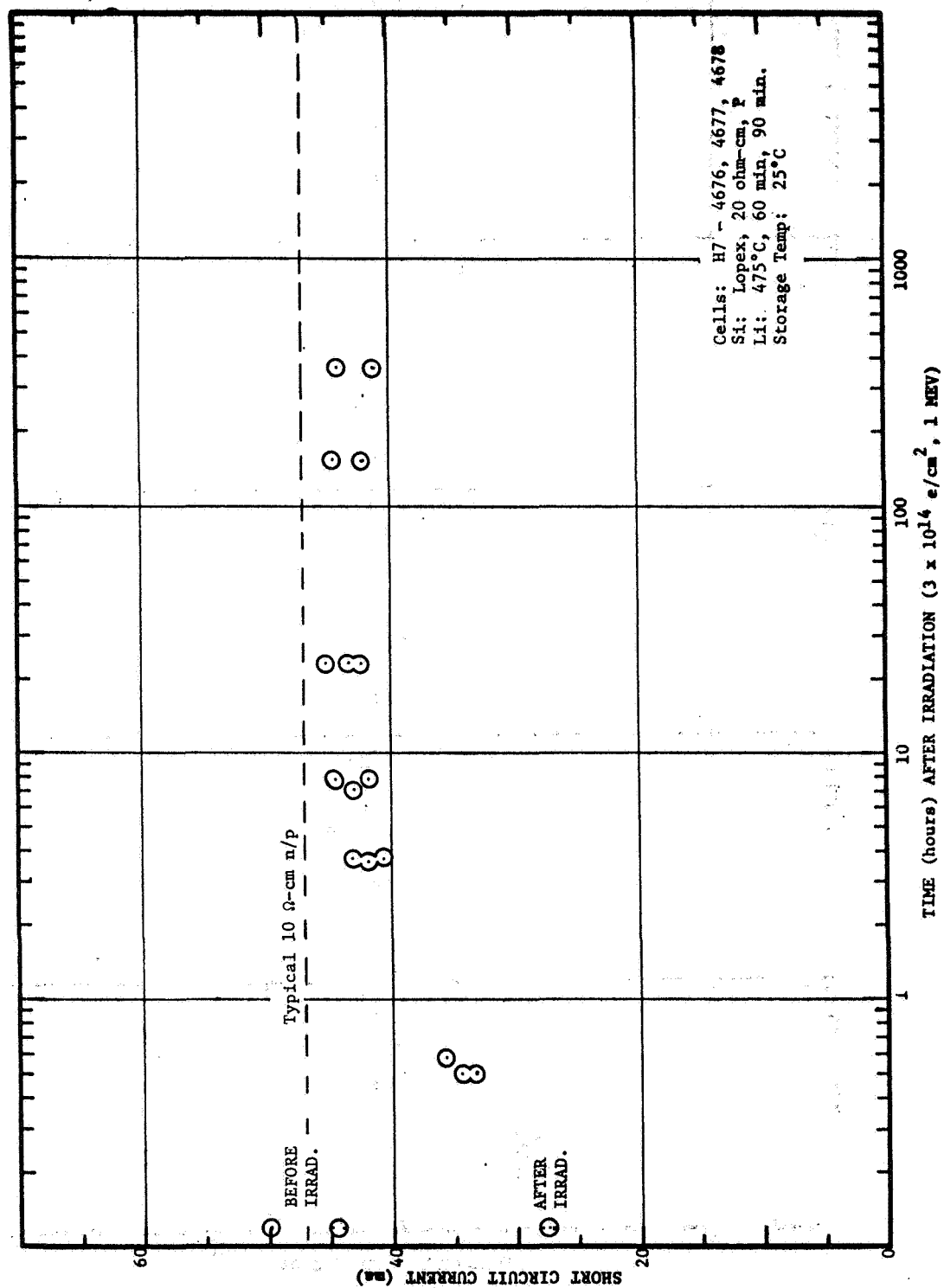


FIG. 56 RECOVERY OF GROUP H7 LITHIUM SOLAR CELLS AFTER  
 $3 \times 10^{14} \text{ e/cm}^2$



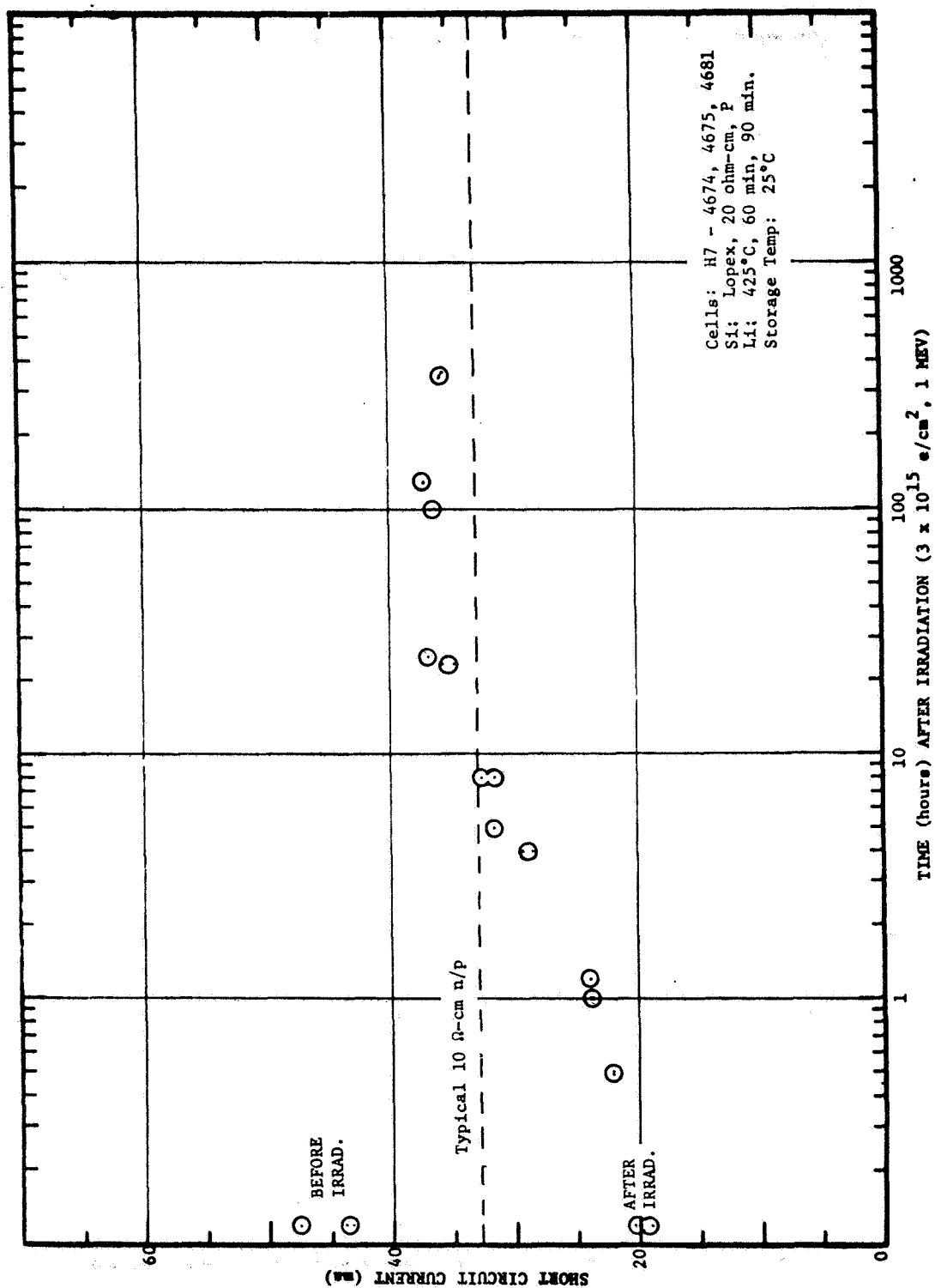


FIG. 57 RECOVERY OF GROUP H7 LITHIUM SOLAR CELLS AFTER  
 $3 \times 10^{15} \text{ e/cm}^2$

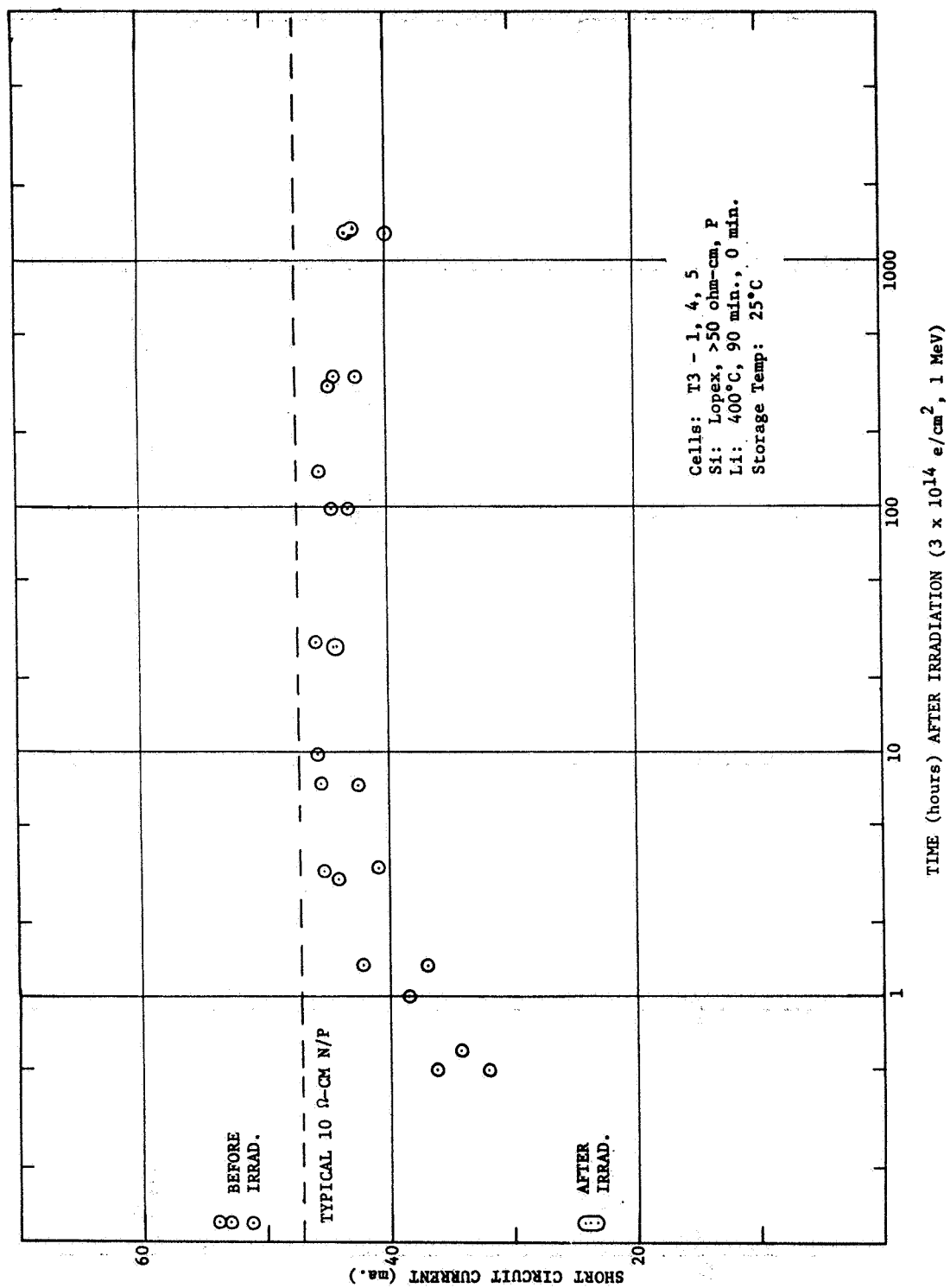


FIG. 58. RECOVERY OF GROUP T3 LITHIUM SOLAR CELLS AFTER  $3 \times 10^{14} \text{ e/cm}^2$

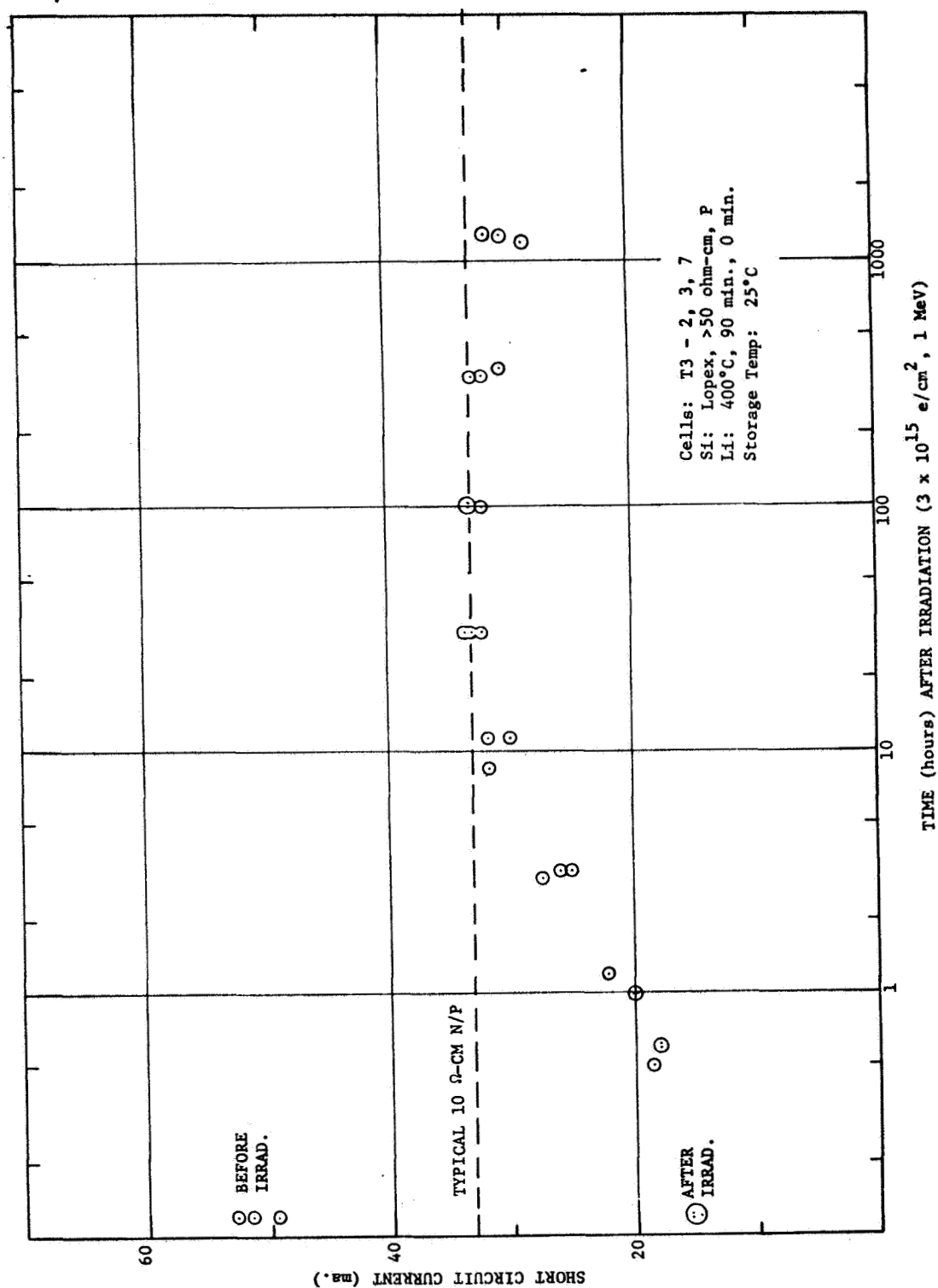


FIG. 59 RECOVERY OF GROUP T3 LITHIUM SOLAR CELLS AFTER  $3 \times 10^{15} \text{ e/cm}^2$

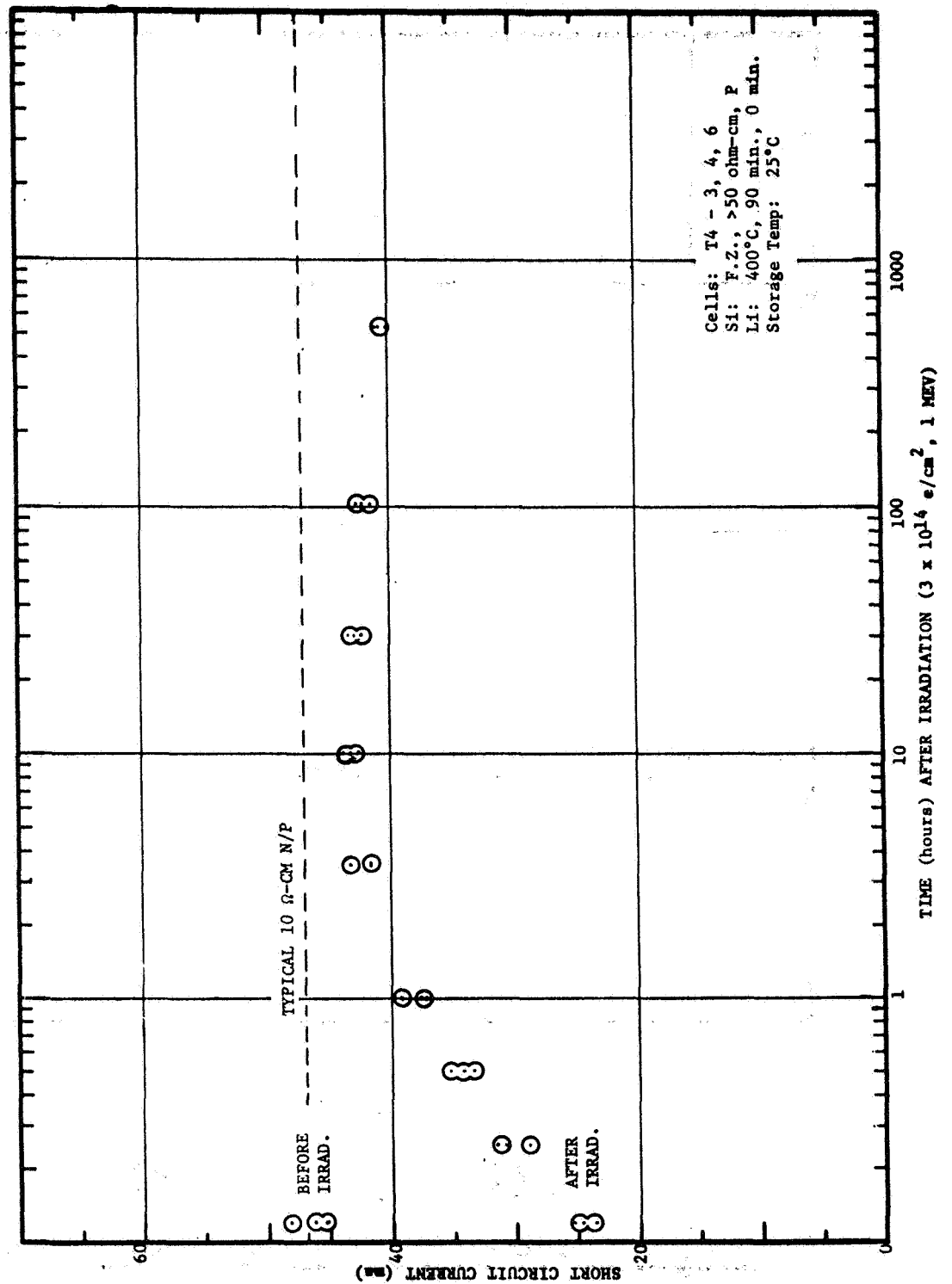


FIG. 60 RECOVERY OF GROUP T4 LITHIUM SOLAR CELLS AFTER  
 $3 \times 10^{14} \text{ e/cm}^2$

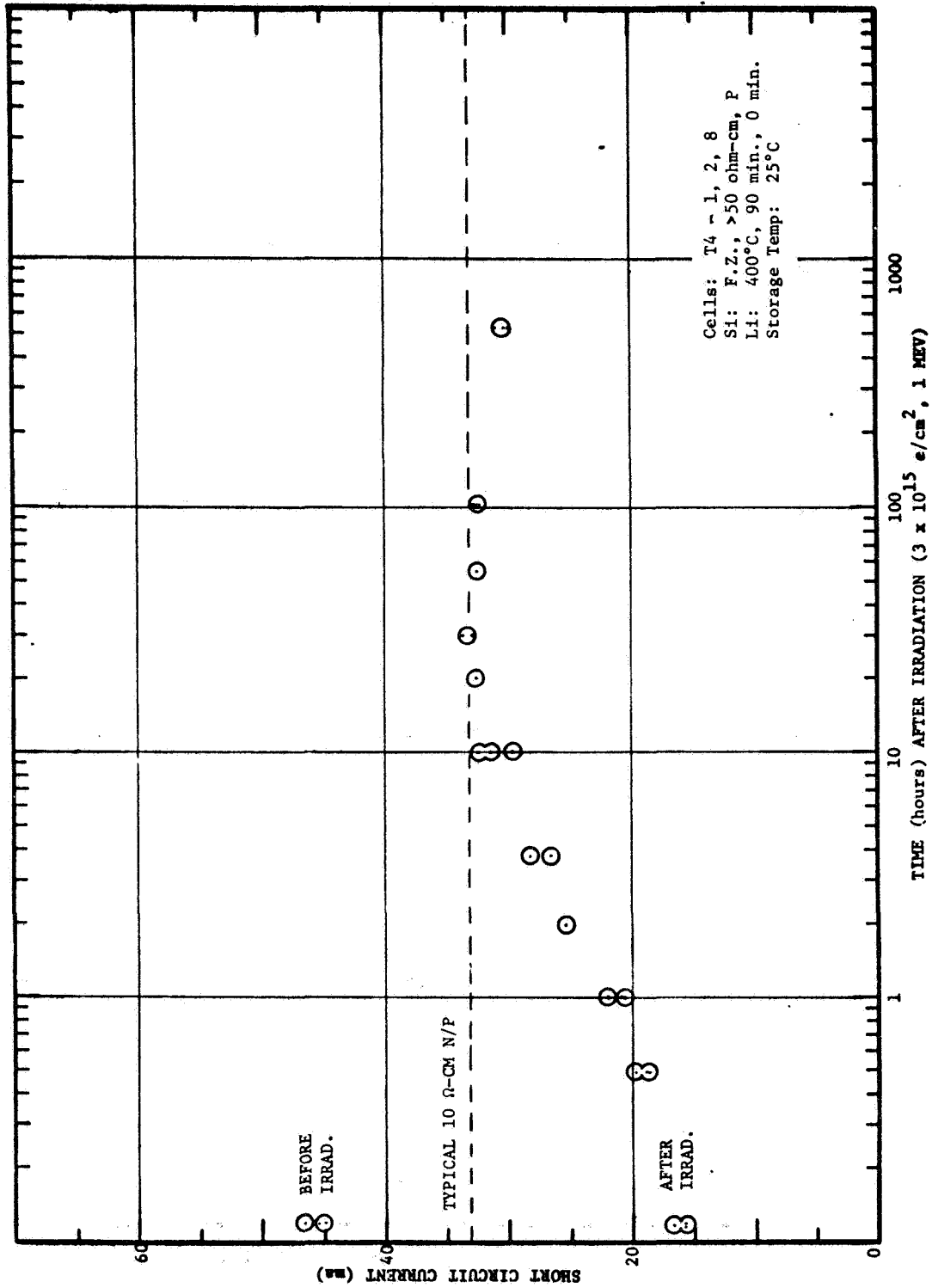


FIG. 61 RECOVERY OF GROUP T4 LITHIUM SOLAR CELLS AFTER  
 $3 \times 10^{15} \text{ e/cm}^2$

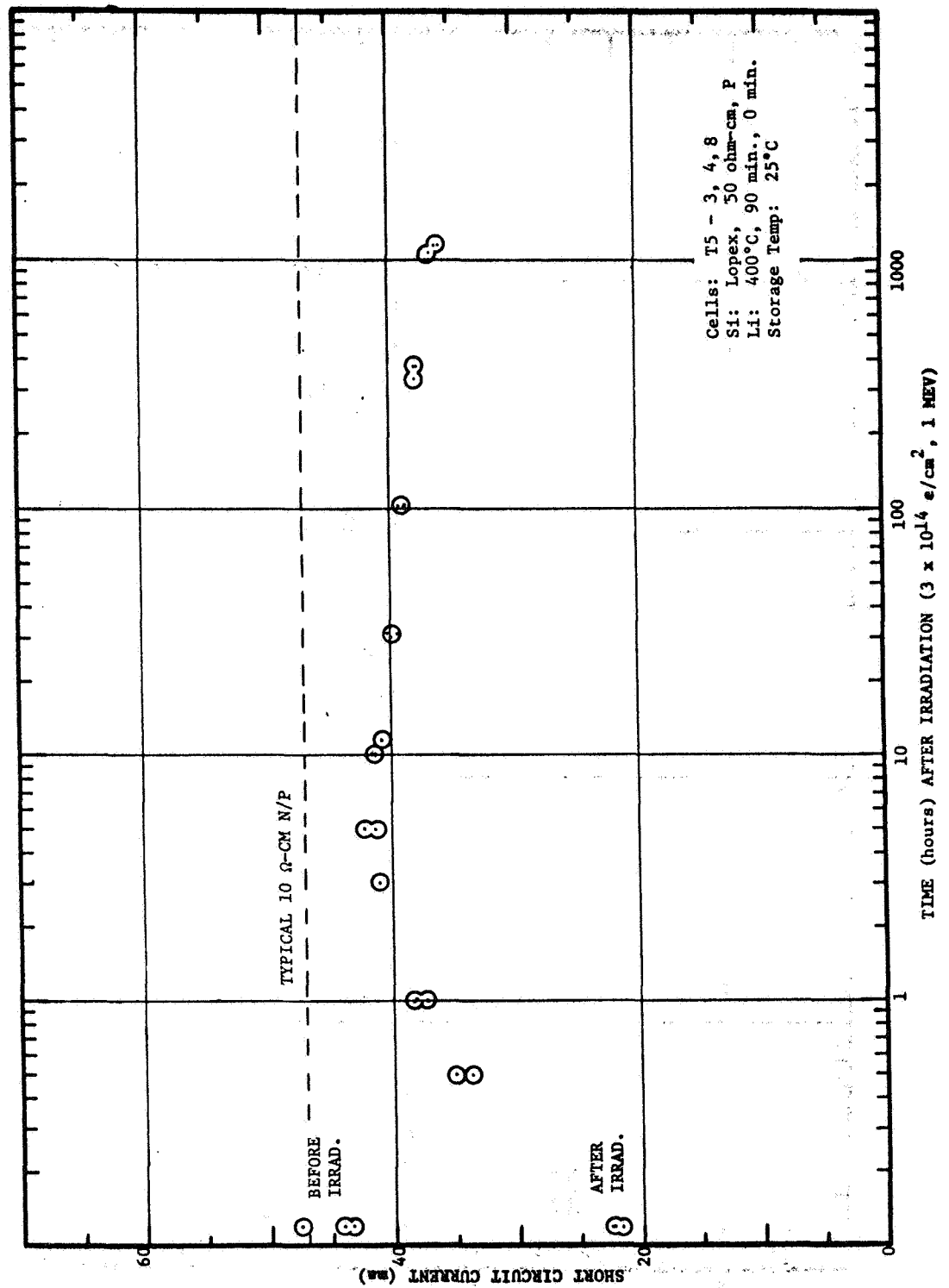


FIG. 62 RECOVERY OF GROUP T5 LITHIUM SOLAR CELLS AFTER  
 $3 \times 10^{14} \text{ e/cm}^2$

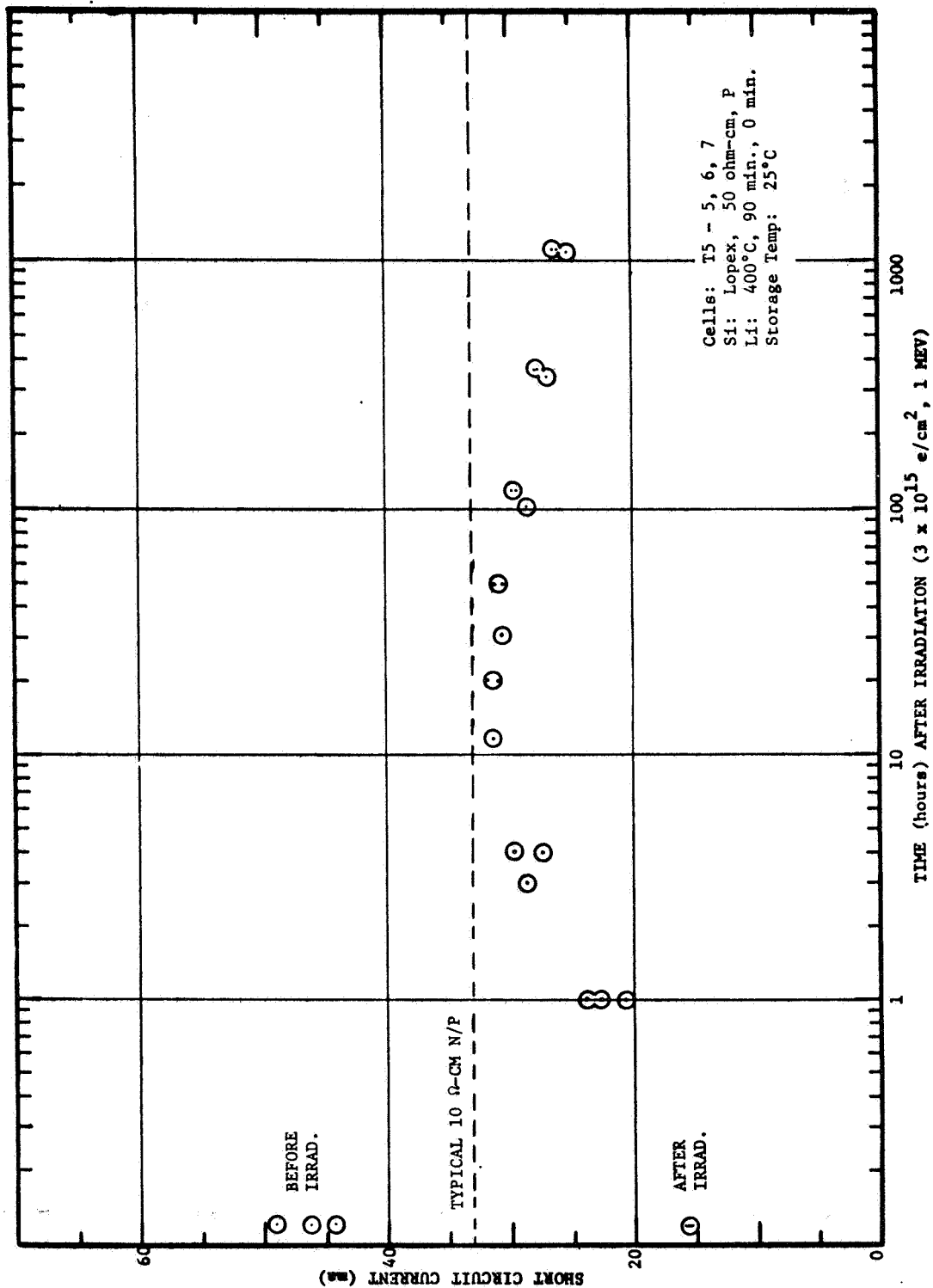


FIG. 63 RECOVERY OF GROUP T5 LITHIUM SOLAR CELLS AFTER  
 $3 \times 10^{15} \text{ e/cm}^2$

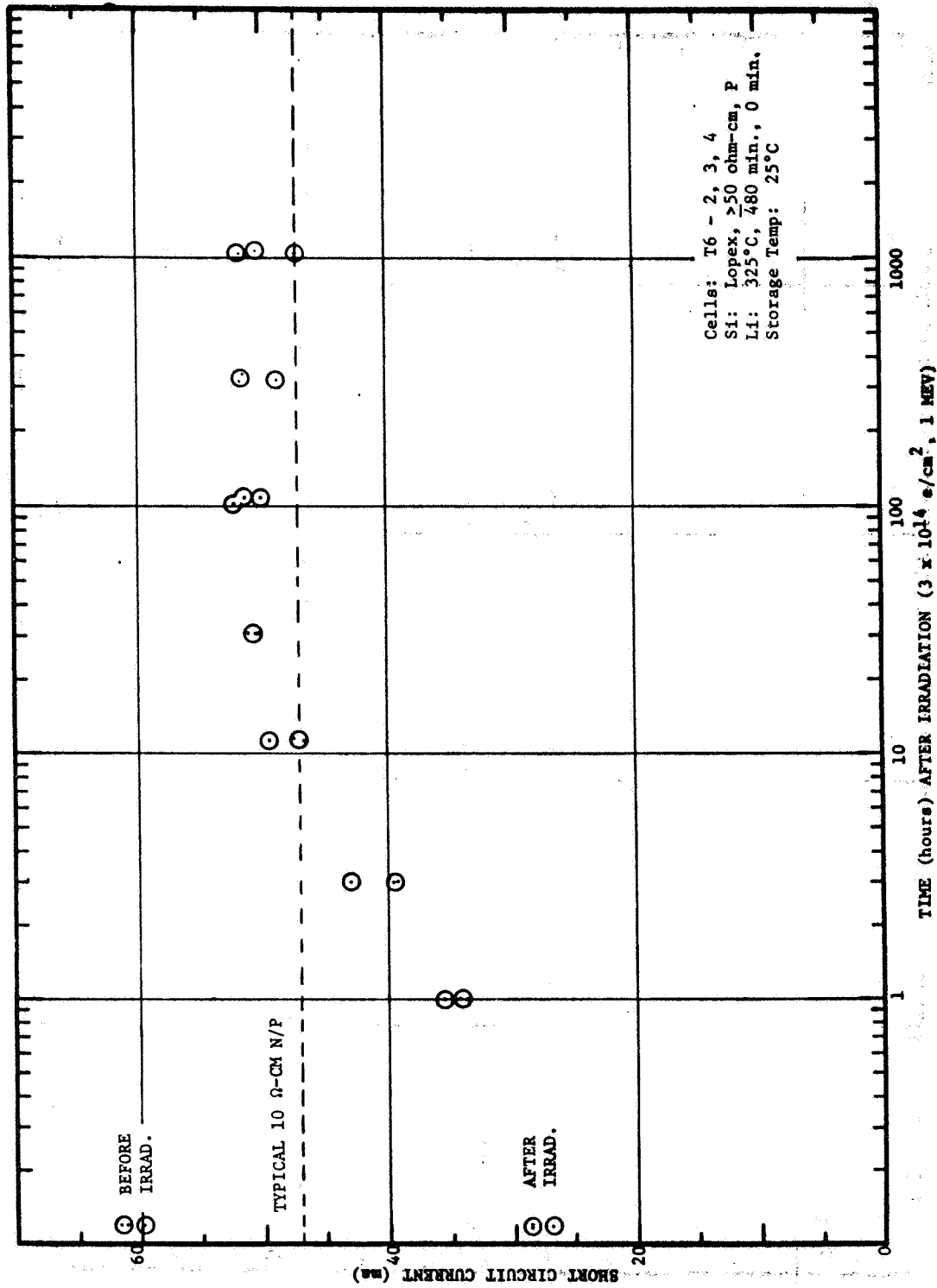


FIG. 64 RECOVERY OF GROUP T6 LITHIUM SOLAR CELLS AFTER  
 $3 \times 10^{14} \text{ e/cm}^2$



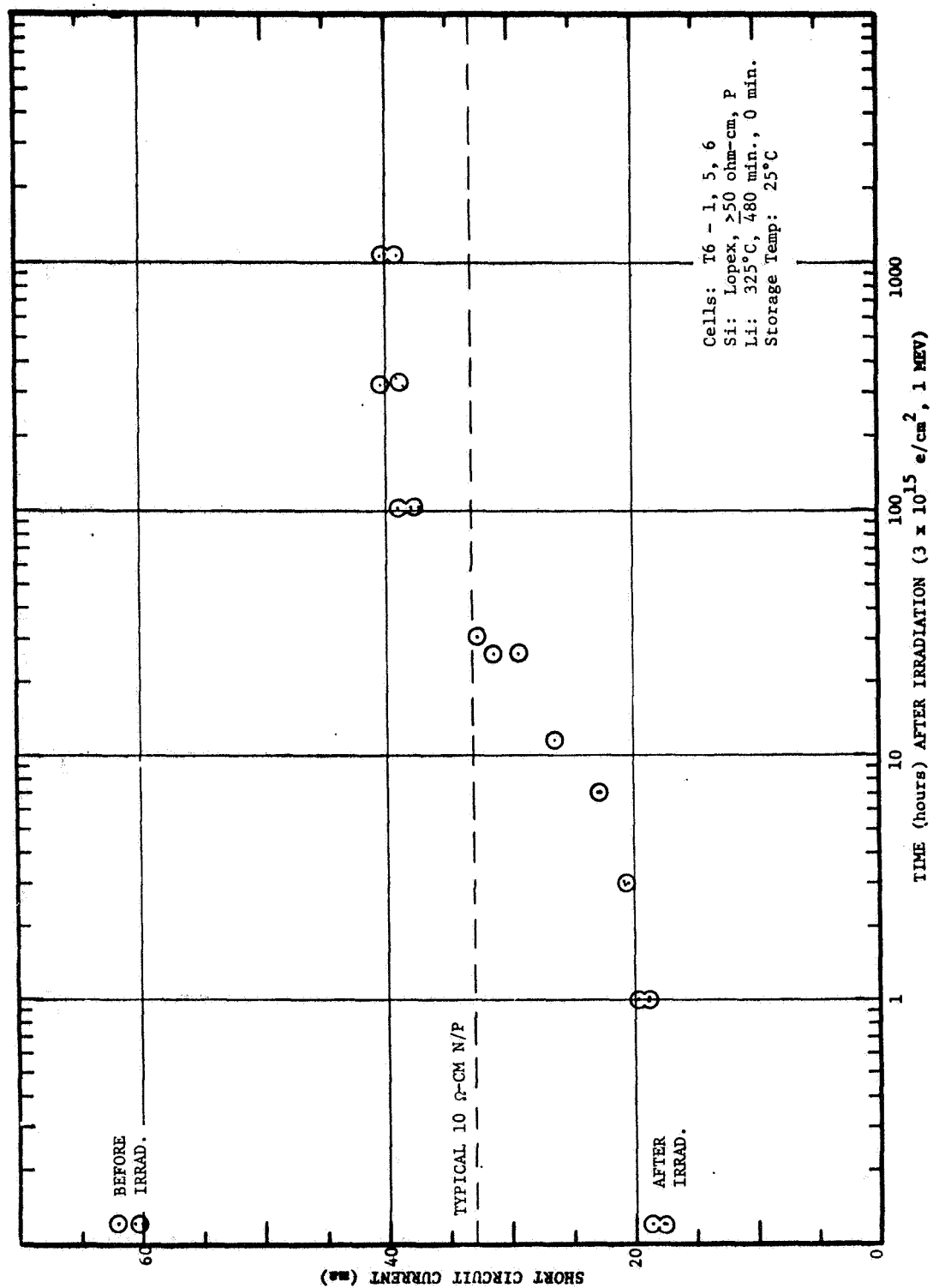


FIG. 65 RECOVERY OF GROUP T6 LITHIUM SOLAR CELLS AFTER  $3 \times 10^{15} \text{ e/cm}^2$

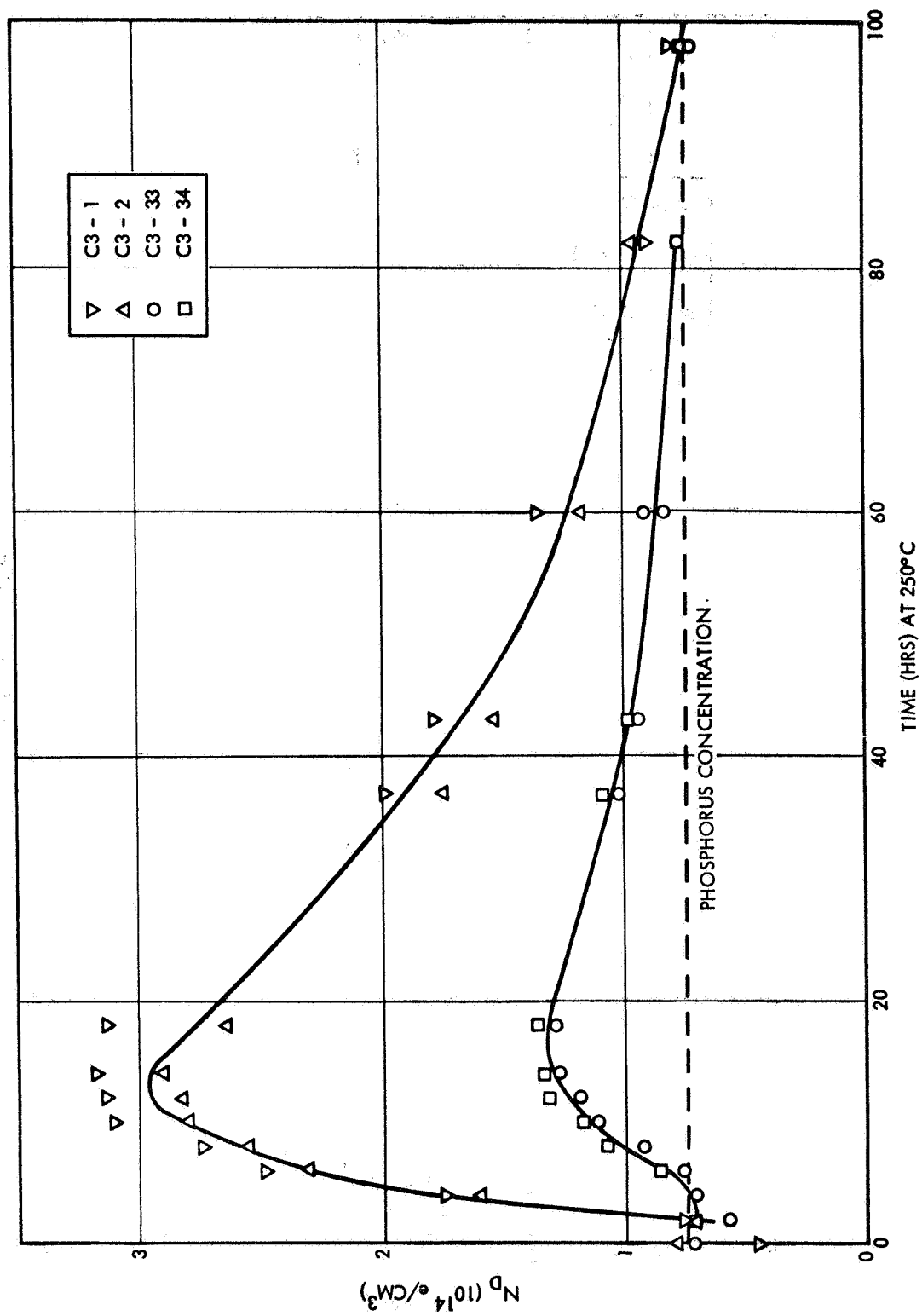


FIG. 66 CHANGES IN DONOR CONCENTRATION DURING REDISTRIBUTION

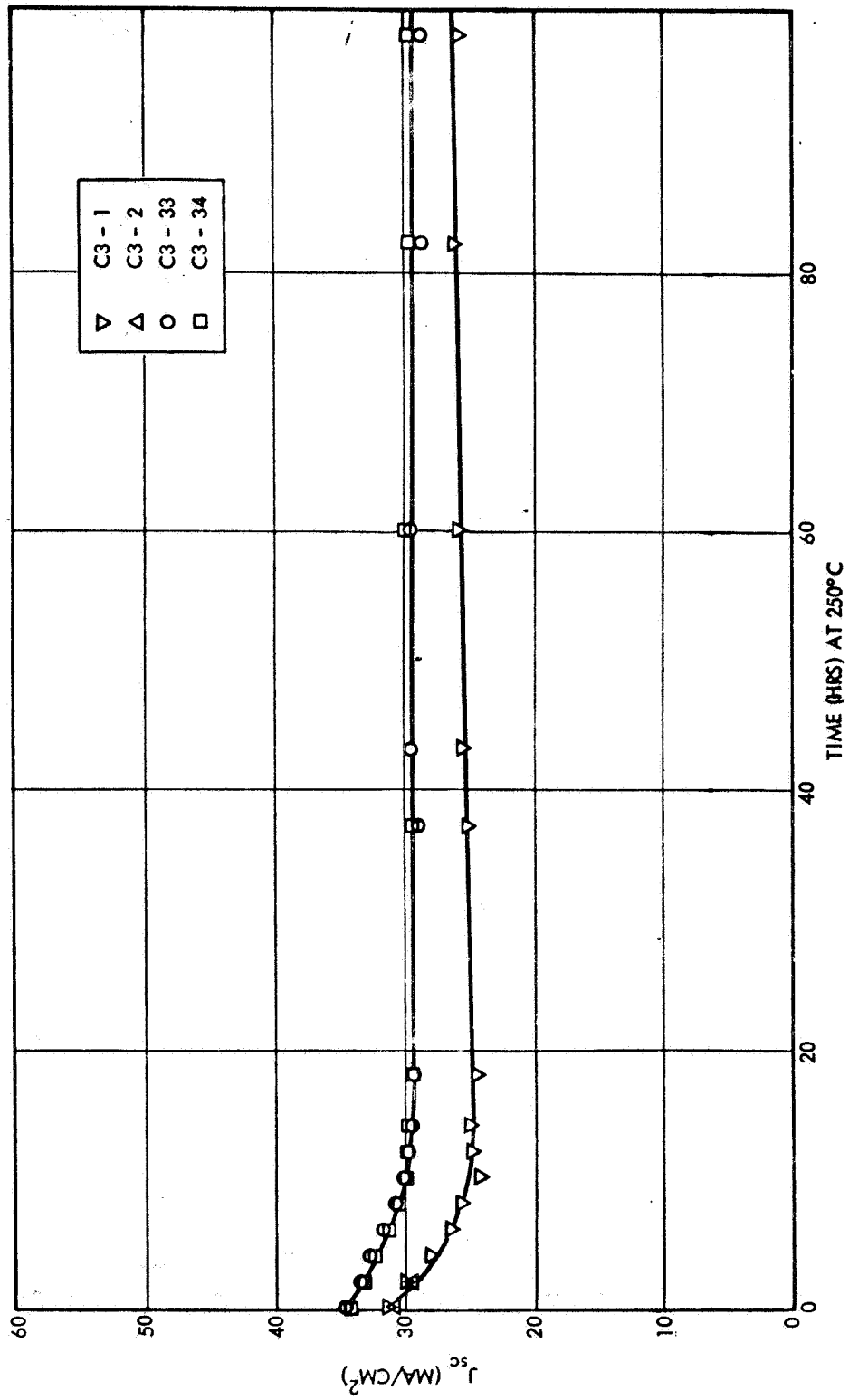


FIG. 67 CHANGES IN SHORT CIRCUIT CURRENT DURING REDISTRIBUTION

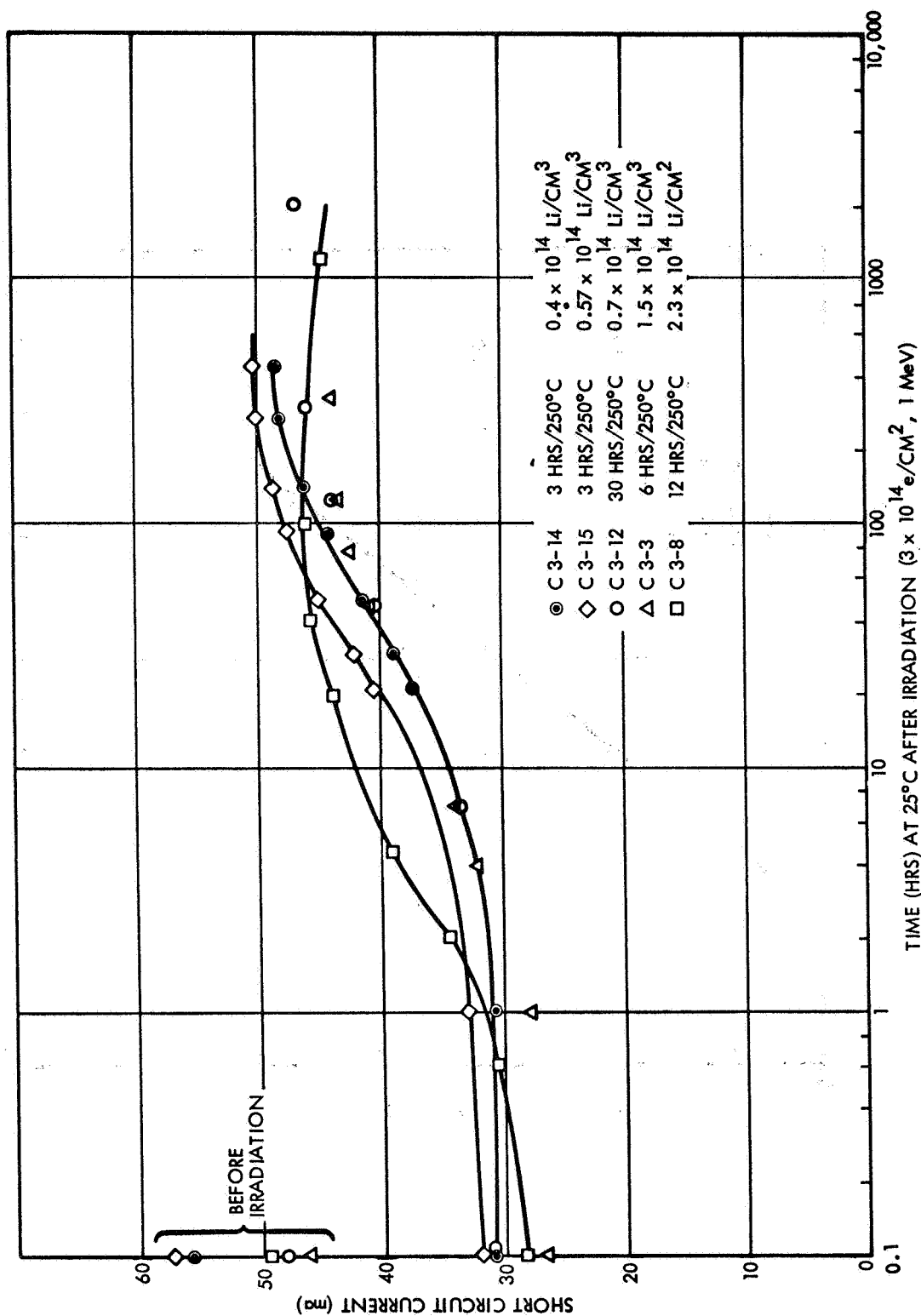


FIG. 68 CHANGES IN SHORT CIRCUIT CURRENT DURING RECOVERY

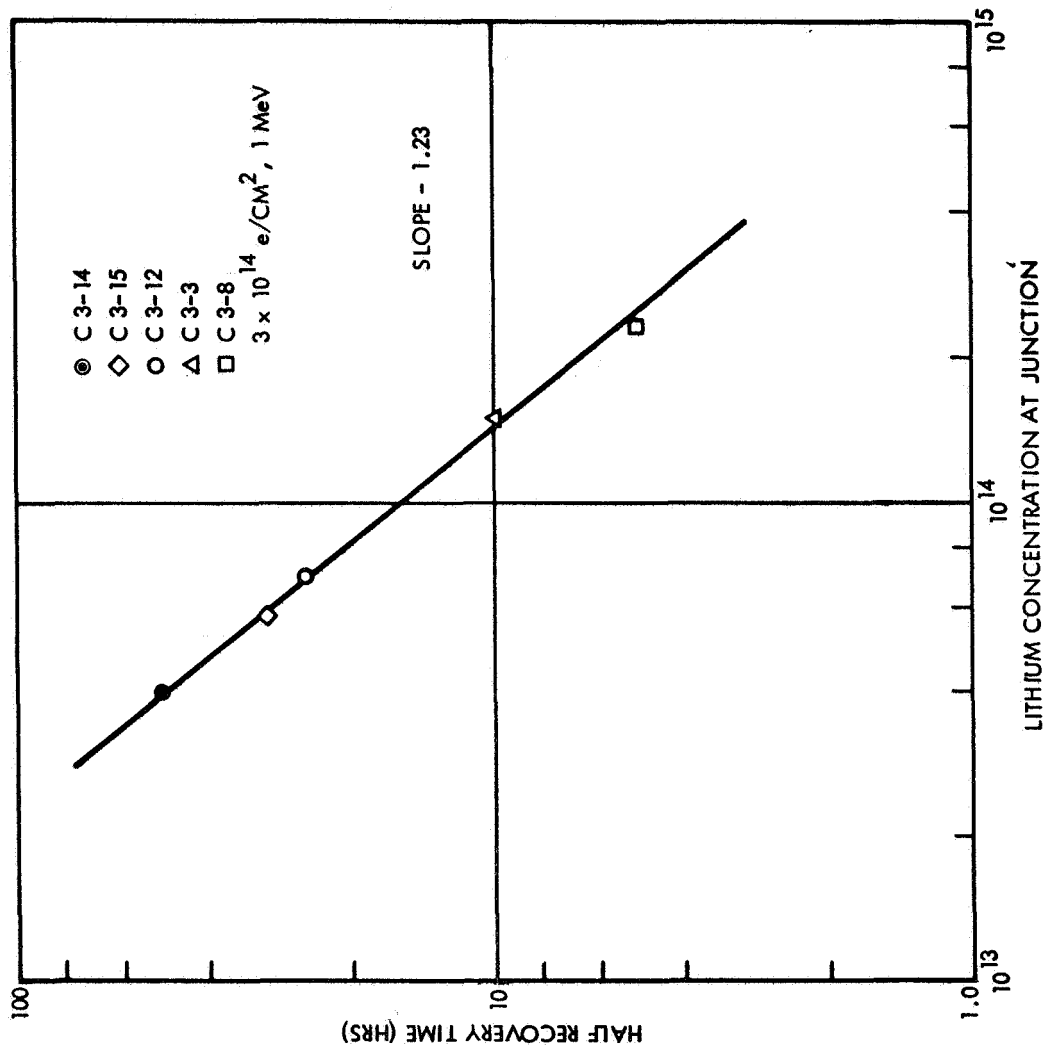


FIG. 69 VARIATION OF RECOVERY HALF TIME WITH LI CONCENTRATION

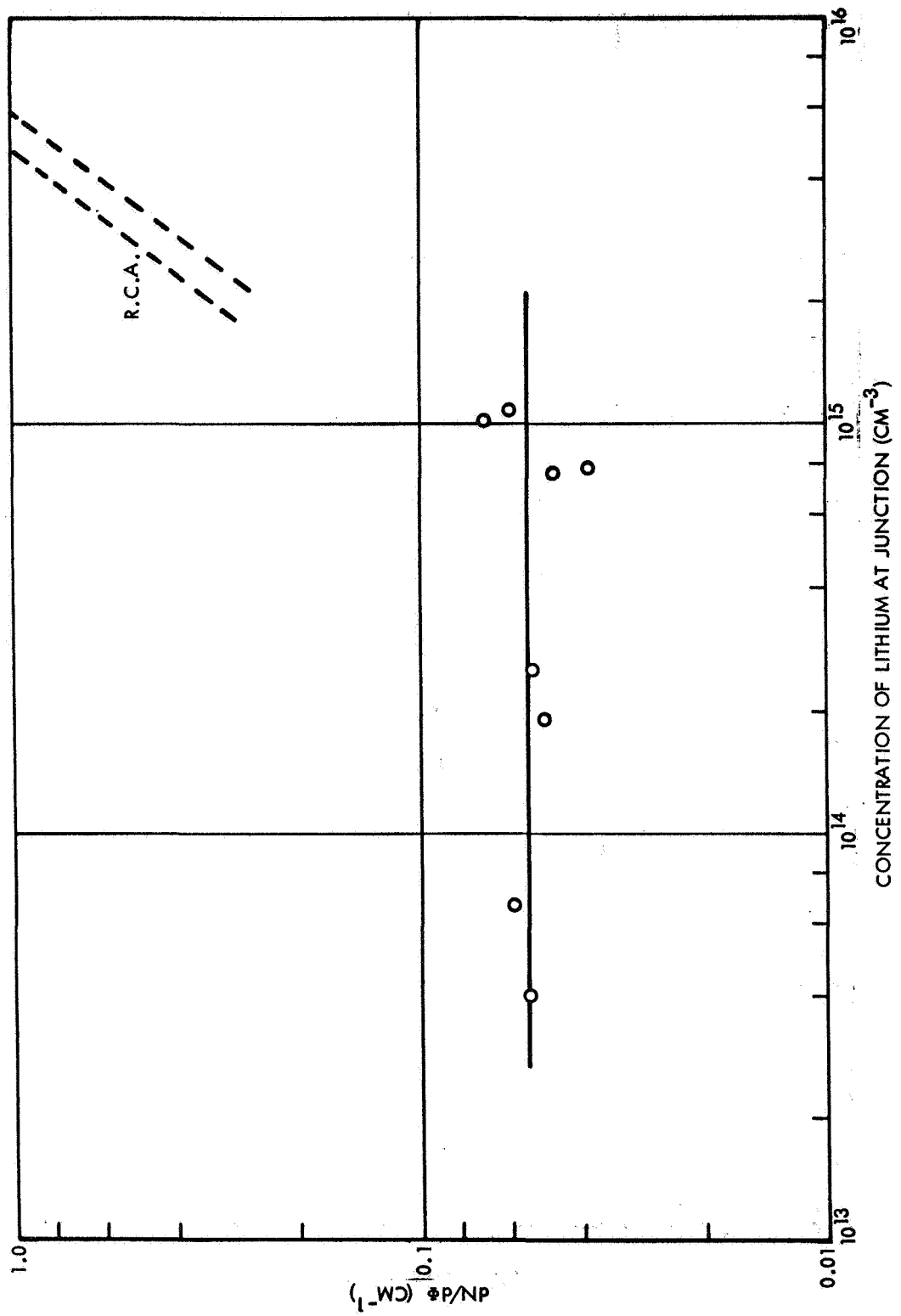


FIG. 70 REMOVAL RATE AT JUNCTION FOR VARIOUS LI CONCENTRATIONS

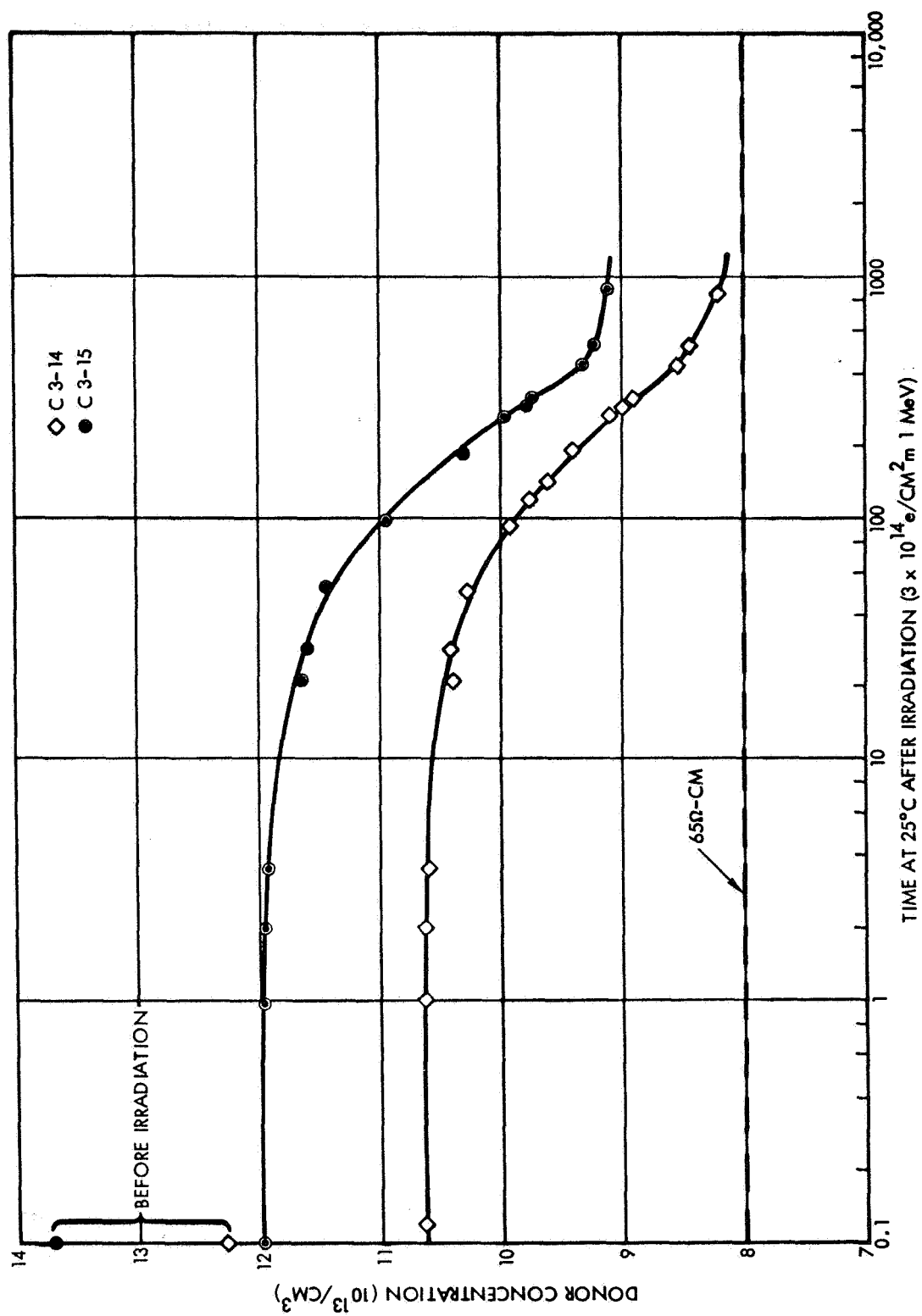


FIG. 71 CHANGES IN LI CONCENTRATION DURING RECOVERY

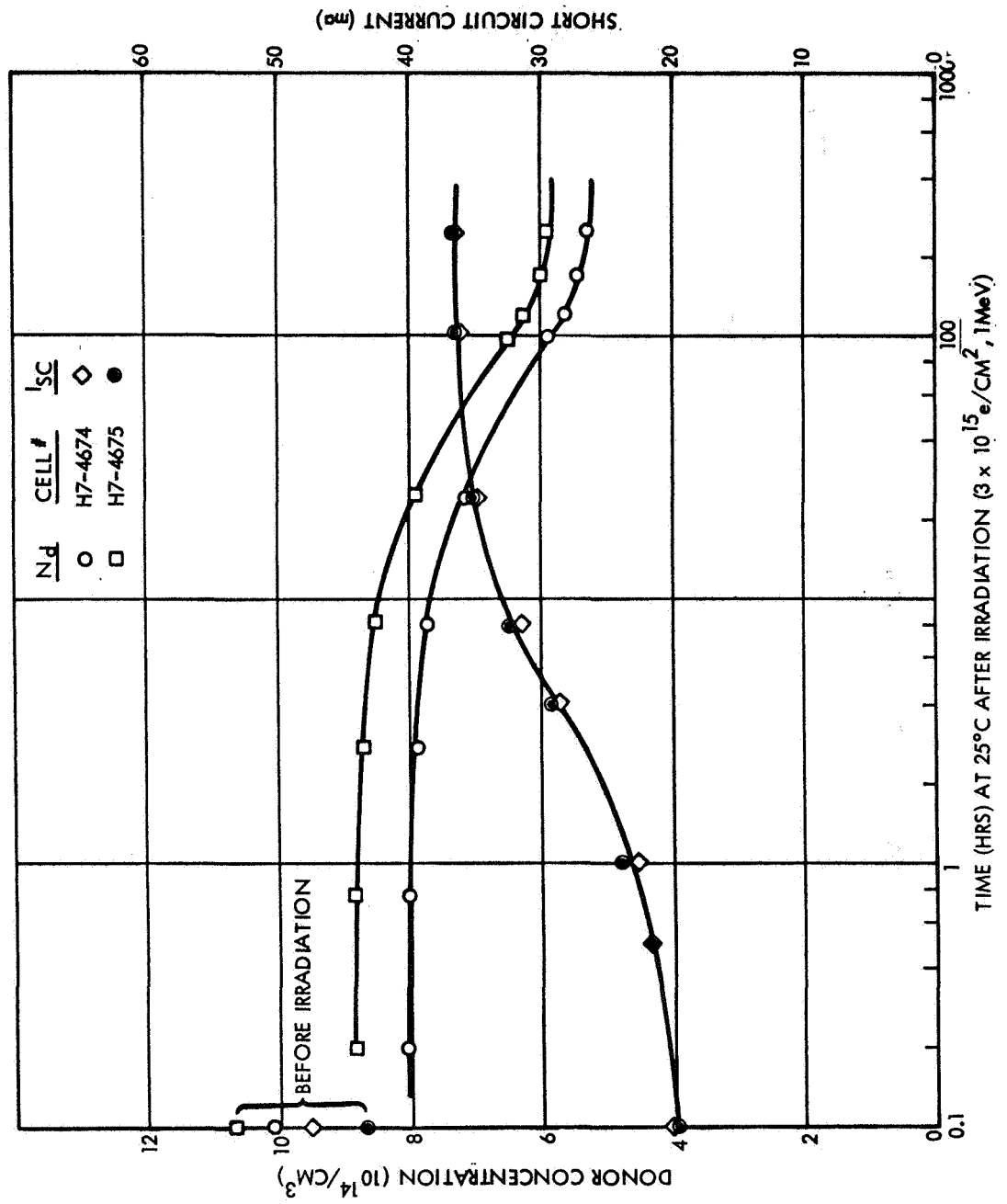


FIG. 72 CHANGES IN LI CONCENTRATION AND SHORT CIRCUIT CURRENT DURING RECOVERY



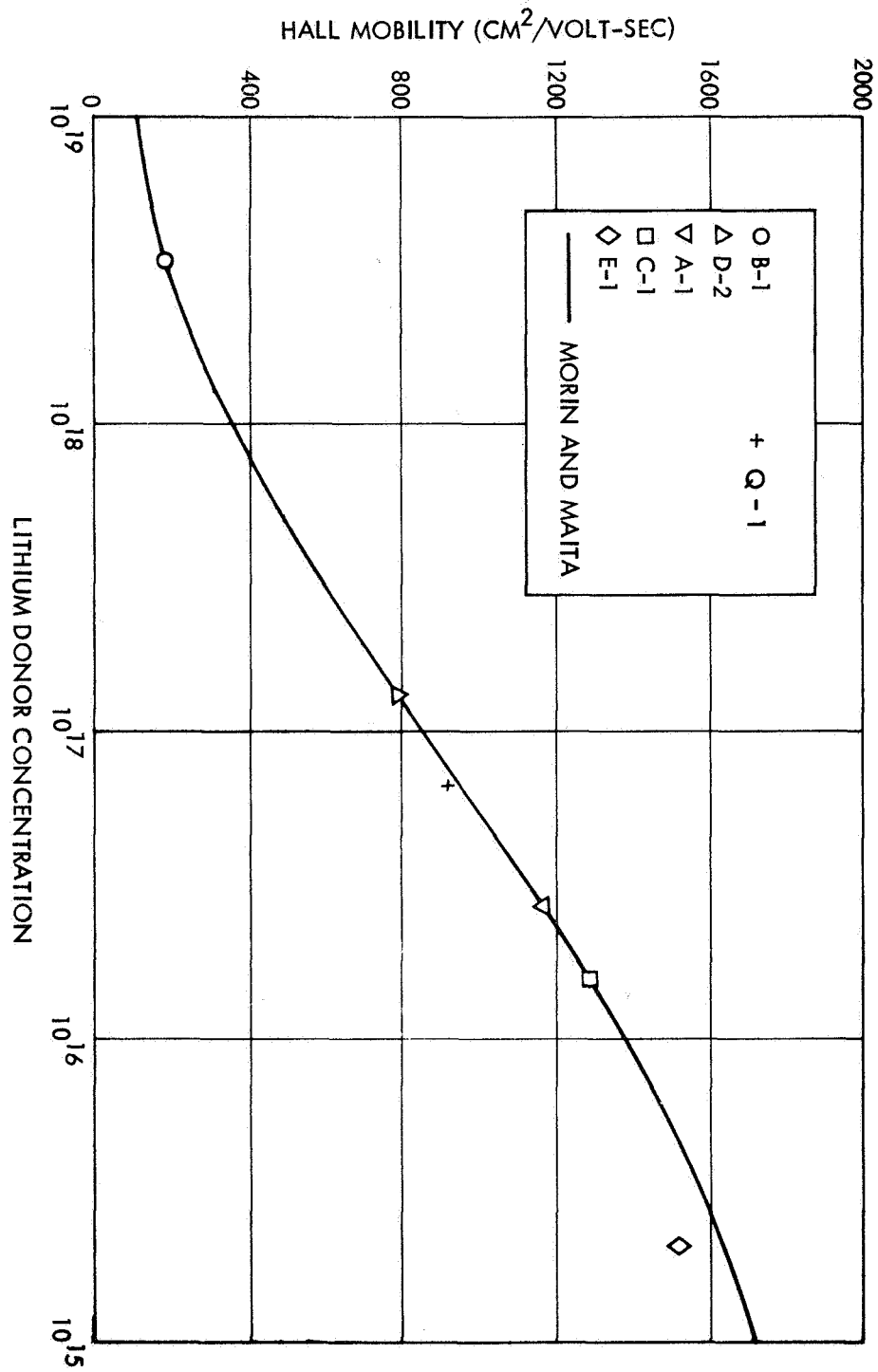


FIG. 73 HALL MOBILITIES OF LITHIUM DOPED SILICON

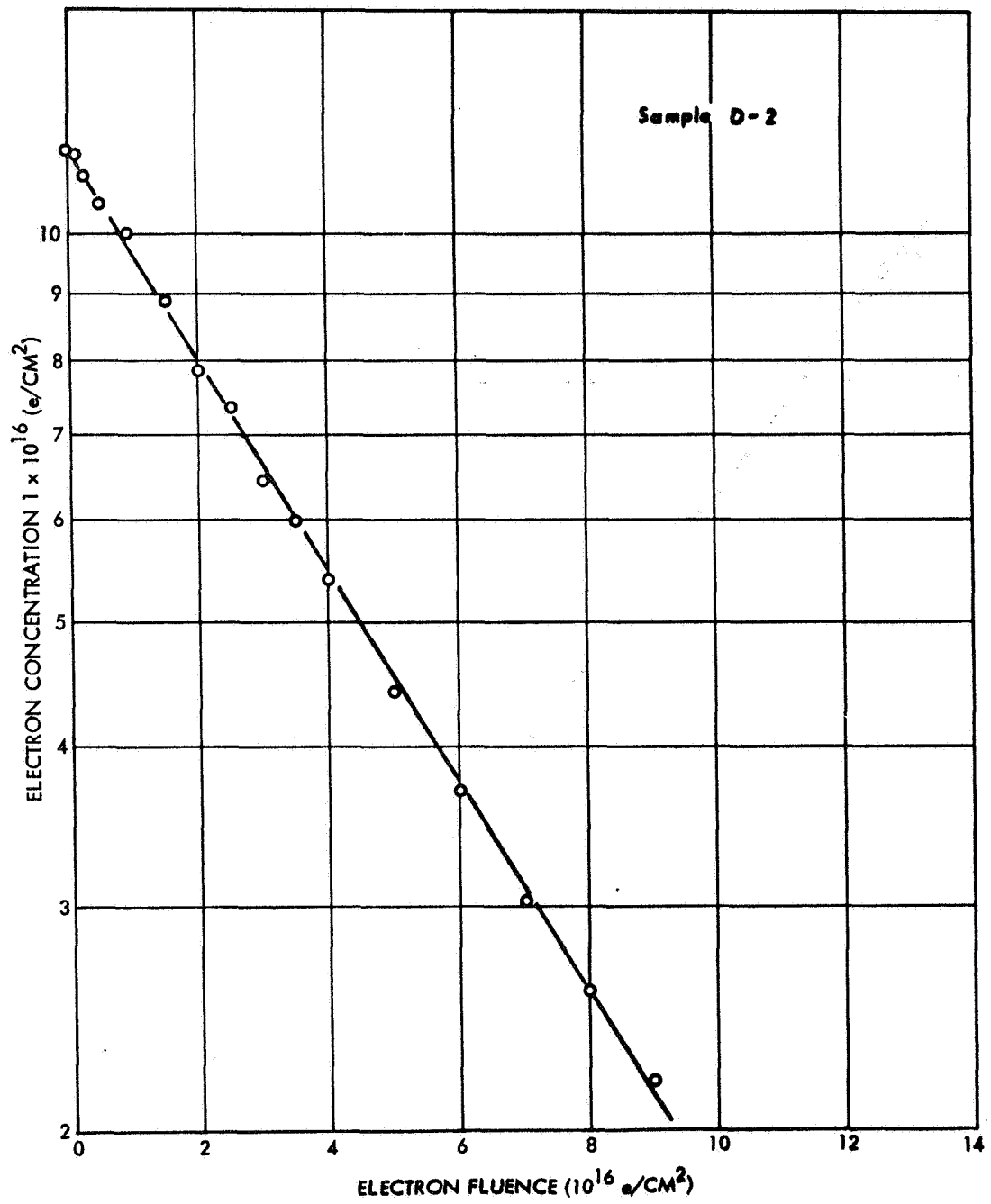


FIG. 74 CARRIER REMOVAL, LITHIUM DOPED F. Z. SILICON

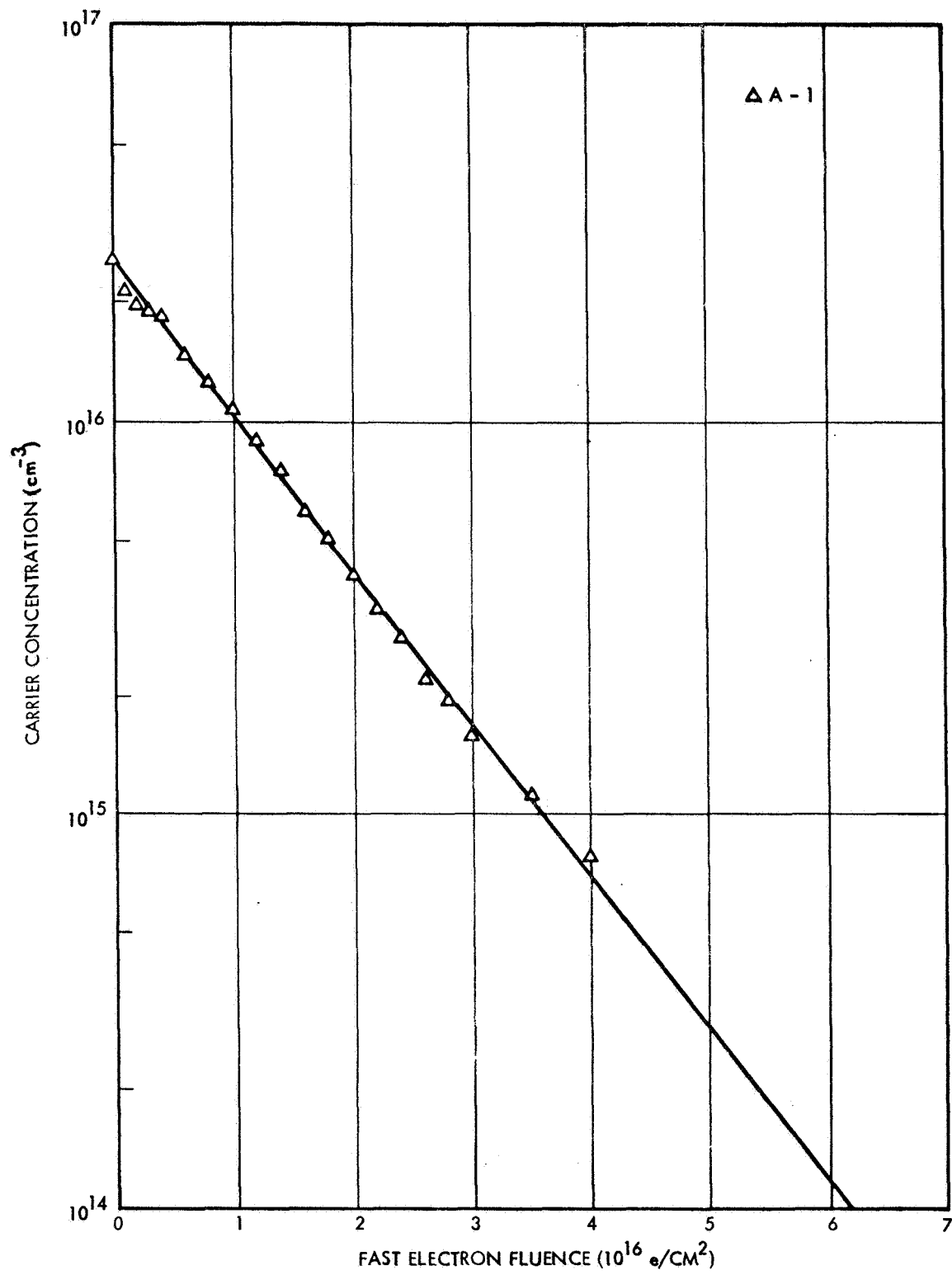


FIG. 75 CARRIER REMOVAL, LITHIUM DOPED F. Z. SILICON

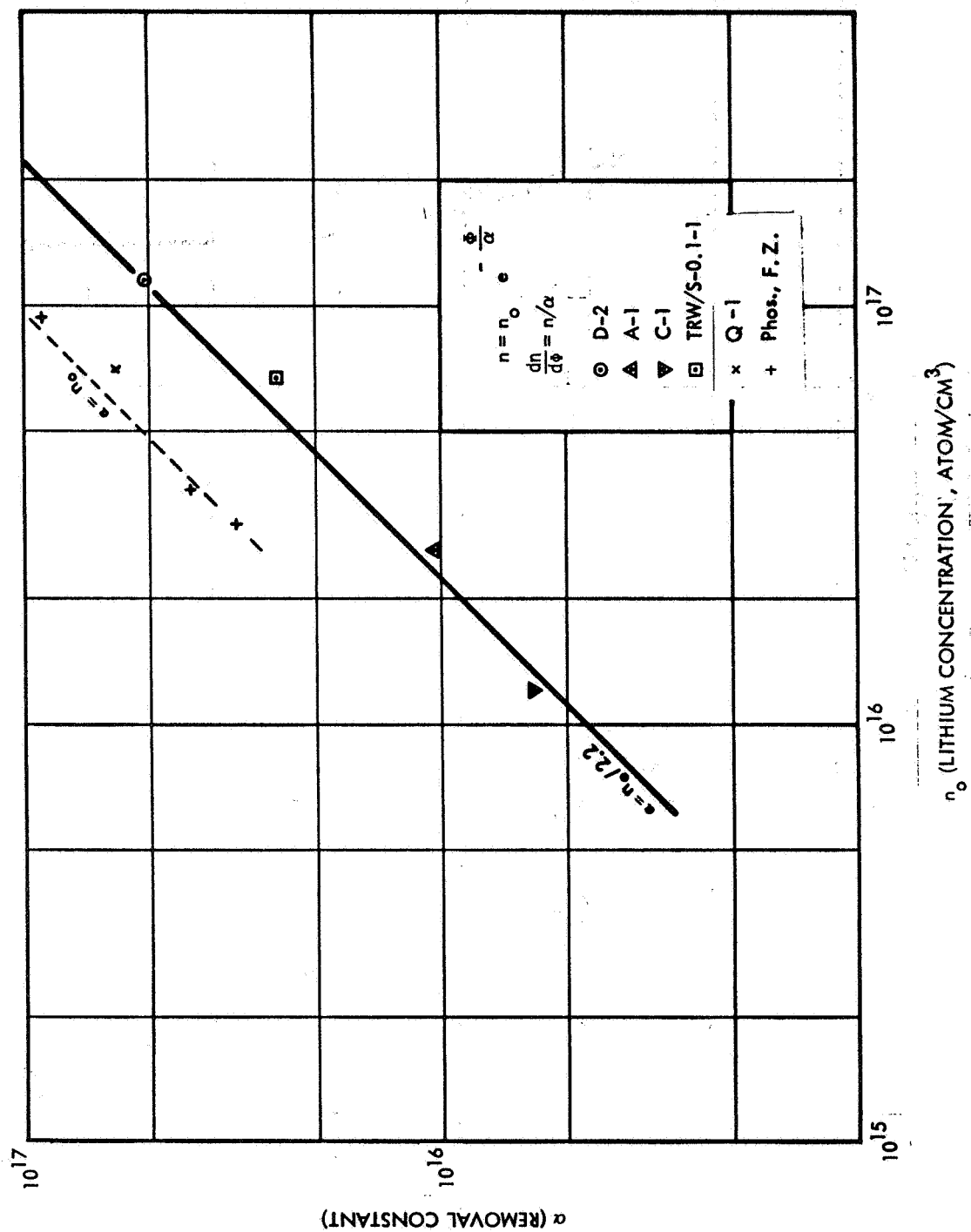


FIG. 76 REMOVAL CONSTANT VS. DONOR CONCENTRATION.

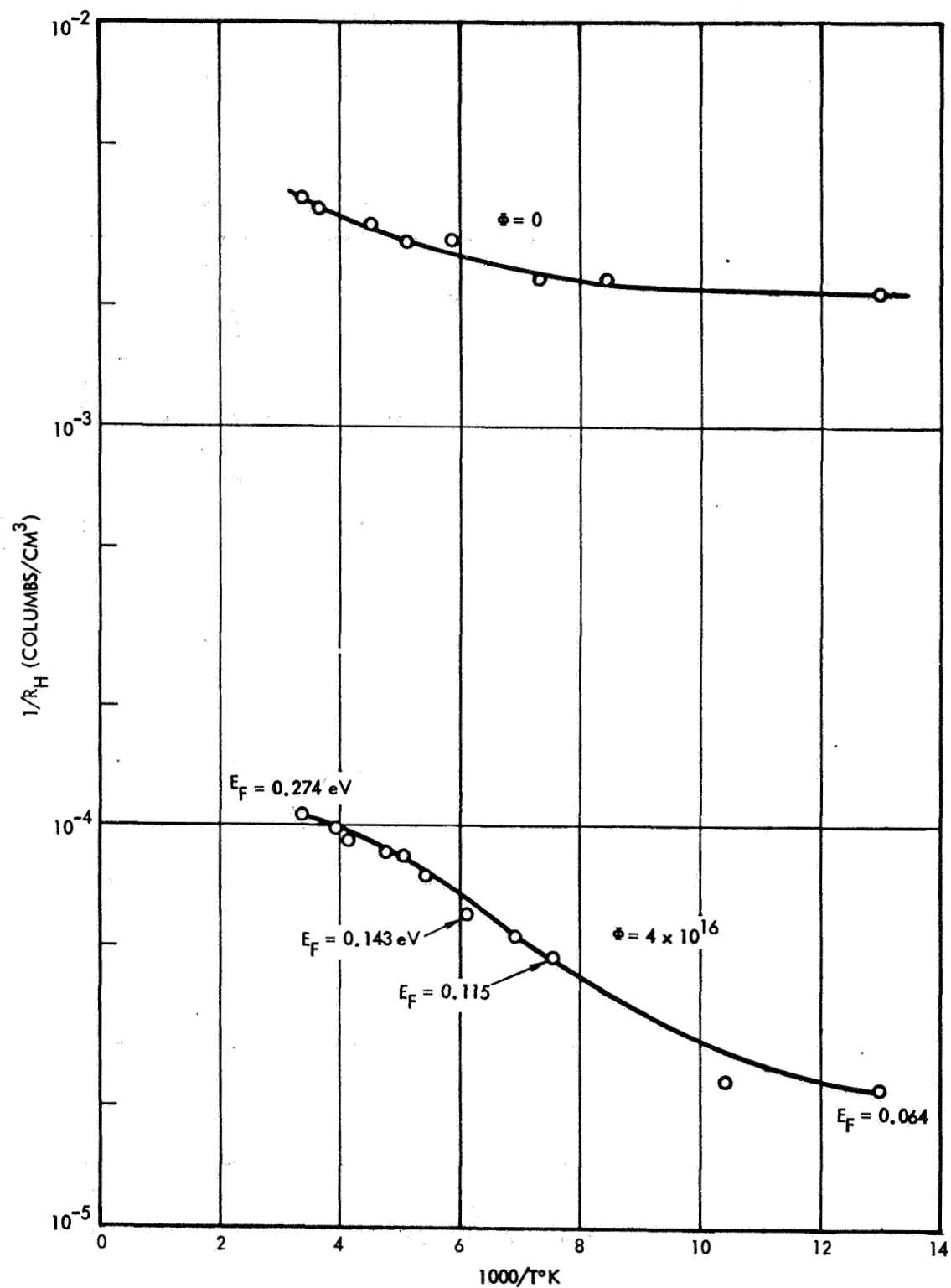


FIG. 77 HALL COEFFICIENT CHANGES DURING IRRADIATION, LITHIUM  
DOPED F. Z. SILICON

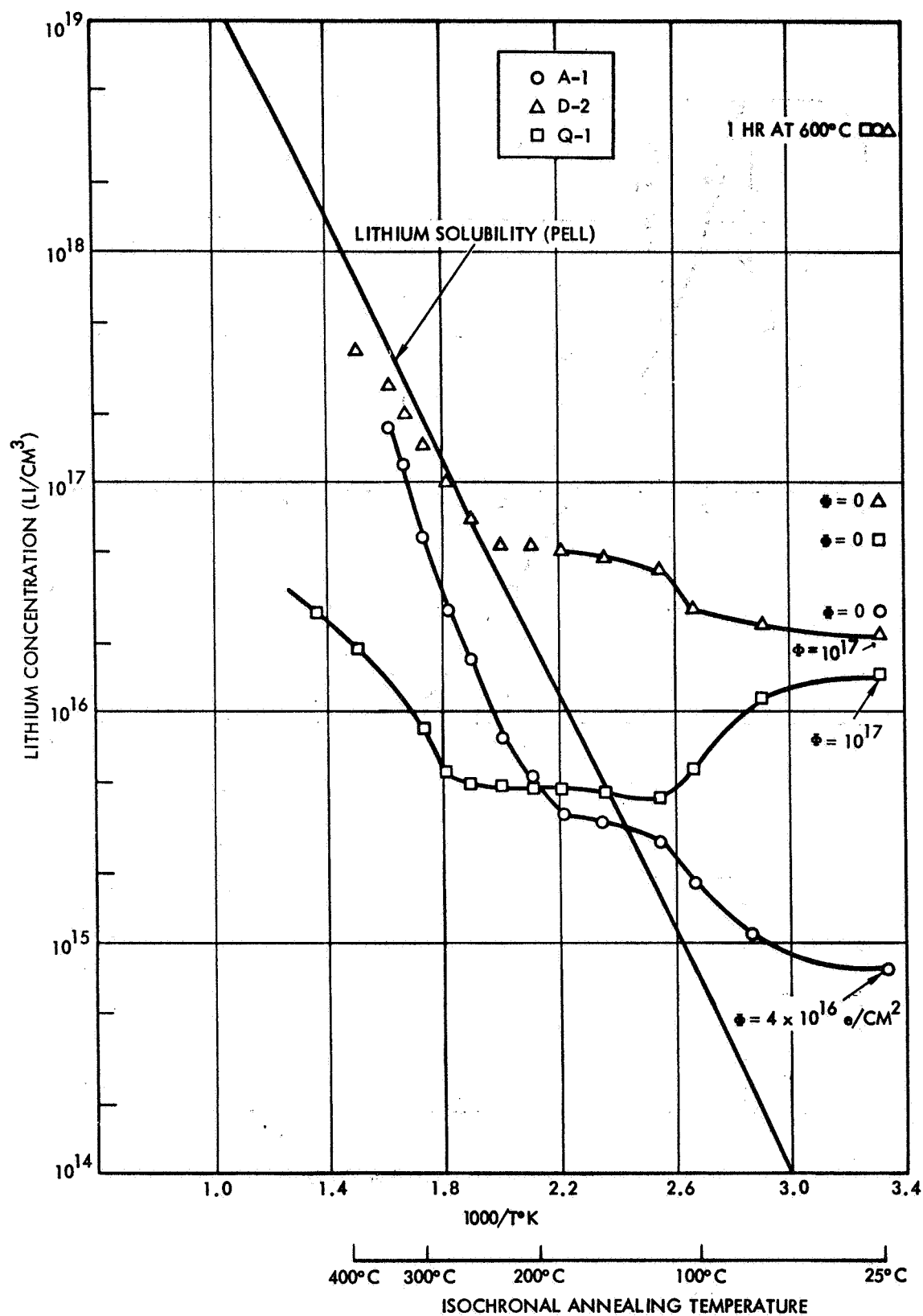


FIG. 78 ANNEALING OF IRRADIATED LITHIUM DOPED SILICON

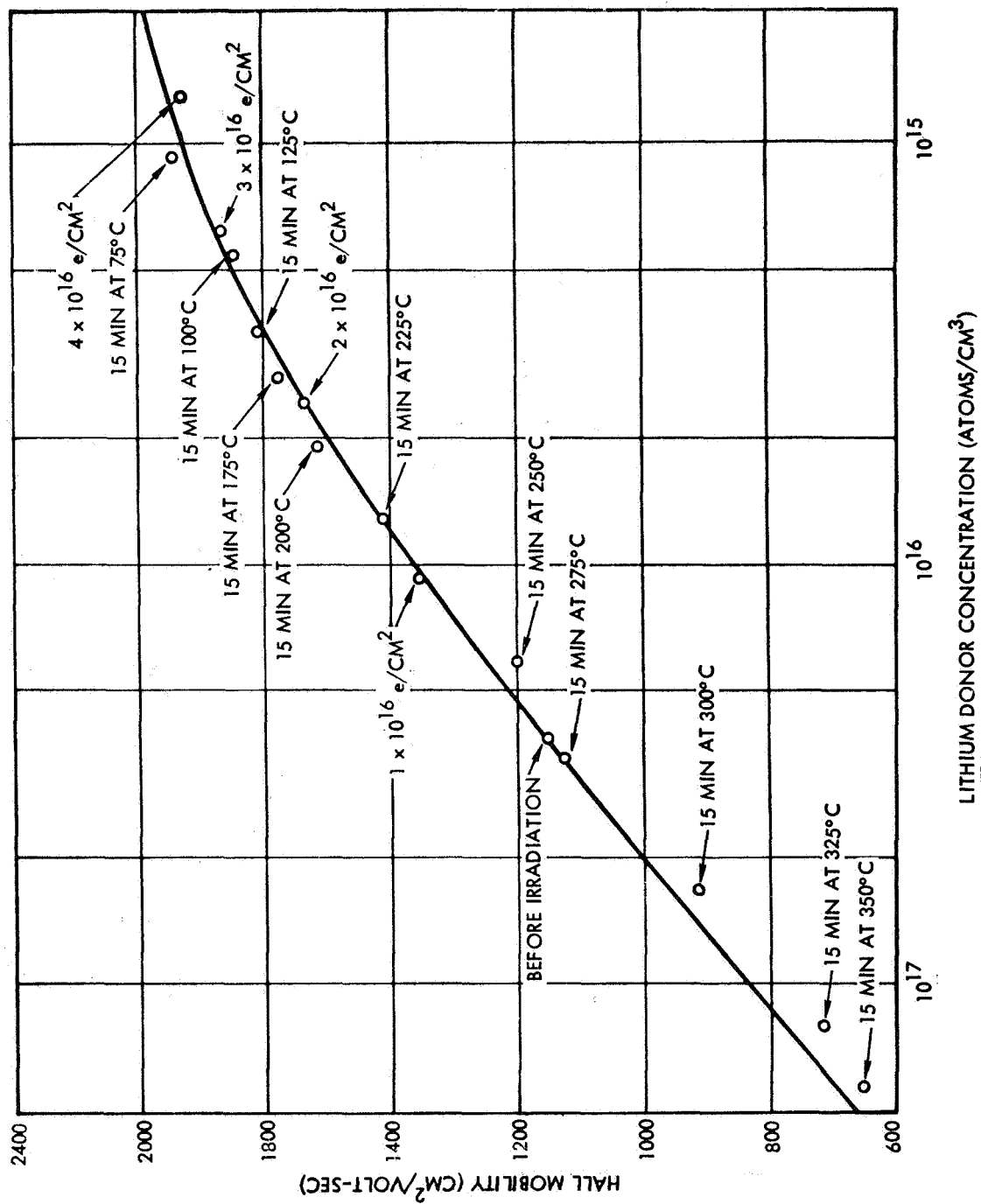


FIG. 79 MOBILITY CHANGES DURING IRRADIATION AND ANNEALING, F.Z.

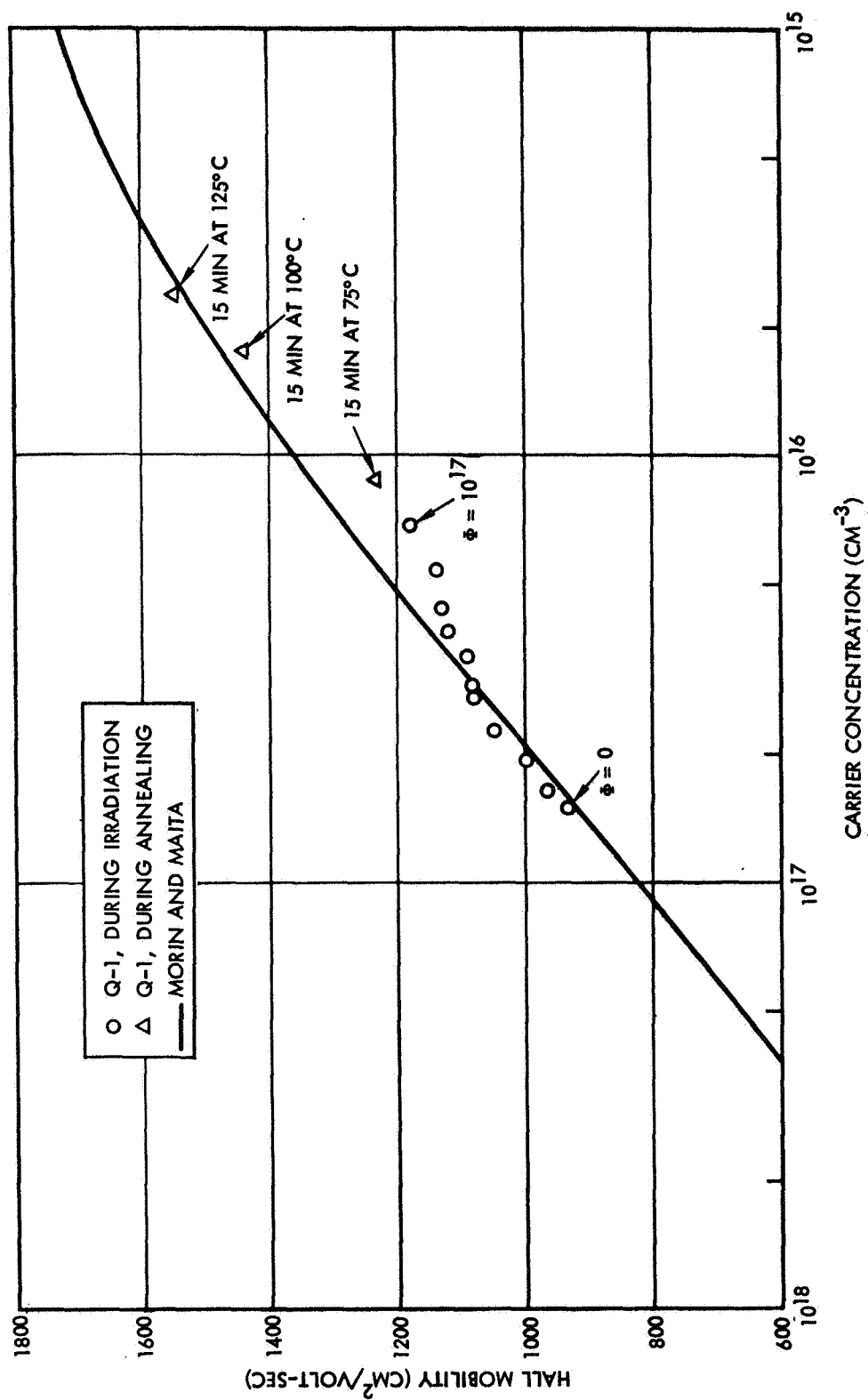


FIG. 80 MOBILITY CHANGES DURING IRRADIATION AND ANNEALING, Q.C.



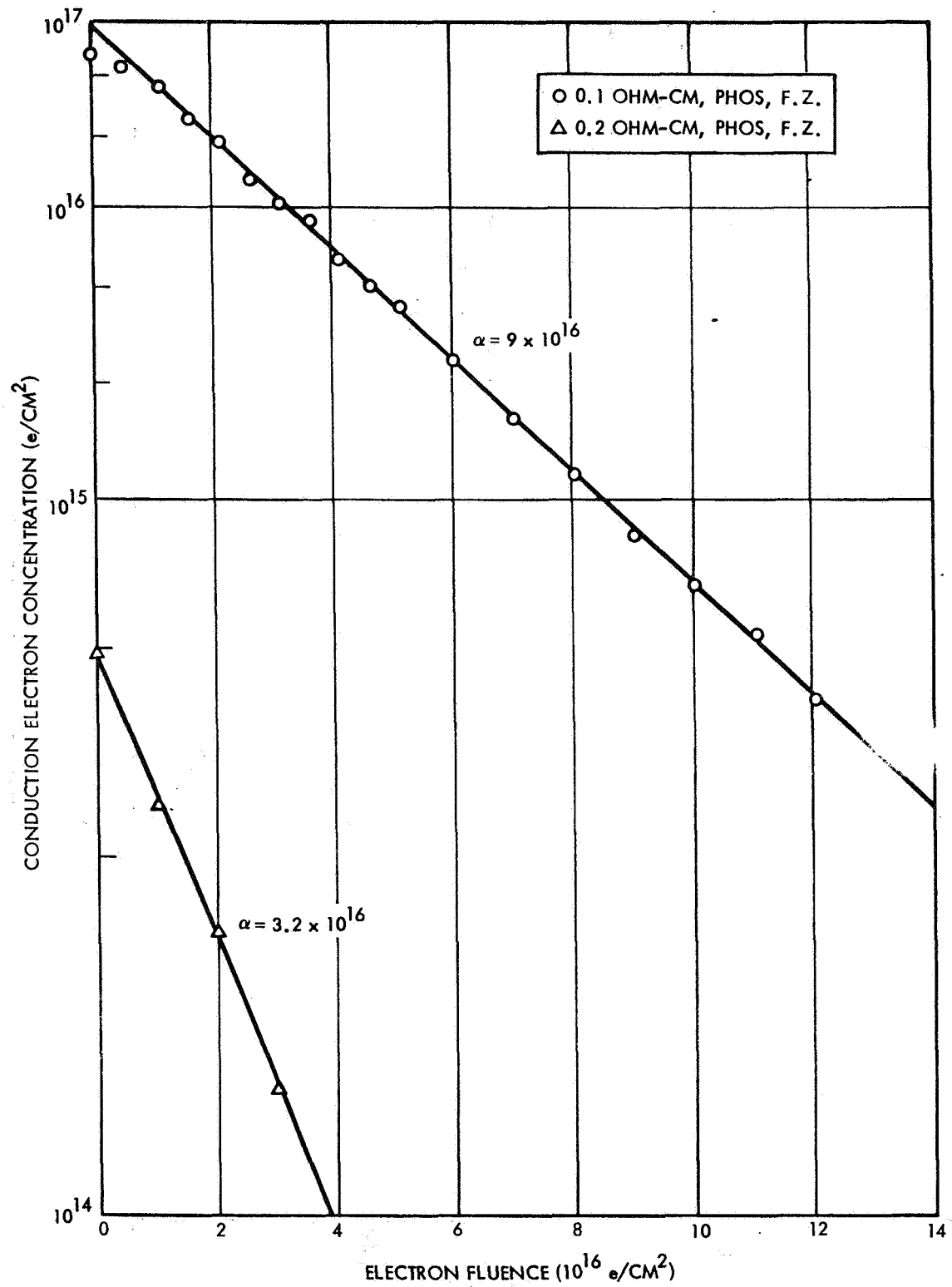


FIG. 81 CARRIER REMOVAL, PHOSPHORUS DOPED F. Z. SILICON

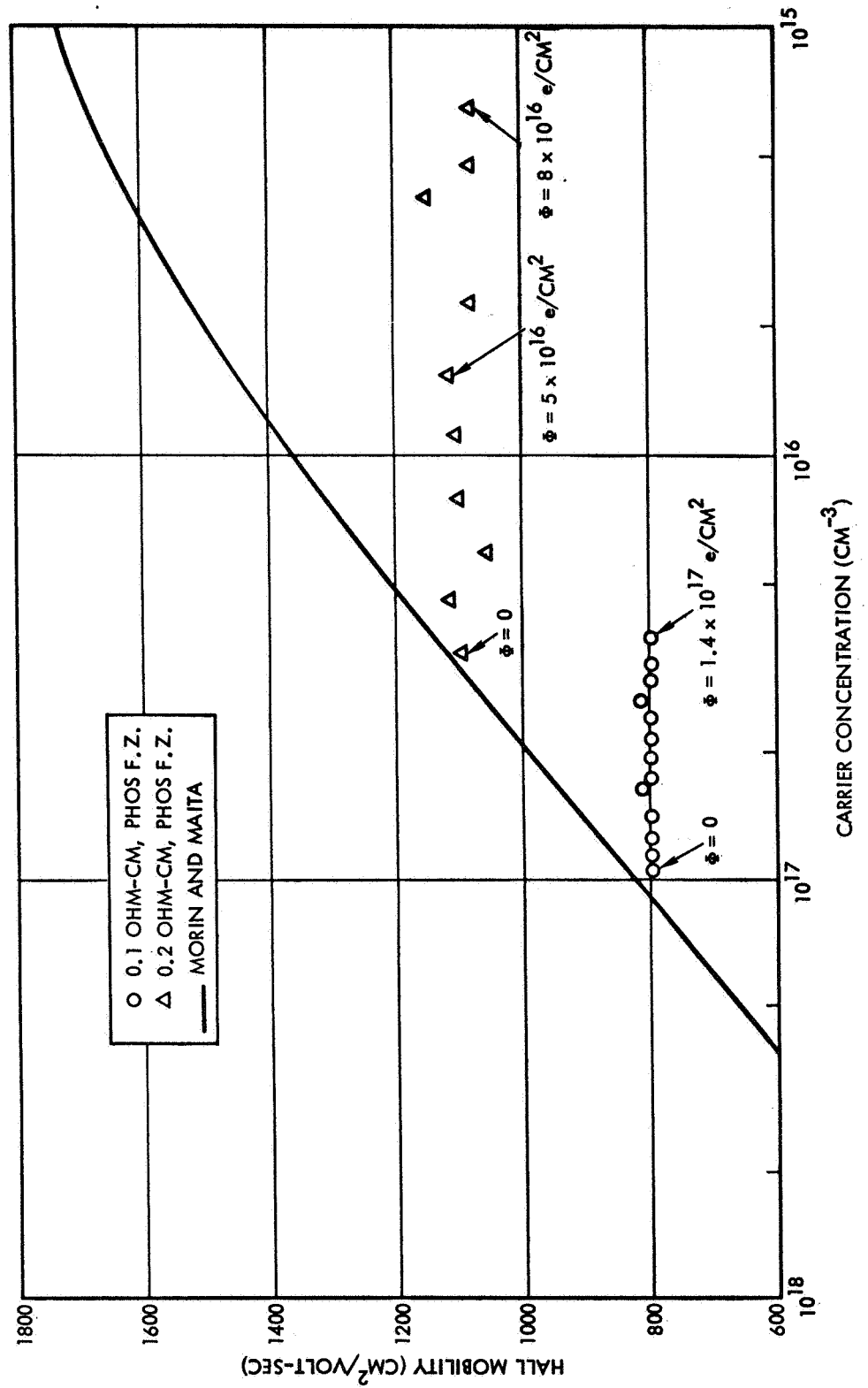


FIG. 82 MOBILITY CHANGES DURING IRRADIATION AND ANNEALING,  
PHOSPHORUS FLOAT ZONE

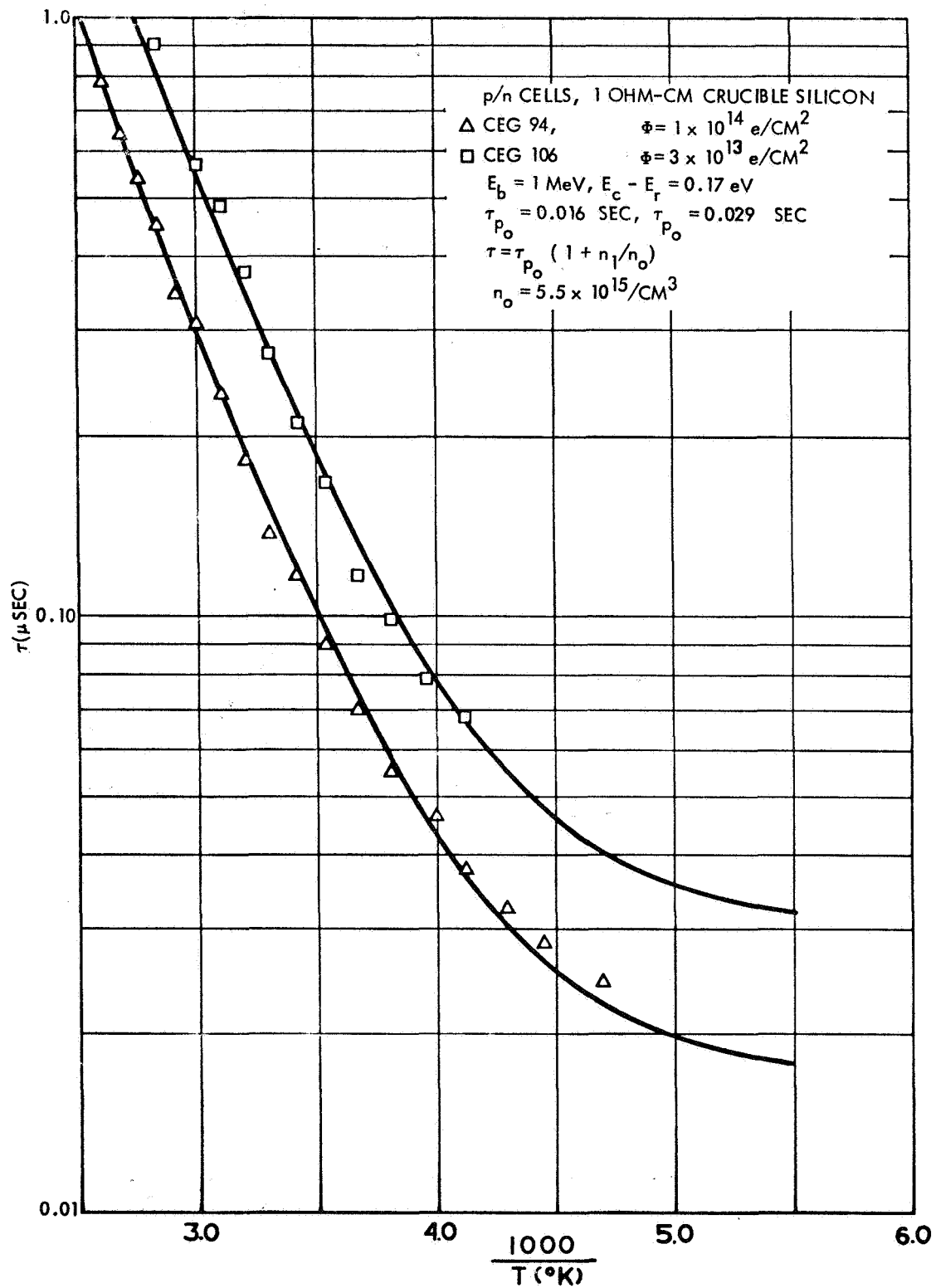


FIG. 83 LIFETIME VERSUS RECIPROCAL TEMP, P/N NON-LITHIUM CELLS

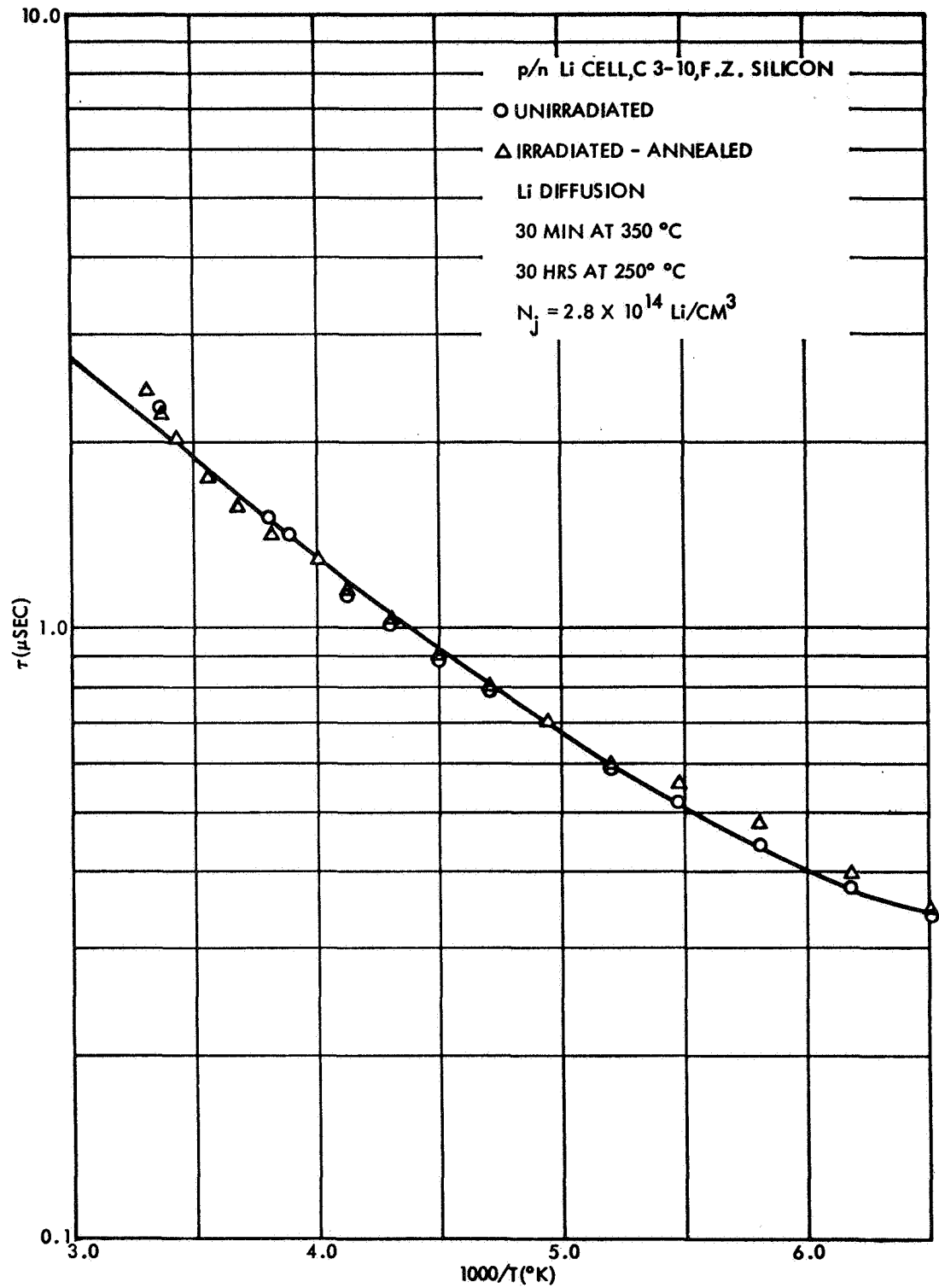


FIG. 84 LIFETIME VERSUS RECIPROCAL TEMP, LITHIUM F. Z. CELLS

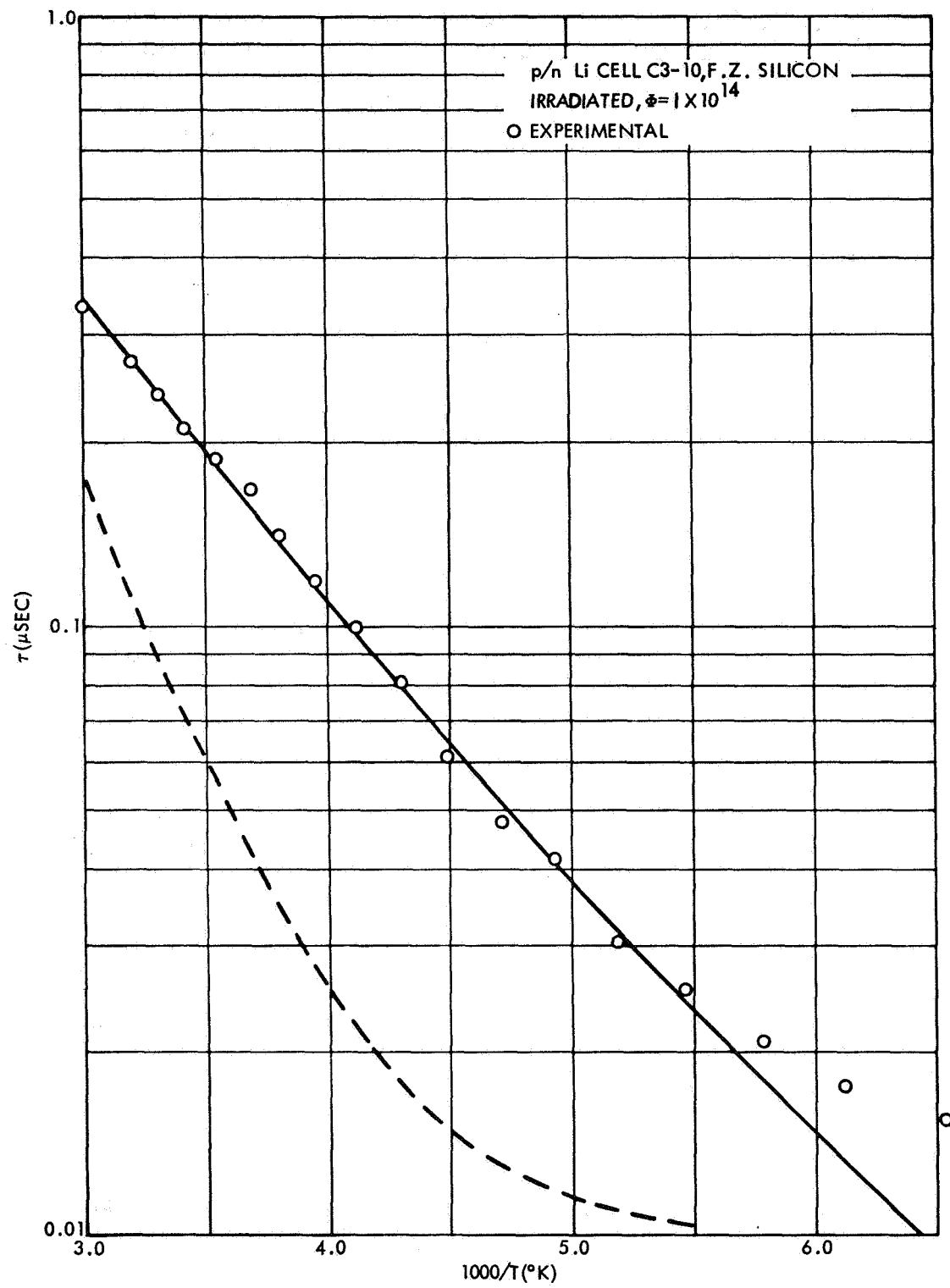


FIG. 85 LIFETIME VERSUS RECIPROCAL TEMP, LITHIUM F.Z. CELLS

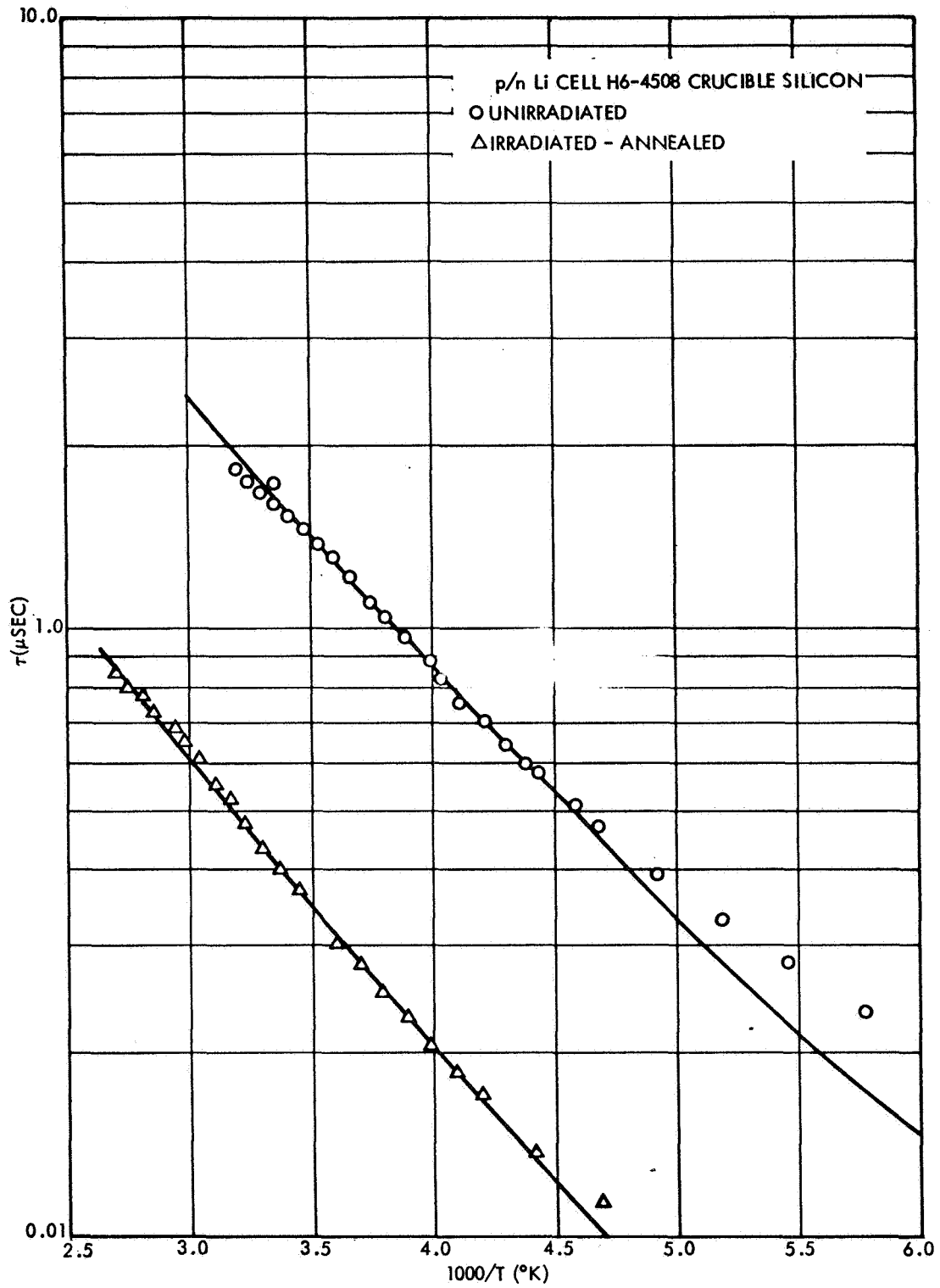


FIG. 86 LIFETIME VERSUS RECIPROCAL TEMP, LITHIUM Q.C. CELLS

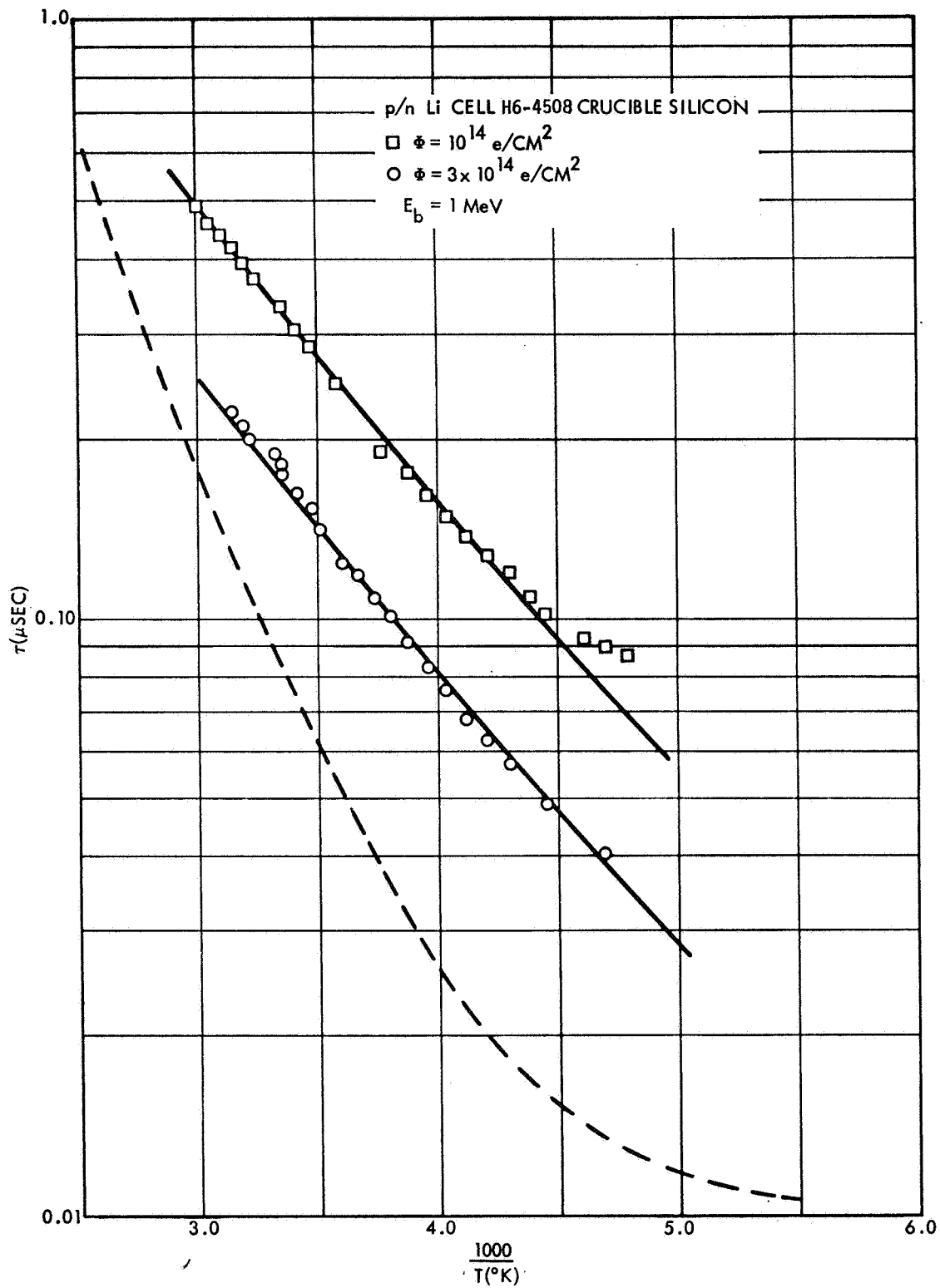


FIG. 87 LIFETIME VERSUS RECIPROCAL TEMP, LITHIUM O.C. CELLS

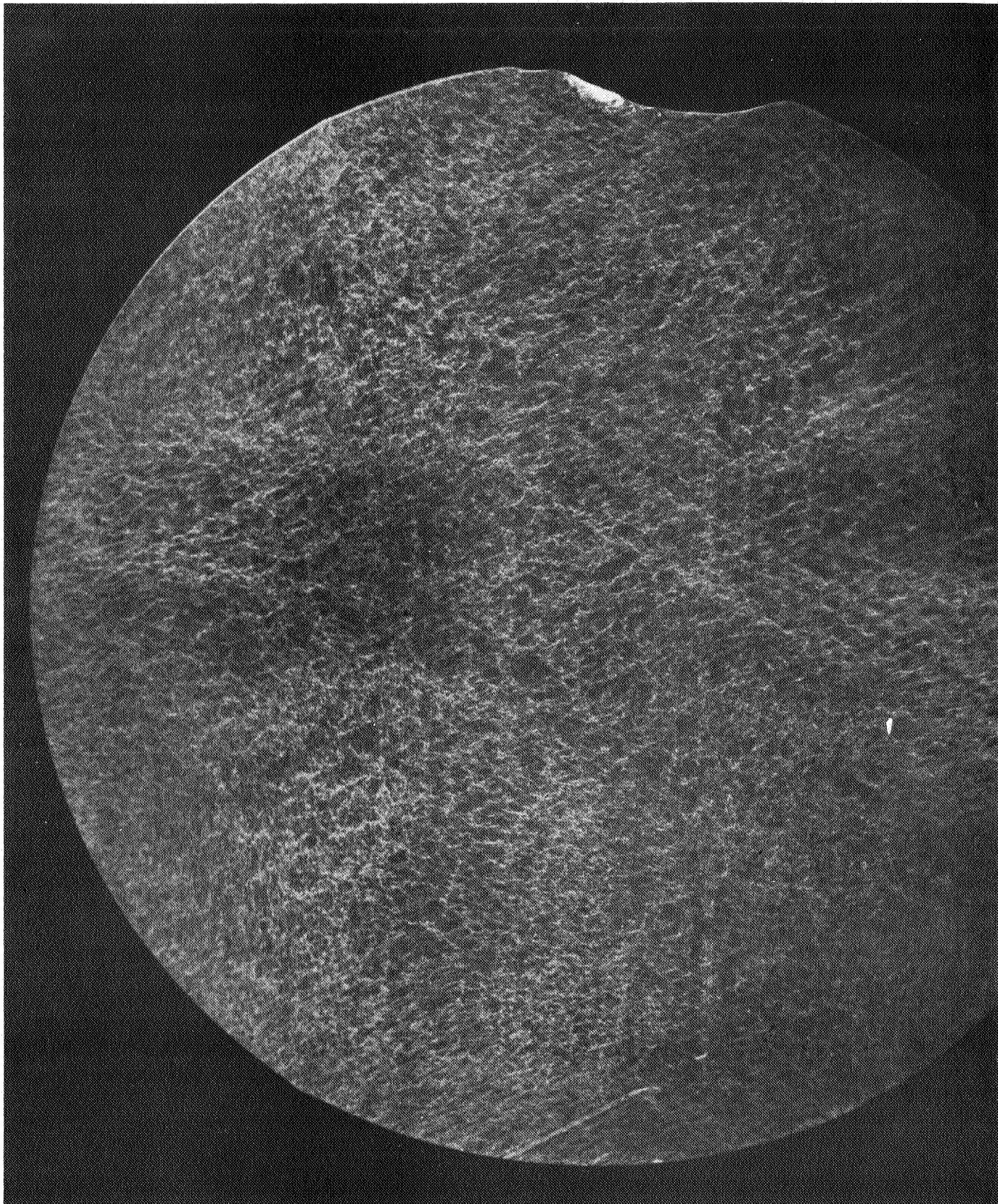


FIG. 88 TOPOGRAPH OF LI DOPED F. Z. SILICON (0.1 ohm-cm), AS RECEIVED



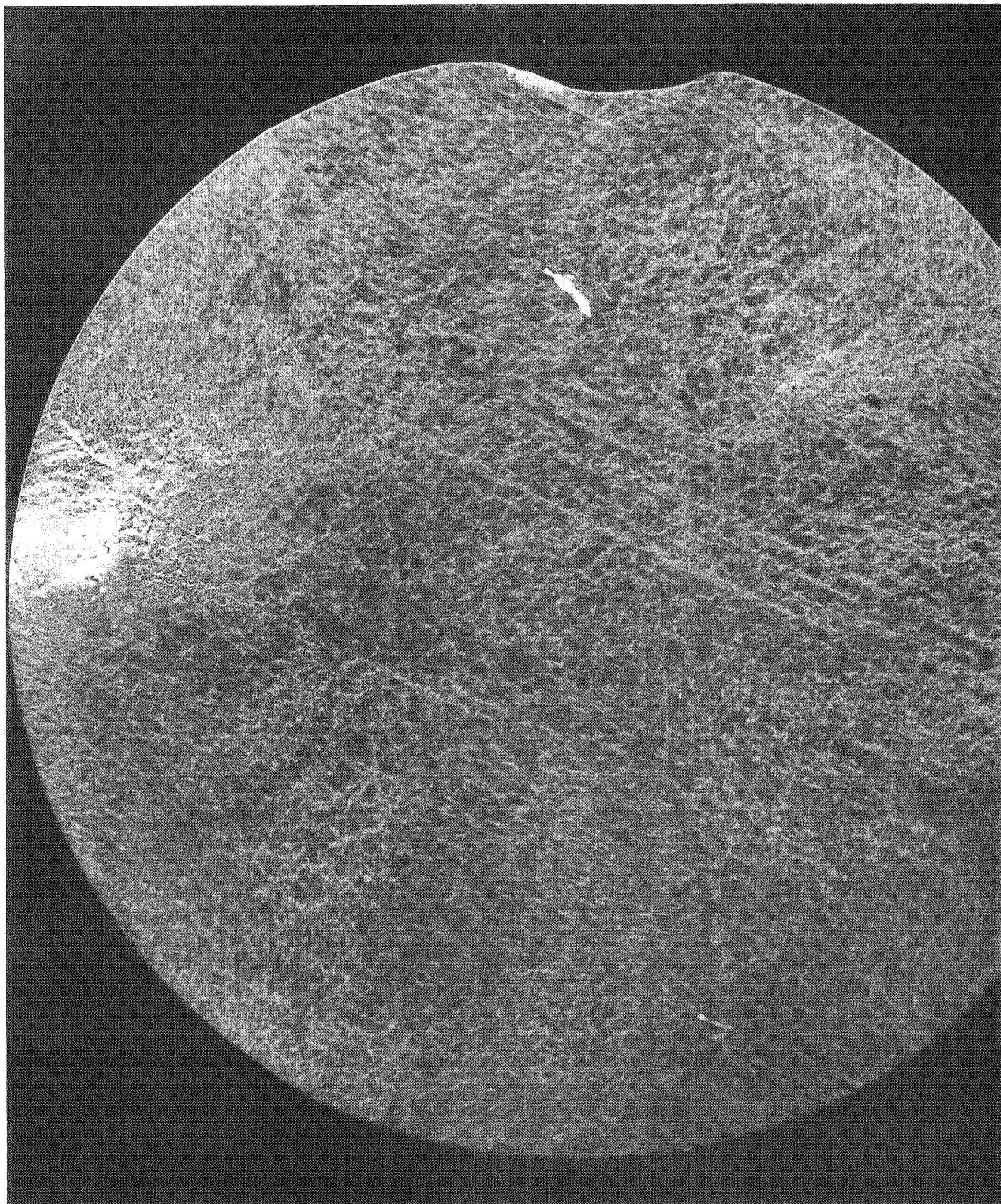


FIG. 89 TOPOGRAPH OF LI DOPED F. Z. SILICON (21 ohm-cm),  
AFTER 18 HRS. AT 400°C, SLOW COOLED

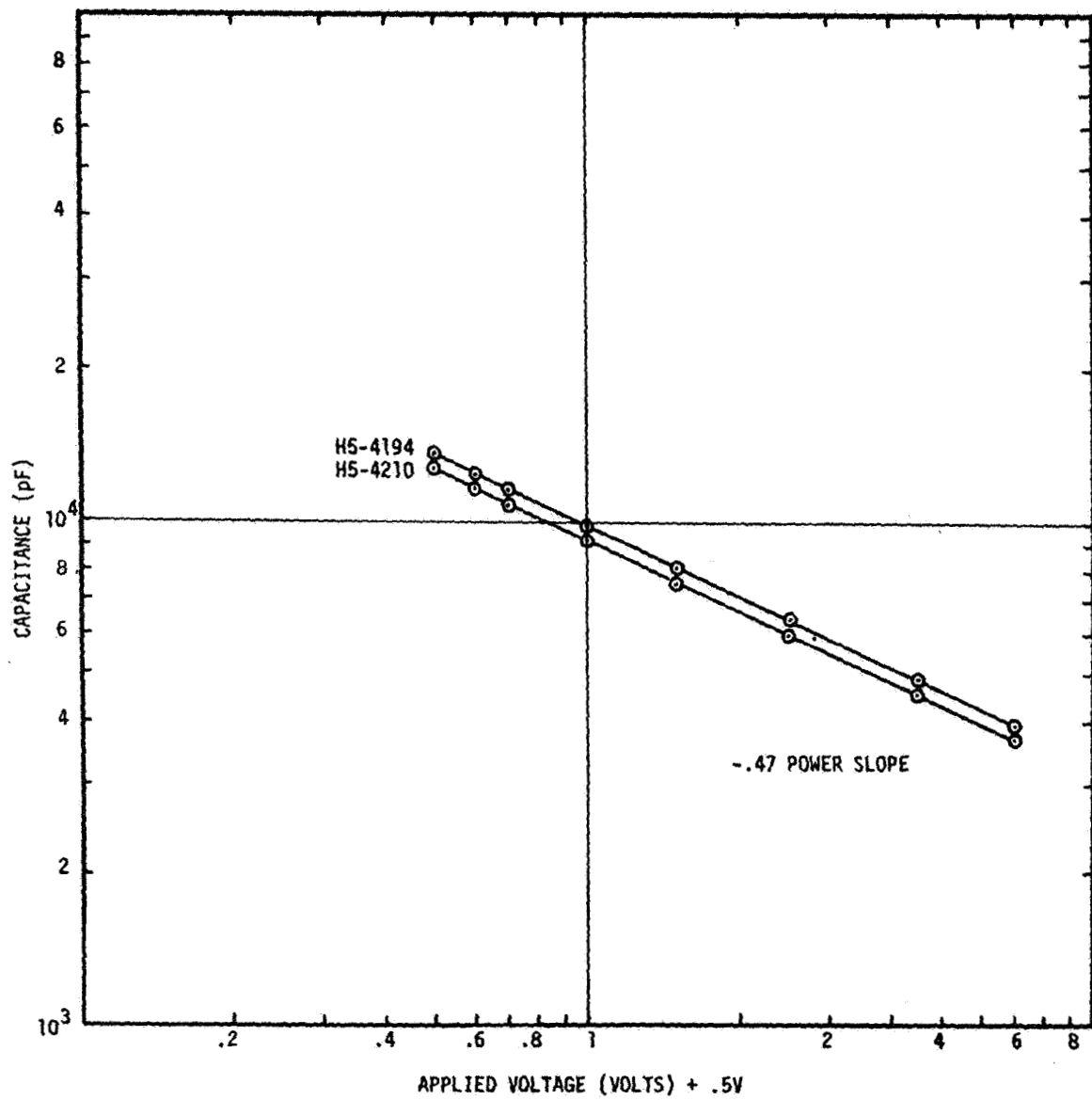


FIG. 90 CAPACITANCE VS. VOLTAGE FOR GROUP H5 LITHIUM SOLAR CELLS SHOWING  $-1/2$  POWER SLOPE

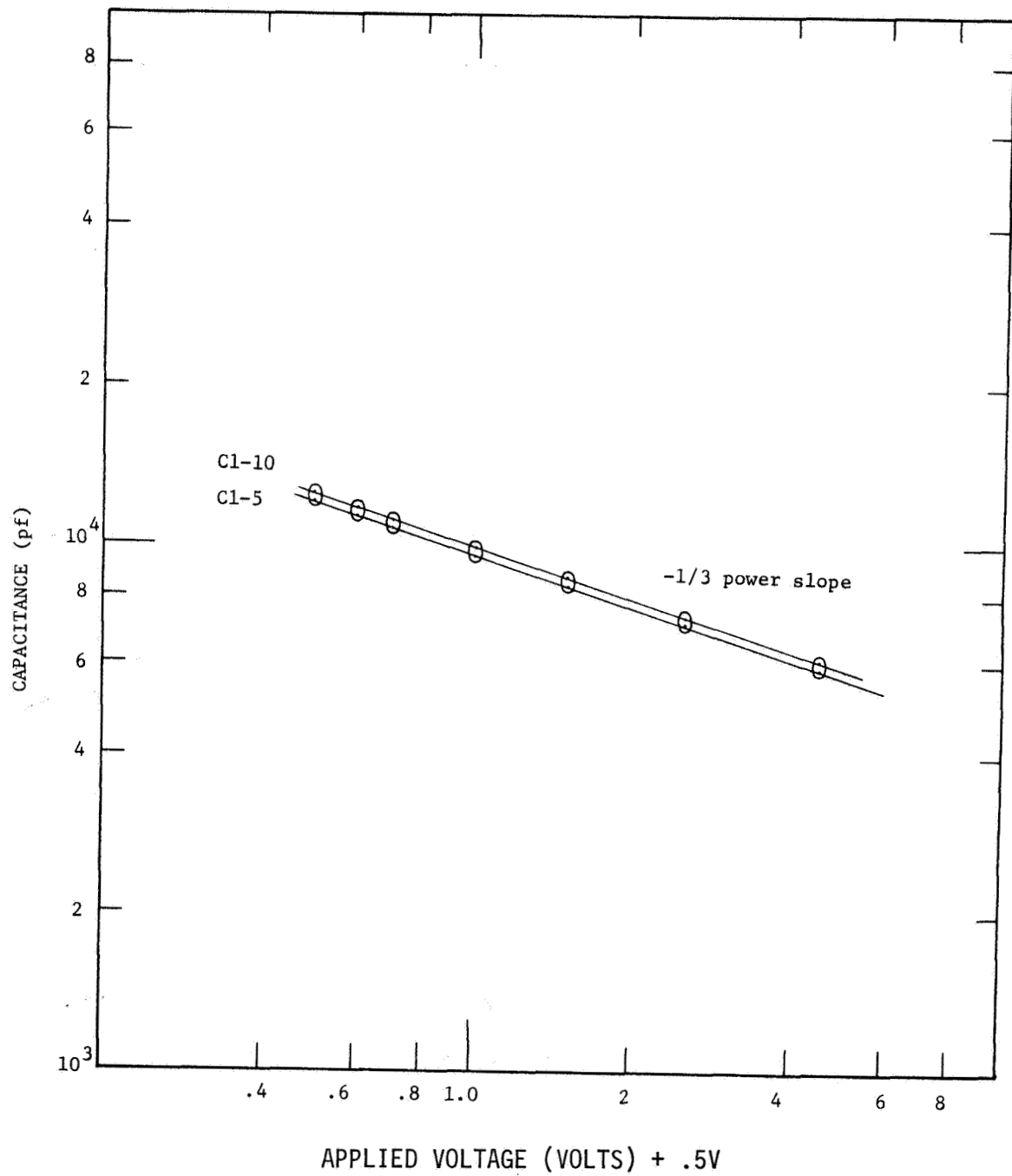


FIG. 91 CAPACITANCE VS. VOLTAGE FOR GROUP C1 LITHIUM SOLAR CELLS SHOWING -1/3 POWER SLOPE

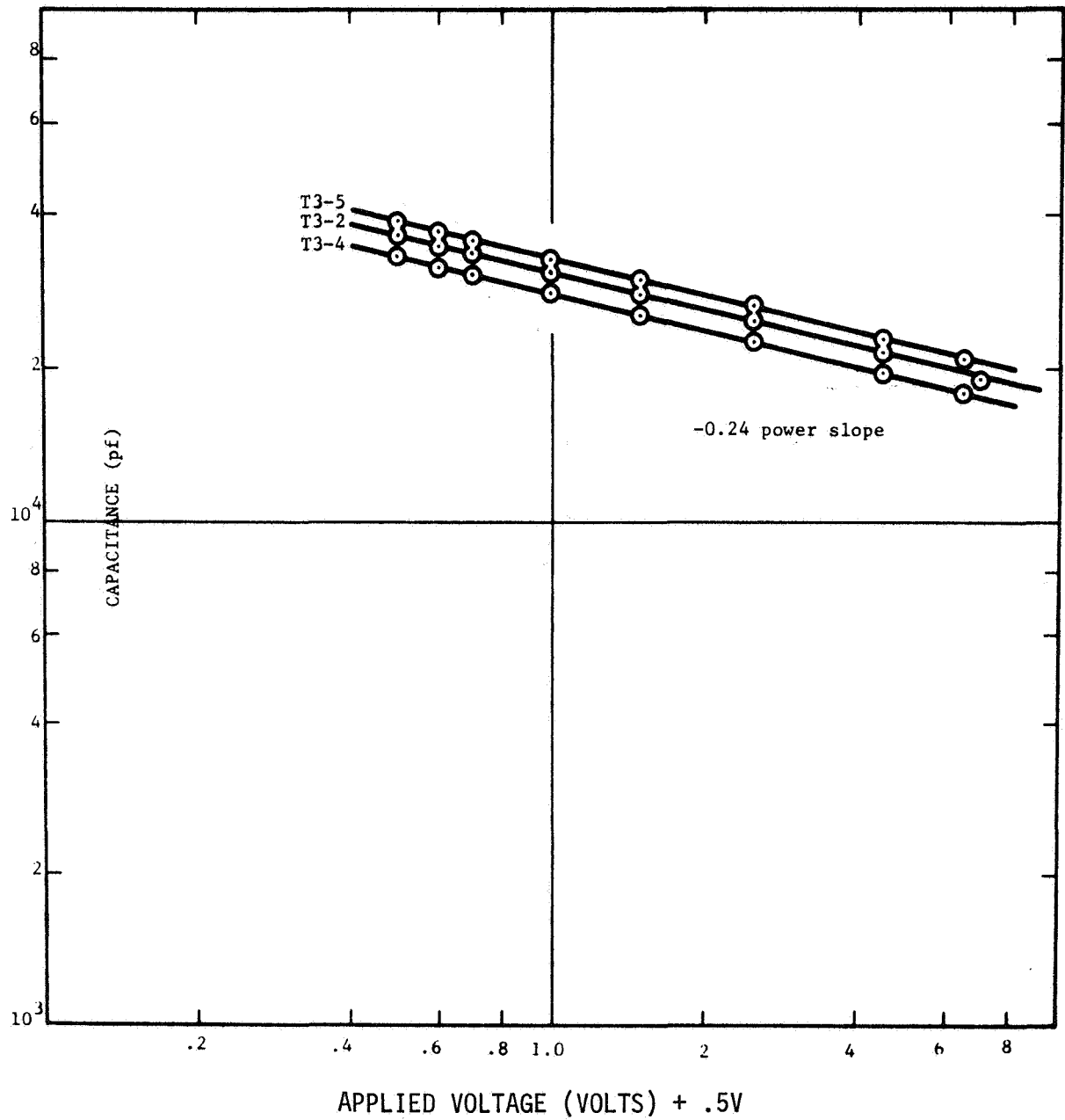


FIG. 92 CAPACITANCE VS. VOLTAGE FOR GROUP T3 LITHIUM SOLAR CELLS SHOWING  $-1/4$  POWER SLOPE

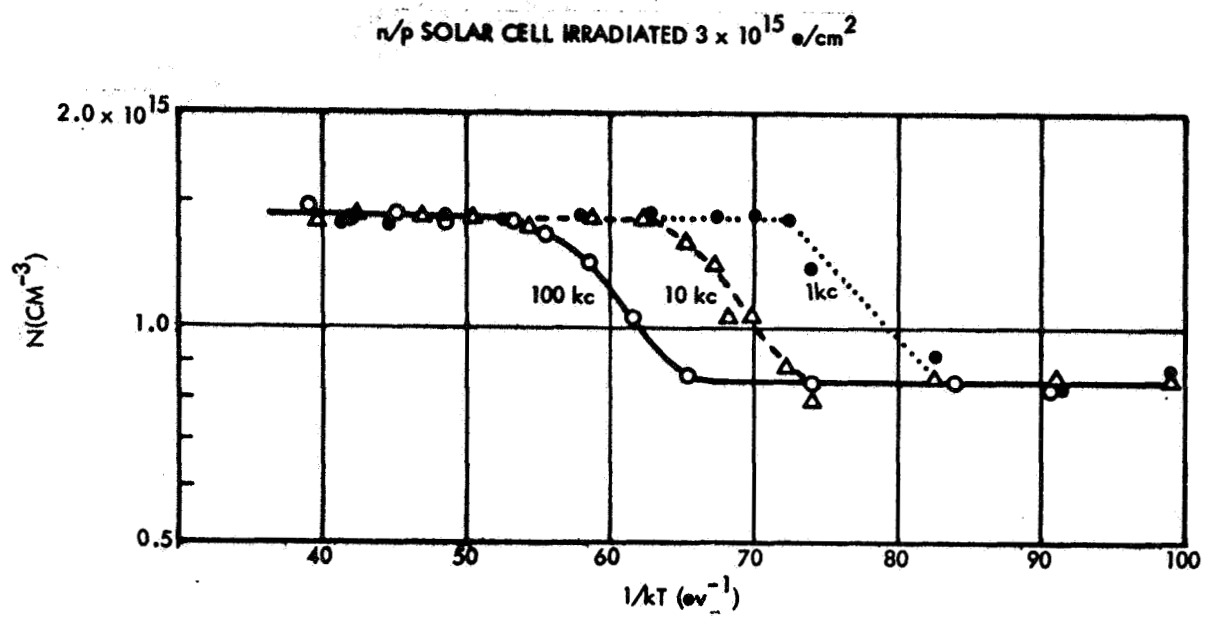


FIG. 93 DONOR CONCENTRATION DETERMINED BY CAPACITANCE